EFFICIENT COMPUTATIONAL TECHNIQUES FOR MODELING OF TRANSIENT RELEASES FOLLOWING PIPELINE FAILURES

A thesis submitted to University College London for the degree of Doctor of Philosophy

By

Navid Jalali

Department of Chemical Engineering

University College London

Torrington Place

London WC1E 7JE

July 2014

I, Navid Jalali confirm that the work presented in this thesis is my own. Where information has been derived from other sources, I confirm that this has been indicated in the thesis.

Abstract

This thesis describes the development and extensive testing of a numerical CFD model and a semi-analytical homogenous flow model for simulating the transient outflow following the failure of pressurised pipelines transporting hydrocarbon mixtures. This is important because these pipelines mainly convey highly flammable pressurised and hazardous inventories and their failure can be catastrophic. Therefore an accurate modelling of the discharge rate is of paramount importance to pipeline operators for safety and consequence analysis. The CFD model involves the development of a Pressure-Entropy (P-S) interpolation scheme followed by its coupling with the fluid flow conservation equations using Pressure (P), Entropy (S), Velocity (U) as the primitive variables, herewith termed as the PSUC. The Method of Characteristics along with the Peng Robinson Equation of State are in turn employed for the numerical solution of the conservation equations. The performance of the PSUC is tested against available experimental data as well as hypothetical test cases involving the failure of realistic pipelines containing gas, two-phase and flashing hydrocarbons. In all cases the PSUC predictions are found to produce reasonably good agreement with the published experimental data, remaining in excellent accord with the previously developed but computationally demanding PHU based CFD model predictions employing Pressure (P), Enthalpy (H) and Velocity (U) as the primitive variables. For all the cases presented, PSUC consistently produces significant saving in CPU run-time with average reduction of ca. 84% as compared to the previously developed PHU based CFD model.

The development and extensive testing of a semi-analytical Vessel Blowdown Model (VBM) aimed at reducing the computational run-time to negligible levels is presented next. This model, based on approximation of the pipeline as a vessel discharging through an orifice, handles both isolated flows as well as un-isolated flows where the flow in the pipeline is terminated upon puncture failure or at any time thereafter. The range of applicability of the VBM is investigated based on the

comparison of its predictions against those obtained using the established but computationally demanding PHU based numerical simulation.

The parameters studied to perform testing the applicability of the VBM include the ratio of the puncture to pipe diameter (0.1 – 0.4), initial line pressure (21 bara, 50 bara and 100 bara) and pipeline length (100 m, 1 km and 5 km). The simulation results reveal that the accuracy of the VBM improves with increasing pipeline length and decreasing line pressure and puncture to pipe diameter ratio. Surprisingly the VBM produces closer agreement with the PHU based CFD predictions for two-phase mixtures as compared to permanent gases. This is shown to be a consequence of the depressurisation induced cooling of the bulk fluid which is not accounted for in the VBM.

Finally, development and testing of the Un-isolated Vessel Blowdown Model (UVBM), as an extension of the VBM accounting for the impact of initial feed flow and fluid/wall heat transfer during puncture is presented. The performance of the UVBM is tested using a 10 km pipeline following a puncture along its length considering three failure scenarios. These include no initial feed flow, cessation of feed flow upon failure and its termination at any set time thereafter. For the ranges tested, the VBM and UVBM are shown to present considerable promise given their significantly shorter computational run-time compared to the PHU based numerical technique whilst maintaining the same level of accuracy.

Acknowledgements

To God Almighty, the giver of life and the source of all the love and wisdom.

To my wife Hiva, for her love, support and encouragement during my PhD studies and to my daughter Salma.

To my parents and my brother for their support and encouragement.

To Max at Howe Baker for his unconditional support.

To my supervisor, Prof. Haroun Mahgerefteh for the trust placed on me, the opportunity to study in this field and for his guidance throughout the project.

To all technical and admin. staff of the Department of Chemical engineering, UCL.

To all my fellow PhD students and office mates Garfield, Aisha, Peng, Sergey, Maria, Shirin, Alex and Vikram, it has been a pleasure meeting and working with you all.

Finally, to Dr. Solomon Brown. Thank you for your friendship and advice through the course of my studies at UCL.

Nomenclature

P	*Fluid pressure*
h	*Fluid enthalpy*
u	*Fluid velocity*
ρ	*Fluid density*
T	*Fluid temperature*
S	*Fluid entropy*
a	*Fluid speed of sound*
φ	*Isochoric thermodynamic function*
g	*Acceleration due to gravity*
θ	*Pipeline angle of inclination*
Q_h	*Heat transferred to the fluid through the pipe wall*
β_x	*Pipeline wall frictional force*
γ	*Ratio of specific heat*
k	*Isothermal coefficient of volumetric expansion*
ξ	*Isobaric coefficient of volumetric expansion*
F_w	*Fanning friction factor*
Re	*Reynolds number*
ε	*Pipe roughness*
r_{in}	*Pipe inside radius*
D	*Pipe inside diameter*
x	*Fluid quality*
z	*Fluid compressibility factor*
R	*Universal gas constant*
M	*Molecular weight*
ω	*Acentric factor*
T_r	*Reduced temperature*
T_c	*Critical temperature*
P_c	*Critical pressure*
$\alpha\ (T_r, \omega)$	*Alpha function*
$a\ (T_c)$	*Parameter for equation of state*
$b\ (T_c)$	*Parameter for equation of state*
a_i *and* b_i	*Constants determined for each component*
x_i	*Component mole fraction*
K_{ij}	*Empirically determined binary interaction coefficient*
α_i *and* α_j	*Alpha function for each component*
ρ_w	*Pipe wall density*
T_w	*Pipe wall temperature*
C_{pw}	*Pipe wall specific heat capacity*
κ_w	*Pipe wall thermal conductivity*
V_w	*Volume per unit length of the pipe*
A_{out} *and* A_{in}	*Outside and inside surface areas per unit length of pipe*
h_{amb}	*Ambient heat transfer coefficient*
h_f	*Fluid heat transfer coefficient*

C_0	*Path line characteristic*
C_+	*Positive characteristic line (Mach line)*
C_-	*Negative characteristic line (Mach line)*
v	*fluid velocity normal to the axial direction (i.e. in y direction)*
A_{pipe}	*Cross sectional area of the pipe*
P_j	*Pump discharge pressure*
u_j	*Pump discharge velocity*
P_{sh}	*Pump shut-off head*
K_{P2} *and* K_{P1}	*Constants dependant on the characteristic of pump*
G	*Mass discharge rate*
g	*Gravitational constant*
W_s	*External work per unit mass*
$C_{pl,u}$	*Specific heat at constant pressure for upstream liquid phase*
$H_{vl,u}$	*Latent heat of vaporisation at upstream condition*
η	*Critical pressure ratio*
C_d	*Discharge Coefficient*
m	*Mass inside the vessel*
V	*Volume of the vessel*
m_{in}	Inlet mass flow rate
t	*Time*
P_{res}	*Reservoir pressure*

Table of Contents

Chapter 1: Introduction

The demand for energy is forecasted to grow by over one-third from 2010 to 2035 underpinned by rising population and living standards (International Energy Agency, 2012). By far the most established method for transportation of the energy is through pressurised oil and gas pipelines therefore the length of these pipelines are expected to increase continually. A recent survey reveals that in 2014, around 110,000 miles of pipelines are either in the planning and design phase or various stages of construction worldwide (Tubb, 2014).

These pipelines mainly convey highly flammable pressurised and hazardous inventories and their failure which can be in the form of full-bore rupture, puncture (i.e. leakage) or longitudinal crack, may result in significant number of fatalities and damage to properties and environment. Corrosion and External forces such as excavation or construction work near the pipelines are the major cause of these incidents of which pipeline puncture is considered to be the most common type of failure (Lydell, 2000) failures

In the US alone, data published by the Office of Pipeline Safety (PHMSA, 2014) indicates over 943 serious pipeline incidents involving all pipelines systems between 1994 and 2014. These resulted in 359 fatalities and over £437 million damage to property.

Following public concern and awareness towards safety of pipelines, the Pipeline Safety Enforcement Program was designed to ensure compliance with applicable pipeline safety regulations and confirm operators are meeting the required expectations for safe, reliable, and environmentally sound operation of their facilities.

In the U.K, for example, the Pipeline Safety Regulations (Health and Safety Executive, 2009) imposes stringent guidelines requiring all the pipeline operators to identify all hazards associated with the pipeline that can potentially lead to major accidents and evaluate the consequences arising from those hazards. An indispensable element in pipeline safety assessment involves prediction of the discharge rate and its variation with depressurisation time following pipeline failure. Accordingly, mathematical modelling is required to accurately predict fluid transient and subsequently the release rate and its variation with time.

The flow in pipelines may be single phase (Gas or Liquid) or two-phase which is flow of two different immiscible phases separated by an infinitesimal thin interface. In this study, simplified two-phase model based on the assumption homogenous equilibrium model is considered assuming that the two phases are in mechanical (i.e. both phases travel at the same velocity) and thermal equilibrium. Calculating the fluid transients as required for modelling pipeline failure and safety analysis involves solution of partial differential equations for which many numerical methods have been developed. These include Finite Difference Method (FDM), Finite Volume Method (FVM) and Method Of Characteristics (MOC).

There are a number of such models available in the open access literature with varying degrees of sophistication producing different levels of accuracy when compared to real data. These differences are mainly due to the assumptions made for simplifying the resulting partial differential equations governing the flow and how the thermo-physical properties of the fluid are obtained. Other important factors include the efficacy of the hydrodynamic correlations such as friction factor, the numerical method employed for the solution of the partial differential equations and the ability to capture the rapid discontinuities in the depressurisation (Kimambo and Thorley, 1995).

Amongst the models available in open literature for predicting the release rate from a puncture in a pressurised pipeline, only a few (e.g. Oke et al., 2003) are capable of handling non-axisymmetric releases where flow in both the axial and radial directions are considered. Other models are based on steady state assumption and/or ignore real fluid behaviour (e.g. Montiel et al., 1998; Young-Do and Bum, 2003).

More thermodynamically rigorous models have focused on the less likely but more catastrophic scenario of full-bore ruptures. Such models (see for example Chen et al. 1995a,b) are also in principle capable of simulating pipeline puncture. However, as these are based on uni-axial flow assumption, they are only applicable for modelling outflow from punctures located at the end of the pipe across its circumference.

The starting point in development of a robust pipeline outflow model involves the formulation of the conservation equations and their coupling with the appropriate correlations for predicting the thermo-physical and flow properties. For numerical calculation of the fluid transient following pipeline blowdown, the hyperbolicity of the flow equations represents a necessary requirement for the correct prediction of decompression waves initiated upon rupture propagating towards the high pressure of the pipe from rupture plane. Given that the resulting set of hyperbolic equations can only be solved using a numerical technique, their resolution can often be computationally demanding.

For example, the computational run-time for the simulation of the complete depressurisation of a 100 km, 0.8 m i.d pipeline conveying natural gas at 100 bara following a 15 cm dia puncture is ca.18 hours using a relatively high specification (e.g 2.66 GHz, 3.0 GB RAM) personal computer. This is in spite of significant progress in the development of fast solution algorithms such as nested grid systems (Oke et al., 2003, Mahgerefteh et al., 2006a and Mahgerefteh et al., 2006b) in which

smaller time and distance discretisation steps are employed near the release plane, interpolation techniques and the more fundamental approaches involving the formulation of the conservation equations using different combinations of primitive variables (Mahgerefteh et al., 2006b).

This study presents the development and extensive testing in terms of accuracy and computational run-time of an efficient numerical CFD and a semi-analytical models for simulating transient outflow following the failure of pressurised pipelines.

The work involves:

1. Development and testing of the computationally efficient CFD model based on the Pressure-Entropy (P-S) interpolation scheme followed by its coupling with the fluid flow conservation equations using Pressure (P), Entropy (S) and Velocity (U) as the primitive variables. This is followed by validation against real data and verification of its performance against the existing UCL pipeline rupture model which employs Pressure (P), Enthalpy (H) and Velocity (U) (PHU) as the primitive variables (Oke et al., 2003). This numerical model together with the P-H interpolation developed by Atti (2006), hereafter referred to as PHU, is based on the solution of the conservation equations using the Method of Characteristics (MOC).

2. Development and extensive testing of a semi-analytical Vessel Blowdown Model (VBM) for predicting release rates following the puncture of pressurised pipelines containing permanent gas or two-phase inventories. The VBM is based on approximating the pipe as a vessel discharging through an orifice. A comparative study is carried out in order to establish the range of applicability of the VBM for both permanent gas and two-phase releases for

three main parameters. These include the ratio of the puncture to pipe diameter, initial line pressure and pipeline length. The efficacy of the VBM is determined by comparison of its predictions against those obtained using the PHU.

3. The extension of the VBM to account for the impact of initial feed flow and fluid/wall heat transfer followed by the testing of its performance against the PHU for three failure scenarios. These include isolated pipe with no initial feed flow, cessation of feed flow upon failure and its termination at any set time after failure.

The above is intended to address the long computational run-times synonymous with simulating pipeline failures using numerically based models whilst maintaining a reasonable level of accuracy as compared to the PHU.

This thesis comprises eight chapters.

Chapter 2 is review of the models available in the open literature for simulation of outflow following pipeline failure. This covers evaluation of the models in terms of robustness, computational efficiency where applicable, and accuracy based on comparison against experimental or field data.

Chapter 3 presents review of the theoretical basis and mathematical modelling of the UCL pipeline outflow model (i.e. PHU). The chapter starts with a brief discussion of the underlying assumptions, considerations made and derivation of the mass, momentum and energy conservation equations governing the flow. This is followed by presentation of the hydrodynamic and thermodynamic relations as well as the

Peng-Robinson equation of state employed in the PHU for predicting the fluid physical properties, heat transfer coefficient and friction factor.

Chapter 4 provides a review of the Method of Characteristics (MOC) used as numerical technique for solving partial differential equations. The chapter commences with describing different methods for discretising the computational domain. This is followed by application of the MOC for numerical solution of the conservation equations. This involves solution of the compatibility equations using the Method of Specified Time intervals and the Euler predictor-corrector technique to improve the accuracy of the numerical results. Next, the appropriate boundary conditions employed to simulate the outflow from a pipeline following a failure and their coupling with the compatibility equations are presented. The boundary conditions considered are closed valve or dead-ended pipe (intact end point), a centrifugal pump (at the flow source) and full-bore rupture/puncture.

With the aim of reducing the computational run-time, chapter 5 presents the development of an interpolation scheme and its coupling with the PSU based conservation equations, herewith referred to as PSUC. Following its validation based on comparison of its predictions using real pipeline rupture data, the PSUC predictions and the associated computational run-times are compared against simulation results obtained using PHU and Brown's (2011) numerical model which is based on Finite Volume Method (FVM).

Chapter 6 presents development and extensive testing of a semi-analytical Vessel Blowdown Model (VBM) for simulating discharge rate and its variation with time. The main assumptions upon which the VBM is based are first presented. This is then followed by calculation procedure for determining the exit pressure and the discharge rate for two-phase and gas inventories. Next, the performance of the VBM for

permanent gases and two-phase mixtures is tested by comparison of its predictions of the transient cumulative mass against those obtained using the PHU. The puncture-pipe diameters ratio, the length of the pipe and the initial feed pressure are the parameters investigated in order to determine the range of applicability of the VBM. Finally, the discussion of the computational run-times associated with the VBM and PHU is presented.

In chapter 7, the underlying assumptions and the formulation of the Unisolated Vessel Blowdown Model (UVBM) accounting for the impact of feed flow and heat transfer during failure are first presented. This is followed by the solution algorithm for simulating the discharge rate and its variation with time. The performance of the UVBM is next tested by comparison of its predictions against those obtained using the PHU for three different scenarios for permanent gas and two-phase pipelines. These include no initial feed flow, cessation of feed flow upon and 50 s after failure.

Chapter 8 presents the conclusions and suggestions for future work.

Chapter 2: Literature Review

2.1 Introduction

In the UK, Health and Safety Executive issued guidance under Pipeline Safety Regulations (Health and Safety Executive, 2009) requiring the pipeline operators to identify all hazards associated with the pipeline that can potentially lead to major accidents and evaluate the risks arising from those hazards. An indispensable part of safety assessment for pressurised pipelines involves prediction of the discharge rate and its variation with the depressurisation time following pipeline failure. Such data serves as the basis for assessing all the consequences associated with pipeline failure including, fire, explosion, atmospheric dispersion and emergency planning.

Inevitably, the development of accurate and robust mathematical models for predicting the transient discharge rate following a pipeline failure has been the focus of substantial attention. The success of all these models invariably relies on their accuracy in predicting real data, level of complexity and computational efficiency (Cumber, 2007). All of these headings in particular, improving the computational efficiency form the focus this study.

In terms of accuracy, a pressurised pipeline outflow model should account for all the important processes and their complex interactions occurring during depressurisation process. These include expansion wave propagation, frictional effects, phase-dependant heat transfer coefficient and use of appropriate equation of state to calculate the fluid properties and phase equilibrium data.

There are a number of pipeline rupture outflow models available in open literature with varying degree of sophistication. Denton (2009) for example presented an extensive review of the commercial as well as the published outflow models with particular attention to the more sophisticated numerically based models. For instance, Chen et al (1995 a,b) developed a two-fluid multi-component, heterogeneous outflow model presenting a comparison of the predictions against experimental data. A heterogeneous model in essence involves a set of conservation equation for each of the constituent phases thereby improving accuracy of the model but in turn making its numerical solution highly complex and computationally demanding.

On the other hand, a large body of work has been published which takes a simplistic approach on modelling blowdown. For example, Tam and Higgins (1990) derived an empirical model for mass discharge rate of the pressurised Liquefied Petroleum Gas (LPG) from pipelines based on the observed characteristics of transient release rate from large scale experimental data. Similarly, Alberta Petroleum Industry Government Environmental Committee (APIGEC, 1978) presented a simplified exponential blowdown model.

In the following, six of the state of the art models for simulating outflow following pipeline failure are reviewed and their validations against available real data are presented. The models include:

1- OLGA (Bendikson et al., 1991)

2- University College London (Mahgerefteh et al., 1997-2000; Oke et al., 2003; Oke, 2004; Atti, 2006; Brown, 2011)

3- Imperial College London (Richardson and Saville, 1991-1996; Haque et al., 1990; Chen et al., 1995 a,b)

4- FRICRUP (Norris III 1993 &1994)

5- SLURP (Cleaver et al., 2003; Cumber, 2007)

6- Webber et al., (1999)

2.2 OLGA (Bendikson et al., 1991)

The first version of OLGA originated in 1979 by Institute for Energy Technology (IFE) and developed for Statoil to simulate slow transients ensued by terrain unevenness, pipeline start-up and shut-down, and variation in production flow rates. The original OLGA model which was based on low pressure air/water mixtures adequately described the bubble/slug flow regimes when compared with the data from SINTEF two-phase flow laboratory in 1983. However it was found unsuccessful in describing the stratified/annular flow regimes (Bendikson et al., 1986).

Bendikson et al. (1991) addressed this problem and extended the model to deal with hydrocarbon mixtures. In this modified two-fluid model, a separate mass conservation equation was applied to three different phases namely gas, liquid bulk and liquid droplets. Two momentum equations were used; one for the liquid phase and the other for the combination of gas and possible liquid droplets entrained in the gas phase. Based on the assumption that the heat capacity of the liquid phase is overwhelmingly larger than that of the gas phase, the model assumes that gas, liquid and interface between the two phases are at the same temperature hence only one energy conservation equation was considered. By combining the three mass conservation equations, a pressure equation was introduced. A step wise time integration procedure was adopted by simultaneous solution of the pressure equation and the momentum equations. Due to inherent numerical limitation, proper phase behaviour was not incorporated in the OLGA model (Chen et al., 1993). All the fluid

properties were provided by a suitable PVT package in a form of table in temperature and pressure.

The finite difference representations of the conservation equations were discretised using a staggered mesh formulation whereby temperatures, pressures, densities, etc. are defined at cell mid-points and velocities and fluxes defined at cell boundaries. An upwind or donor cell technique was applied for the mass and energy equations.

OLGA was validated by Shoup et al. (1998) under transient condition against experimental data for “slow” and “rapid” depressurisations. The experimental data was obtained by Deepstar for blowdown of a 5.28 km long and 0.102 m i.d. condensate pipeline at 47.6 atm pressure, discharging through 12 mm (corresponding to slow blowdown) and 25 mm choke openings (corresponding to rapid blowdown). The comparisons against the experimental data established that reasonable agreement was obtained for slow blowdown. For rapid blowdown, the model prediction performed poorly throughout the depressurisation as compared to the field data.

Based on the result obtained by Shoup et al. (1998) for rapid blowdown whereby choke opening to pipe diameter ratio was 1 to 4, it may be postulated that OLGA will produce even greater error for the case of Full Bore Rupture (FBR) where the release area is equal to the cross-section of the pipe.

Recently, OLGA was validated against experimental decompression data by Botros et al. (2007) for studying the effect of decompression wave speed on fracture control following pipeline failure. The study of decompression wave speed using shock tube tests is of particular interest as the events following a pipeline failure have similar characteristics.

The decompression tests were conducted at the TCPL gas dynamic test facility in Canada. The facility comprised a 172 m long, 49.5 mm i.d. instrumented shock-tube rig containing inventories ranging from pure nitrogen to typical rich gas mixtures. The decompression of the pipe was initiated upon failure of a rupture disc. Comparison between OLGA prediction and those obtained by experiments are only presented for case 2 at locations 23.1 m (P14), 47.1 m (P19) and 71.1 m (P24) from the rupture point. The inventory contained in the pipe had a composition of 95.6 % methane representing a rich gas mixture initially at 105.8 bara and 25.6 ºC. The corresponding variation of pressure with time at different locations along the pipe is presented in Figure 2.11.

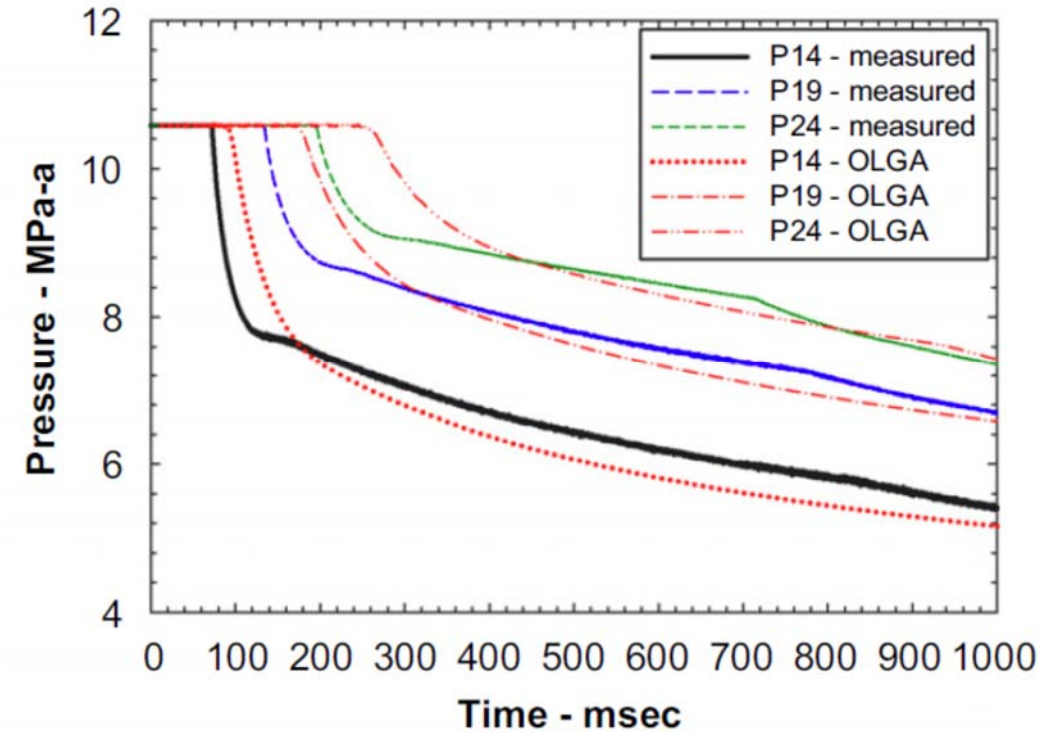

Figure 2.1: Comparison between experimental data and OLGA predictions for variation of pressure against time at different locations from the rupture disc for case 2 (Botros et al., 2007).

As observed by the Botros et al. (2007), OLGA predicted a lower speed at the front of the decompression wave as compared to the measured data hence the delay in initial pressure drop. The reason for this discrepancy as given by authors is due to the isothermal calculation of speed of sound used in OLGA as opposed to isentropic calculation. In addition, the predicted pressure drop imparted by the expansion waves was larger than the measured data. In terms of computational run-time of OLGA, no information is publicly available.

2.3 University College London (Mahgerefteh et al., 1997-2006 a,b; Oke et al., 2003; Oke, 2004; Atti, 2006; Brown, 2011)

As part of a continuing research on modelling pipeline failure, Mahgerefteh and co-workers at UCL published a number of papers studying different aspects of transient outflow modelling following rupture of pipelines conveying pressurised hydrocarbons.

In the first publication, Mahgerefteh et al. (1997) developed a full bore rupture outflow model for one-dimensional high pressure gas pipelines. The mass, momentum and energy equations were utilised and the numerical solution to these conservation equations was based on the classical inverse marching Method of Characteristics (Zucrow and Hoffman, 1976). The inventory was assumed to follow the ideal gas law. The model was applied to simulate the effects of isolation valve positioning with respect to rupture plane and delay in valve closure on total inventory released.

The dynamic response of Emergency Shut-Down Valves (ESDV) following rupture was modelled based on a real North Sea pipeline with a length and diameter of 145 km and 0.87 m respectively. The pipeline conveyed methane at flow velocity of 10

m/s with the line pressure and temperature of 133 bar and 10 ^{o}C respectively. The pipeline was assumed to be partially insulated and a constant heat transfer coefficient of 5 W/m^{2}C was used for the heat transfer calculations. Mahgerefteh et al. (1997) model considered a closed boundary condition i.e. assuming instantaneous closure for check valve closure and for ball valve closure the variation of flow properties were evaluated as a function of time during valve closure. The ball valve was assumed to trigger on sensing 10 bar pressure drop below the normal operating pressure with a constant closure rate of 2.54 cm/s.

Under worst case scenario whereby rupture occurs at the high pressure end of the pipeline, Mahgerefteh et al. (1997) studied the effect of valve closure and its proximity to the rupture plane on the total inventory released. Figure 2.2 presents the variation of total inventory released with respect to the distance of shut-down valve from the rupture plane for both check and ball type valves. From the data presented in figure 2.2, it can be seen that a check valve would give a better protection in terms of limiting the amount of inventory loss as compared to ball valve providing they are located within approximately 5 km away from rupture plane.

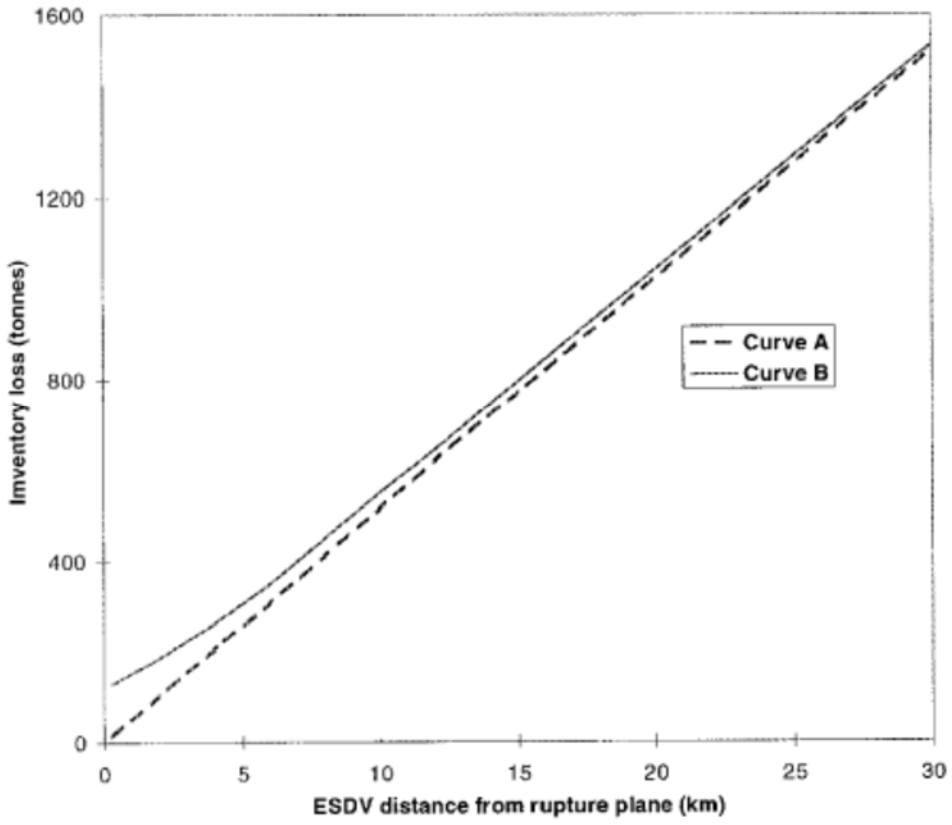

Figure 2.2: The variation of inventory loss as a function of ESDV proximity to the rupture plane (Mahgerefteh et al., 1997).

Curve A: Check valve

Curve B: Ball valve

In a later publication, Mahgerefteh et al. (1999) incorporated the real fluid behaviour in their earlier (Mahgerefteh et al., 1997) outflow model. The thermodynamic and phase equilibrium data were obtained using Peng-Robinson Equation of State (Peng and Robinson, 1976). This in turn introduced much longer computational run-times as opposed to the ideal gas based outflow model. The authors partly addressed this problem by introducing Compound Nested Grids System (CNGS) as well as adopting second order characteristics (curved characteristics see Zucrow and

Hofftman, 1976) by which the linear characteristics are replaced with arcs of parabolas. The CNGS utilises fine grids closer to the rupture plane in order to capture the highly transient behaviour of the fluid whilst for locations away from the rupture plane coarse grids are utilised (Mahgerefteh et al., 1999). The model was also extended to account for two-phase fluid flow on the basis of Homogeneous Equilibrium Model (HEM) assumption whereby the constituent phases are assumed to be travelling at the same velocity and that they are simultaneously at thermal, and phase equilibrium.

Mahgerefteh et al. (1999) validated the extended model by comparison of its predictions against Isle of Grain LPG depressurisation tests P40 and P42 (Tam and Higgins, 1990). For brevity, only P40 validation is presented here. The model was also validated against the recorded intact end pressure during rupture of the sub-sea pipeline connecting Piper Alpha to MCP-01 platforms in North Sea.

Figure 2.3 and 2.4 respectively present the model predictions for pressure-time and temperature-time profiles for the P40 test compared with the experimental data at open pipe end and closed pipe end locations. The test involved full bore rupture of 100 m pipe at 21.6 bara pressure containing a mixture of 95 % propane 5 % n-butane. The inventory was initially liquid but became two-phase upon depressurisation. Curve A and B show the measured data whilst curve C and D represent the corresponding simulated data using Compound Nested Grid System Method Of Characteristics (CNGS-MOC). As it may be observed from figure 2.3, relatively good agreement is achieved between the predicted and measured data. However the model fails to accurately predict the large initial rapid pressure drop at open end which is due to the almost instantaneous change of phase from liquid to flashing two-phase. Mahgerefteh et al. (1999) attributed this to the immediate transition to saturation condition without considering the non-equilibrium effect caused by delayed bubble nucleation. The corresponding predicted data for

temperature profiles in figure 2.4 shows a reasonable agreement with measured data. The relatively large discrepancy between the measured and predicted temperatures which can be observed towards the end of the depressurisation at both open and closed ends may be due to the constant heat transfer coefficient used in the calculation.

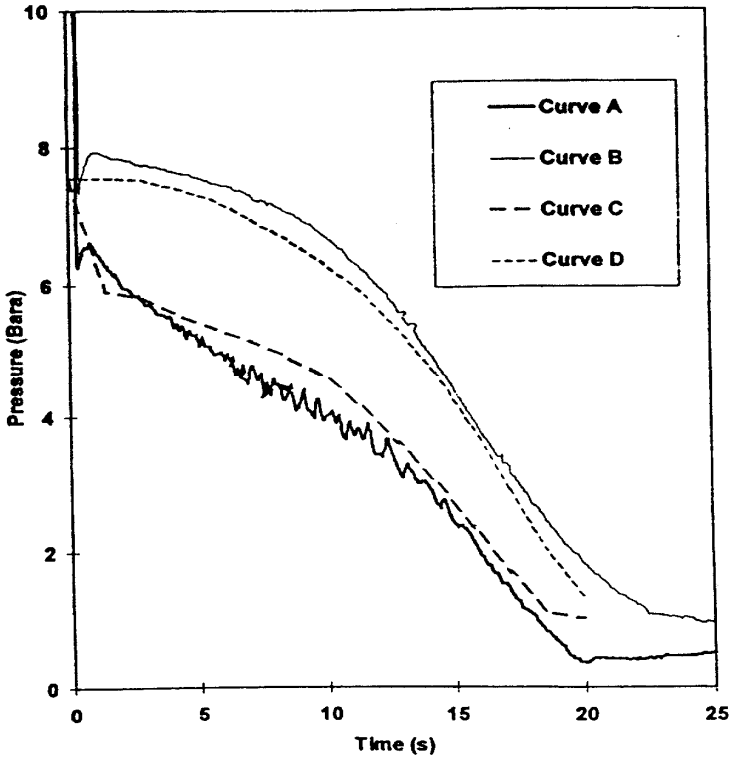

Figure 2.3: Pressure-time profiles at closed and open ends for the P40 test (Mahgerefteh et al., 1999).

Curve A: Experimental data (open end)

Curve B: Experimental data (closed end)

Curve C: CNGS-MOC (open end)

Curve D: CNGS-MOC (closed end)

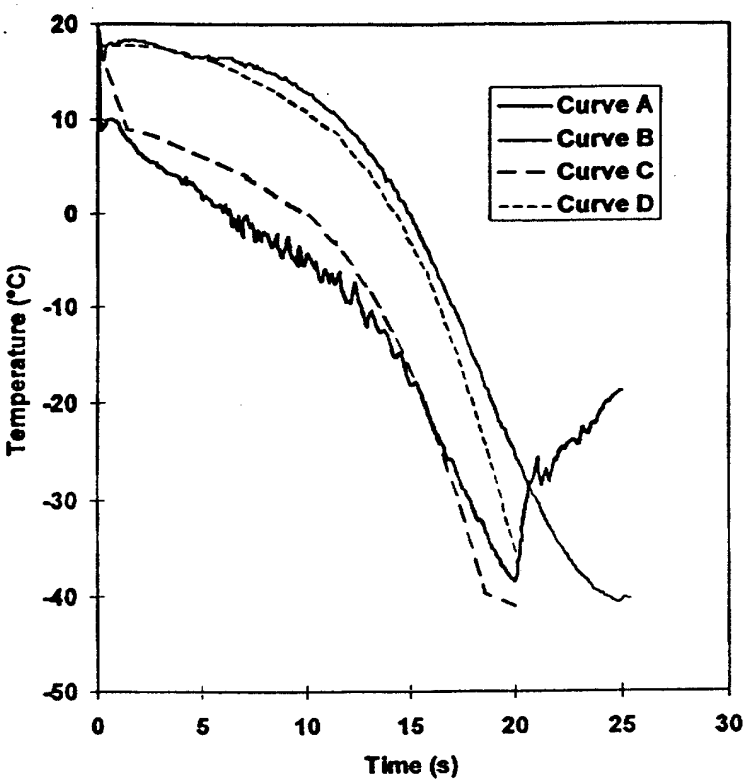

Figure 2.4: Temperature-time profiles at closed and open ends for the P40 test (Mahgerefteh et al., 1999).

Curve A: Experimental data (open end)

Curve B: Experimental data (closed end)

Curve C: CNGS-MOC (open end)

Curve D: CNGS-MOC (closed end)

Figure 2.5 shows variation of pressure at intact end against time following FBR of Piper Alpha to MCP-01 subsea pipeline. Curve A presents the recorded data during the incident whilst the curve B presents predictions using curved characteristics CNGS-MOC. Curve C shows the corresponding simulated data using first order characteristics in conjunction with ideal gas (CNGS-Ideal) model as described by

Mahgerefteh et al. (1997). As it may be observed, there is a good agreement between the model prediction and measured data. The marked difference between the CNGS-Ideal and CNGS-MOC models highlights the importance of considering real fluid behaviour when accurate predictions are required. Accounting for real fluid behaviour introduces a significant increase in the total computational run-time from 1.5 min corresponding to CNGS-Ideal to approximately 6 days corresponding to CNGS-MOC (Mahgerefteh et al., 1999).

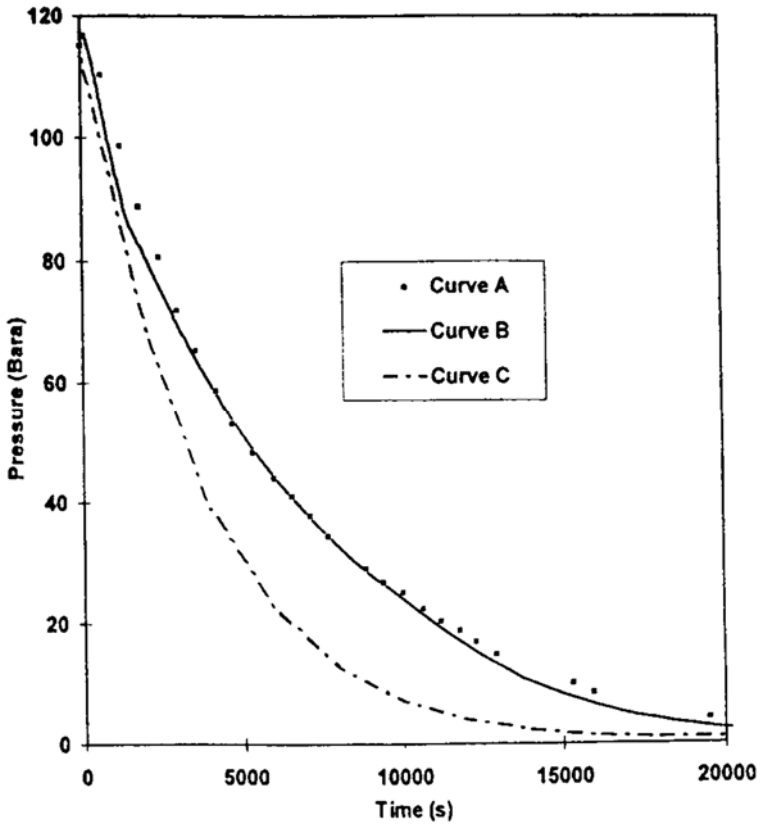

Figure 2.5: Intact end pressure against time profiles for Piper Alpha-MCP pipeline (Mahgerefteh et al., 1999).

Curve A: Field data

Curve B: CNGS-MOC; CPU time = 6 days

Curve C: CNGS-Ideal; CPU time = 1.5 min

Mahgerefteh et al. (1999) presented a case study using different numerical discretisation methods for FBR simulation of Piper Alpha to MCP-01 sub-sea line. The authors demonstrated that the use of second order characteristics in conjunction with CNGS results in approximately 75 fold reduction in total computational run-time as compared to use of first order characteristics with Simple Grid System (SGS) whereby a 10 m constant grid spacing was used.

In the later publication, by accounting for real fluid behaviour, Mahgerefteh et al. (2000) investigated the effect of fluid phase transition on dynamic response of emergency shutdown valves. Based on their findings, the authors successfully demonstrated, that the change of phase in the fluid from gas to two-phase delays the valve closure which consequently leads to greater loss of inventory.

Given that all the previously published models by Mahgerefteh and co-workers were developed specifically for simulation of FBR, Oke et al. (2003) and Oke (2004) presented a HEM based pipeline outflow model dealing with punctures along the length of the pipeline. The puncture model was based on the MOC in which the conventional Pressure (P), Density (D) and velocity (U) (PDU) conservation equations were represented in the form of Pressure (P), enthalpy (H) and velocity (U) (PHU) as well as Pressure (P), entropy (S) and velocity (U) (PSU) using the appropriate thermodynamic transformation.

The impact of using the above three different formulations of the conservation equations on the total computational run-time as well as simulation accuracy were compared against the Isle of Grain P40 LPG test (Richardson and Saville, 1996). Figure 2.6 presents the variation of open end pressure against time for experimental data of P40 test as compared to model predictions based on PHU, PSU and PDU.

All the simulations were performed on IBM Pentium IV 2.4 GHz PC. The corresponding CPU run-times of 12 min, 13 min and 86 min was reported by Oke (2004) for PHU, PSU and PDU respectively. As it may be observed from the simulation results presented in figure 2.6, the PHU based model performed best both in terms of accuracy and computational run-time followed by PSU and PDU based models.

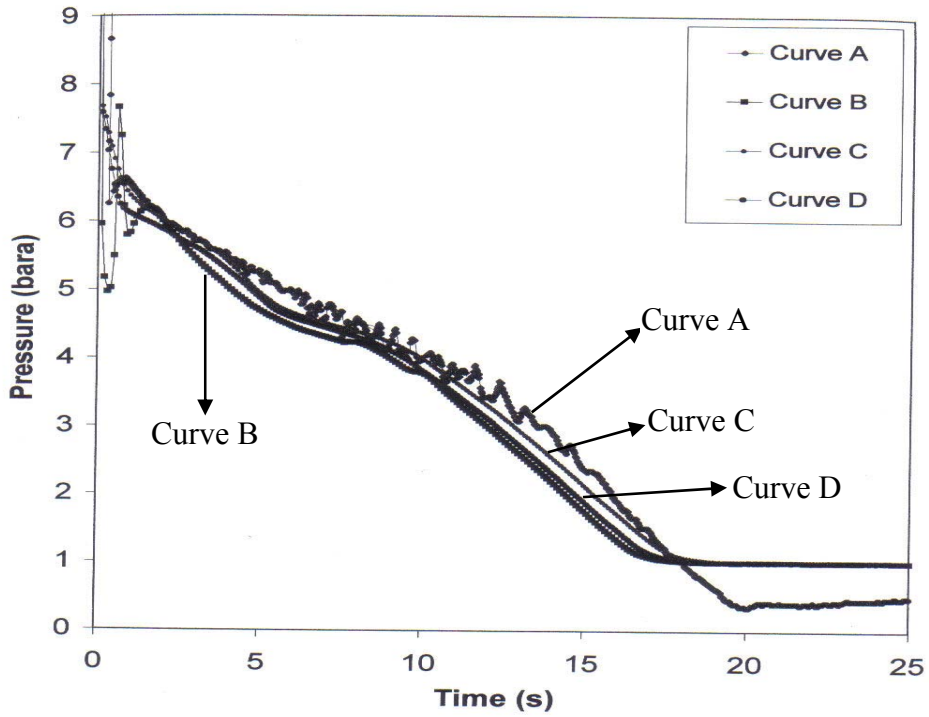

Figure 2.6: Pressure against time at open end for P40 LPG test showing results for different formulation of conservation equations as compared to measured data (Oke, 2004).

Curve A: Measured open end pressure

Curve B: Predicted open end pressure using the PDU model; CPU time= 86 min

Curve C: Predicted open end pressure using the PHU model; CPU time= 12 min

Curve D: Predicted open end pressure using the PSU model; CPU time= 13 min

The puncture outflow model developed by Oke et al. (2003) was employed to simulate the fluid flow behaviour following the mid-point puncture of a hypothetical 16 km pipe transporting a 10 component condensable hydrocarbon gas mixture operating at 117 bara and 9.85 ºC. The initial flow rate was 0.3 m^3/s and a centrifugal pump was located at high pressure end to maintain the flow rate for the first 90 seconds following pipe failure whilst the other end was assumed to be a closed end boundary. Figure 2.7 shows the corresponding variation of the in-pipe fluid flow dynamic for the first 90 seconds following failure.

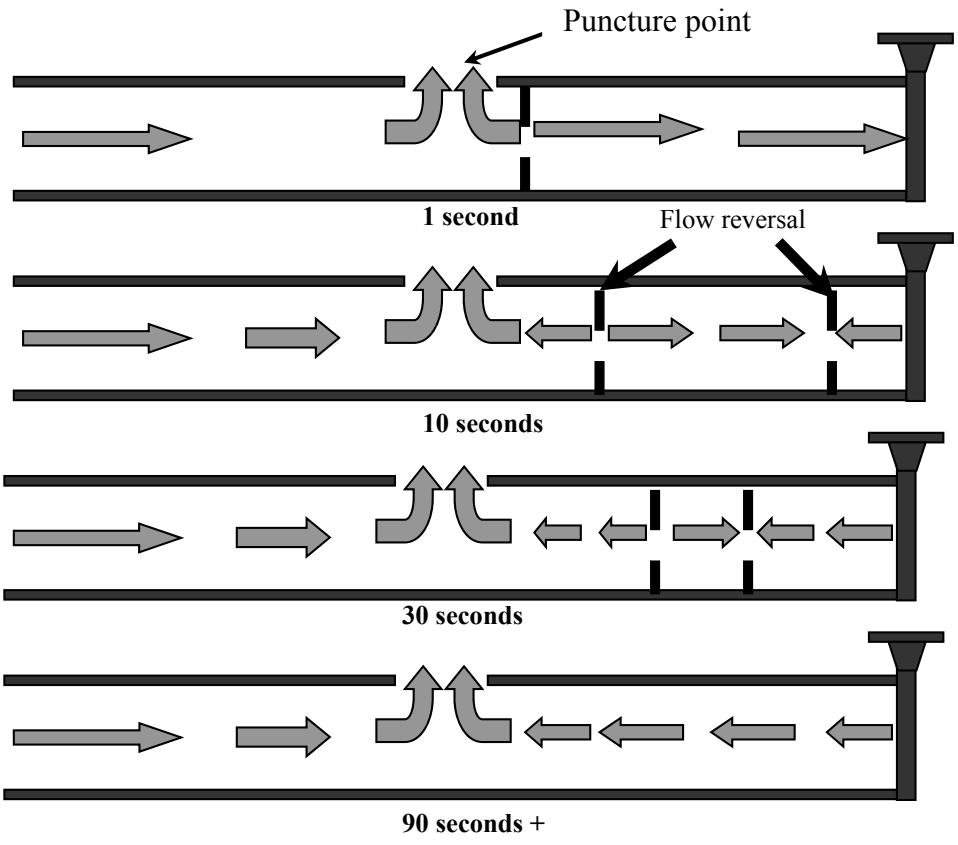

Figure 2.7: Schematic representation of the flow patterns within the pipe following a puncture in the middle of pipeline (Oke et al., 2003).

The pipeline is assumed to be isolated downstream upon puncture. This in turn creates a flow reversal at the closed end. Also, the marked difference in pressure between the ambient and the downstream of the puncture plane, causes another flow reversal to occur and travel towards the closed end to the point that these flow reversals are joined. Thereafter the flow is unified towards the puncture location.

Atti (2006) highlighted the errors in the boundary condition given by the authors (Oke et al., 2003; Oke, 2004) and proposed the required solutions. Atti (2006) also partly addressed the long computational run-time inherent in the previously presented models by introducing an interpolation technique for determination of the fluid physical properties. Based on the findings of Oke (2004), the PHU formulation of the conservation equations were used by Atti (2006) which requires pressure-enthalpy flash calculations for determining the fluid properties along the pipe.

The reduction in computational workload using the interpolation technique firstly involved the determination of maximum and minimum fluid enthalpies (h_{min},h_{max}) bounded at the likely fluid pressures (P_{min},P_{max}) and temperatures (T_{min},T_{max}).

P_{min} and P_{max} correspond to ambient and feed pressure respectively. T_{max} is the greater of feed and ambient temperatures whilst T_{min} corresponds to isentropic expansion temperature of fluid from P_{max} and T_{max} to P_{min}.

Atti (2006) showed that the use of interpolation scheme results in a maximum 0.01% difference between the interpolated values and those obtained from direct flash calculation for a range of inventories such as permanent gases, two-phase mixtures, flashing liquids and permanent liquids.

Atti (2006) validated the model by comparison against the Isle of Grain P40 LPG depressurisation test and against the field data obtained for the intact end pressure during rupture of the sub-sea pipeline connecting Piper Alpha to MCP-01 platforms in North Sea. For brevity, only comparison against Piper Alpha incident is presented in this review. Figure 2.9 presents the variation of intact end pressure against time for Piper Alpha-MCP pipeline. As it may be observed, the simulated data is in good accord with the field data. The interpolation scheme achieved a significant reduction c.a. 80% in the total computational run-time (c.f. 27 h versus 5.5 h).

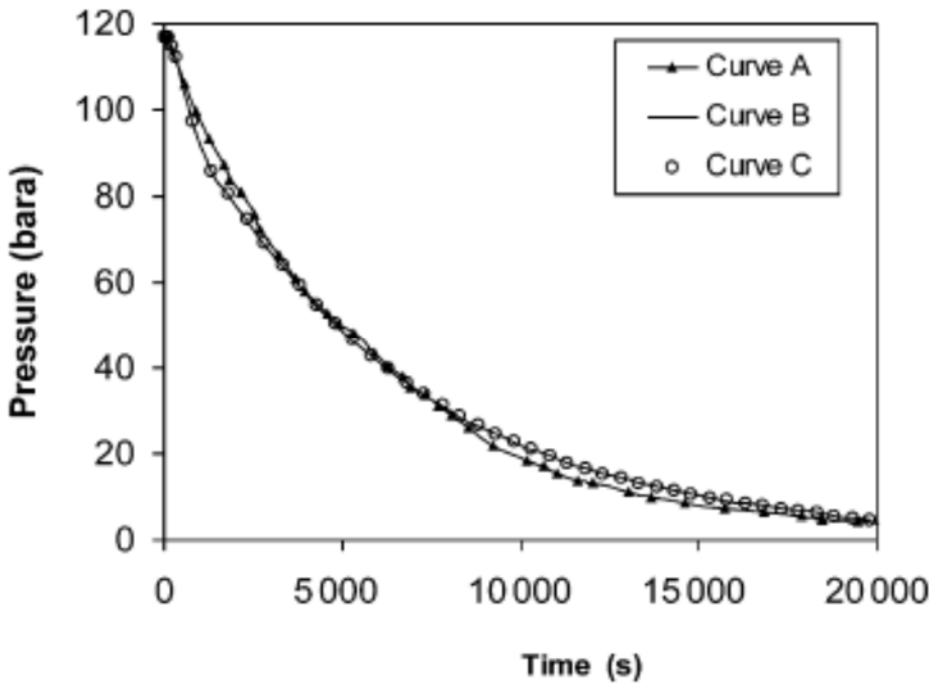

Figure 2.8: Intact end pressure against time profiles for Piper Alpha-MCP pipeline (Atti, 2006):

Curve A: Field data

Curve B: Simulation data without interpolation scheme; CPU time = 27 h

Curve C: Simulation data with interpolation scheme; CPU time = 5.5 h

More recently, in an attempt to reduce the computational run-time even further, Brown (2011) developed an outflow model based on the numerical solution of the conservation equations using Finite Volume (FV) scheme in place of the MOC. The FV based model when coupled with the numerical boundary conditions previously developed by Mahgerefteh et al. (1997-1999) and Oke (2004) has the following advantages over the MOC:

1- It is a non-iterative numerical technique as opposed to the MOC in which a large number of iterations are required in the corrector step (Atti, 2006).

2- A fixed number of calculations are required without compromising numerical accuracy (Brown, 2011).

Brown (2011) utilised the PHU formulation of the conservation equations for development of the FV based model. The source terms of the governing conservation equations were initially ignored and solved separately using an explicit Euler method based on operator splitting (Leveque, 2002). The primitive centred PRICE-T scheme of Toro and Siviglia (2003) was applied to the remaining hyperbolic systems of equations. Brown (2011) reformulated the Random Choice Method (RCM) of Gottlieb (1988) in terms of average sampling. Figure 2.9 presents the staggered grid discretisation along the time (t) and space (x) axes of RCM for grid (i). The primitive variables (flow variables) are assumed to be known at positions i-1,i and i+1 at time (n). Using the staggered grid RCM, the flow variables are obtained for Q_i^{n+1} (i.e. at next time step t+Δt) in two steps solution algorithm.

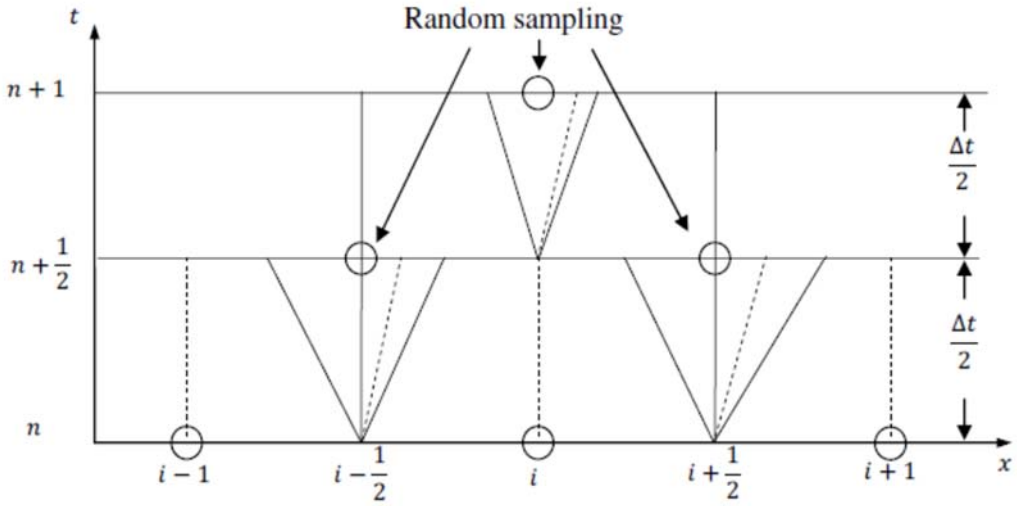

Figure 2.9: Schematic representation of the RCM for grid point (i) along the time (t) and space (x) axes on staggered grids (Brown, 2011).

Brown (2011) validated the FV based model against experimental data in which simulation accuracy and total computational run-time were investigated. Brown (2011) also presented some case studies comparing the FV simulation results with those obtained from the MOC. In some of the cases, Brown (2011) model achieved 23 to 78 % saving in the CPU run-times as compared to Atti's (2006) model.

The validation and verification case studies of the FV model are presented and reviewed in chapter 5.

2.4 Imperial College London (Richardson and Saville, 1991-1996; Haque et al., 1990; Chen et al., 1995 a, b)

Hague et al. (1990) developed a computer code namely "BLOWDOWN" in order to simulate the rapid depressurisation of pressure vessels particularly to address the low steel temperature reached. The model accounts for existence of vapour at the top zone (with consideration of liquid droplets formation) and liquid at bottom zone of the vessel.

The solution algorithm adopted by Haque et al. (1990) involved introducing a pressure reduction to the system and performing isentropic flash calculation on each zone followed by the calculation of the discharge rate. Once heat transfer coefficients are calculated for each zone, the corresponding temperature in each zone is determined by applying energy and mass balances over the content of each zone. Based on the above, the total inventory released can be calculated.

Richardson and Saville (1991) developed an extension to the BLOWDOWN program which was capable of simulating the depressurisation of pipelines following failure. The authors classified the pipelines with respect to their inventories namely:

- Permanent gas
- Permanent liquid
- Volatile liquid

Separate models were presented for each type of inventory. In the following, for brevity, only the more sophisticated model for volatile or flashing liquid is presented and discussed.

The following distinct stages were reported upon commencement of the failure in a pipeline containing flashing liquids (Richardson and Saville, 1991):

1- Propagation of the expansion waves from the failure location to the high pressure end
2- Quasi-steady frictional flow once the expansion wave reaches the high pressure end. This regime will continue until the pressure immediately upstream the rupture plane falls to saturation pressure
3- Quasi-steady frictional two-phase flow when the pressure inside the pipe falls sufficiently low and two-phase mixture is formed throughout the pipe

Due to much larger drop in pressure occurring during FBR as compared to punctures, the evolution of gas is expected to start almost instantaneous hence stage 2 occurs almost at the same time as stage 1. Richardson and Saville (1991) derived analytical solutions for predicting discharge rate during each stage. The pipeline is then discretised into number of elements and mass, momentum and energy balances are set up for each element considering the following assumptions:

1. Homogenous Equilibrium Model
2. Quasi-steady approximation

The second assumption implies that the flow rate at a given time is constant in every element. The discharge pressure is obtained by performing an energy balance across the release plane assuming that the fluid emanating the pipe follows an isentropic process.

The fluid properties are calculated using PREPROP, a computer package which utilises the Corresponding States Principle (CSP) based on an accurate equation of state for methane (Saville et al., 1982) in order to calculate the thermo-physical properties of a multi-component mixture.

The pipe is discretised into a number of sufficiently small elements such that change in physical properties between consecutive elements can be neglected. The initial state and velocity at the inlet are known, then for each element:

- An energy balance is performed to determine the state and speed of the material leaving the element
- A momentum balance is performed to determine the pressure drop over the element considering the gravitational forces

The balances are then linked together and solved iteratively to satisfy the boundary conditions. The model was validated against the Isle of Grain P42 test.

Figure 2.10-11 respectively present variation of intact end pressure and total inventory within the pipe against the depressurisation time. Given that BLOWDOWN does not consider the induced expansion wave propagation, it may be observed from figure 2.10 that the model unsurprisingly fails to predict the sharp pressure drop at the intact end of the pipe upon arrival of the expansion waves. However, soon after, the inventory becomes two-phase throughout the pipe and quasi-steady frictional two-phase governs the flow and the model predictions closely match the experimental data. Thereafter, the inventory follows a phase transition from two-phase to gas and the model predictions start deviating from the experimental data. In figure 2.11, the prediction of the total inventory inside the pipe

is initially in good accord with measured data and continues to diverge towards the end of depressurisation.

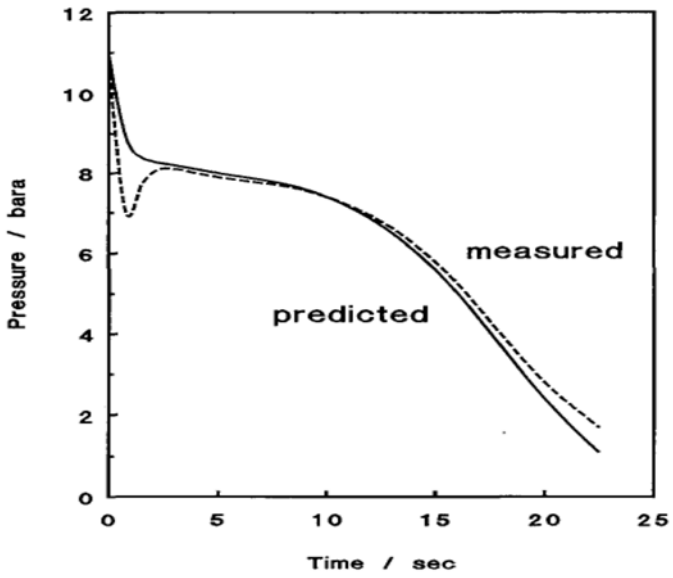

Figure 2.10: Variation of intact end pressure with time for P42 LPG test (Richardson and Saville, 1991).

Broken Line: Experimental data

Solid Line: Blowdown prediction

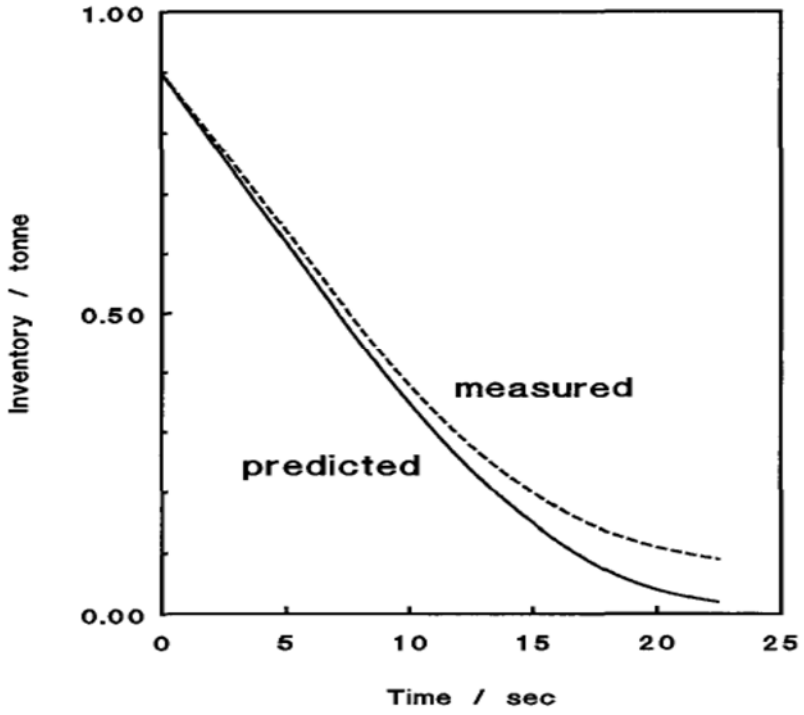

Figure 2.11: Variation of total inventory with time for P42 LPG test (Richardson and Saville, 1991).

Broken Line: Experimental data

Solid Line: Blowdown prediction

Richardson and Saville (1996) published a more detailed and more substantiated validation of their model against the complete Isle of Grain LPG depressurisation tests. For brevity, only validation of BLOWDOWN against P40 test is presented in this section.

It is assumed that authors have made some general modifications in the new version of the BLOWDOWN. For instance, Richardson and Saville (1996) developed a much more comprehensive heat transfer calculation in addition to what they have previously presented (Richardson and Saville, 1991). The heat transfer accounts for

forced convection between fluid and pipe wall, transient conduction through the wall and forced/natural convection between pipe and the surroundings.

In terms of computational run-time of, a complete simulation of one of the Isle of Grain test using BLOWDOWN took typically ‘few’ hours on a 386 or 486 machine fitted with an 860 co-processor.

Figures 2.12-14 respectively show the variations of the pressure, inventory and temperature against depressurisation time for Isle of Grain P40 test. Reasonable agreement may be observed between model predictions and experimental data even though the temperature predictions of BLOWDOWN (specifically at the closed end) have deviated from experimental data and the model almost consistently under-predicted the temperature. Added to this, the predicted inventory remaining in the pipeline is consistently greater than the measured data. The authors have attributed this to the quasi-steady and the HEM assumptions which are considered in development of BLOWDOWN model for simulating the pipeline failures.

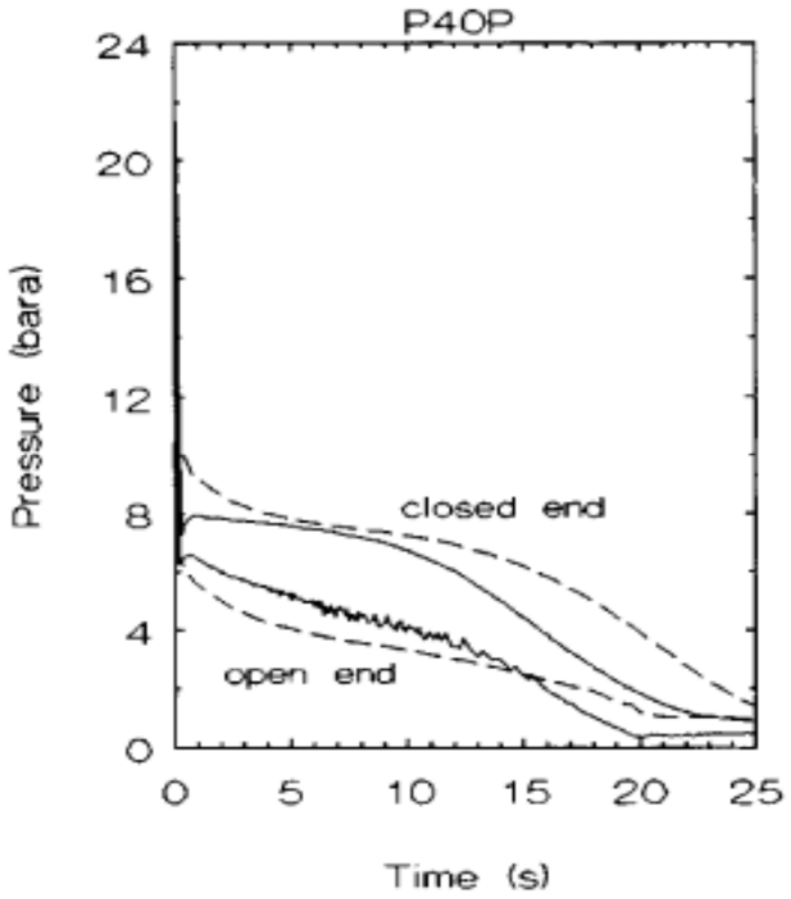

Figure 2.12: Variation of pressure with depressurisation time for P40 LPG test (Richardson and Saville, 1996).

Solid Line: Experimental data

Broken Line: BLOWDOWN prediction

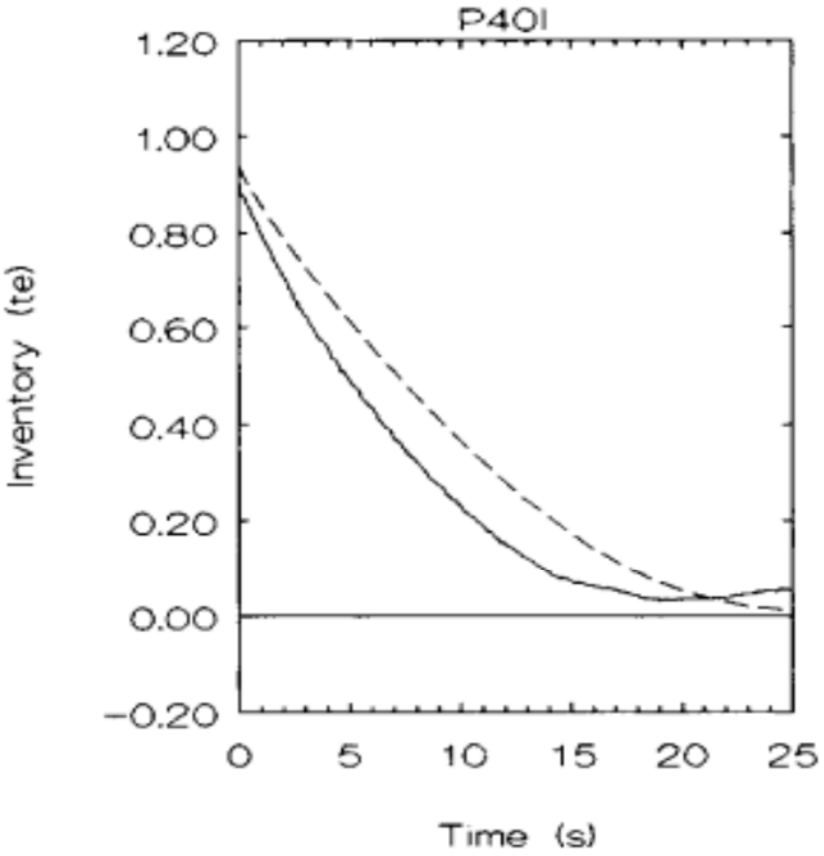

Figure 2.13: Variation of total inventory with depressurisation time for P40 LPG test (Richardson and Saville, 1996).

Solid Line: Experimental data

Broken Line: BLOWDOWN prediction

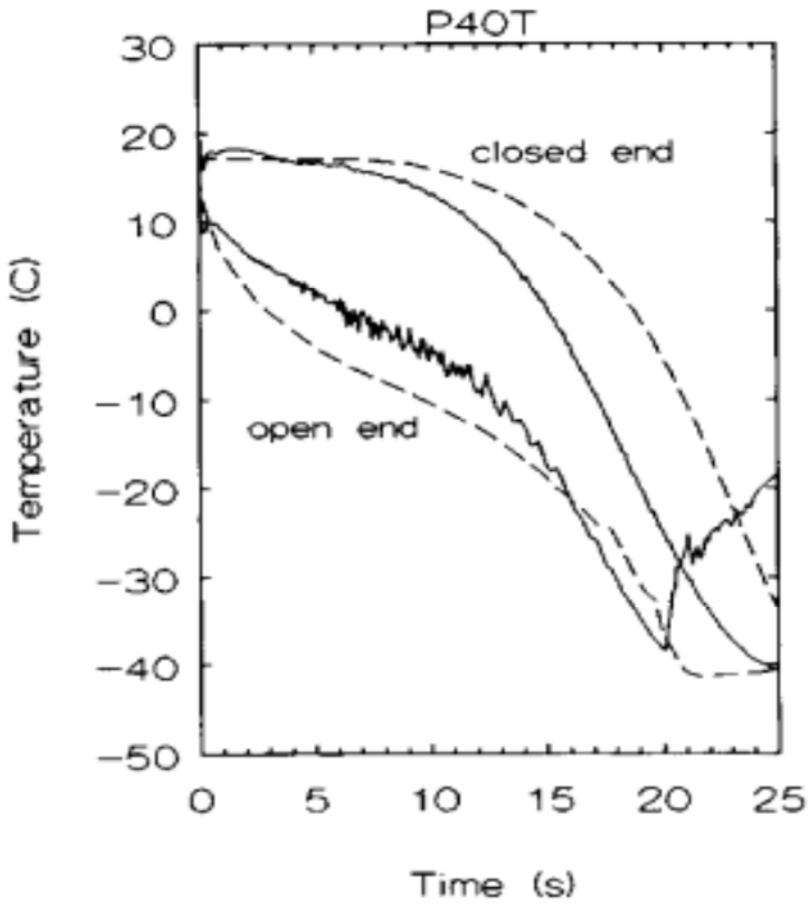

Figure 2.14: Variation of temperature with depressurisation time for P40 LPG test (Richardson and Saville, 1996).

Solid Line: Experimental data

Broken Line: BLOWDOWN prediction

Chen et al., (1995a, b) investigated the effects of HEM flow assumption on the accuracy of their simulations by developing heterogeneous model and comparing its performance against the HEM based model. Unlike HEM, the constituent phases in a heterogeneous model are not in thermodynamic and mechanical equilibrium (i.e. both phases are not traveling at the same speed). Chen et al., (1995a) successfully

demonstrated that the non-equilibrium behaviour can be explicitly expressed in terms of the velocity difference between the liquid and the vapour phases. Considering this and in order to conserve the hyperbolicity of the system of equations, the authors forced the flow to be marginally stable. That is, all the information related to the structure of the flow which is not accounted for under the basis of non-dissipative and inviscid flow is assumed to be embedded in the inertial coupling constant.

In their second paper (Chen et al., 1995b), the authors modified their earlier model (Chen et al., 1993) which was based on MOC and ideal gas law, using a simplified finite difference method for equilibrium two-phase flow and applied the marginal stability model for multi-component mixtures. In this model, the flow channel is discretised using staggered grids where the flow velocity is defined at the cell boundary with all other variables defined at cell centre. Following the guidelines of the Fourier stability analysis, the scheme solves the convection term of the momentum equation explicitly and the flow velocity is expressed in terms of pressure. In order to reduce the complexity of the heterogeneous model, the authors investigated the effect of the concentration stratification by assuming fully dispersed flow and also by relaxing the assumption. The fluid properties were calculated using the PREPROP computer package.

Chen et al. (1995a) validated their model against the Isle of Grain P40 test. Figure 2.15 (a-d) presents the predicted pressure and temperature profiles obtained from the heterogeneous as well as homogeneous models with comparison against the measured data. The heterogeneous models are referred to as MSM-CS (Marginally Stable Model-Concentration Stratification) and MSM- no CS (Marginally Stable Model-Without Concentration Stratification). The agreement of the META-HEM (META referring to the name of the main computer program) is sufficient enough to suggest that such non-equilibrium effects can generally be ignored. On the other hand, the poor performance of the MSM model can primarily be a consequence of

the uncertainties associated with empirical correlations used in formulation of the model.

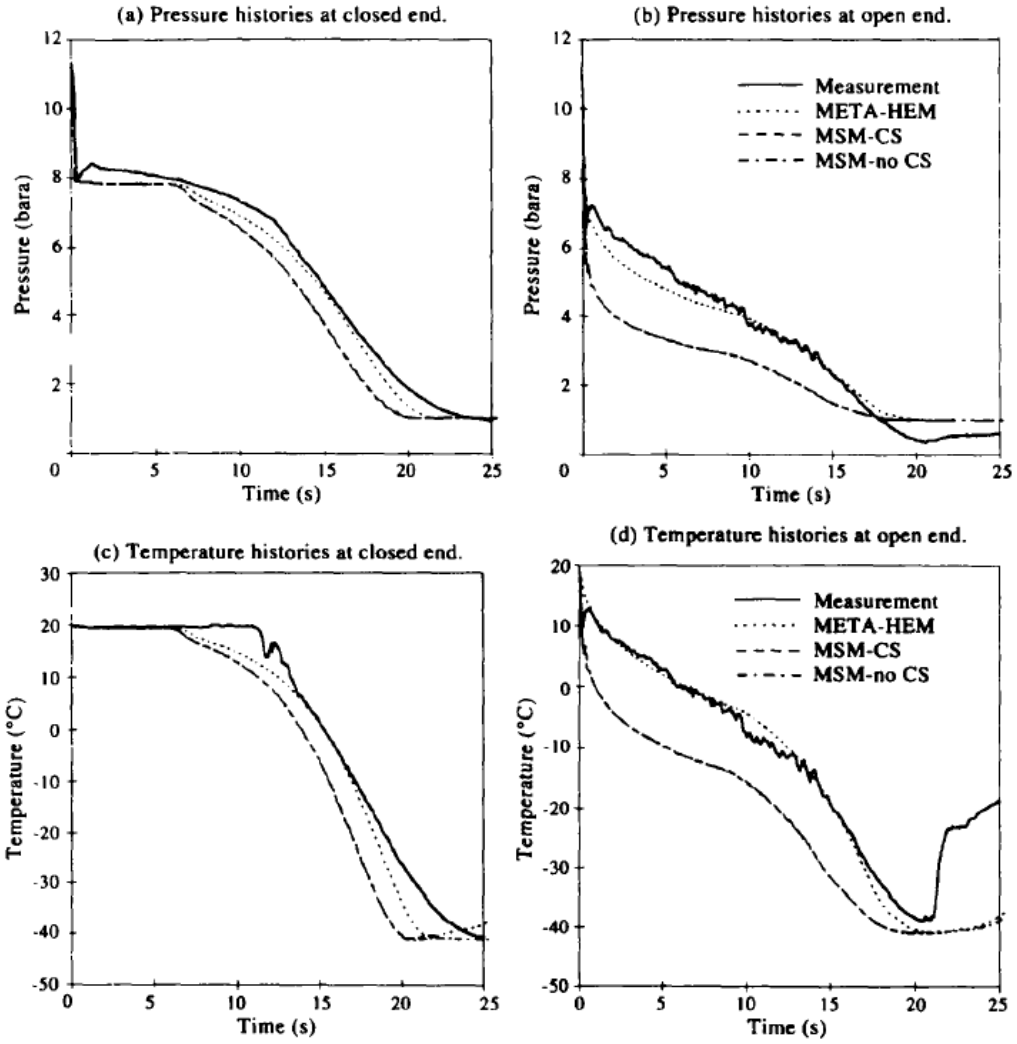

Figure 2.15(a-d): Comparison of results for two-component system (Chen et al., 1995a).

25 uniform meshes of 4 m long were used to perform the above simulations. The time steps were in the range of 0.0004 - 0.04 s. The reported computational run-time using a DEC 5000/240 station were 20 h for MSM and 8 h for META-HEM.

2.5 FRICRUP (Norris and Puls, 1993; Norris, 1994)

A series of small scale blowdown experiments were conducted by Exxon using gas bottles connected to coiled tubing. Alongside the experimental tests, a mechanistic homogenous equilibrium model was developed in an attempt to develop a simplistic model describing the blowdown of both vessels and pipelines. Efficacy of the FRICRUP was demonstrated through comparison against experimental data.

In what follows, a brief description of the experimental set up is presented. The test facility comprises of nozzle controlled by a quick-opening valve attached to an interchangeable "vessels" and "pipelines". The vessel consisted of a single gas cylinder (0.05 m^3 volume) with a liquid delivery tube or three gas cylinders manifolded together. The cylinders were constructed with seamless steel similar to those normally used for delivery of compressed gas. The 'pipeline' comprised a 610 m long coil of tubing (L) with outside diameter of 15 mm (inside diameter of 10 mm) with the total volume of the pipeline being 0.048 m^3.

The vessels (gas bottles) or pipeline (tubing) rested on an electronic scale allowing for mass efflux during blowdown to be measured using the time history of the scale readings. The pressures and temperatures were measured for both upstream of the nozzle and upstream of pipe/vessel. The analogue data was converted in to digital data and stored in a spread sheet for further analysis. The scans through all the channels were made at a varying rate.

Figure 2.16-17 respectively show the geometry used in the development of the FRICRUP model and the schematic representation of the test facility.

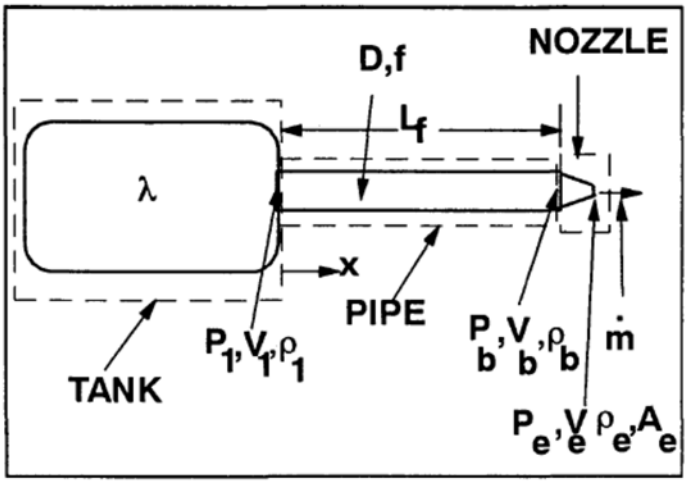

Figure 2.16: The geometry used for the FRICRUP model development (Norris and Puls, 1993).

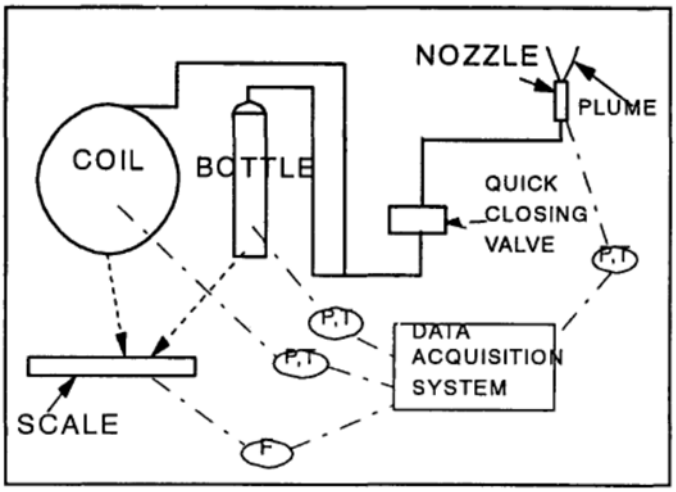

Figure 2.17: Schematic view of the test facility (Norris and Puls, 1993).

The time dependence of the depressurisation was obtained by solution of the mass balance across the vessel. The Moody friction factor was utilised to determine the pressure drop across the pipe. Since the discharge through nozzle during depressurisation is assumed to be a frictionless process, for momentum balance

across the nozzle, the friction term is removed. The authors assumed that flow through the pipe is steady state (i.e. the mass flux is constant). The vessel and pipe are assumed to follow an isothermal path. However the temperature profiles obtained from experimental data demonstrated a considerable drop in temperature for the vessel and less profound drop of temperature for the pipeline.

A series of isothermal and isentropic flashes were performed using an equation of state (BWRS method). The results were curve fitted in the form of a quadratic polynomial such that if either temperature or entropy is specified, the density can be obtained as a function of pressure.

Returning to figure 2.16, the total length of the pipeline (L) is replaced with the effective frictional length (L_f) that is the length where most of the frictional pressure drop near the discharge takes place. Therefore for integration of the momentum balance, L_f is used as the upper limit of the integral.

V_l and V_b are calculated using the steady state assumption. Choked flow algorithm was applied assuming the exit velocity V_e is equal to the isentropic speed of sound at P_e. The momentum equations of pipe and nozzle were solved simultaneously through a nested iteration loop in order to determine P_b and P_e. The mass flux was determined once P_b and P_e were calculated. By introducing a time step, the time history of pressures, velocities and mass effluxes can be determined through the use of a simple mass balance across the vessel.

In order to determine L_f, the authors made the following ambiguous assumption that the blowdown of pipe is approximated as a linear mass source such that it satisfies the following:

$$\rho V = \left(\frac{\dot{m}}{A}\right)\frac{x}{L} \tag{2.1}$$

Where,

ρ= density

V= velocity

$\dot{m}$= is mass efflux rate

A= is cross sectional area of the pipe

x= is the distance along pipe from the high pressure length

The above equation is not consistent with the steady state assumption earlier made for development of FRICRUP and invalidates the simplified momentum equation obtained by assuming steady state. Despite this, using the analogy between the two momentum equations (with and without the above assumption), the author presented the following relationship between, L and L_f:

$$L_f = \frac{1}{3}L \tag{2.2}$$

For simulating vessel blowdowns using FRICRUP, L_f must be equated to zero. Figure 2.18 and 2.19 respectively present blowdown of carbon dioxide from coil and vessel. The initial pressures of 55-69 bar and initial temperature of 27 ^{o}C were used in the experiments.

As it may be observed, the model predictions are not in good accord with the experimental data and the model consistently under-predicted the discharge rate. As expected, the experimental data suggests that the discharge rates from vessel blowdowns are considerably higher than the coil blowdowns indicating the importance of frictional effect within the pipe.

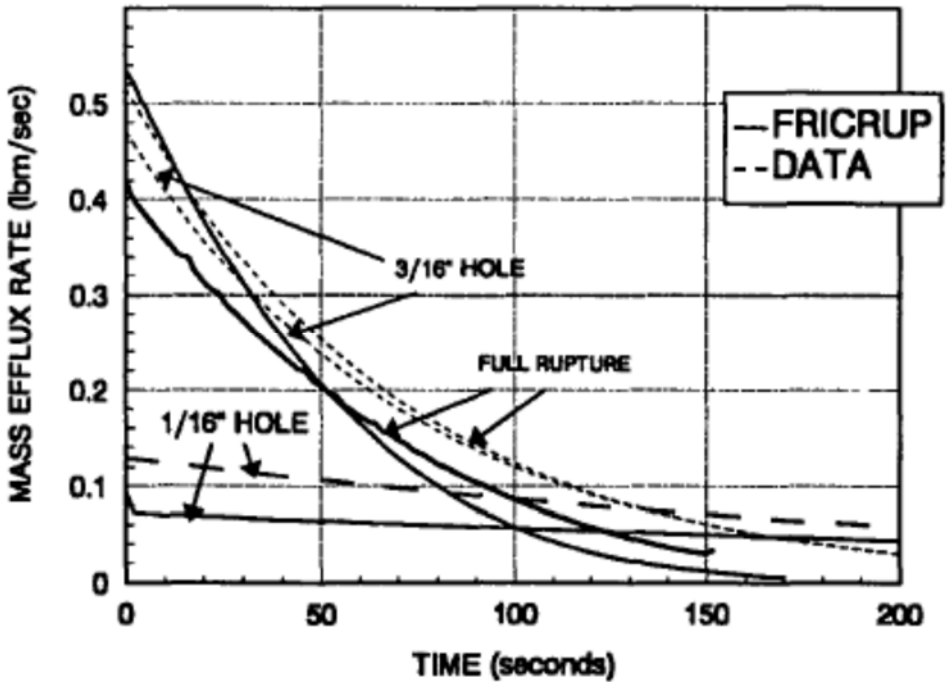

Figure 2.18: Comparison between FRICRUP predictions and experimental data for the Blowdown of Carbon Dioxide in the coil with 1.6 mm and 4.8mm openings and FBR (Norris and Puls, 1993).

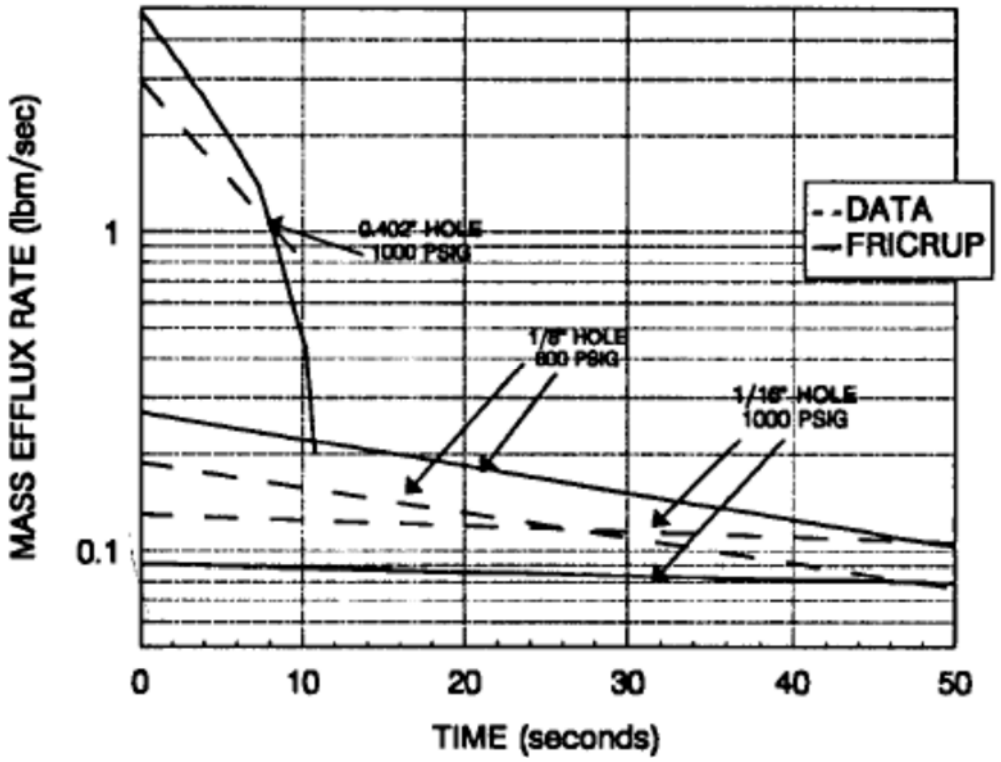

Figure 2.19: Comparison between FRICRUP predictions and experimental data of the Carbon Dioxide blowdown of vessel for 1.6 mm and 3.2 mm openings and FBR (Norris and Puls, 1993).

Comparison between the data presented in figures 2.18 and 2.19, leads to a very interesting discovery which was not reported by Norris and Puls (1993). That is for smaller size apertures, the blowdown behaviour of vessel and pipe becomes very similar. In contrast, for case of FBR, there is a distinct difference between the two blowdown behaviours which evidently is the result of larger pressure gradient across the pipe during its depressurisation.

In a later publication, Norris and Puls (1994) conducted further experiments for blowdown of three hydrocarbon gasses, including 99.92% pure methane, light gas (MW=17.64 g/mol) and heavy gas (MW=17.70 g/mol).

The experimental data for vessel blowdown indicated condensation of gas in the nozzle. Due to highly transient nature of vessel blowdown particularly for the larger nozzles, the temperature was sufficiently low for gas to condense. The thermodynamic analysis using isentropic flashes demonstrated that liquid volume fraction for the range of pressures tested, does not exceed 0.33% and 0.14% for light gas and heavy gas respectively. Despite the fact that the liquid volume fraction is considered to be relatively small, a noticeable amount of condensate was observed by the near invisibility of the discharged jet. The authors attributed this to the fact that a lower sonic velocity is expected as a result of the condensation and that fluid emanating through the nozzle, under such condition, requires lesser acceleration to reach the sonic velocity. This results in higher pressure at the exit plane relative to what it would have been in the case of a single phase flow hence higher density at the exit plane. The increase in fluid density at the exit plane more than compensates for the lower sonic velocity.

In addition to the above, the following observations were made by Norris and Puls (1994):

1. The hydrocarbon blowdown behaviour described above for vessel and pipe matches the earlier finding of Norris and Puls (1993) for air and carbon dioxide blowdowns
2. The FRICRUP predictions for the hydrocarbon (light and heavy gases) blowdowns were compared with experimental data and the discrepancies with the initial discharge rates were found to be within ca. 20% error band
3. For vessel blowdowns with very high initial discharge rates, FRICRUP predictions were significantly lower than the measured data

Figure 2.20 presents comparison between FRICRUP predictions and measured data. For better demonstration, the data was presented in logarithmic scale. As it may be observed, majority of the data rests within the 20% error band.

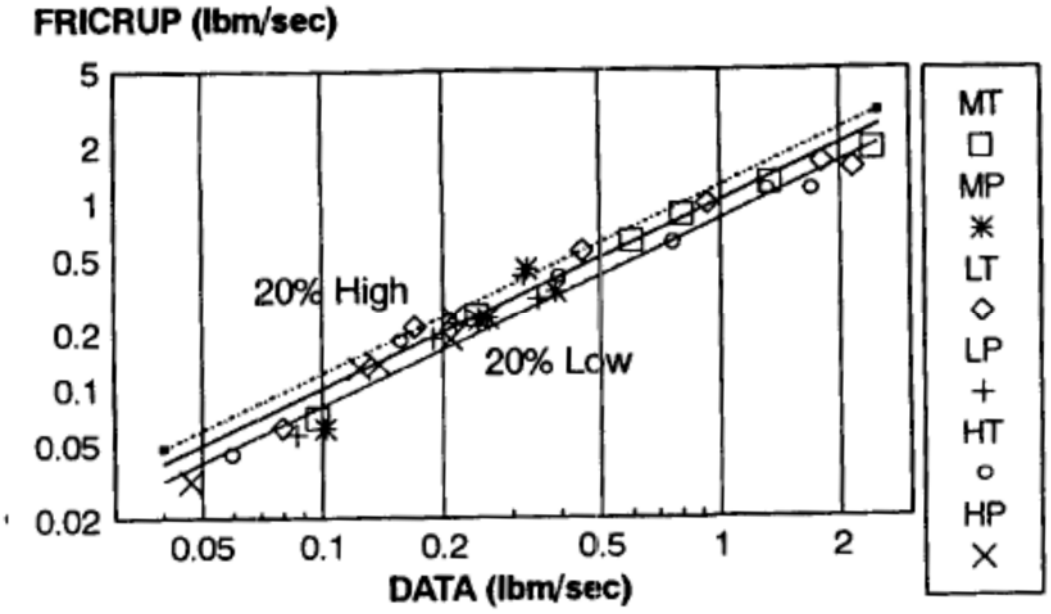

Figure 2.20: Comparison of measured data and FRICRUP predictions for initial mass release rate (Norris and Puls, 1994).

MT and MP refer to methane tests for vessel and pipeline respectively

LT and LP refer to light gas tests for vessel and pipeline respectively

HT and HP refer to heavy gas tests for vessel and pipeline respectively

There is no information publicly available for FRICRUP computational run-time. However, given that the FRICRUP is an analytical model, the associated computational run-time is expected to be negligible.

2.6 SLURP (Cleaver et al., 2003; Cumber, 2007)

SLURP is a model for predicting outflow from pipelines transporting compressed volatile liquids. It was first developed by Morrow (1982) and further extended by Cleaver et al. (2003) in terms of calculation of the thermodynamic properties together with minor corrections to the mathematical basis.

The model is solely developed to handle compressed volatile liquids. Accordingly, it is assumed that upon rupture the pipeline pressure at the rupture plane decreases rapidly to saturation pressure resulting in liquid flash to a two-phase state creating a moving boundary between the two-phase and liquid regions which propagates towards the high pressure end. Figure 2.21 is a schematic representation of the moving boundary between the two-phase region and liquid region following FBR of pipeline containing compressed volatile liquids.

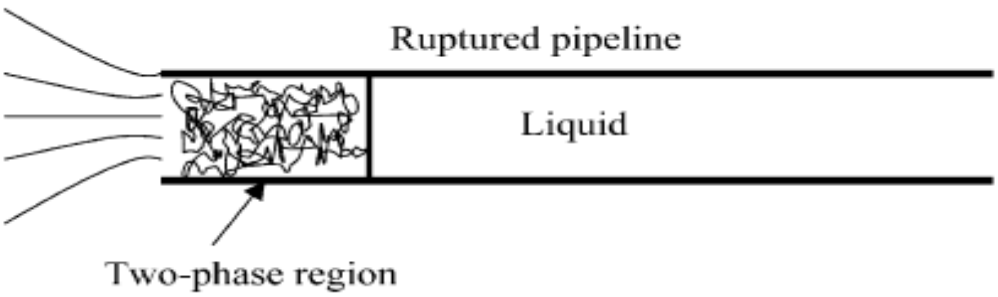

Figure 2.21: Represents the moving boundary (Cleaver et al., 2003).

SLURP comprises three sub-models:

1- A critical two-phase discharge flow model to calculate the choked pressure at the pipe exit considering velocity slip model

2- A relationship for the pressure gradient in the two-phase section of the pipe

3- A model for predicting voidage within the pipe

The following assumptions were made by the authors:

- The flow of fluid inside the pipe follows an isenthalpic process
- Immediately upon rupture, the pressure at rupture is equal to the saturation pressure
- The specific volume of the liquid in the two-phase region remains constant
- The pipe is infinitely long such that outflow from each end is unaffected by the other
- Choke pressure always exceeds the atmospheric pressure

The physical properties of the inventories such as saturation temperature, specific gas volume, specific liquid volume and heat of vaporization were estimated using correlations derived as functions of the saturation pressure in the form of polynomial.

Curve fitting coefficients were determined by generating physical properties of interest on the saturation line using the Peng-Robinson EoS (Peng and Robinson, 1976). For liquid phase, the COSTALD method was used for the phase density prediction (Cleaver et al., 2003).

Cleaver et al. (2003) validated their model by comparing the model predictions against the measured mass release rate and measured pipe inventories obtained from the Isle of Grain LPG pipeline depressurisation tests (Tam and Cowley, 1988). The authors verified SLURP outflow prediction by comparison against PROFES (Hyprotech, 2003) prediction which is a numerically based two-phase pipeline flow

model. Table 2.1 summarises the Isle of Grain experimental test conditions used in the validation.

The Isle of Grain tests T61, T63 and T65 were used consisting of a pipe with 51 mm i.d and l00 m long containing mainly LPG (assumed to be 95 mole% propane and 5 mole% n-butane). Validation against T65 FBR test is only presented in this study for brevity.

Table 2.1: Experimental conditions used in the Isle of Grain experiments (Cleaver et al., 2003).

Test	Initial Pressure (Bara)	Initial Temperature (^oC)	Orifice Diameter (mm)	Orifice Shape
T61	21.2	Unknown	51	Circular
T63	22.5	18.4	35	Circular
T65	11.6	13.8	51	Circular

Figure 2.22 present the variation of pipe inventory against depressurisation time for T65 test. As it may be observed, SLURP performs poorly towards the end of the depressurisation showing marked disagreement with the measured data.

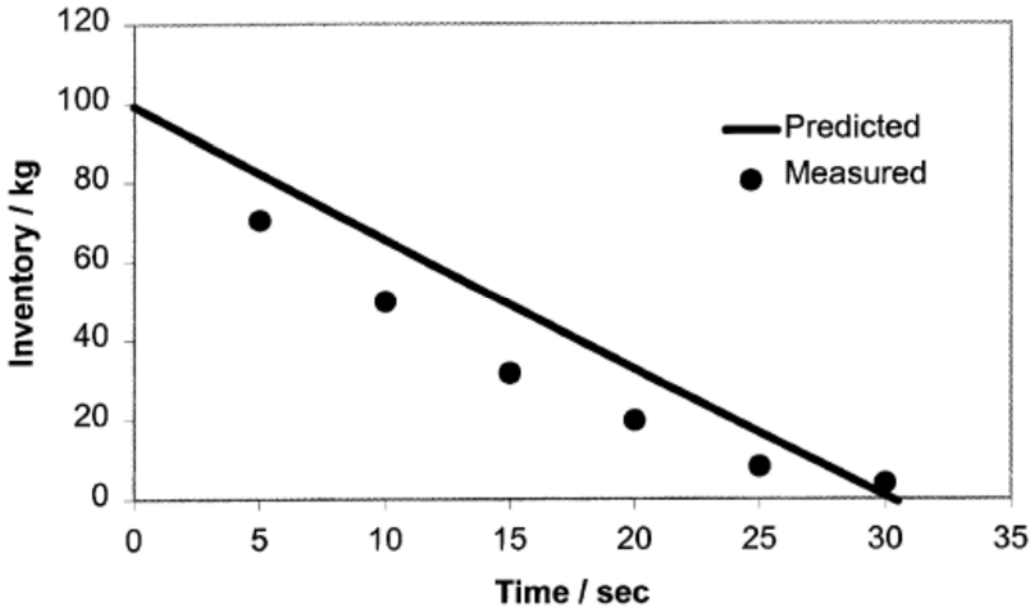

Figure 2.22: Comparison between SLURP predictions and measured variation of pipeline inventory with time for test T65 (Cleaver et al., 2003).

In a later publication, Cumber (2007) improved the efficacy of SLURP by incorporating the heat transfer from the pipe wall to the flowing fluid and investigating the effect of other slip models on the model's performance.

Cumber (2007) verified these improvements through comparison against number of LPG outflow simulations obtained using PROFES for which no validation against experimental data is available in the open literature.

2.7 Webber et al. (1999)

Webber et al. (1999) developed a mathematical model for a pipeline conveying compressed volatile liquids following an accidental breach. The model is in principle similar to SLURP (Cleaver et al., 2003) and yet differs in some aspects. For example,

the model includes heat transfer from the pipe wall to the fluid. The model is also particularly developed for pipeline transporting compressed volatile liquids such as LPG and ethylene.

The authors presented a very much simplistic but reasonable thermodynamic model applicable to single component inventories. The model assumptions are as follows:

- Liquid specific volume is constant
- Liquid specific enthalpy follows the ideal gas law (i.e liquid specific heat capacity is constant)
- Vapour pressure is obtained using Clausius-Clapeyron equation

The model is based on HEM flow assumption and quasi-steady fluid flow. A constant Fanning Friction factor of 0.0029 was used for simulation.

Webber et al. (1999) claimed that, in general, the following four successive regimes are expected to occur following an accidental breach in a pipeline containing volatile liquids:

1. **Rapid Depressurisation**; immediately after the failure, the pressure in the pipe follows a rapid decrease which is governed by the speed of sound in the liquid (or supercritical fluid). Hence the authors assumed that the expansion in this flow regime to end very rapidly resulting in saturated liquid. During this regime the loss of fluid from the pipe is small
2. **Flash Front Propagation**; following regime 1, the liquid which is effectively at rest, starts to vaporise forming an interface (b) between zone 1 (saturated liquid) and zone 2 (two-phase). Figure 2.23 presents the state of the inventory

in the pipe during regime 2. The pressure at open end (e) starts to drop to the value p_e at which the maximum discharge rate is achieved

3. **Further Two-phase Flow**; following regime 2, once the flash front interface has reached the closed end, the upstream pressure starts to drop resulting in a pressure gradient which drives flow out of the pipe. Figure 2.24 presents the state of the flow in the pipe during regime 3
4. **Unpressurised Flow**; at the end of regime 3, almost the entire inventory within the pipe has been forced out and discharge rate during this regime is negligible

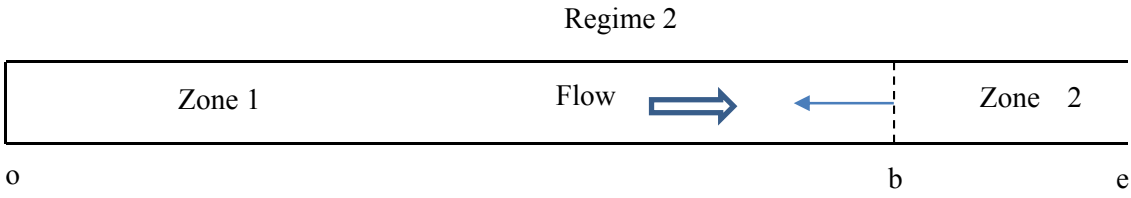

Figure 2.23: Schematic representation of the regime 2 (Webber et al., 1999).

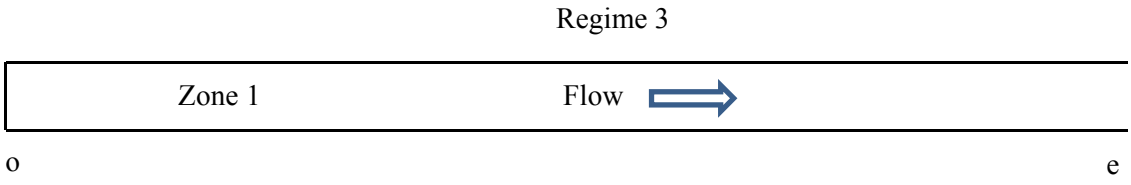

Figure 2.24: Schematic representation of the regime 3 (Webber et al., 1999).

Webber et al (1999) neglected the discharge rate during regimes 1 and 4 and developed a simplistic model that both dynamically and thermo-dynamically describes regimes 2 and 3. The novelty of the Webber et al. (1999) model lies in approximation of the momentum equation whereby it is approximated using the profile functions based on earlier work of Fannelop and Ryhming (1982).

In their isothermal flow case studies of gas pipelines, Fannelop and Ryhming (1982), ignored the inertia term in the momentum equations claiming that for sufficiently long pipelines, friction term governs the flow. Based on this, the authors integrated the momentum equation using various spatial profiles of pressure and flow rate which satisfied the boundary conditions. In order to verify the validity of these profiles, an integral method was developed and the solutions were compared with the corresponding numerical solution of Partial Differential Equations (PDE) governing the flow. The accuracy of the results was claimed to be adequate for engineering purposes (Fannelop and Ryhming, 1981).

For approximation of the energy equation, based on the analogy to the gas pipelines, Webber et al. (1999) assumed a constant stagnation enthalpy.

Webber et al. (1999) validated their model against the Isle of Grain P42 test. Figures 2.26 and 27 show comparison of the measured pressure and temperature at both open and closed end of the pipe against model predictions for Isle of Grain P42 test.

As it may be observed from the figures 2.25-26, the model performs better when heat transfer from pipe wall to fluid is considered as opposed to isothermal model. The model predictions are also in good accord with measured pressure and temperature at the closed end of the pipe whilst at open end of the pipe there are marked differences between predicted and measured data. Webber et al.'s (1999) model consistently under-predicts the open end pressures and temperatures. The authors attributed the differences to the HEM assumption.

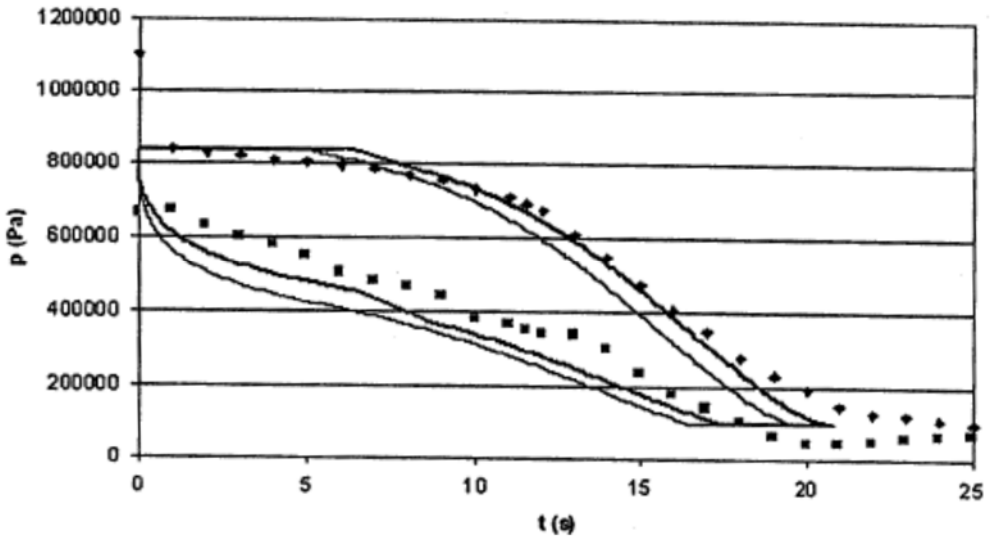

Figure 2.25: Comparison of the model prediction and measured pressure against time at open end (marked with squares) and closed end (marked with diamond) of the Isle of Grain trial P42 LPG test (Webber et al., 1999).

Thick Line: Model prediction with heat transfer

Thin Line: Model prediction without heat transfer

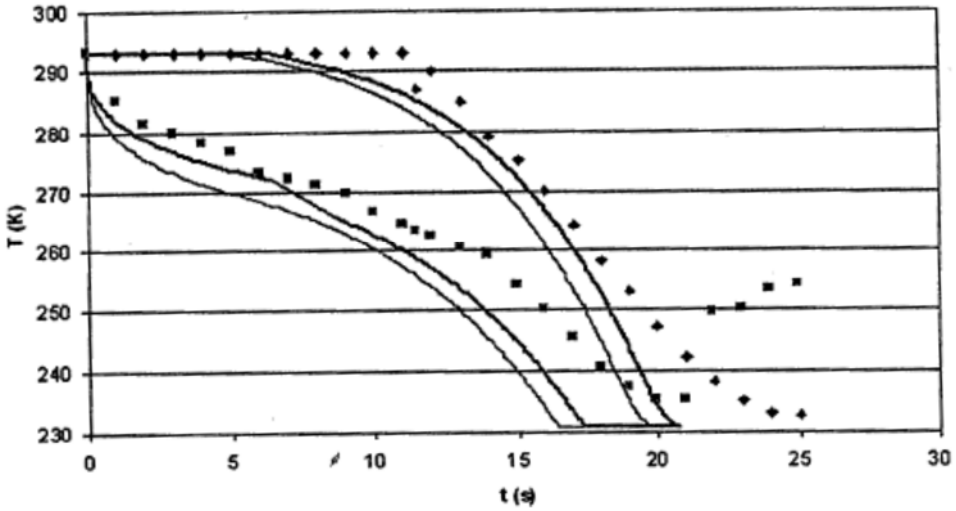

Figure 2.26: Comparison of the model prediction and measured temperature against time at open end (marked with squares) and closed end (marked with diamond) of the Isle of Grain trial P42 LPG test (Webber et al., 1999).

Thick Line: Model prediction with heat transfer

Thin Line: Model prediction without heat transfer

The computational run-time of Webber et al.'s (1999) model is expected to be relatively small, although such data has not been reported by authors.

2.8 Concluding Remarks

A number of models with various degree of sophistication were presented for simulating outflow following failure of pressurised pipeline. Some of which were based on numerical solution of the conservation equations whilst others are relying on simplistic approach both in terms of fluid dynamics and thermodynamics.

Nevertheless, simulation of the complete blowdown of long pipelines (>100 km) requires significant computational resource which makes the use of numerical models impracticable when design and safety assessment of pipelines are concerned. Hence, ways of further reduction of the computational run-time need to be investigated. Given that such models serve as a tool for safety engineers to carry out the consequence analysis, substantial progress has been made to improve the accuracy as well as reducing the computational run-time. However, considering the models reported in the open literature, there is still a significant scope available for further improvement of pipeline failure models.

For instance, the HEM based models of Chen et al. (1995a, b) and Atti (2006) are the most robust with the latter performing best in relation to accuracy and computational run-time However, computational run-time associated to failure simulation of long pipelines are is still a major impracticality particularly when these simulations are carried out for various possible scenarios common to consequence analysis. These may include different operating conditions, failure location and other scenarios. Hence, further reduction of the computational run-time by way of efficient modelling and computation needs to be explored.

Based on the above review, considering the heat transfer between the fluid and pipe wall may improve accuracy of the simulated data. This is particularly due to the energy that is stored within the pipe wall itself which is readily available.

Based on the experimental study presented by Norris and Puls (1993) an interesting similarity between the vessel and pipe puncture type failures was observed. That is, for smaller size apertures, the blowdown behaviour of vessel becomes similar to that observed during blowdown of pipe. This in turn poses the interesting question that

when and under what conditions the pipe can be approximated as vessel discharging through an aperture.

Chapter 3: Fundamental Theory for Modelling Transient Flow in Pipeline

3.1 Introduction

For development of a mathematically robust and accurate pipeline outflow model, the followings should be accounted for:

- The underlying theoretical foundation of transient flow in a pipe which involves derivation of the governing conservation equations. As a result, a detailed model must contain equations of mass, momentum and energy conservation equations for the constituent phases
- An appropriate Equation of State (EoS) order to determine the thermo-physical behaviour of the mixture
- The appropriate boundary conditions and hydro-dynamic relations such as frictional effects and dissipative fluid/wall interactions for analysis of transient energy transport across the pipe

For the case of fluid flow in the pipe, the Navier-Stokes equations provide the most complete formulation. The solution of the resulting complex system of equations is numerically based and demands significant computational resources. Accordingly, depending upon the characteristics of the flow, simplifying assumptions may be applied (see section 3.23.2) and some terms may be safely removed from the governing equations. Considering such simplifying assumptions, the resulting system of equations may be linear, quasi-linear or non-linear, parabolic or hyperbolic in nature. Accordingly, the appropriate numerical resolution should be selected.

In what follows, the main model assumptions and the mathematical formulation of the transient flow following pipeline failure used in this work are presented.

3.2 Model Assumptions

The main simplifying assumptions made in development of the transient flow following pipeline failure are:

- Isothermal steady state flow exists prior to failure

- The flow in the pipeline is mainly one-dimensional along the pipeline's axis. However, for the case of puncture along the length of the pipe, the rate of change of flow variables are resolved in the normal and axial directions in the proximity of the puncture
- The flow is based on Homogenous Equilibrium Model (HEM) whereby it is assumed that all the constituent phases are travelling at the same velocity and that they are simultaneously at thermal and phase equilibrium. As such, one set of mass, momentum and energy conservation equations is applied to the constituent phases
- Pipeline is assumed to be firmly supported and its elasticity is neglected
- All puncture geometries are represented with equivalent orifice diameter

3.3 Formulation of the Governing Conservation Equations

The total derivative of density with respect to time (derived based on conservation of mass within finite element of the pipe) is represented in terms of fluid pressure and enthalpy resulting in a system of conservation equations with Pressure (P), Enthalpy (H) and Velocity (U) being the primitive variables (PHU). As presented in the preceding chapter, Oke (2004) demonstrated that this reformulation provides better accuracy with considerable reduction in computational run-time. Hence the same formulation is used in this work as the basis of the underlying theory for transient flow. The conforming mass, momentum and energy conservations are respectively given as (Oke, 2004):

$$(\rho T + \varphi)\left(\frac{\partial P}{\partial t} + u\frac{\partial P}{\partial x}\right) - \rho\varphi\left(\frac{\partial h}{\partial t} + u\frac{\partial h}{\partial x}\right) + \rho^2 a^2 T\frac{\partial u}{\partial x} = 0 \qquad (3.1)$$

$$\rho\left(\frac{\partial u}{\partial t} + u\frac{\partial u}{\partial x}\right) + \frac{\partial P}{\partial x} = \beta_x + \rho g\sin(\theta) \qquad (3.2)$$

$$\rho\left(\frac{\partial h}{\partial t} + u\frac{\partial h}{\partial x}\right) - \left(\frac{\partial P}{\partial t} + u\frac{\partial P}{\partial x}\right) = Q_h + u\beta_x \qquad (3.3)$$

Where,

P = fluid pressure

h = fluid enthalpy

u = fluid velocity

ρ = fluid density

T = fluid temperature

a = fluid speed of sound

φ = isochoric thermodynamic function of the homogeneous fluid with respect to time, t and distance, *x*

g = acceleration due to gravity

θ = pipeline angle of inclination

Q_h= the heat transferred to the fluid through the pipe wall

β_x = pipeline wall frictional force

Isochoric process, also known as constant-volume process, is a thermodynamic process during which the volume of the closed system undergoing such a process remains constant. The speed of sound and isochoric thermodynamic function for real multi-component single phase homogeneous fluids are respectively defined as (Walas ,1985):

$$a^2 = \left(\frac{\partial P}{\partial \rho}\right)_s \tag{3. 4}$$

$$\varphi = \left(\frac{\partial P}{\partial s}\right)_\rho \tag{3. 5}$$

Where, subscripts *s* and ρ respectively denote the constant specific entropy and density.

3.4 Hydrodynamic and Thermodynamic Relations for Homogeneous Mixtures

3.4.1 Evaluation of Single and Two-phase Speed of Sound

The speed of sound for single phase homogeneous mixtures can be derived analytically as given by Picard and Bishnoi (1987):

$$a^2 = \frac{\gamma}{k\rho} \tag{3. 6}$$

Where, γ and *k* are respectively the ratio of specific heat and isothermal coefficient of volumetric expansion given by Walas (1985):

$$\gamma = \frac{C_p}{C_v} \tag{3. 7}$$

$$k = -\rho \left(\frac{\partial V}{\partial P}\right)_T \tag{3. 8}$$

$\left(\frac{\partial V}{\partial P}\right)_T$ can be obtained directly from differentiation of the EoS (see section 3.5). Nevertheless, for two-phase mixtures, determination of the γ and C_p turn into a complex problem and the speed of sound must therefore be evaluated numerically as given by (Mahgerefteh, 2000):

$$a^2 = \left(\frac{\Delta P}{\left(\rho(T,P) - \rho(T^*, P - \Delta P)\right)}\right)_s \tag{3. 9}$$

Where, ΔP (taken as 1×10^{-6} atm) and T^* represent the infinitesimal change in fluid pressure and the corresponding temperature obtained from the pressure-entropy flash calculation at the decremented fluid pressure.

3.4.2 Evaluation of the Isochoric Thermodynamic Function

The isochoric thermodynamic function, φ for real multi-component single phase homogeneous fluids is defined as (Walas, 1985):

$$\varphi = \left(\frac{\partial P}{\partial S}\right)_{\rho} = \frac{\rho \xi T a^2}{C_p} \tag{3. 10}$$

$$\xi = \frac{1}{V}\left(\frac{\partial V}{\partial T}\right)_{P} \tag{3. 11}$$

Where, ξ is the isobaric coefficient of volumetric expansion.

Analogous to the speed of sound calculation, the isochoric thermodynamic function for two-phase mixture becomes complex and therefore should be determined numerically.

For the case of the two-phase mixtures, using Maxwell's thermodynamic relations, equation (3.5) can be represented as (Walas, 1985):

$$\left(\frac{\partial P}{\partial S}\right)_{\rho} = \rho^2 \left(\frac{\partial T}{\partial \rho}\right)_{S} \tag{3. 12}$$

The same numerical solution algorithm adopted in section 3.4.1 speed of sound can be used for evaluation of the isochoric thermodynamic function.

3.4.3 Fanning Friction Factor

Solution of the momentum equation requires the pipe wall frictional forces to be determined. Accordingly, the fanning friction factor, f_w, must be calculated for the various flow regimes namely laminar, transitional and turbulent.

For laminar flows, f_w is calculated using the following equation (Rohsenow et al. 1998):

$$f_w = \frac{16}{Re} \tag{3. 13}$$

For the case of transitional and turbulent flows in rough pipes, f_w is determined from Chen (1979):

$$\frac{1}{\sqrt{\mathrm{f_w}}} = 3.48 - 1.7372 \ln\left(\frac{\varepsilon}{r_{in}} - \frac{16.2446}{Re} lnA\right) \tag{3. 14}$$

Where,

$$A = \frac{\left(\frac{\epsilon}{r_{in}}\right)^{1.0198}}{6.0983} + \left(\frac{7.149}{Re}\right)^{0.8981} \tag{3. 15}$$

and ϵ, r_{in} and Re respectively are pipe roughness, pipe inside radius and Reynolds' number. In case of a smooth pipeline, the fanning friction factor for turbulent flow is calculated using the recommendation of Rohsenow et al. (1998):

$$\frac{1}{\sqrt{f_w}} = 1.7372 ln \frac{Re}{(1.694Re - 3.8215)} \tag{3. 16}$$

As reported by Rohsenow et al. (1998), the predictions of the above correlation for turbulent flows when compared with the experimental data are within the 2% error band.

3.4.4 Two-phase Mixture Density (Atti, 2006)

In line with the HEM assumption, for two-phase flow, the pseudo mixture density is calculated from:

$$\rho = \frac{\rho_l \rho_g}{(\rho_g(1-x)+\rho_l x)} \quad (3.17)$$

$$\rho_l = \frac{PM_l}{Z_l RT} \quad (3.18)$$

$$\rho_g = \frac{PM_g}{Z_g RT} \quad (3.19)$$

Where,

ρ=fluid density

x=fluid quality (i.e liquid mass fraction)

z=fluid compressibility factor

R=universal gas constant

M= Molecular weight

Subscripts g and l respectively denote gas and liquid phases.

3.4.5 Thermal Conductivity and Viscosity Calculations

The vapour thermal conductivity and viscosity are required in order to determine the Nusselt, Reynolds and Prandtl numbers which are in turn used for the calculation of pipe wall frictional forces and the heat transfer through the pipe. Throughout this study, for non-polar gases, the method of Ely and Hanley (1981, 1983) is used to

calculate these properties. For brevity and due to complexity of the methods, no correlation is presented. However, the accuracy of these methods for determining the vapour thermal conductivity and viscosity is claimed (Assael et al., 1996) to be reasonable for a large number of non-polar gases over wide-ranging conditions.

The semi-empirical scheme proposed by Assael et al. (1996) is adopted for determining the thermal conductivity and viscosity of liquid mixtures containing alkanes. Over 2000 measurements of viscosity and thermal conductivity were carried out by the authors for temperatures ranging from 7 ºC to 127 ºC and pressures from saturation up to 990 atm. The uncertainty of the scheme for the range tested is claimed to be less than 5 % (Assael et al., 1996).

In the case of a two-phase mixture, the correlations proposed by Design Institute for Physical Properties (DIPPR) as reported by Daubert and Danner, (1990) are employed.

3.5 Application of the Cubic Equation of State

In order to obtain the thermodynamic properties and phase equilibrium data, the Peng-Robinson EoS (PR EoS) (Peng and Robinson, 1976) is used throughout this study. PR EoS is widely applied to high pressure hydrocarbon mixtures (Walas, 1985).

Peng-Robinson (1976) proposed the following equation for a pure component:

$$P = \frac{RT}{V - b_V} - \frac{a_V(T)}{V^2 + 2b_V - (b_V)^2} \tag{3. 20}$$

$$a_V(T) = a(T_C) \times \alpha(T_r, \omega) \tag{3. 21}$$

Where,

ω = acentric factor

T_r = reduced temperature

α = dimensionless function of T_r and ω which equals unity at critical temperature

At the critical point, parameters *a* and *b* are expressed in terms of the critical properties:

$$a(T_C) = 0.45724 \frac{R^2 T_C^2}{P_C^2} \quad (3.\ 22)$$

$$b(T_C) = 0.0778 \frac{RT_C}{P_C} \quad (3.\ 23)$$

Where,

T_c = critical temperature of the component

P_c = critical pressure of the component

For mixtures, parameters b and a are defined as:

$$b = \sum_i^N x_i b_i \quad (3.\ 24)$$

$$a = \sum_i^N \sum_j^N (1 - K_{ij}) \sqrt{(a_i \alpha_i)(a_j \alpha_j)} \quad (3.\ 25)$$

Where,

a_i and b_i = constants determined for each component

x_i = the component mole fraction

K_{ij} = empirically determined binary interaction coefficient

α_i and α_j = the alpha function for each component

Twu et al. (1995) developed a generalized function of the attractive pressure term in equation (3. **21)**, known as alpha function, in order to improve the prediction of the PREoS. This function is only dependant of temperature and acentric factor.

The range of applicability of the generalized alpha function is from the triple point to the critical point (Twu et. al., 1995). The absolute average error in the prediction of the hydrocarbon vapour pressures calculated by original PREoS (1976) when compared with experimental data was 12.08 %. Utilising the generalised alpha function, the absolute average error was reduced to 3.28 % (Twu et. al., 1995). This indicates the improvement in accuracy of the alpha function in predicting the vapour pressure.

3.6 Phase Stability and Flash Calculations

One of the main problems associated in the flash calculations, for example at a given temperature and pressure, is that the number of equilibrium phases are not known in advance. The conventional approach, which requires high computational resources, is to assume the number of phases present at equilibrium and then estimate initial values for the equilibrium factors. The material balance is solved and the new phase compositions provide new values of the equilibrium factors. This procedure is continued until convergence is achieved (King, 1980).

The stability analysis method, which is based on the tangent plane criterion proposed by Michelsen (1982a,b), is a preliminary step in isothermal flash calculations in order to determine the thermodynamic state of a fluid mixture at given temperature and pressure. The equilibrium mixture is said to be stable at a known temperature and pressure if and only if the total Gibbs free energy is at its global minimum. Therefore equilibrium condition between the phases can be formulated as a Gibbs free energy minimization problem (Michelsen, 1982a, b, Michelsen, 1987).

Stability analysis is suggested as a preliminary step in isothermal flash calculations in order to determine thermodynamic state of a fluid mixture at given temperature and pressure. The advantage of such scheme is when the lack of stability (i.e. two-phase) is verified by converging to a solution, the converged K_i (equilibrium factors for component i) values provide appropriate initial estimates for subsequent flash calculations. The above procedure is also computationally more efficient as opposed to the conventional approach (i.e Rachford-Rice procedure).

3.7 Fluid/Wall Heat Transfer (Atti, 2006)

Following pipeline failure, the sudden drop in pressure and temperature may lead to a phase change resulting in a significant variation in the heat transfer coefficient. This will contravene the validity of the assumption of using a constant heat transfer coefficient during the depressurisation process.

In such a case, in order to properly model the heat transfer occurring at the pipe wall, a transient energy balance across the fluid-wall-ambient surfaces based on a lumped body approach is employed (see Atti, 2006). In this approach the wall temperature is updated after a given time step, therefore the heat input to the fluid in the next time interval can be estimated. Figure 3.1 shows a schematic representation of the heat transfer across the cross-section of a pipe and the parameters used in the formulation.

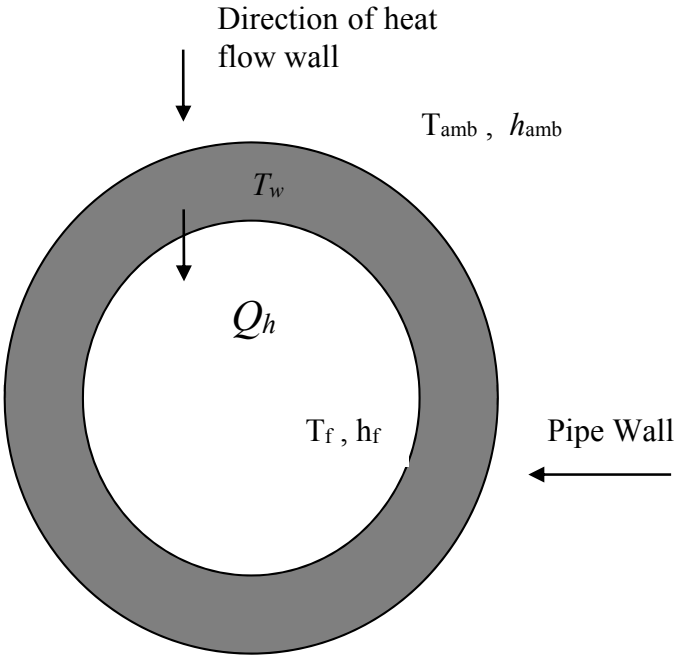

Figure 3.1: Schematic representation of the heat transfer across the cross-section of a pipe. T_{amb}, h_{amb} and T_w respectively represent the ambient temperature, heat transfer coefficient of the ambient, and wall temperature. T_f, h_f and Q_h respectively represent the fluid's temperature, heat transfer coefficient, and the quantity of heat transferred to it (Atti, 2006).

In the lumped body approach the following simplifying assumptions are employed:

- No temperature stratification across the pipeline wall
- Wall density ρ_w, specific heat capacity, C_{pw} and thermal conductivity, κ_w remain constant
- In a given time step, the fluid and ambient heat transfer coefficients remain constant
- No longitudinal heat conduction (i.e. heat transfer occurs predominantly across the pipeline wall)

Considering the above assumptions the transient energy balance across the pipeline can be re-written as (Myers, 1971):

$$h_{amb}^{i-1}A_{amb}(T_{amb}-T_w)-h_f^{i-1}A_{in}\left(T_w-T_f\right)=\rho_w C_{pw}V_w\frac{dT_w}{dt} \quad (3.\ 26)$$

Where,

V_w = the volume per unit length of the pipeline

A_{out} and A_{in} = the outside and inside surface areas per unit length along the walls of the pipeline respectively

T_w will get updated at each time step and used in Newton's cooling law to calculate the rate of heat transferred to the fluid (Q_h) in a given time step:

$$Q_h=\frac{4}{D_{in}}h_f^{i-1}(T_w-T_f) \quad (3.\ 27)$$

3.8 The Steady State Isothermal Flow Model (Oke, 2004)

Based on the main simplifying assumptions listed in section 3.2, the isothermal steady state solution is required prior to failure. The isothermal steady state model is based on one-dimensional continuity and momentum equations as given in section 3.3.

The steady state condition requires all fluid properties to be time invariant. Therefore, the one-dimensional mass continuity can be written as:

$$u\frac{d\rho}{dx}+\rho\frac{du}{dx}=0 \quad (3.\ 28)$$

Separation of variables and integration yields:

$$\rho_i u_i=\rho_{i-1}u_{i-1} \quad (3.\ 29)$$

Where the subscripts *i* and *i-1* represent the current and penultimate grid point respectively based on discretising the length of the pipe into set number of grids. Equation (3. **28)** is valid for steady state flow in a constant diameter pipe.

Similarly, by setting the time derivatives to zero in equation (3. **2)**, the steady state one-dimensional momentum equation can be written as:

$$\rho u \frac{\partial u}{\partial x} + \frac{\partial P}{\partial x} = \beta_x + \rho g \sin(\theta) \tag{3. 30}$$

The frictional force term (β_x) is given by:

$$\beta_x = \frac{2\rho u|u| f_w}{D} \tag{3. 31}$$

Where, D is the pipe diameter.

Substituting equation (3.31) in to (3.30) and rearranging yields (Oke, 2004):

$$\rho dP - \left(\rho u^2 \frac{dP}{\rho}\right) = -\left(\frac{2f_w(\rho u)^2}{D} + \rho^2 g sin(\theta)\right) dx \tag{3. 32}$$

Integration of equation (3. **32)** yields to the following expression which is used in the calculation of the pressure drop under isothermal steady state condition prior to pipe failure (Oke, 2004):

$$\frac{1}{2}\left[\frac{\rho}{(K_2+\rho^2 K_3)_{P_i}} + \frac{\rho}{(K_2+\rho^2 K_3)_{P_{i-1}}}\right] + \frac{K_1}{2K_2}\left[2ln\left(\frac{\rho_i}{\rho_{i-1}}\right) ln\left(\frac{(K_2+\rho_i^2 K_3)}{(K_2+\rho_{i-1}^2 K_3)}\right)\right] = x_i - x_{i-1} \tag{3. 33}$$

$$K_1 = -(\rho u)^2 \tag{3. 34}$$

$$K_2 = -\frac{2f_w(\rho u)^2}{D} \tag{3. 35}$$

$$K_3 = -gsin(\theta) \tag{3. 36}$$

Given the fluid/flow condition at pipeline inlet (e.g. fluid pressure, temperature and velocity), the following algorithm is used for calculating the pressure drop along the pipe for isothermal steady state flow (Oke, 2004):

1. The pipeline is discretised into number of grid points separated by a length of $\Delta x = x_i - x_{i-1}$
2. Guess the pressure at the next grid point (i.e. P_i)
3. Using the appropriate EoS, with the pressure and temperature, evaluate the left hand side of equation (3. **33)**
4. The guessed pressure is adopted as the correct pressure if equation (3. **33)** is satisfied and the velocity at the next grid point can be obtained from equation (3. **29)**. Otherwise, go back to step 2 and update the guessed pressure (i.e. P_i)
5. Update fluid properties at this grid point and calculate the pressure drop at the next grid point

3.9 Hyperbolicity of the Governing Conservation Equations

The partial differential equations relating to the conservation of mass, momentum and energy coupled with the PR EoS constitute a system of equations with source terms.

The conservation equations (i.e. equations (3.1) to (3.3)) can be rewritten in the general matrix form:

$$A\frac{\partial F}{\partial t} + B\frac{\partial F}{\partial x} = C \tag{3. 37}$$

Where,

$$F = \begin{pmatrix} P \\ h \\ u \end{pmatrix} \tag{3. 38}$$

$$A = \begin{pmatrix} \rho T + \varphi & -\rho\varphi & 0 \\ 0 & 0 & \rho \\ -1 & \rho & 0 \end{pmatrix} \tag{3. 39}$$

$$B = \begin{pmatrix} (\rho T + \varphi)u & -\rho\varphi u & \rho^2 a^2 T \\ 1 & 0 & \rho u \\ -u & \rho u & 0 \end{pmatrix} \tag{3. 40}$$

$$C = \begin{pmatrix} 0 \\ \Phi \\ \psi \end{pmatrix} \tag{3. 41}$$

$$\Phi = \beta_x + \rho g \sin\theta \tag{3. 42}$$

$$\psi = q_h + u\beta_x \tag{3. 43}$$

Prior to selecting the appropriate numerical technique for the solution of the governing partial differential equations, the knowledge of their mathematical nature is required. In what follows, it is demonstrated that above system of conservation equations are quasi-linear and hyperbolic in nature. The application of an appropriate numerical technique for solution of hyperbolic conservation equations is presented in chapter 4.

A partial differential equation is said to be quasi-linear if all derivatives of the dependent function (i.e. $\frac{\partial F}{\partial t}$ and $\frac{\partial F}{\partial x}$) are linear, while their corresponding coefficients such as density (ρ) and fluid speed of sound (a) are non-linear functions of F (i.e. the primitive variables P, h and u) (Prasad and Ravindran, 1985).

A system of partial differential equations presented in equation (3.37), is said to be hyperbolic if the eigenvalues (λ) satisfying the following equation are real and distinct (Prasad and Ravindran, 1985).

$$det|B - \lambda A| = \begin{pmatrix} (\rho T + \varphi)(u - \lambda) & \rho\varphi(\lambda - u) & \rho^2 a^2 T \\ 1 & 0 & \rho(u - \lambda) \\ (\lambda - u) & \rho(u - \lambda) & 0 \end{pmatrix} = 0 \tag{3. 44}$$

Hence:

$$-(\rho T + \varphi)(u - \lambda)\rho^2(u - \lambda)^2 + \rho^2\varphi(\lambda - u)^2(u - \lambda) + \rho^3 a^2 T(u - \lambda) = 0 \tag{3. 45}$$

Factorising and solving equation (3. **45)** yields to the following real and distinct solutions (Oke, 2004):

$$\lambda_1 = u \tag{3.46}$$

$$\lambda_2 = u - a \tag{3.47}$$

$$\lambda_3 = u + a \tag{3.48}$$

Thus, the system of quasi-linear partial differential equations for mass, momentum and energy conservation are hyperbolic.

3.10 Concluding Remarks

In this chapter the mass, momentum and energy conservation equations for the transient fluid flow in a pipeline following its failure were presented. These were expressed in terms of the dependent variables pressure, enthalpy and velocity. The governing system of conservation equations were shown to be quasi-linear and hyperbolic in nature. Consequently, the method of numerical resolution must be selected appropriately.

The various hydrodynamic and thermodynamic relations for predicting the pertinent fluid properties such as the fluid speed of sound, isochoric thermodynamic function and phase dependent friction factor were presented. For brevity, the work carried out for determination of fluid viscosity and thermal conductivity was only reported.

The calculation procedure for isothermal steady state pressure drop prior to failure was outlined. Finally, the lumped body approach for modelling the fluid phase dependent heat transfer effects were presented.

Chapter 4 : Application of the Method of Characteristics to the Simulation of Puncture/Full Bore Rupture of Pipeline

4.1 Introduction

Understanding compressible flow is of great interest particularly for civilian and military applications. Accordingly, the study of compressible flow which requires the solution differential equations has received special attention and many numerical methods have been developed for this purpose. These include:

1. Finite Difference Method (FDM)
2. Finite Volume Method (FVM)
3. Method Of Characteristics (MOC)

The FDM is the oldest numerical method which is widely applied to Partial Differential Equations (PDE). The method in general involves replacing the derivative terms, at each grid point, by its approximation in terms of the nodal values of the function using Taylor series expansion or polynomial fitting. The substituted finite approximations result in a system of algebraic equations. Due to the numerical diffusion, this numerical method is unsuitable for modelling highly transient flow which is expected following a pipeline failure (Mahgerefteh et al., 2006). As such it is not further discussed in the context of this work. The FVM, as its starting point, requires the integral form of the conservation equations. The solution domain is subdivided into a finite number of control volumes. Unlike FDM whereby the

approximation of the derivative term at the grid point has to be selected, with FVM, one has to select the methods for approximating the surface and volume integrals using suitable quadrature formulae. In recent years, application of the FVM to hyperbolic PDEs has been centre of considerable attentions (see for example Leveque, 2002; Toro, 2009; Brown, 2011). Some of the important advantages are as follows:

- It is the simplest numerical method to understand and to implement
- The method is conservative by construction
- It is a non-iterative numerical technique hence computationally efficient
- Can accommodate any type of grids hence suitable for complex geometry

The MOC on the other hand, is the general mathematical technique particularly suited for solution of quasi-linear hyperbolic PDEs with two independent variables of time and distance. The method involves transformation of the PDEs into ordinary differential equations (referred to as compatibility equations) by means of change of coordinates. This means that these compatibility equations are only valid along the characteristic lines. MOC is particularly suitable for systems with complex boundary conditions, as each node point and boundary conditions are analysed individually at each time step (Denton, 2009).

The primary drawback of the MOC is the Courant stability criterion which governs choice of time steps and the time step-distance interval relationship (Courant et al., 1967; Mahgerefteh et al., 2009). This results in demanding higher computational resources which has somewhat been compensated for with the arrival of fast computers.

In this study, the MOC has been chosen for solution of the conservation equations together with a interpolation scheme to model the transient outflow following pipeline rupture.

In the following, the formulation and implementation of the MOC for the solution of the conservation equations governing single/two-phase homogeneous flow along with the relevant boundary conditions required for modelling transient pipeline outflow are presented.

4.2 Methods of Discretisation

The two methods of discretisation used in MOC are Characteristic Grids (CG) also known as Natural Method of Characteristics (Wylie and Streeter, 1993) and the Method of Specified Time intervals (MST) also known as the Inverse Marching Method (Flatt, 1986).

In the CG method, the intersection of the characteristic lines, originated from points where solution is already known, determine the location of the new solution which is not known in advance. By adopting this method, a free-floating grid construction will be developed in the *x*-*t* plane as shown in Figure 4.1.

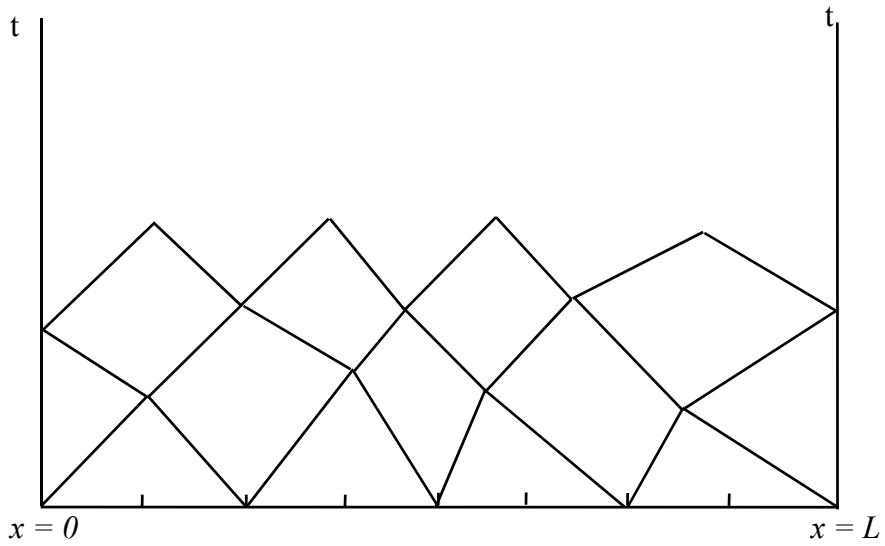

Figure 4.1: The grid construction using Characteristic Grid (CG) method.

In contrast to CG method, with the MST, the location of the new solution in the space and time domain is known in advance and the characteristic lines at each grid point are traced backwards in time to intersect a time line at their previous points as schematically shown in Figure 4.2.

The MST allows control of the time at which input variables are given at boundaries. However using this method requires interpolation in order to locate the intersection of all the three characteristic lines on the previous time line. This in turn results in loss of accuracy. In this respect, the CG method is more accurate than the MST, but it does not allow for introducing the prevailing boundary conditions which is commonly applied in modelling pipeline failures such as pump shut-off and valve closure at specified time and distance along the pipe. For this reason, the MST is adopted throughout this study.

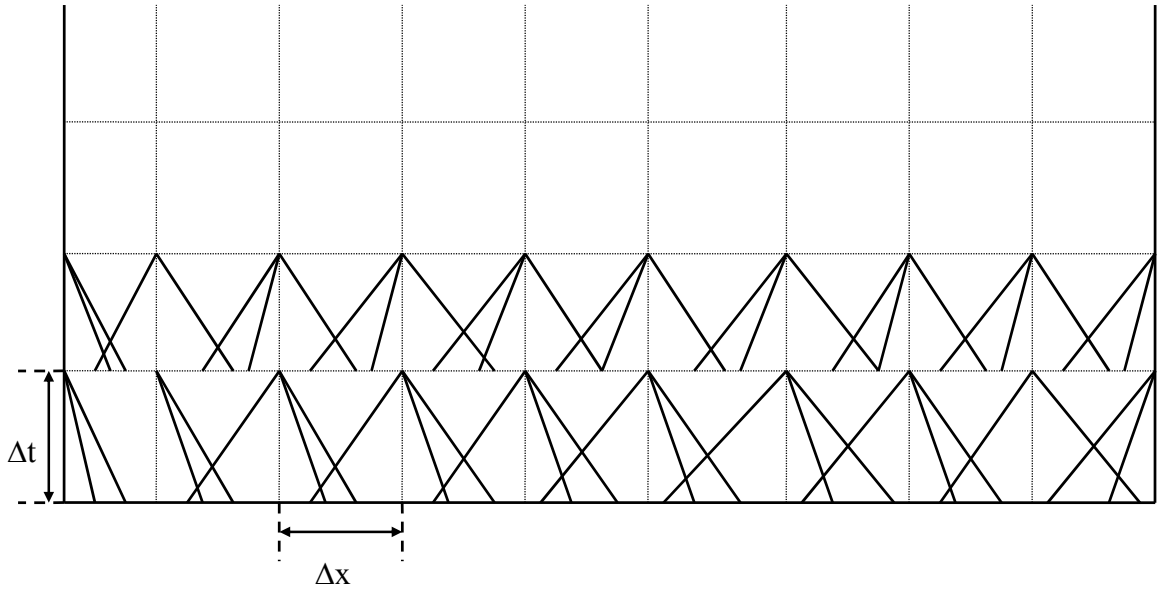

Figure 4.2: The grid construction based on Method of Specified Time (MST).

4.3 Numerical Formulation and Implementation of the MOC

In general, the solution of the conservation equations based on MOC can be summarised into the following two steps:

1. Deriving a system of Ordinary Differential Equations (ODE) by converting the PDEs into compatibility equations
2. Solution of the compatibility equations along the characteristic lines and employing Euler predictor-corrector technique (Zucrow and Hoffman, 1975). The Euler predictor-corrector technique is used to improve the accuracy of the numerical results

Step 1: Conversion of the PDEs to ODEs

The governing conservation equations (i.e. PDEs) presented in chapter 3 for mass momentum and energy conservation equations are repeated here:

$$(\rho T + \varphi)\left(\frac{\partial P}{\partial t} + u\frac{\partial P}{\partial x}\right) - \rho\varphi\left(\frac{\partial h}{\partial t} + u\frac{\partial h}{\partial x}\right) + \rho^2 a^2 T\frac{\partial u}{\partial x} = 0 \quad (3.1)$$

$$\rho\left(\frac{\partial u}{\partial t} + u\frac{\partial u}{\partial x}\right) + \frac{\partial P}{\partial x} = \beta_x + \rho g\sin(\theta) \quad (3.2)$$

$$\rho\left(\frac{\partial h}{\partial t} + u\frac{\partial h}{\partial x}\right) - \left(\frac{\partial P}{\partial t} + u\frac{\partial P}{\partial x}\right) = Q_h + u\beta_x \quad (3.3)$$

The above conservation equations may be replaced by three compatibility equations, which are valid along the respective characteristic lines. The three compatibility equations are given by Zucrow and Hoffman (1975):

Path line compatibility equation:

$$\rho_0 d_0 h - d_0 P = \psi d_0 t \quad (4.1)$$

Valid along the path line characteristic (C_0)

$$\frac{d_0 t}{d_0 x} = \frac{1}{u} \quad (4.2)$$

Positive compatibility equation:

$$d_+P + \rho a d_+u = \left(\frac{\varphi\psi}{\rho T} + a(\beta_x + \rho g \sin(\theta)\right) d_+t \tag{4.3}$$

Valid along the positive characteristic line (Mach line) (C_+):

$$\frac{d_+t}{d_+x} = \frac{1}{u+a} \tag{4.4}$$

Negative compatibility equation:

$$\rho a d_- u - d_- P = \left(a(\beta_x + \rho g \sin(\theta) + \frac{\varphi\psi}{\rho T}\right) d_- t \tag{4.5}$$

Valid along the negative characteristic line (Mach line) (C_-):

$$\frac{d_-t}{d_-x} = \frac{1}{u-a} \tag{4.6}$$

Notations d_+, d_- and d_o represent positive, negative and path compatibility equations and characteristic lines. The path line dictates the rate of flow at any given point along the pipeline whereas the positive and negative characteristic lines (i.e. Mach lines) respectively govern the speed at which expansion and compression waves travel along the length of the pipeline.

Step 2: Solution of the compatibility equations

Figure 4.3 illustrates a schematic representation of path line and Mach lines based on the MST grid construction. The fluid properties pertaining to grid points *i-1, i* and *i+1* are known in advance. This means that the information at the previous time step (either from isothermal steady state solution or the previous time step calculation) is available. Next, the fluid properties at the foot of the characteristics (i.e. points *p*, *o* and *n*) are obtained using linear approximation. Finite difference approximation form of the compatibility equations are employed for solution of the flow variables (*P*, *h*

and u) for the next time step $t_1+\Delta t$ at point j which is the intersection of the characteristic lines.

The numerical stability of the solution based on MOC requires the following time step (Δt)-distance interval (Δx) relationship to be maintained (Courant et al., 1967):

$$\Delta t \leq \frac{\Delta x}{|u+a|_{max}} \tag{4.7}$$

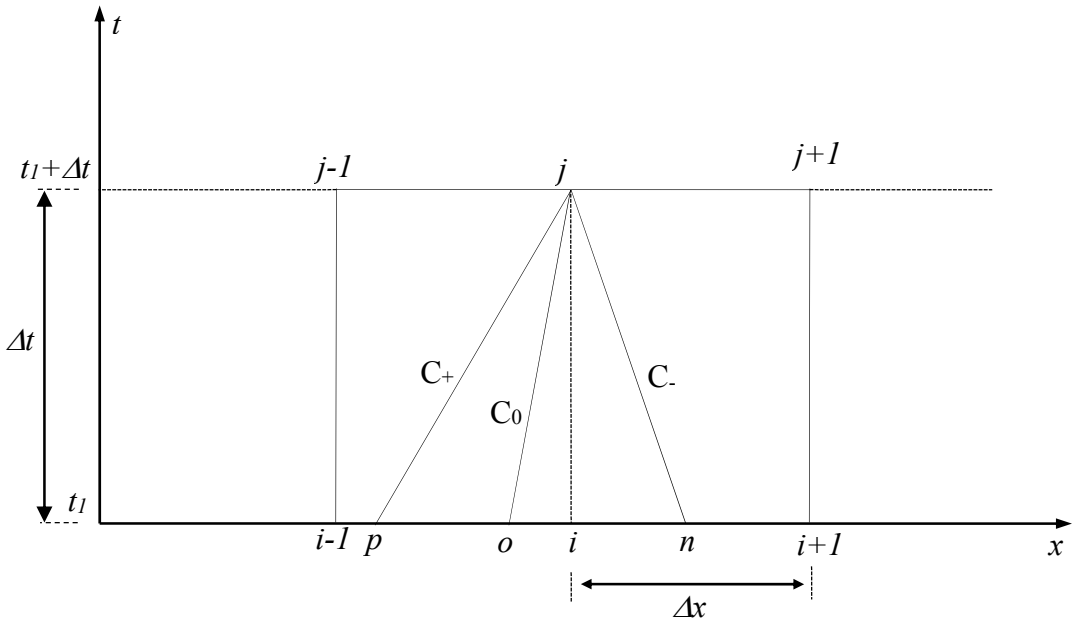

Figure 4.3: Schematic representation of the Path line (C_0) and Mach lines (C_+ and C_-) based on the MST grid construction along the time (t) and distance (x) axes.

4.4 Solution of the Compatibility Equations Based on FDM

Euler predictor-corrector step is employed to resolve the system of ODEs (equations 4.1-4.6). A detailed description of the method is given elsewhere (see for example Zucrow and Hoffman, (1975) hence, a brief account is given in this section stressing the salient points. The method consists of a predictor step (first order approximation), an explicit Euler method used to provide an estimate of the flow variables at the solution point. Next, the corrector step (a second order approximation) is used to improve on the initial approximation of the predictor step.

First Order Approximation: Predictor Step

In predictor step, the compatibility equations (4.1, 4.3 and 4.5) are replaced with their finite difference approximations as (Oke, 2004):

Path line compatibility:

$$\rho_o(h_j - h_o) - (P_j - P_o) = \psi_0(t_j - t_o) \tag{4.8}$$

Positive mach line compatibility:

$$(\rho a)_p(u_j - u_p) - (P_j - P_p) = \left(a(\beta_x + \rho g \sin(\theta) + \frac{\varphi\psi}{\rho T}\right)_p (t_j - t_p) \tag{4.9}$$

Negative mach line compatibility:

$$(\rho a)_n(u_j - u_n) - (P_j - P_n) = \left(a(\beta_x + \rho g \sin(\theta) + \frac{\varphi\psi}{\rho T}\right)_n (t_j - t_o) \tag{4.10}$$

The subscripts in the above equations represent the location in space and time domain as marked in Figure 4.3. When the locations x_p, x_o and x_n are determined

using first order finite difference approximation of equations (4.2), (4.4) and (4.6) the fluid properties are then obtained using linear interpolation between points *i*, *i+1* and *i-1* (Atti, 2006).

Second Order Approximation: Corrector Step

For improvement of the solution accuracy obtained in predictor step, a second order approximation of the compatibility equations are employed as given by Atti (2006):

Path line compatibility:

$$\frac{1}{2}(\rho_0 + \rho_j)(h_j - h_0) - (P_j - P_0) = \frac{1}{2}(\psi_0 + \psi_j)(t_j - t_0) \tag{4.11}$$

Positive mach line compatibility:

$$\frac{1}{2}((\rho a)_p + (\rho a)_j)(u_j - u_p) - (P_j - P_p) = \frac{1}{2}\left(\left(\psi(\beta_x + \rho g \sin(\theta) + \frac{\varphi\psi}{\rho T}\right)_p + \frac{1}{2}\left(\psi + \frac{\varphi\psi}{\rho T}\right)_j\right)(t_j - t_p) \tag{4.12}$$

Negative mach line compatibility:

$$\frac{1}{2}((\rho a)_n + (\rho a)_j)(u_j - u_n) - (P_j - P_n) = \frac{1}{2}\left(\left(\psi(\beta_x + \rho g \sin(\theta) + \frac{\varphi\psi}{\rho T}\right)_n + \frac{1}{2}\left(\psi(\beta_x + \rho g \sin(\theta) + \frac{\varphi\psi}{\rho T}\right)_j\right)(t_j - t_n) \tag{4.13}$$

Similarly, the locations x_p, x_o and x_n are determined using second order finite difference approximation of equations (4.2), (4.4) and (4.6) whereby the corresponding fluid properties at these points are obtained by linearly interpolating between points *i*, *i+1* and *i-1*. This calculation procedure is continued iteratively until the acceptable tolerance (ca. 10^{-5}) is satisfied for all three independent flow parameters.

4.5 Formulation of the Boundary Conditions for Simulating the Pipeline Failure

In this section, the boundary conditions used in simulation of the outflow from pipelines are presented. These boundary conditions are required for closure of the governing flow equations. These are:

- Intact end of pipeline (closed end)
- Full bore rupture or puncture at the pipe end
- Puncture along the pipe length
- Pump at pipe inlet

4.5.1 The Intact End Boundary Condition

The intact end boundary condition defines the inlet/upstream condition whereby only path line and negative mach line are valid. Accordingly, only two compatibility equations are applicable.

Figure 4.4 depicts the schematic presentation of the active characteristics for closed end boundary condition. Given that the velocity is equal to zero at the closed end, accordingly the equation **(4.10)** which is the first order finite difference approximation of the negative compatibility equation may be reduced to:

$$P_j = K_2 + (\rho a u)_n + P_n \tag{4.14}$$

Where K_2 is given by:

$$K_2 = \left(\frac{\varphi\psi}{\rho T} - a(\beta_x + \rho g \sin(\theta)\right)_n \Delta t \tag{4.15}$$

Using the first order finite difference approximation of the path line compatibility (equation **(4.8)**), the upstream enthalpy at solution point *j* may be calculated:

$$h_j = \frac{\psi_0 \Delta t + (P_j - P_0) + \rho_0 h_0}{\rho_0} \tag{4.16}$$

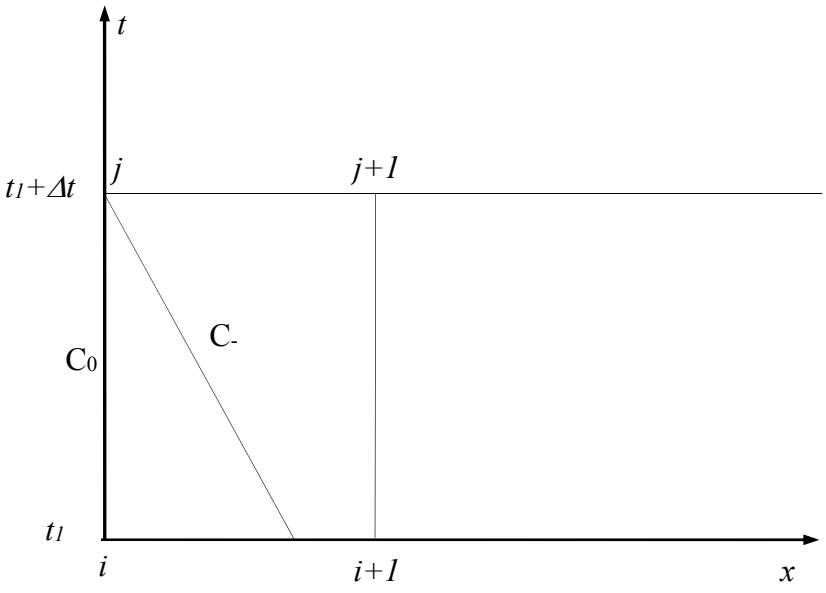

Figure 4.4: Schematic representation of the active characteristics lines at closed inlet point.

Since the initial solution at point, *j* is approximated, the corrector step which is second order finite difference approximation is subsequently utilised (as discussed in section 4.2.3) for obtaining more accurate flow variables at this point.

4.5.2 Full Bore Rupture and Puncture at the Downstream End

When a Full Bore Rupture (FBR) or Puncture occurs at the downstream end of a pressurised pipeline (i.e. low pressure end), depending on the upstream and downstream pressures, the outflow may be either chocked or unchocked.

For the case of choked flow, the fluid is assumed to follow an isentropic expansion, discharging at the choked pressure and the flow exiting the release plane becomes independent of the downstream pressure (i.e the disturbances downstream of the release plane cannot propagate inside the pipe). Once the discharge pressure has reached the ambient pressure this flow is said to be unchoked and discharge of the remaining inventory is driven only by momentum of the fluid.

For a single phase fluid, as defined in equation (3.4), the flow at the release plane is assumed to follow an isentropic trajectory with the fluid traveling at the speed of sound. For choked two-phase flow, equation (3.4) must be solved numerically as shown in section 3.4.1.

At the release plane, only path and positive characteristic lines are available within the computational domain. A simple analytical relationship is therefore required to describe the expansion process and determine the required properties at the release plane. Accordingly, an imaginary cell or a ‘ghost’ cell is considered outside of the physical pipe as depicted in Figure 4.5 within which the negative characteristic can be assumingly included in the computational domain. As it may be observed in

Figure 4.5, the ghost cell is a fictitious node (*i+1*) positioned same as node *i* permitting the solution along the C- line.

With the introduction of the C-, the solution at point *j* can be obtained using the same calculation procedure as for the interior points described in section 4.4.

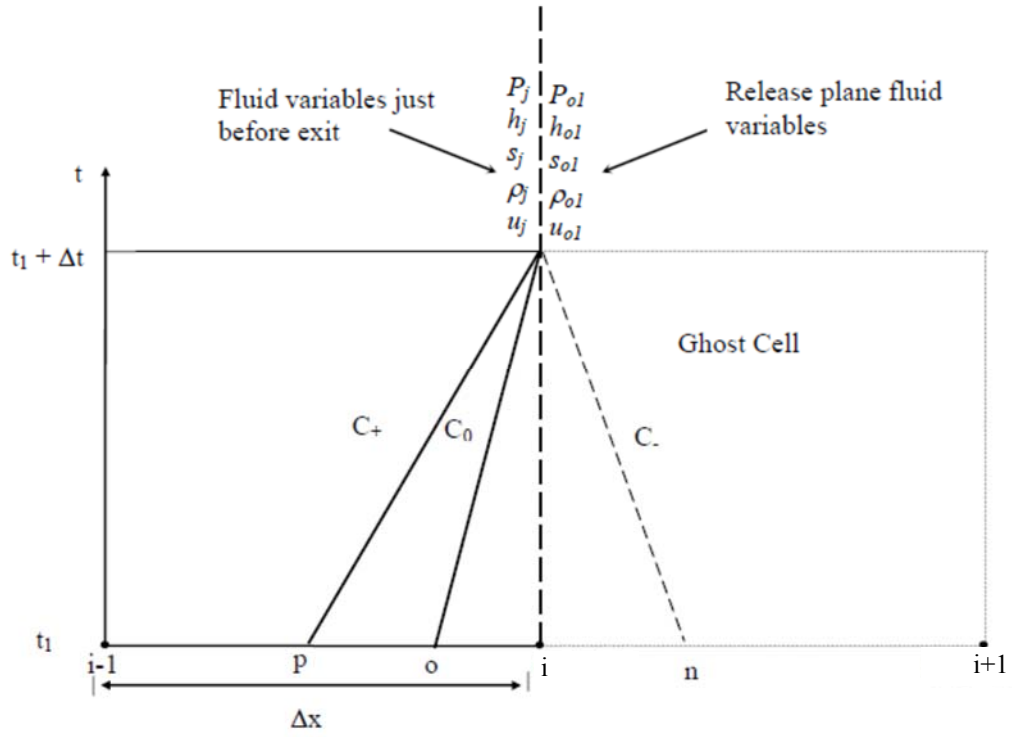

Figure 4.5: Schematic representation of the characteristic lines around the release plane based on 'ghost' cell approach.

The variables at release plane (i.e ρ_{o1}, u_{o1} and h_{o1}) as shown in Figure 4.5 are calculated using the critical discharge algorithm described in the section 4.5.3.

For the case of puncture at the pipe end, although it is assumed that the expansion process across the release plane is isentropic, nonetheless, non-isentropic effect is

expected due to hydraulic resistance posed by the opening. Accordingly the release rate based on the latter is smaller than that of isentropic flow. The ratio of the actual release rate which is determined by conservation of mass and the isentropic equivalent release rate is expressed in terms of Discharge Coefficient, C_d:

$$C_d = \frac{\rho_j u_j A_{pipe}}{\rho_{o1} u_{o1} A_{o1}} \tag{4.17}$$

Where, A_{pipe} and A_{o1} are respectively the area of the pipe and orifice. The fluid properties denoted by *o1* are at release plane.

4.5.3 Algorithm for Obtaining Discharge Rate

Figure 4.6 shows all the pertinent pressures across the release plane during the discharge process. The P_j, P_{o1} and P_d respectively present the fluid approaching the release plane (upstream), release plane and ambient (downstream) pressures.

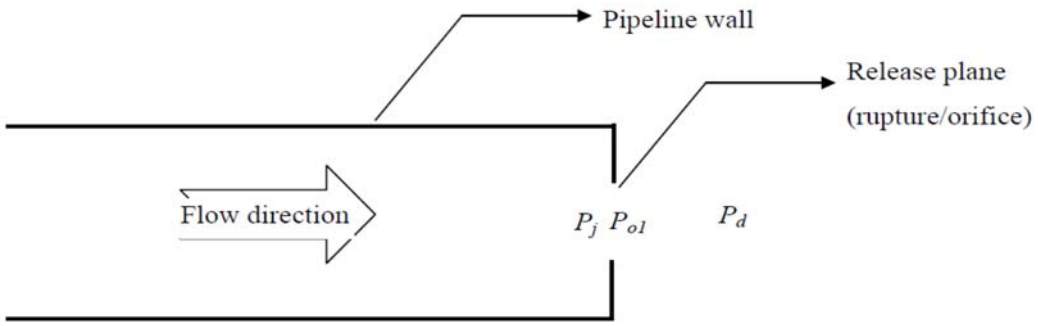

Figure 4.6: Schematic representation of the pertinent pressures across the release plane governing the discharge process for the case of rupture/puncture at the end.

For choked flow condition, the release rate is calculated by applying the energy balance across the release plane. Ignoring the potential energy difference between the upstream and release plane, the energy balance is reduced to:

$$h_j + \frac{1}{2}u_j^2 = h_{o1} + \frac{1}{2}u_{o1}^2 \quad (4.18)$$

The calculation algorithm for determining the discharge pressure and other pertinent flow variables at the release plane is depicted in Figure 4.7.

The solution of equation **(4.18)** under choked flow condition is carried out iteratively by assuming a discharge pressure P_{o1} and replacing the u_{o1} with the corresponding speed of sound obtained from the pressure-entropy (P_{o1}-s_j) flash calculation. The Brent iteration method (Press et al., 1992) is adopted for fast convergence. Once equation (4.18) is satisfied, other corresponding variables at the release planes such as ρ_{o1}, T_{o1} and h_{o1} are determined.

For unchoked flow, no iteration is required as the discharge pressure, P_{o1}, is equal to the ambient pressure (P_d). Other pertinent variables at the release plane (i.e ρ_{o1}, T_{o1} and h_{o1}) are determined using the corresponding pressure-entropy (P_{o1}-s_j) flash calculation and subsequently the discharge velocity can directly be calculated from equation (4.18).

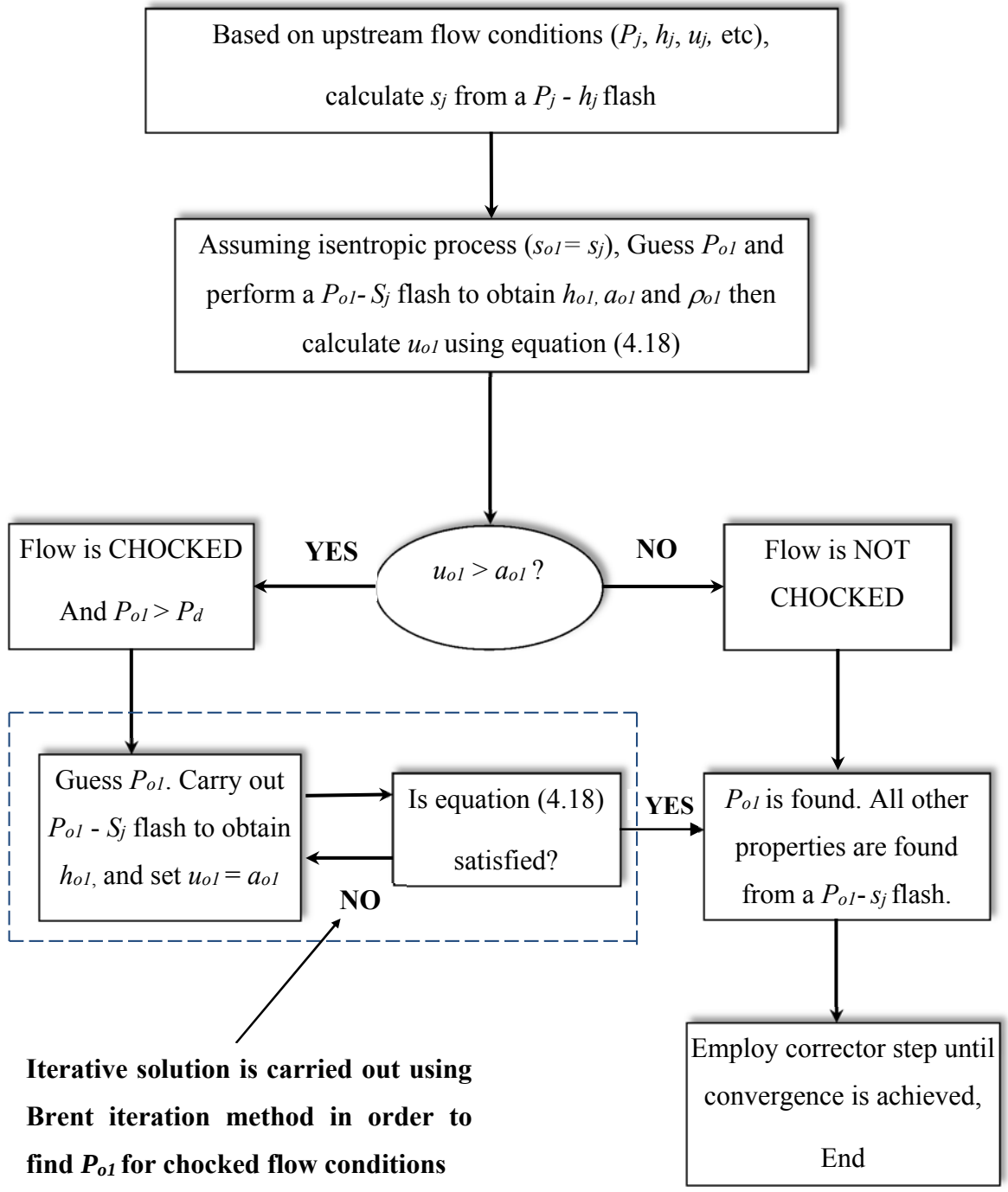

Figure 4.7: Calculation algorithm for determining the pressure and other pertinent flow variables at the release plane.

4.5.4 Puncture on the Pipe Wall Boundary Condition

As mentioned in chapter 2, Oke et al., (2003) developed the boundary condition for simulating flow through a puncture on the pipe wall. Atti (2006) later corrected the invalid constant density assumption across the release plane in Oke's model. Atti's (2006) puncture boundary is therefore employed in this study. For the sake of completeness it is reproduced below.

For punctures on the pipe wall, the pipe is assumed to split into two sections. The control volume around the puncture location poses three boundaries as depicted in Figure 4.8:

- Upstream section boundary (B_1)
- Downstream section boundary (B_2)
- Release plane boundary (B_3)

For the upstream boundary (B_1), only the positive characteristic and path lines lie within the computational domain. Similarly, for the downstream boundary (B_2), the negative characteristic line and path line are applicable within this domain.

The solution as proposed by Atti (2006) requires the pressure within the control volume to remain constant at the current time step. This implies that the pressure at the boundaries B_1, B_2 and B_3 denoted by j_1,j_2 and j_{01} respectively to be equal:

$$P_{j_1} = P_{j_2} = P_{j_{01}} \tag{4.19}$$

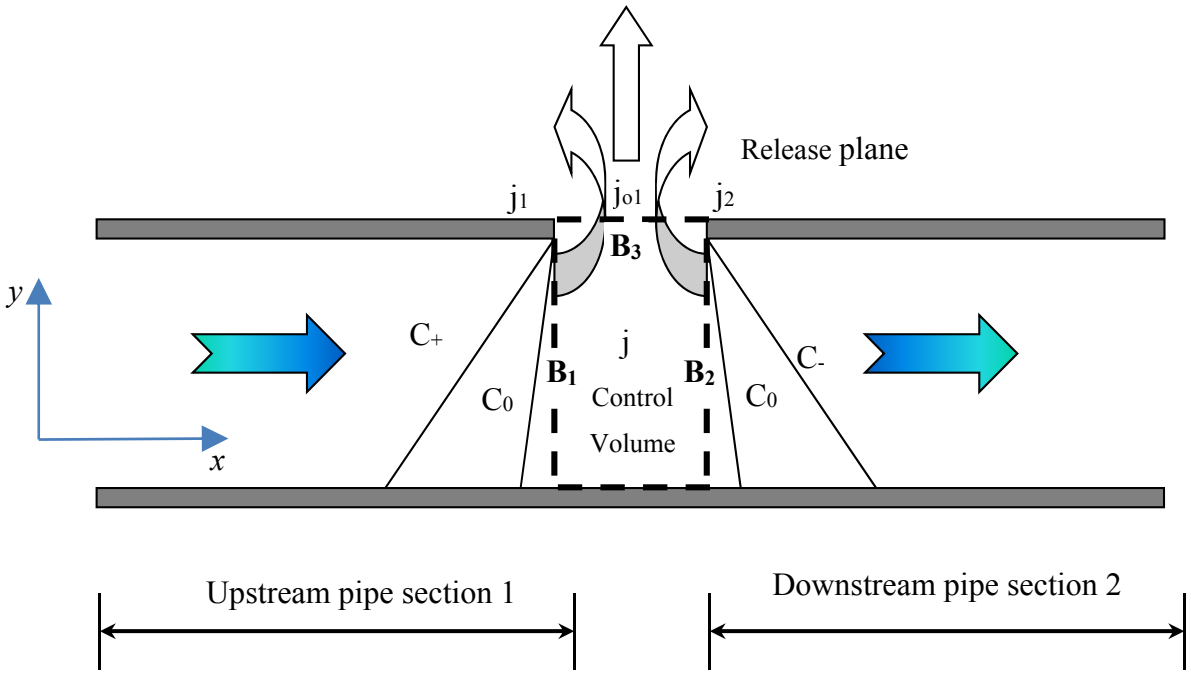

Figure 4.8: Schematic representation of the applicable characteristic lines and fluid flow analysis following pipeline puncture.

The properties at the control volume are averaged such that:

$$s_j = \frac{1}{2}(s_{j_1} + s_{j_2}) \tag{4.20}$$

Where properties denoted by *j* represent the value at the centre of the cell. The flow through boundary B_3 is assumed to be isentropic therefore the following relation is valid:

$$s_j = s_{o1} \tag{4.21}$$

The flow through the control volume is both in radial and axial direction. Accordingly, the mass conservation equation for the control volume is casted as:

$$V\frac{d\rho}{dt} + A_{pipe}\frac{\partial(pv)}{\partial x} + A_{o1}\frac{\partial(pv)}{\partial y} = 0 \tag{4.22}$$

Where,

V= volume of the control volume

v=fluid velocity normal to the axial direction (i.e. in *y* direction)

Integration of equation (4.22) with respect to, t, over interval [t_1,t_2] yields:

$$V\left(\rho_{j|t=t_2} - \rho_{j|t=t_1}\right) + A_{pipe}\int_{t_1}^{t_2}\left[(\rho u)_{x_2} - (\rho u)_{x_1}\right]dt + A_{o1}\int_{t_1}^{t_2}\left[(\rho v)_{y_2} - (\rho v)_{y_1}\right]dt = 0 \tag{4.23}$$

Given that $(\rho v)_{j|y=y_1}$ is equal to zero, numerical evaluation of the integrals gives:

$$V\left(\rho_{j|t=t_2} - \rho_{j|t=t_1}\right) + \left\{A_{pipe}\left[(\rho u)_{j|x=x_2} - (\rho u)_{j|x=x_1}\right] + A_{o1}\left((\rho v)_{j|y=y_2}\right)_{ave}\right\}\Delta t = 0 \tag{4.24}$$

The subscript *ave* denotes the average of the value in the brackets over interval [t_1, t_2]. The x_2 and x_1 presents the B_2 and B_1 boundaries along the *x*-axis of the control volume.

Equation (4.24) is based on the assumption that discharge process follows an isentropic path. The non-isentropic effects are accounted for by introducing the discharge coefficient (C_d) in to equation (4.24) yields:

$$V\left(\rho_{j|t=t_2} - \rho_{j|t=t_1}\right) + \left\{A_{pipe}\left[(\rho u)_{j|x=x_2} - (\rho u)_{j|x=x_1}\right] + C_d A_{o1}\left((\rho v)_{j|y=y_2}\right)_{ave}\right\}\Delta t = 0 \quad (4.25)$$

The boundary condition solution algorithm employed for puncture on pipe wall is depicted in Figure 4.9.

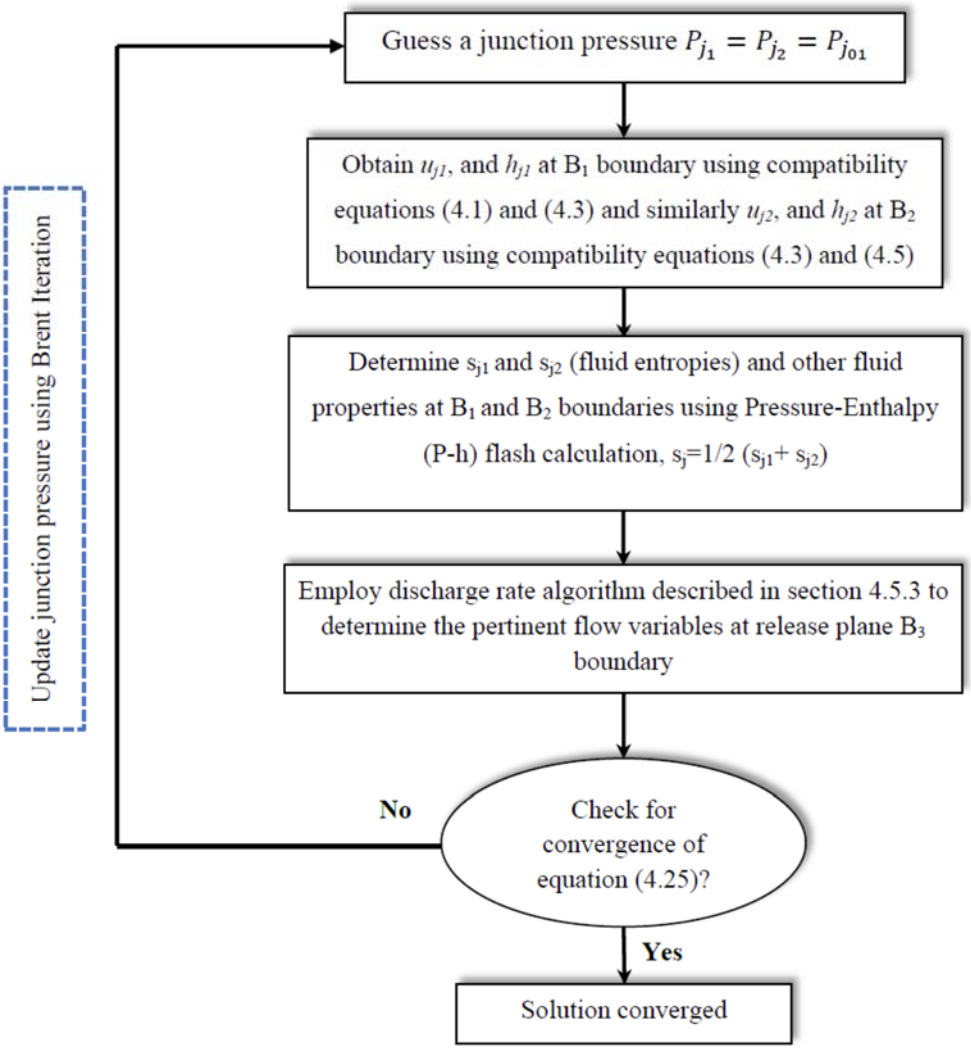

Figure 4.9: Calculation algorithm for determining the pressure and other pertinent flow variables at the release plane for puncture on the pipe wall.

4.5.5 Centrifugal Pump at Pipe Inlet

Centrifugal pump pipe inlet boundary condition accounts for simulating the failure of an un-isolated pipe where the inventory continues to be fed into the system despite the failure.

Wylie and Streeter (1993) presented the performance characteristic curve of the centrifugal pump to describe the behaviour of the pump discharge pressure as a function of its discharge rate or velocity:

$$P_j = K_{P2}u_j^2 + K_{P1}u_j + P_{sh} \quad (4.26)$$

Where,

P_j= Pump discharge pressure

u_j=Pump discharge velocity

P_{sh}= Pump shut-off head (maximum discharge pressure of the pump)

$K_{P2}\ and\ K_{P1}$ = Constants dependant on the type of pump used and usually given by pump manufacturer

Alternatively, if the steady state pump head vs discharge data is available, equation **(4.26)** can be curve fitted to obtained P_{sh}, $K_{P2}\ and\ K_{P1}$.

Similar to the intact end boundary condition described in section 4.5.1, only negative compatibility and path lines are valid within the computational domain. Negative compatibility is rearranged for u_j such that:

$$u_j = \frac{P_j}{(\rho a)_n} - \frac{P_n}{(\rho a)_n} - \frac{K_2}{(\rho a)_n} + u_n \tag{4.27}$$

Equation **(4.27)** shows the linear relationship between discharge pressure and velocity. Further simplification yields:

$$u_j = K_{nu1} P_j - K_{nu2} \tag{4.28}$$

Where,

$$K_{nu1} = \frac{1}{(\rho a)_n}$$

$$K_{nu1} = \frac{P_n + K_2}{(\rho a)_n} - u_n$$

Substituting **(4.26)** into equation **(4.28)** gives:

$$K_{nu1} K_{P2} u_j^2 + (K_{nu1} K_{P1} - 1) u_j + K_{nu1} P_{sh} - K_{nu2} = 0 \tag{4.29}$$

The positive root of the above equation is the pump discharge velocity and the corresponding discharge pressure can be determined using equation **(4.26)**.

4.6 Concluding Remarks

In this chapter, application of the MOC to the conservation equations was presented. Different methods of discretisation for MOC were next discussed together with their advantages and disadvantages.

The formulation of the MOC based on MST discretisation method was presented. The formulation was based on the assumption that the fluid properties at the current time step vary linearly with distance. Accordingly, the algebraic expressions for the fluid variables at the next time step along the pipeline length were obtained.

The solution of governing conservation equations using MOC involves representation of the PDEs by converting the compatibility equations using their finite difference approximation. These compatibility equations are then solved along the respective characteristic lines using the Euler predictor-corrector technique.

For closure of the system of equations, the appropriate boundary conditions are required to represent the fluid dynamics behaviour following the puncture/rupture of pipeline. These relevant boundary conditions and their applications to MOC were presented and discussed.

Chapter 5: Development of a Computationally Efficient Numerical Solution for Outflow Simulation Following Pipeline Failure

5.1 Introduction

In chapter 2, the validation of MOC for simulating pipeline failures was reviewed. However, this method of solution suffers from long computational run-times, largely due to the requirement to determine the real fluid properties, hence the solution of the EoS at p, n and o locations (see chapter 4: figure 4.3) for all time and space grid points along the pipeline.

As discussed in chapter 2, Atti (2006) partially addressed this issue through the use of PHU based conservation equations for simulating the transient fluid flow. The above coupled with the introduction of a Pressure-Enthalpy (P-H) interpolation scheme led to as much as 80 % reduction in computational run-time as compared to the use of the PHU based conservation equations.

However, the above reduction in the computational run-time is a consequence of the reduction in the number of flash calculations at the grid points only along the length of the pipeline. The P-H interpolation scheme becomes redundant at the rupture plane given that the expansion process is isentropic.

Given the iterative calculation algorithm at the rupture plane (see chapter 4: section 4.5.3), a large number Pressure-Entropy (P-S) flash calculations are required for calculating the critical discharge pressure thus contributing significantly to the overall computational run-time. An analysis of the CPU time spent in flash

calculations during the first 2000 s simulation of the Piper Alpha pipeline depressurisation case (see section 5.6 for pipeline characteristics and prevailing conditions) was performed using the time profiling utility built in SILVERFROST FORTRAN compiler. The results reveal that despite the P-H interpolation, the CPU time spent in the flash calculations still accounts for approximately 95% of the overall CPU run-time. Furthermore, the vast majority of these flash calculations are performed at the release plane.

In this chapter, development of a computationally efficient pipeline rupture outflow model based on PSU conservation equations coupled with a P-S interpolation scheme herein referred to the PSU Coupled (PSUC) model is presented.

Following validation of its performance using real pipeline rupture data, the PSUC predictions and the associated computational run-times are compared against simulation results obtained using PHU and FVM (Brown, 2011). All simulations presented in this work were conducted on a Dell 2.66 GHz Intel Dual Core PC.

5.2 Scheme for Reducing Computational Run-time of MOC

The interpolation scheme developed by Atti (2006) first involves a *priori* generation of a look-up table containing the relevant thermodynamic properties at set intervals within a predefined range of pressures and enthalpies. Subsequently, the intermediate values are determined using interpolation.

However, the solution at the discharge plane still remains computationally expensive as the P-S flash calculations are performed interactively in separate subroutines using direct call to the flash subroutine.

An analysis of the CPU time spent in flash calculations during the first 2000 s simulation of the Piper Alpha pipeline depressurisation case (see section 5.6 for pipeline characteristics and prevailing conditions) was performed using the time profiling utility built in SILVERFROST FORTRAN compiler. The results reveal that despite the P-H interpolation, the CPU time spent in the flash calculations still accounts for approximately 95% of the overall CPU time. Furthermore, the vast majority of these flash calculations are performed at the release plane.

As such the PSU based conservation equations are employed in this study to unite the P-S flash calculations required within the computational domain. Therefore, reducing the number of these flash calculations will unvaryingly reduce the overall computational run-time. This is achieved by generation of P-S look-up table and utilising an interpolation scheme for determination of the fluid properties at intermediate points.

5.3 Formulation of the PSU Compatibility Equations

For any given fluid, the following relations between enthalpy and entropy exist as given by (Walas, 1985):

$$dh = Tds + \frac{1}{\rho} dP$$

or

$$\frac{1}{T}\left[\frac{dh}{dt} - \frac{1}{\rho}\frac{dP}{dt}\right] = \frac{ds}{dt} \tag{5.1}$$

Using thermodynamic transformation, the PHU formulation of the conservation equations (see equations (3.1), (3.2) and (3.3)) can be represented with pressure (P), entropy (S) and velocity (U) as the primitive variables (PSU) (Ade, 2004):

$$\left(\frac{\partial P}{\partial t}+u\frac{\partial P}{\partial x}\right)-\varphi\left(\frac{\partial s}{\partial t}+u\frac{\partial s}{\partial x}\right)+\rho^2 a^2 T\frac{\partial u}{\partial x}=0 \tag{5.2}$$

$$\rho\left(\frac{\partial u}{\partial t}+u\frac{\partial u}{\partial x}\right)+\frac{\partial P}{\partial x}=\beta_x+\rho g\sin(\theta) \tag{5.3}$$

$$\rho\left(\frac{\partial s}{\partial t}+u\frac{\partial s}{\partial x}\right)=Q_h+u\beta_x \tag{5.4}$$

The above conservation equations are quasi-linear as all the derivative terms are linear and hyperbolic in nature (see chapter 3). The hyperbolicity is because the system of equations has three distinct and real roots (Prasad and Ravindran, 1985). Following the same approach as taken for solution of PHU conservation equations, the above equations are replaced by three compatibility equations which are valid along the respective characteristic lines. The three PSU compatibility equations are given by (Ade, 2004):

Path line compatibility equation

$$d_0 s=\left[\frac{\psi}{\rho T}\right]d_0 t \tag{5.5}$$

Valid along the path line characteristic (C_0)

$$\frac{d_0 t}{d_0 x}=\frac{1}{u} \tag{5.6}$$

Positive compatibility equation

$$d_+ P+\rho a d_+ u=\left(\frac{\varphi\psi}{\rho T}+a(\beta_x+\rho g\sin(\theta))\right)d_+ t \tag{5.7}$$

Valid along the positive characteristic line (mach line) (C_+)

$$\frac{d_+ t}{d_+ x}=\frac{1}{u+a} \tag{5.8}$$

Negative compatibility equation

$$d\_P+\rho a d\_u=\left(\frac{\varphi\psi}{\rho T}-a(\beta_x+\rho g\sin(\theta)\right) d\_t \quad (5.9)$$

Valid along the negative characteristic line (mach line) (C-)

$$\frac{d\_t}{d\_x}=\frac{1}{u-a} \quad (5.10)$$

As it may be observed, the positive and negative compatibility equations for both PHU and PSU are identical. Therefore only the path line compatibility equation depends on the selection of primitive variables of the conservation equations.

5.4 Methodology Employed for P-S Interpolation

The following describes development of P-S interpolation technique which unifies the flash calculations throughout the computational domain including boundary conditions. This scheme involves generation of a database containing the relevant thermodynamic properties in the form of the look-up table for subsequent determination of the intermediate values using interpolation. Figure 5.1 presents the P-S interpolation domain.

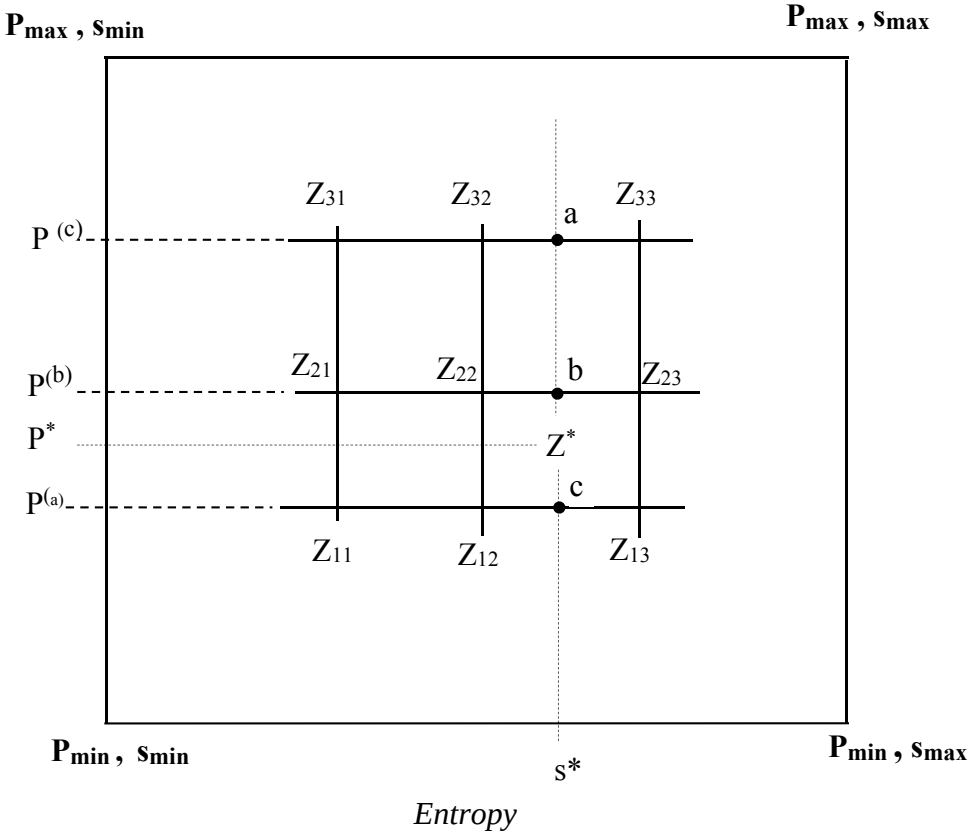

Figure 5.1: Schematic presentation of the Pressure-Entropy (P-S) interpolation domain.

The interpolation domain is established by determination of the likely range of fluid entropies, S_{min} and S_{max}. This is achieved by determining the maximum and minimum possible pipeline pressures, P_{max}, P_{min} and temperatures, T_{max}, T_{min}.

P_{max} is equal to the pipeline feed or inlet pressure. P_{min} on the other hand is taken as the ambient pressure. In order to define the temperature range, the highest temperature (be it the inlet fluid or ambient temperature) is taken as T_{max} and the minimum fluid temperature, T_{min} is determined by performing an isentropic flash from P_{max} and T_{max} to P_{min}.

S_{min} and S_{max} are obtained by performing the corresponding Pressure-Temperature flash calculations.

Since the PSU conservation equations are employed, the pressure and entropy are chosen as the independent axes. Once the interpolation domain is established as depicted in figure 5.1, it is then discretised along the pressure and entropy axes using predefined intervals.

Returning to figure 5.1, Z_{11}-Z_{33} represent the predetermined nodal fluid properties based on P-S flash calculations. The fluid properties Z* is obtained at a specific P and S (P*- S*).

The pertinent fluid thermo-physical properties, Z (= *f* (*P*, *s*, composition) at each node are then determined by performing P-S flash. This leads to a 3 dimensional array comprising pressure, entropy and fluid properties. The calculated fluid properties are selected such that no further flash calculations would be necessary for subsequent numerical calculations.

The fluid properties, Z required at any intermediate pressure and entropy values can then be determined directly from interpolation as opposed to time consuming flash calculations which require the solution of the equation of state. The Lagrange Polynomial Method (Hoffmann, 1992) is employed in this scheme for the quadratic interpolation given its high accuracy and computational efficiency.

The interpolation is carried out in two steps. First, the intermediate values of Z at points a, b and c corresponding to the entropy, s* are determined as depicted in figure 5.1. This is achieved by interpolating between points Z_{11}-Z_{13} , Z_{21}-Z_{23}, and Z_{31}-Z_{33} respectively using the following interpolation formulas (Hoffmann, 1992):

$$Z^{(a)} = \frac{(s^* - s_{12})(s^* - s_{13})}{(s_{11} - s_{12})(s_{11} - s_{13})} Z_{11} + \frac{(s^* - s_{11})(s^* - s_{13})}{(s_{12} - s_{11})(s_{12} - s_{13})} Z_{12} + \frac{(s^* - s_{11})(s^* - s_{12})}{(s_{13} - s_{11})(s_{13} - s_{12})} Z_{13} \quad (5.11)$$

$$Z^{(b)} = \frac{(s^* - s_{22})(s^* - s_{23})}{(s_{21} - s_{22})(s_{21} - s_{23})} Z_{21} + \frac{(s^* - s_{21})(s^* - s_{23})}{(s_{22} - s_{21})(s_{22} - s_{23})} Z_{22} + \frac{(s^* - s_{21})(s^* - s_{22})}{(s_{23} - s_{21})(s_{23} - s_{22})} Z_{23} \quad (5.12)$$

$$Z^{(c)} = \frac{(s^* - s_{32})(s^* - s_{33})}{(s_{31} - s_{32})(s_{31} - s_{33})} Z_{31} + \frac{(s^* - s_{31})(s^* - s_{33})}{(s_{32} - s_{31})(s_{32} - s_{33})} Z_{32} + \frac{(s^* - s_{31})(s^* - s_{32})}{(s_{33} - s_{31})(s_{33} - s_{32})} Z_{33} \quad (5.13)$$

Finally, at the second stage of interpolation, Z^* is obtained by interpolating between $Z^{(a)}$, $Z^{(b)}$ and $Z^{(c)}$ along the pressure axis using the following equation:

$$Z^* = \frac{(P^* - P^b)(P^* - P^c)}{(P^a - P^b)(P^a - P^c)} Z^a + \frac{(P^* - P^a)(P^* - P^c)}{(P^b - P^a)(P^b - P^c)} Z^b + \frac{(P^* - P^b)(P^* - P^b)}{(P^c - P^a)(P^c - P^b)} Z^c \quad (5.14)$$

The above methodology ensures that fluid properties are determined using efficient interpolation scheme at a given pressure and entropy.

Flash calculation are employed in the event that any pressure or entropy fall outside the interpolation domain. Depending on the interpolation domain, typical computation run-time for the generation of an interpolation table is in the range 20–40 s.

The P-S interpolation in comparison to P-H interpolation has a slightly higher CPU run-time as the table being generated includes additional fluid properties required for release plane calculations. However, its impact on the total computation run-time for the simulation of the entire pipeline depressurisation duration is insignificant.

5.5 P-S Interpolation Scheme Accuracy

In order to determine the accuracy of P-S interpolation scheme, its predictions are compared against those obtained directly from P-S flash calculations for different types of hydrocarbon systems at given pressures and entropies. Table 5.1 presents the comparisons between the fluid densities, speed of sound and corresponding temperatures obtained using P-S interpolation and direct flash calculation. As it may be observed, the differences between the predictions are indeed very small (0.006% max error) indicating that the computationally expensive flash calculations can be replaced with the interpolation scheme without comprising accuracy.

Table 5.1: Comparisons between the fluid density, speed of sound and corresponding temperature obtained from P-S interpolation and P-S flash calculation.

Fluid State	*Fluid Mixture*	*Pres. (bar)*	*Entr. (s/R)*	*Fluid Properties*	*Interpolated Values*	*Direct P-S Flash Values*	*Error %*
Gas	85% methane 15% ethane	10.94	-2.2858	Speed of Sound (m/s)	378.9533	378.9681	0.0039
				Density (kg/m^3)	9.8322	9.8325	0.003
				Temperature (C)	255.9601	255.9745	0.0056
Two-phase	50% methane 50% n-pentane	12.14	-5.5889	Speed of Sound (m/s)	163.9285	163.9289	0.0002
				Density (kg/m^3)	45.2975	45.2970	0.0011
				Temperature (C)	287.1413	287.1468	0.0019
Liquid	95% n-butane 5% propane	3.95	-7.9697	Speed of Sound (m/s)	714.3376	714.3376	0.0000
				Density (kg/m^3)	599.4141	599.4143	0.0000
				Temperature (C)	294.2850	294.2850	0.0000

5.6 Validation of PSUC against Experimental Data

In this section, the performance of the PSUC in reducing the computational run-time as compared to PHU, and where available FVM, and accuracy based on comparison with real pipeline rupture data are investigated. The three sets of field data include:

1. Measured mass discharge rate from the TransCanada pipeline accident (HSE, 2004)
2. Intact end pressure at natural gas riser connecting the Piper Alpha to the MCP01 platform (Chen, 1993)
3. Release pressure, release temperature and cumulative mass released measurements obtained for a series of pipeline FBR experiments carried out by Shell and BP on the Isle of Grain (Richardson and Saville, 1996)

For validation against puncture failures, the performances of PSUC and PHU are compared against the field data for P45 and P47 puncture tests carried out by Shell and BP on the Isle of Grain (Richardson and Saville, 1996).

5.6.1 Full Bore Rupture

The TransCanada natural gas pipeline is a 76 km long pipe with 894.4 mm i.d. The pipeline operated at 61 bara and assumed to contain 100 % methane (HSE, 2004). The isolated pipeline (no flow prior to rupture) underwent FBR at 38 km along its length. Table 5.2 presents the remaining pipeline characteristics and prevailing conditions used for the simulations.

Figure 5.2 shows the corresponding variation of the mass release rate with depressurisation time. Curve A represents the measured data whilst curves B, C and D are the predicted results obtained using the PHU, FVM and PSUC (the present scheme) respectively. There is no measured data reported for the first 10 s following FBR. The corresponding CPU run-times for the above as well as those for the proceeding investigations are given in the figure captions.

As it may be observed, the PHU predictions are in marginally better agreement with measured data with FVM and PSUC producing almost identical results throughout the simulation. The finite discrepancies between theory and measurement may be due to the assumption of the pipeline inventory being 100% methane. In practice, heavier hydrocarbons may have been present in the pipeline; however no accurate feed composition data is available (Brown, 2011). In terms of computational run-time, PSUC performs remarkably well with total computational run-time of 43 s. This as compares with 210 s for PHU and 414 s for FVM, representing 80 % reduction in the total CPU run-time as compared to PHU.

Table 5.2: Pipeline characteristics and prevailing conditions for the simulation of TransCanada (HSE, 2004) pipeline rupture.

Input		Value
Inlet Parameters	Number of components	1
	Feed composition (mole %)	methane 100%
	Feed inlet temperature (K)	283
	Feed inlet pressure (bara)	61
	Ambient temperature (K)	283
	Ambient pressure (bara)	1.01
Pipe Characteristics	Length (m)	76000
	External diameter (mm)	914.4
	Wall thickness (mm)	10
	Roughness (mm)	0.05
	Orientation to the horizontal plane (deg)	0
Rupture Conditions	Failure mode	Full Bore Rupture
	Failure location relative to high pressure end (m)	38000
	Rupture diameter (mm)	894.4
	Discharge coefficient	1
Other Parameters	Feed flow rate prior to rupture (m^3/s)	0
	Pumping cessation time following pipeline failure (s)	0
	Pump shut-off head (bara)	NA
	Grid system used	Simple
	Number of grid points specified	3000
	Equation of State	Peng Robinson (Peng and Robinson, 1976)
	Friction factor correlation	Chen (Chen 1979)
	Heat transfer coefficient (W/m^2K)	5
	Total depressurisation time (s)	60

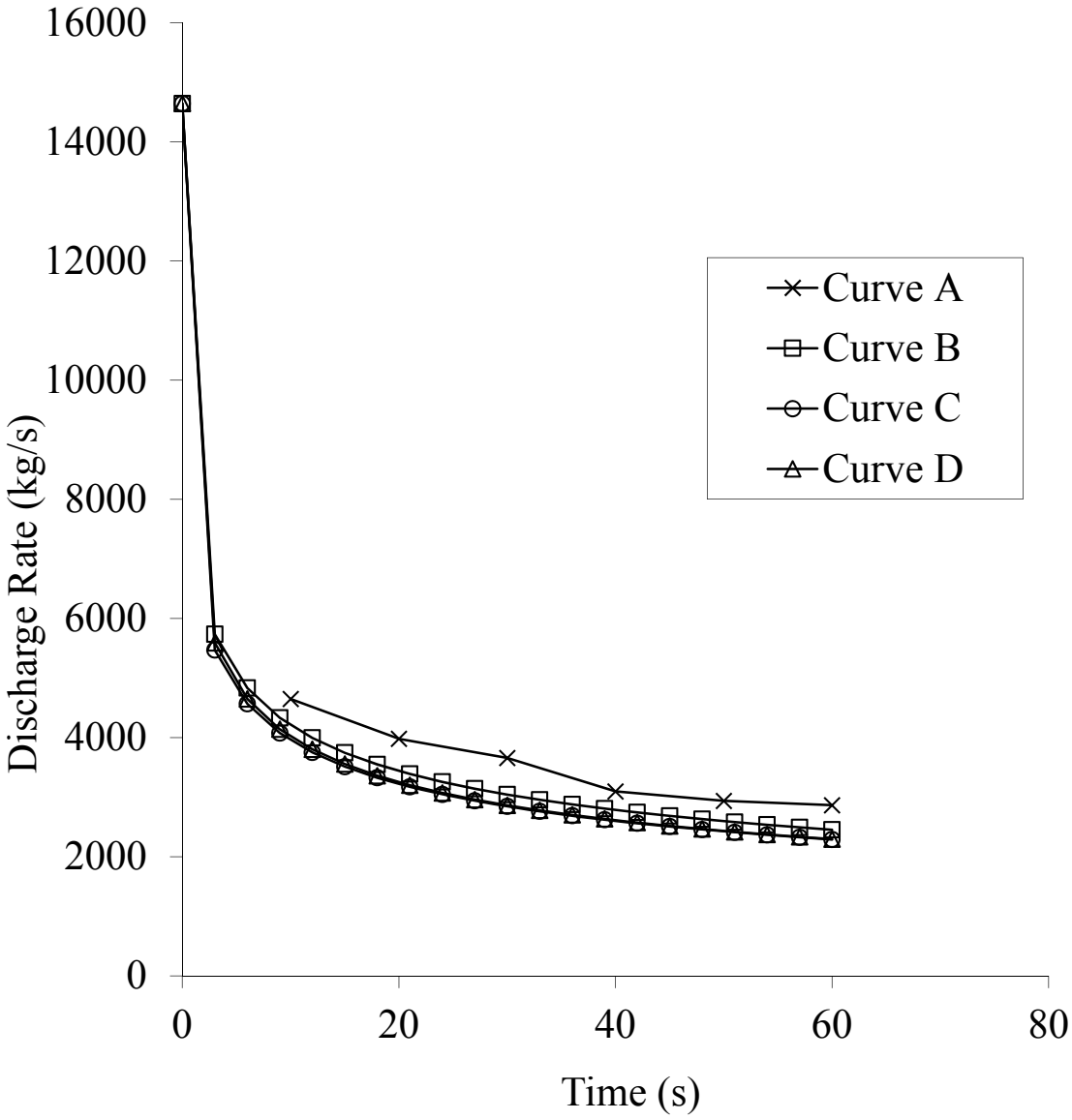

Figure 5.2: Comparison of the measured and simulated variation of discharge rate with time following FBR of TransCanada.

Curve A: Experimental data (HSE, 2004)

Curve B: PHU, CPU run-time = 210 s

Curve C: FVM, CPU run-time = 414 s (Brown, 2011)

Curve D: PSUC, CPU run-time = 43 s

The Piper Alpha was a North Sea oil production platform. The Piper Alpha tragedy involved the FBR of the 54 km subsea natural gas riser connecting the Piper Alpha to the MCP01 platform (Cullen, 1990). During the incident only pressure-time data at high pressure end of the pipeline (intact end) was recorded. Table 5.3 shows the pipeline characteristics and prevailing conditions used in simulation of Piper Alpha pipeline rupture. Figure 5.3 shows the corresponding variation of the closed end pressure with depressurisation time for Piper Alpha pipeline. Curve A shows the measured data, whereas curves B and C show the PHU and PSUC simulations respectively.

Table 5.3: Pipeline characteristics and prevailing conditions for simulation of the Piper Alpha (Sylvester and Evans, 1991) pipeline rupture.

Input		Value
Inlet Parameters	Number of components	9
	Feed composition (mole %)	methane- 73.6
		ethane-13.4
		propane-7.4
		i-butane-0.4
		butane-1.0
		i-pentane-0.08
		pentane-0.07
		hexane-0.02
		nitrogen-4.3
	Feed inlet temperature (K)	283
	Feed inlet pressure (bara)	117
	Ambient temperature (K)	292.15
	Ambient pressure (bara)	1.01
Pipe Characteristics	Length (m)	54000
	External diameter (mm)	457.12
	Wall thickness (mm)	19.01
	Roughness (mm)	0. 259
	Orientation to the horizontal plane (deg)	0
Rupture Conditions	Failure mode	Full Bore Rupture
	Failure location relative to high pressure end (m)	54000
	Rupture diameter (mm)	419
	Discharge coefficient	1
Other Parameters	Feed flow rate prior to rupture (m^3/s)	0
	Pumping cessation time following pipeline failure (s)	0
	Pump shut-off head (bara)	NA
	Grid system used	Nested
	Number of grid points specified	108
	Equation of State	Peng Robinson (Peng and Robinson, 1976)
	Friction factor correlation	Chen (Chen 1979)
	Heat transfer coefficient (W/m^2K)	1.136
	Total depressurisation time (s)	10,000

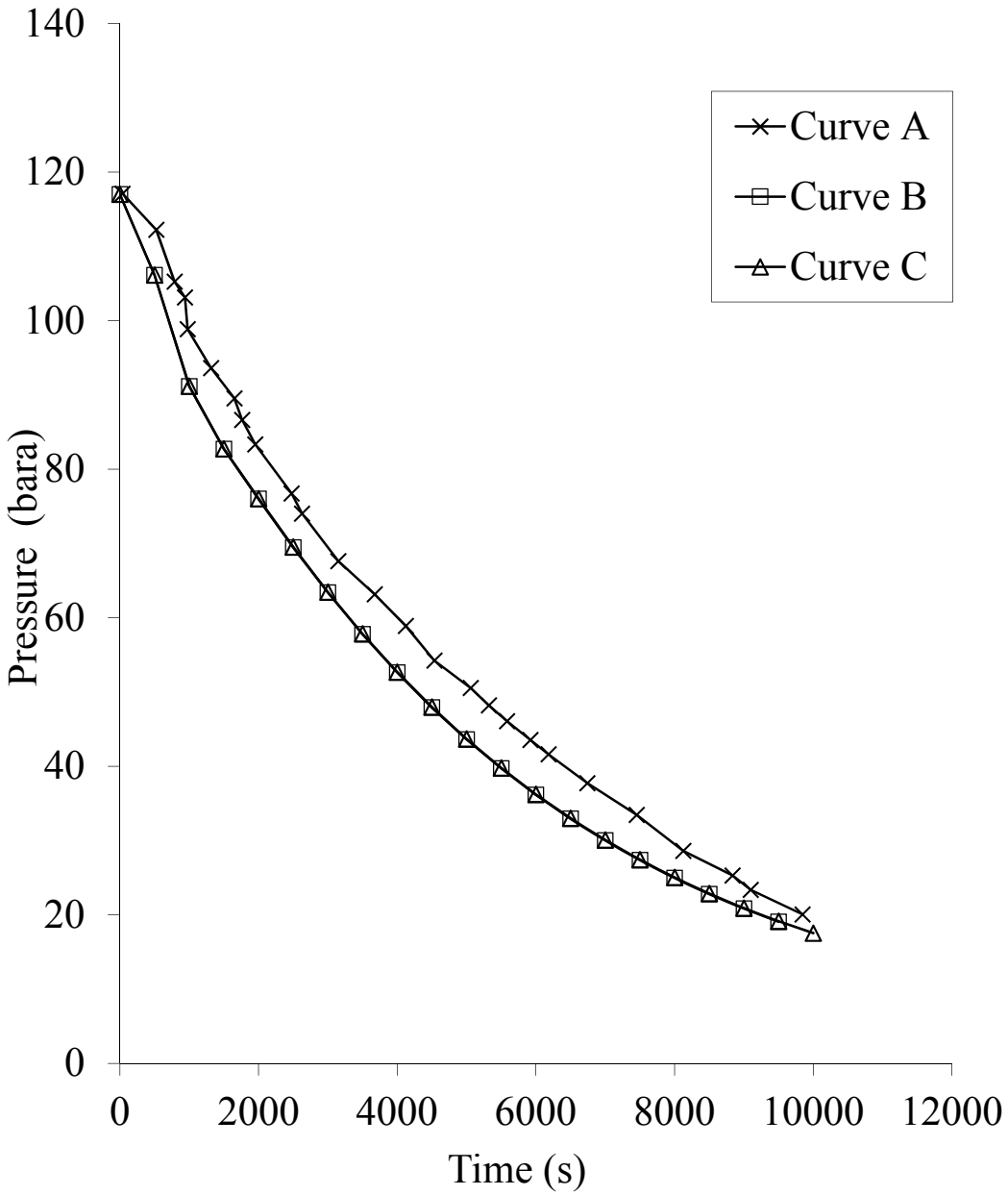

Figure 5.3: Comparison of the variation of intact end pressure with time following the FBR of the Piper Alpha-MCP01 pipeline.

Curve A: Field data (Cullen, 1990)

Curve B: PHU, CPU run-time = 92,506 s

Curve C: PSUC, CPU run-time = 2,736 s

As it may be observed from the comparison presented in figure 5.3 between the predicted and measured data, PHU and PSUC under predict the intact end pressure whilst both model predictions are in good accord with each other for the entire depressurisation duration. The average difference in predicted intact pressure between the PHU and PSUC is ca. 0.23 %.

The CPU run-time for PHU and PSUC is 92,506 s (ca. 26 hours) and 2,736 s respectively. While maintaining almost the same level of accuracy as compared to PHU, the PSUC achieved a remarkable reduction in computational run-time of ca. 97%.

Performing a multi-component flash calculations is computationally more demanding than that for a single-component flash. Accordingly, more significant reduction in CPU run-time for the Piper Alpha pipeline as compared to the methane gas Trasncanada pipeline (figure 5.2) is due to longer CPU run-time required by PHU to perform P-S flash calculations at the release plane.

The PSUC prediction is validated against the Isle of Grain FBR field tests (i.e. P40 and P42). Details of the test facility and procedures are given elsewhere (see for example Chen, 1993; Richardson and Saville, 1996) hence only a brief account is provided here. The tests involved the use of a 150 mm carbon steel pipe incorporating punctures with equivalent diameter up to FBR. The inventory for these tests was commercial propane; that is a mixture of propane and other low molecular weight hydrocarbons. The mixture was assumed to comprise of 95% propane and 5% n-butane (Richardson and Saville, 1996). The initial state of the inventory was liquid however due to the highly volatile nature of the mixture, it rapidly became two-phase upon depressurisation.

Other pipeline characteristics and prevailing conditions used in simulation of Isle of Grain FBR tests are presented in Table 5.4 .

The predicted release (open end) pressure, release (open end) temperature and cumulative mass released are compared against measured data. These are respectively presented in figures 5.4, 5.5 and 5.6 for Isle of Grain P40 test. Curve A represents the measured data whilst curves B and C represent the predicted data obtained using PHU and PSUC respectively.

As it may be observed in figure 5.4, upon rupture, the phase transition from initial LPG to two-phase is marked by almost instantaneous drop from 21.6 bara to the discharge pressure ca. 10 bara. The slight under-prediction of the release pressure (curve B and C) from the measured open end pressure during the early stage of depressurisation is postulated to be due to the non-equilibrium effects caused by delayed bubble nucleation. Given that the overall impact of such non-equilibrium effects on the total discharge for FBR failure is considered to be marginal (Brown, 2011), such phenomenon is not considered in this study. The rapid depressurisation is then followed by a steady drop in pressure which corresponds to gradual transition from two-phase to vapour phase at about 20 s ensuing rupture. As can be seen from figure 5.4, there is good agreement between the simulated data (i.e. curves B and C) for the entire simulation showing no discernible differences and the predictions are closely matching the measured data. It is noteworthy that the measured open-end pressure drops below 1 bara towards the end of the depressurisation which is almost inline the measurement uncertainty range of +/-0.5 bara.

Table 5.4: Shows the pipeline characteristics and prevailing conditions used for simulation of Isle of Grain P40 and P42 (Richardson and Saville, 1996).

Input		Isle of Grain P40	Isle of Grain P42
Inlet Parameters	Number of components	2	2
	Feed composition (mole %)	propane- 95 %	propane- 95 %
		n-butane-5 %	n-butane-5 %
	Feed inlet temperature (K)	293.15	293.15
	Feed inlet pressure (bara)	21.6	11.6
	Ambient temperature (K)	292.25	292.25
	Ambient pressure (bara)	1.01	1.01
Pipe Characteristics	Length (m)	100	100
	External diameter (mm)	168.6	168.6
	Wall thickness (mm)	7.3	7.3
	Roughness (mm)	0.05	0.05
	Orientation to the horizontal plane (deg)	0	0
Rupture Conditions	Failure mode	FBR	FBR
	Failure location relative to high pressure end (m)	100	100
	Rupture diameter (mm)	-	-
	Discharge coefficient	1	1
Other Parameters	Feed flow rate prior to rupture (m^3/s)	0	0
	Pumping cessation time following pipeline failure (s)	0	0
	Pump shut-off head (bara)	NA	NA
	Grid system used	Simple	Simple
	Number of grid points specified	50	50
	Equation of State	Peng Robinson (Peng and Robinson, 1976)	Peng Robinson (Peng and Robinson, 1976)
	Friction factor correlation	Chen (Chen 1979)	Chen (Chen 1979)
	Heat transfer coefficient (W/m^2K)	Automatically Determined	Automatically Determined
	Total depressurisation time (s)	25	25

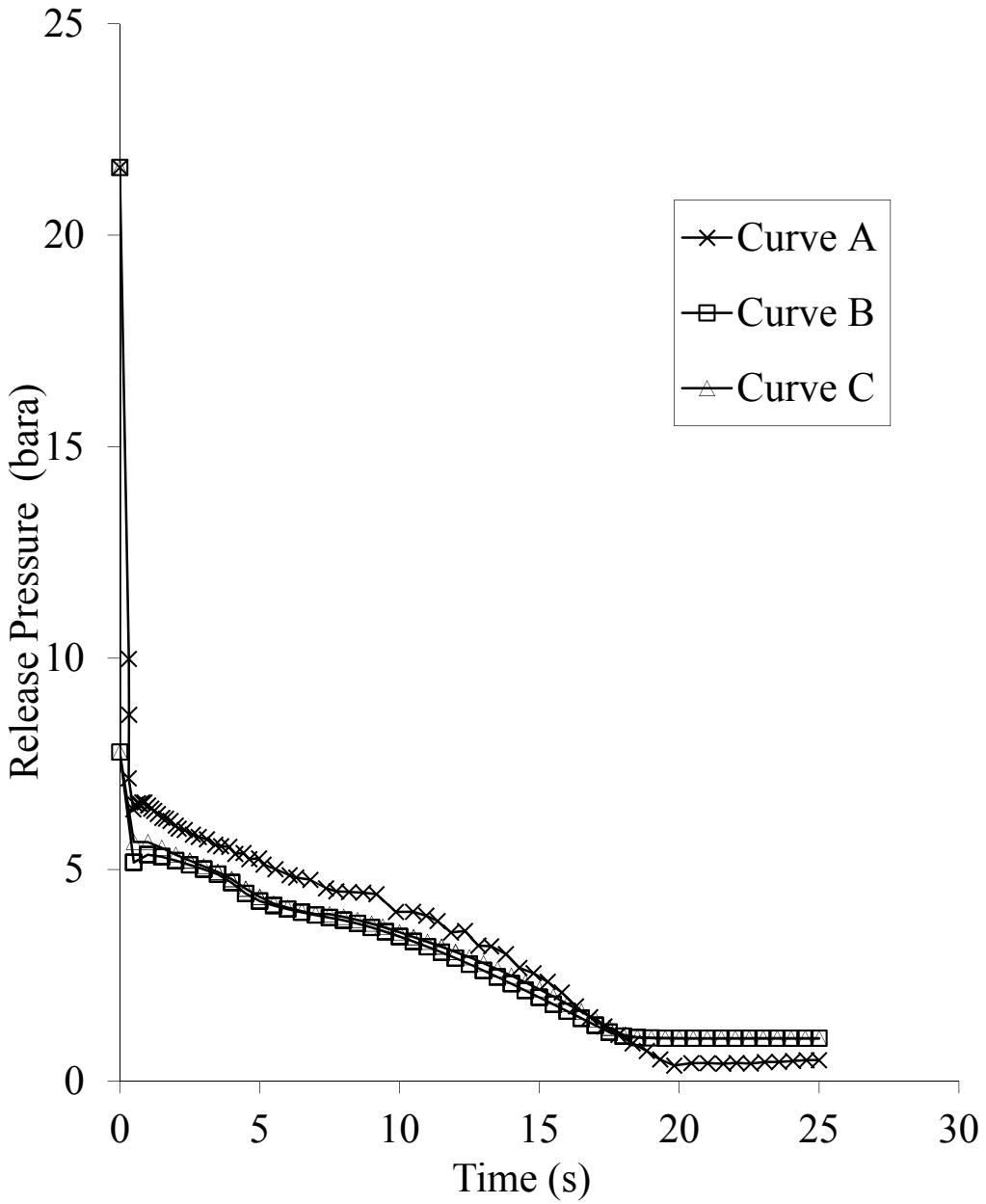

Figure 5.4: Comparison of the measured and simulated variation of open end pressure with time following FBR of Isle of Grain P40 test.

Curve A: Experimental (Richardson and Saville, 1996)

Curve B: PHU, CPU run-time = 585 s

Curve C: PSUC, CPU run-time = 100 s

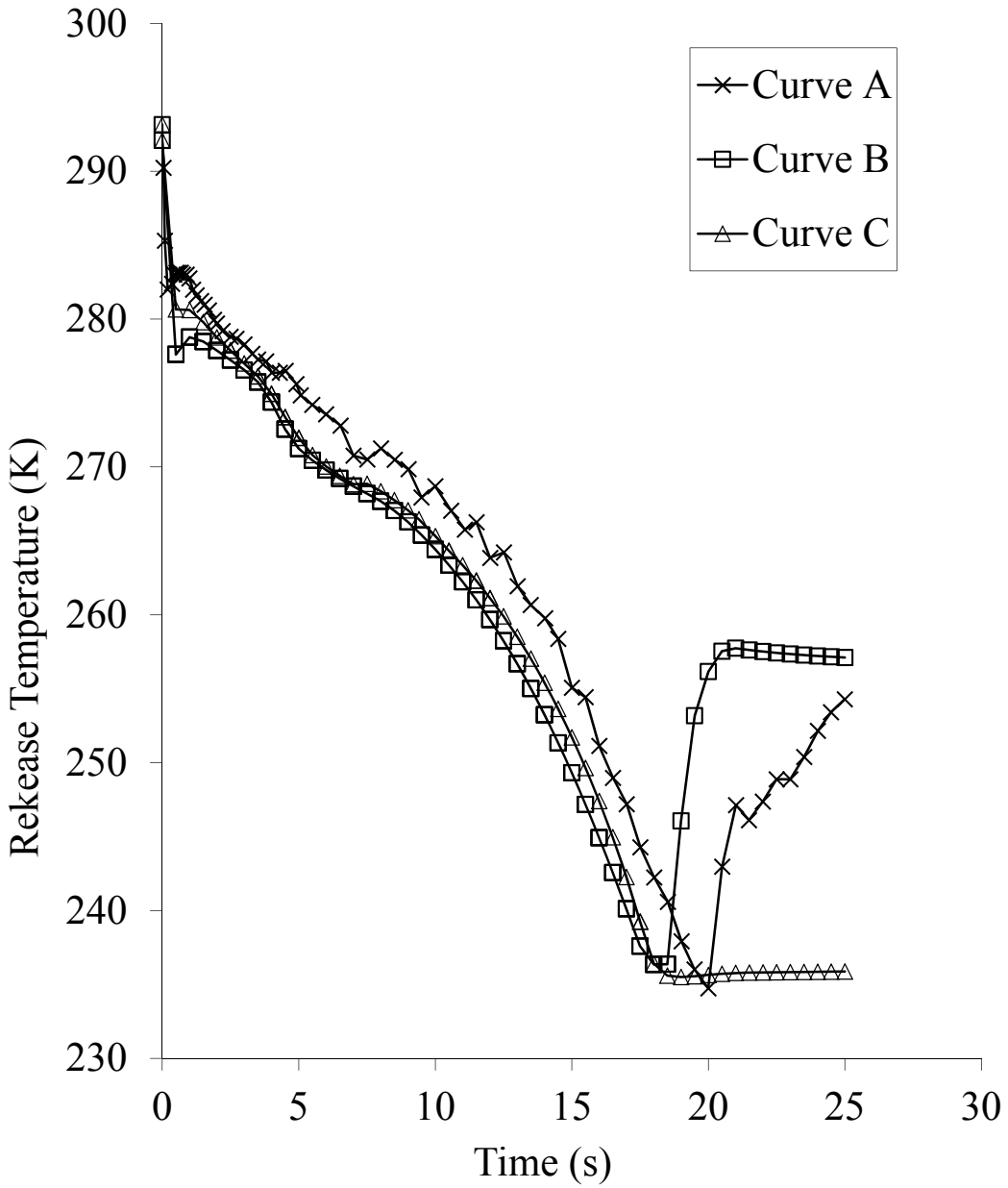

Figure 5.5: Comparison of the measured and simulated variation of open end temperature with time following FBR of Isle of Grain P40 test.

Curve A: Experimental (Richardson and Saville, 1996)

Curve B: PHU, CPU run-time = 585 s

Curve C: PSUC, CPU run-time = 100 s

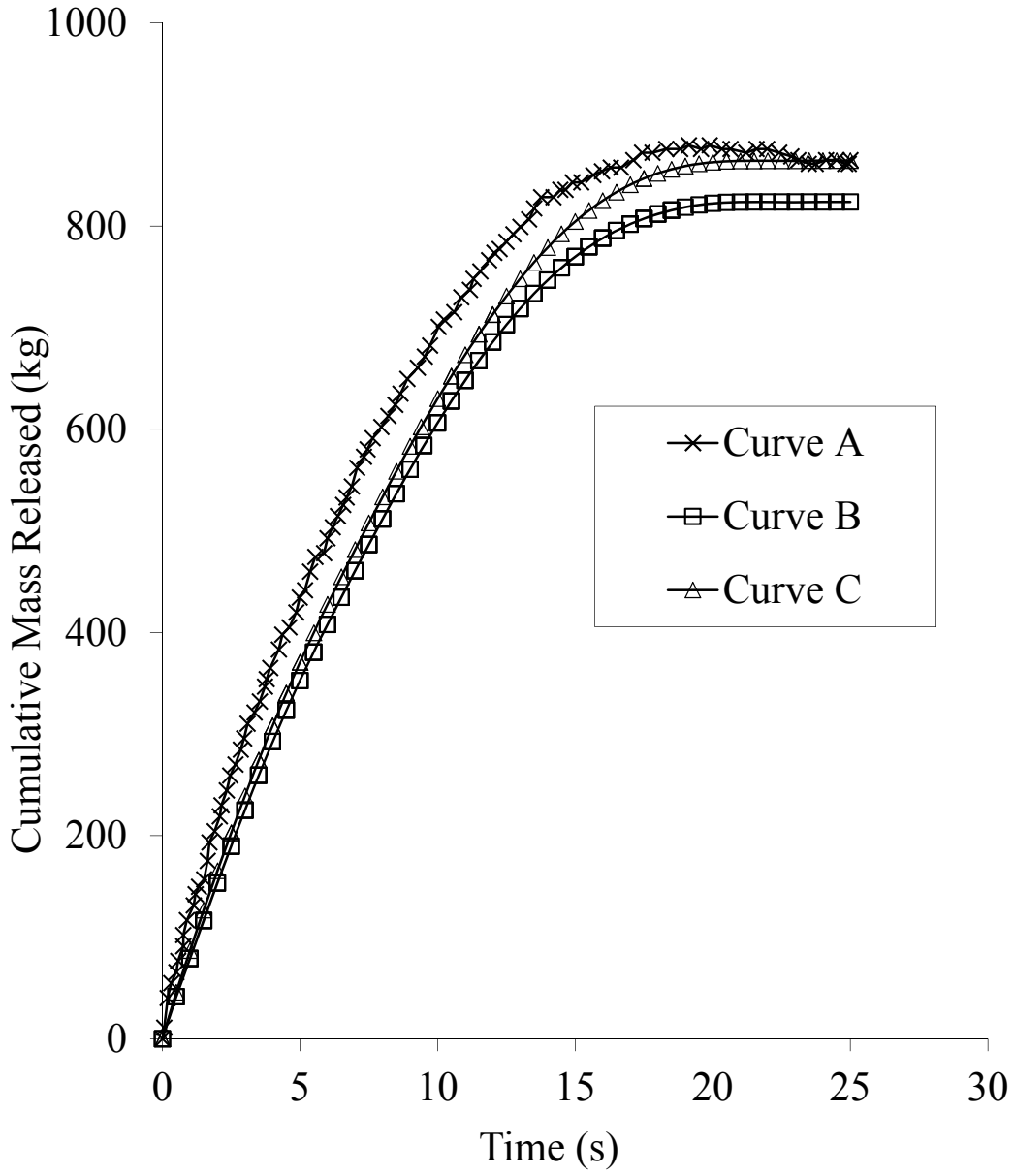

Figure 5.6: Comparison of the measured and simulated variation of commutative mass released with time following FBR of Isle of Grain P40 test. Curve A: Experimental (Richardson and Saville, 1996)

Curve B: PHU, CPU run-time = 585 s

Curve C: PSUC, CPU run-time = 100 s

Brown (2011) reported that FVM predictions for P40 and P42 tests were found to be unstable at the initial time steps due to the rapid discontinuity in the fluid properties. Hence no data is available for FVM relating to P40 and P42.

As can be seen in figures 5.5 and 5.6, both sets of simulated data are in good agreement with one another for most of the depressurisation duration. In figure 5.5, the PSUC prediction (curve C) is in good accord with measurements (curve A) up to the phase transition from two-phase to vapour occurring at approximately 20 s following rupture. Thereafter, in contrast to the PSUC, the measurements and PHU prediction show a temperature recovery. This phenomenon has not been reported by earlier works (see for example Chen, 1993 and Fairuzov, 1998) or indeed observed in the measured data for Isle of Grain P45 puncture test (see figure 5.11). As such it is not certain if the recorded temperature recovery is real or due to an experimental artefact such as the ingress of the warmer surrounding air into the pipeline.

Returning to figure 5.6 showing the variation of cumulative mass released against time, it is noteworthy that after 20 s following rupture, 'negative mass' is being discharged from the pipe (the cumulative mass release declines with time). The above may be attributed to the measurement uncertainty in the load cell, estimated to be ca. ± 5 % (Richardson and Saville, 1996). The corresponding CPU run-time for PHU and PSUC are 585 and 100 s respectively representing ca. 83 % saving in the overall computational run-time when PSUC is employed.

The comparisons of the predicted and measured data for release pressure, release temperature and cumulative mass released against time for the Isle of Grain P42 test are presented in figures 5.7, 5.8 and 5.9 respectively. Curve A represents the measured data whilst curves B and C represent the predicted data obtained from PHU and PSUC respectively.

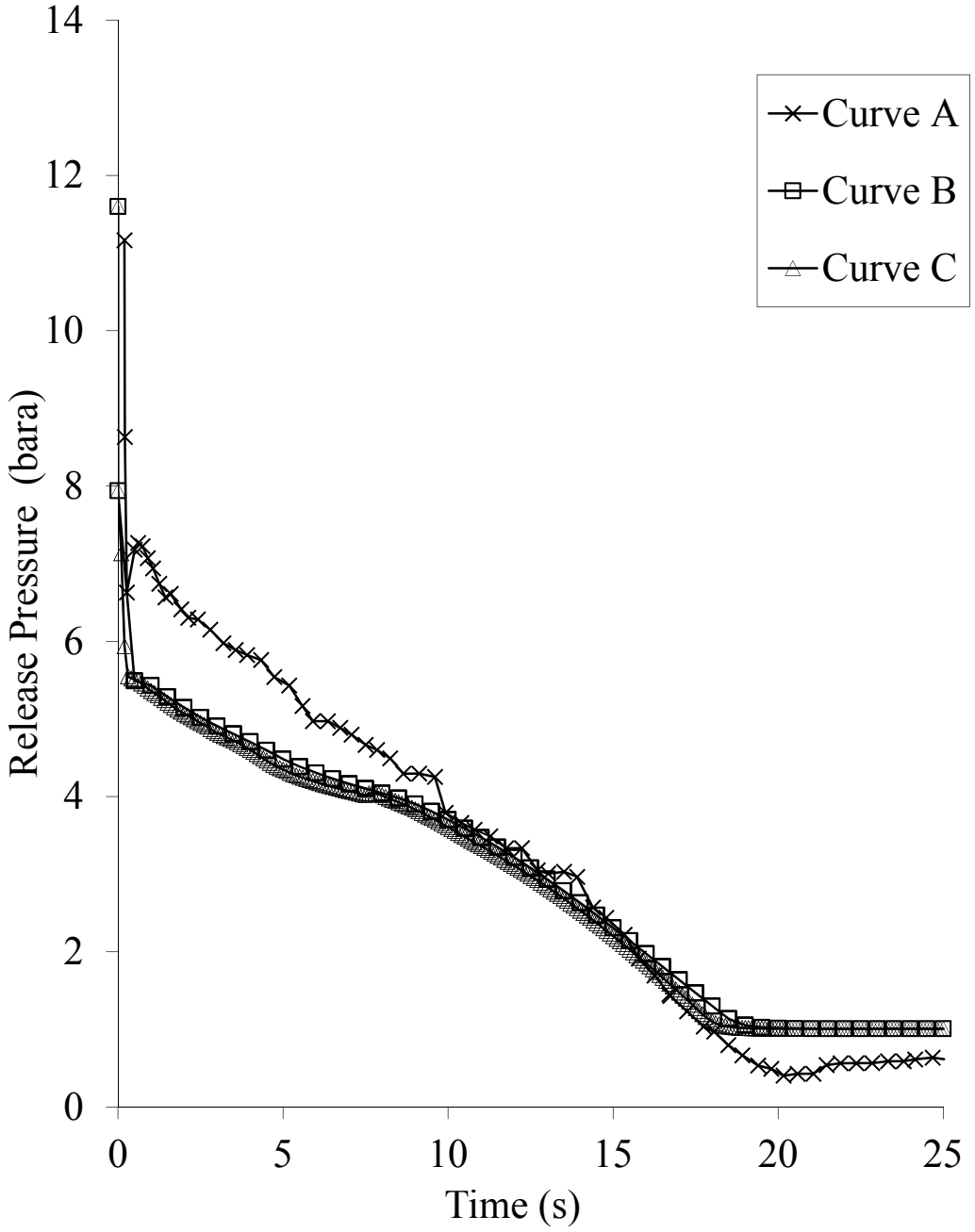

Figure 5.7: Comparison of the measured and simulated variation of open end pressure with time following FBR of Isle of Grain P42 test.

Curve A: Experimental (Richardson and Saville, 1996)

Curve B: PHU, CPU run-time = 578 s

Curve C: PSUC, CPU run-time = 69 s

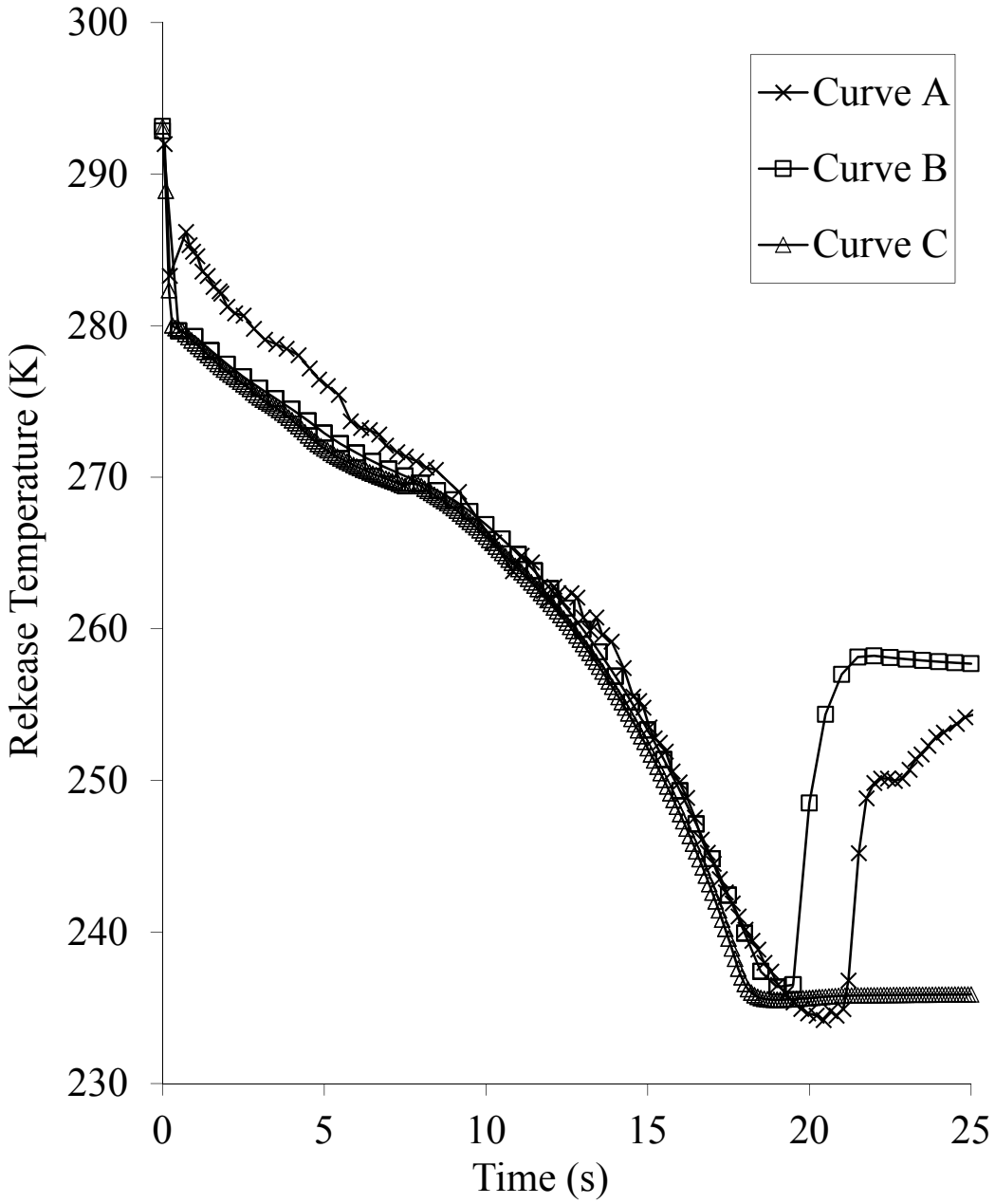

Figure 5.8: Comparison of the measured and simulated variation of open end temperature with time following FBR of Isle of Grain P42 test.

Curve A: Experimental (Richardson and Saville, 1996)

Curve B: PHU, CPU run-time = 578 s

Curve C: PSUC, CPU run-time = 69 s

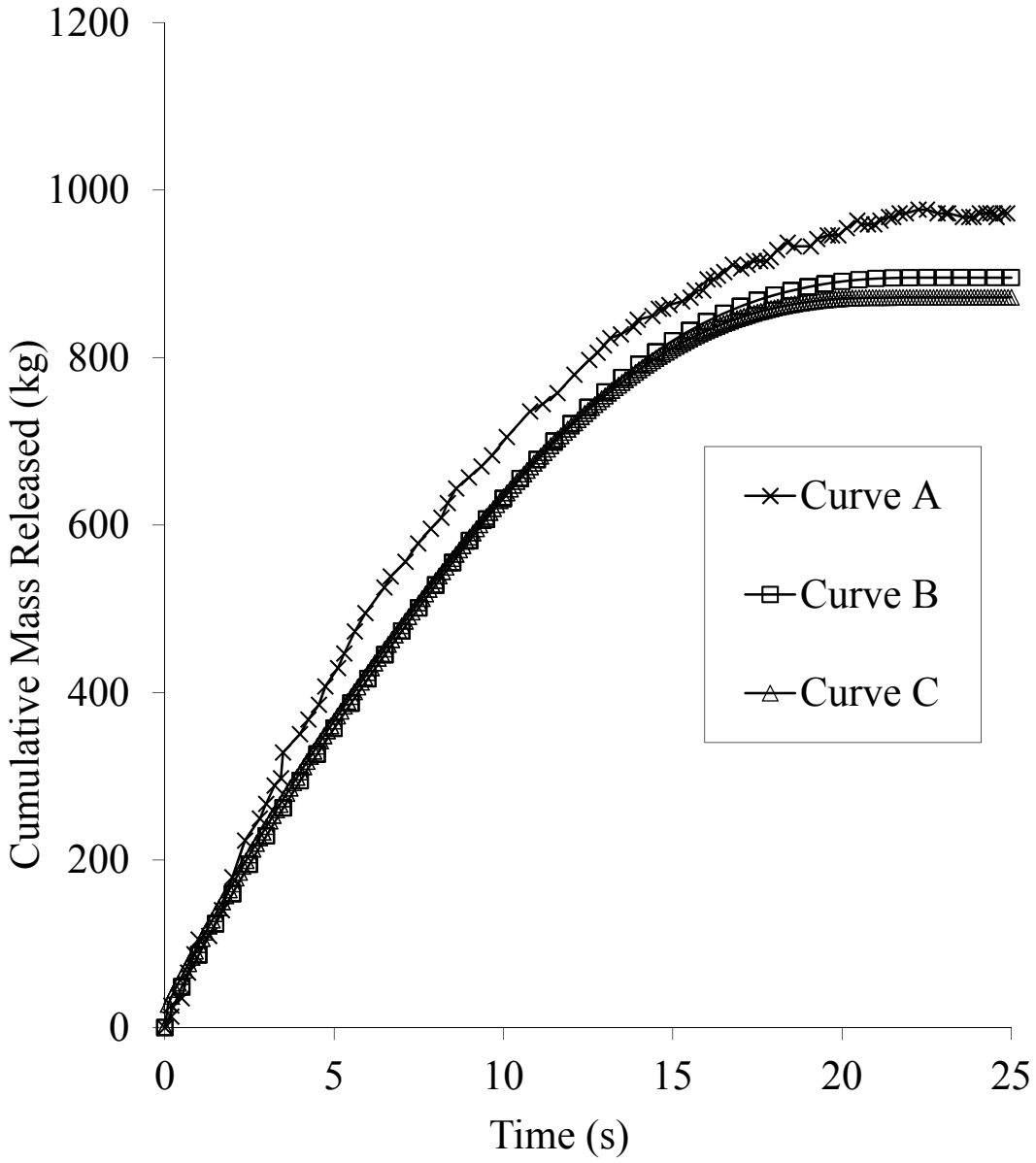

Figure 5.9: Comparison of the measured and simulated variation of commutative mass released with time following FBR of Isle of Grain P42 test. Curve A: Experimental (Richardson and Saville, 1996)

Curve B: PHU, CPU run-time = 578 s

Curve C: PSUC, CPU run-time = 69 s

As it may be observed from the above figures, the model predictions are in reasonably good agreement with measured data. Similarly, as seen in figure 5.4, an under-prediction of the release pressure (curves B and C) during the early stage of depressurisation is observed. The corresponding CPU run-times for PHU and PSUC are 578 and 69 s respectively. This represents ca. 88 % saving in CPU run-time.

5.6.2 Puncture

In this section, the PSUC is validated against Isle of Grain P45 and P47 puncture tests. The inventory, pipeline characteristics and prevailing conditions used for simulation of the P45 and P47 tests are presented in table 5.5. Due to the uncertainty in the measurements, the effective orifice diameters for P45 and P47 tests are adopted as 95 and 70 mm respectively (Richardson and Saville, 1996). Additionally, a discharge coefficient of 0.8 is assumed based on experimental findings of Haque et al. (1992b).

Figures 5.10 and 5.11 respectively present the comparison of release (open end) pressure, release (open end) temperature between the simulated and measured data for P45 puncture test. The corresponding data for test P47 is presented in figures 5.12 and 5.13. In all the cases, curve A represents measured data, while curves B, C and D show the predicted data obtained from PHU, FVM and PSUC respectively.

As it may be seen from figures 5.10 -13, all model predictions are in reasonably good agreement with measurements during most of the depressurisation period, following similar trends for both P45 and P47 tests. Referring to figure 5.13, 120 s post depressurisation, the measured release temperature indicates a temperature recovery similar to that observed by PHU data (curve B) whilst the same trend is not seen in

FVM and PSUC predictions. The reason for this discrepancy is not clear considering that the temperature recovery is not observed for P45 test.

The corresponding CPU run-time of P45 test for PHU, FVM and PSUC are 695 s, 694 s and 80 s respectively. Based on the above, employing PSUC results in a saving of ca. 88% in the computational run-time when compared to PHU.

Similarly, the corresponding CPU run-time of P47 test for PHU, FVM and PSUC are 1,305 s, 1,625 s and 133 s respectively. Based on the above, employing PSUC results in a saving of ca. 90% in the computational run-time when compared to PHU.

Table 5.5: Shows the pipeline characteristics and prevailing conditions used for simulation of Isle of Grain P45 and P47 (Richardson and Saville, 1996).

Input		Isle of Grain P45	Isle of Grain P47
Inlet Parameters	Number of components	2	2
	Feed composition (mole %)	propane- 95 %	propane- 95 %
		n-butane-5 %	n-butane-5 %
	Feed inlet temperature (K)	290.45	288.75
	Feed inlet pressure (bara)	11.4	21.6
	Ambient temperature (K)	292.25	291.75
	Ambient pressure (bara)	1.01	1.01
Pipe Characteristics	Length (m)	100	100
	External diameter (mm)	168.6	168.6
	Wall thickness (mm)	7.3	7.3
	Roughness (mm)	0.05	0.05
	Orientation to the horizontal plane (deg)	0	0
Rupture Conditions	Failure mode	Puncture	Puncture
	Failure location relative to high pressure end (m)	100	100
	Puncture (orifice) diameter (mm)	95	70
	Discharge coefficient	0.8	0.8
Other Parameters	Feed flow rate prior to rupture (m^3/s)	0	0
	Pumping cessation time following pipeline failure (s)	0	0
	Pump shut-off head (bara)	NA	NA
	Grid system used	Simple	Simple
	Number of grid points specified	50	50
	Equation of State	Peng Robinson (Peng and Robinson, 1976)	Peng Robinson (Peng and Robinson, 1976)
	Friction factor correlation	Chen (Chen 1979)	Chen (Chen 1979)
	Heat transfer coefficient (W/m^2K)	Automatically Determined	Automatically Determined
	Total depressurisation time (s)	65	150

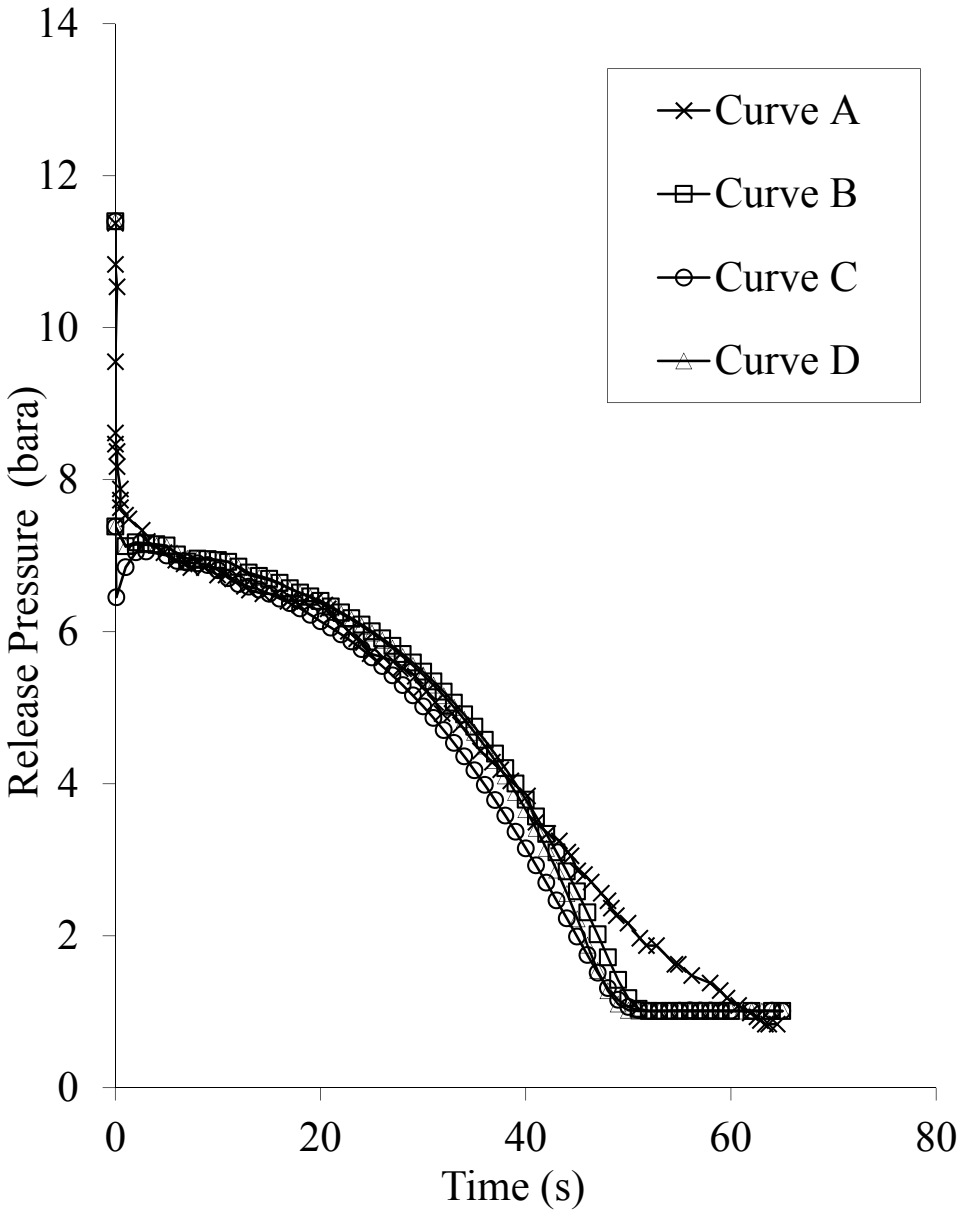

Figure 5.10: Comparison of the measured and simulated variation of open end pressure with time following puncture at the end (P45 test).

Curve A: Experimental (Richardson and Saville, 1996)

Curve B: PHU, CPU run-time = 695 s

Curve C: FVM, CPU run-time = 694 s (Brown, 2011)

Curve D: PSUC, CPU run-time = 80 s

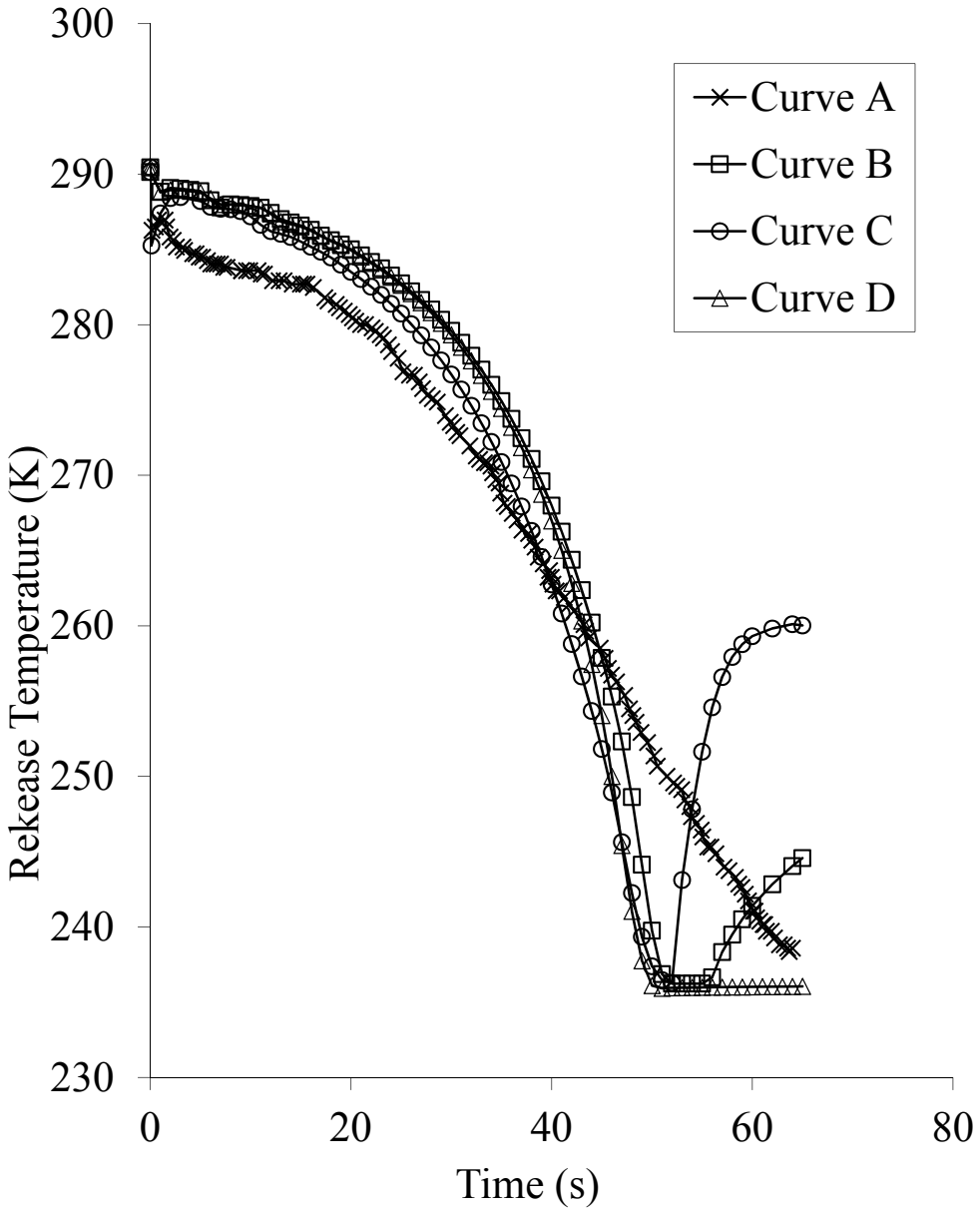

Figure 5.11: Comparison of the measured and simulated variation of open end temperature with time following puncture at the end (P45 test).

Curve A: Experimental (Richardson and Saville, 1996)

Curve B: PHU, CPU run-time = 695 s

Curve C: FVM, CPU run-time = 694 s (Brown, 2011)

Curve D: PSUC, CPU run-time = 80 s

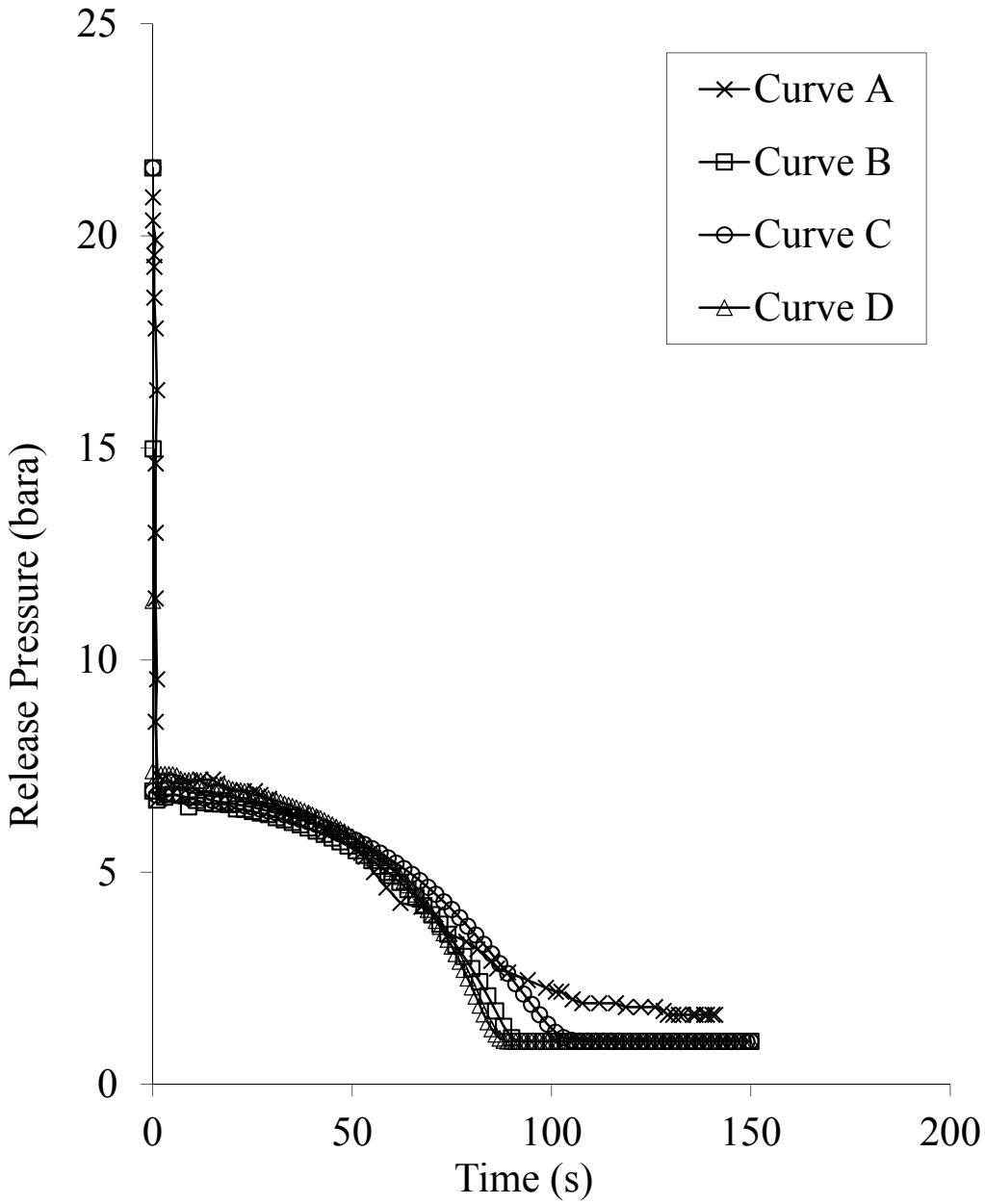

Figure 5.12: Comparison of the measured and simulated variation of open end pressure with time following puncture at the end (P47 test).

Curve A: Experimental (Richardson and Saville, 1996)

Curve B: PHU, CPU run-time = 1,305 s

Curve C: FVM, CPU run-time = 1,625 s (Brown, 2011)

Curve D: PSUC, CPU run-time = 133 s

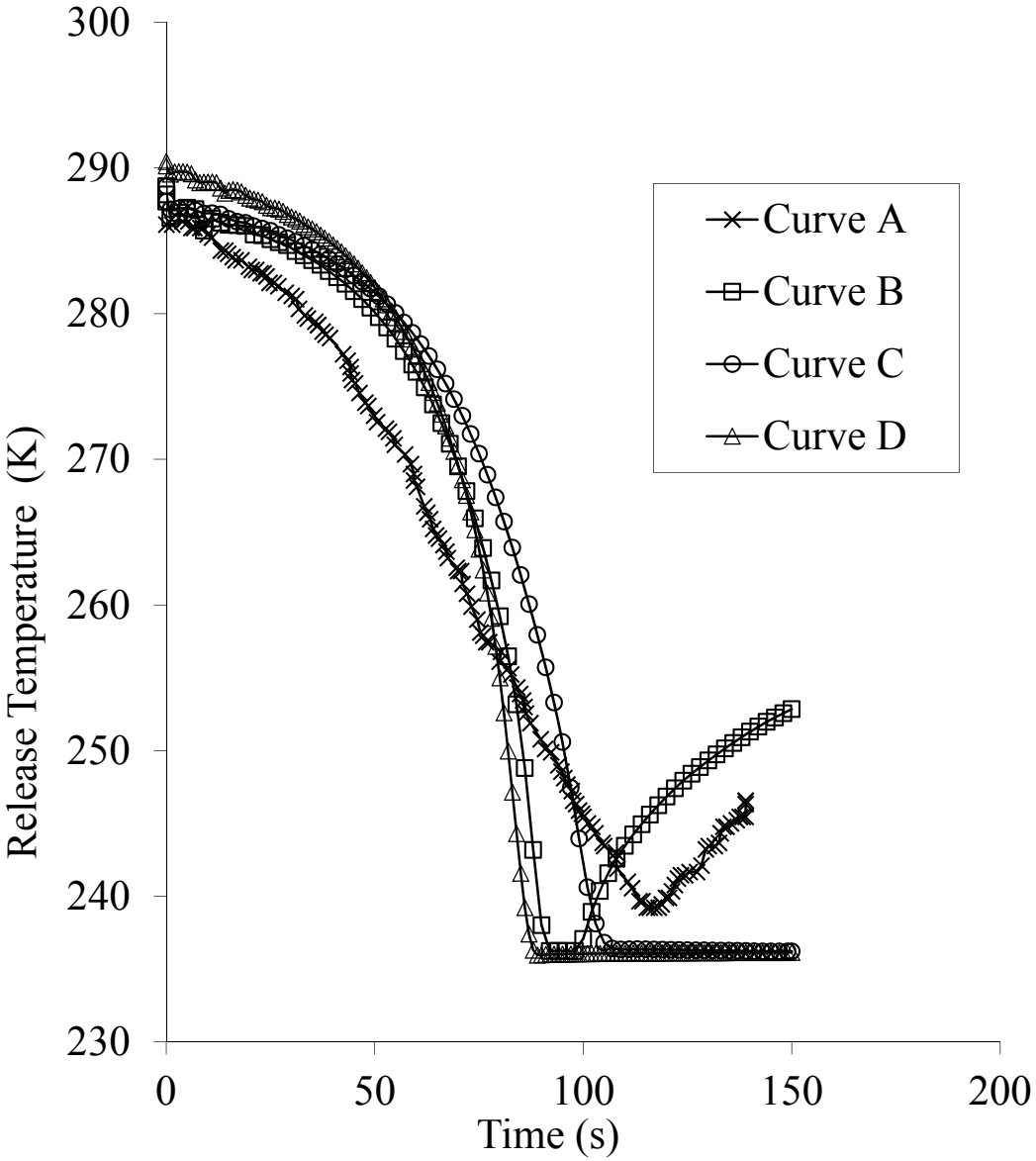

Figure 5.13: Comparison of the measured and simulated variation of open end temperature with time following puncture at the end (P47 test).

Curve A: Experimental (Richardson and Saville, 1996)

Curve B: PHU, CPU run-time = 1,305 s

Curve C: FVM, CPU run-time = 1,625 s (Brown, 2011)

Curve D: PSU, CPU run-time = 133 s

5.7 Verification Case Study

In the preceding section, the PSUC model was validated against a series of available experimental data. In the following, the performance of the PSUC based on comparison against predictions of the PHU and FVM for series of verification case studies is assessed. These simulations are based on the failure of a hypothetical 1 km pipeline containing both permanent gas and two-phase inventories. Pressurised liquid pipelines are of no concern in this study given the almost instantaneous depressurisation to ambient conditions upon failure. The corresponding pipeline characteristics and prevailing conditions for these investigations are given in table 5.6.

5.6.3 Permanent Gas

Variation of predicted release pressure, temperature and discharge rate against depressurisation time for the puncture type failure are respectively presented in figures 5.14-16. The pipeline is assumed to contain a mixture of methane and ethane at 60 barg. Under the conditions given in table 5.6 for case of permanent gas, the inventory will remain in gaseous phase for the entire duration of the depressurisation. Curve C represents PSUC predictions whilst curves A and B represent PHU and FVM predictions respectively. Similarly, the variation of predicted release pressure, temperature and discharge rate against depressurisation time for FBR failure are presented in figures 5.17-19 respectively.

As can be seen from figures 5.14-19, with the exception of the release temperature in figure 5.18, all three sets of predictions are in excellent agreement showing no discernible differences. As it may be observed in figure 5.18, the release plane temperature follows a large initial drop in temperature followed by recovery stage.

The PHU and PSUC predictions exhibit similar trends. The release temperature as predicted by PSUC are ca. 2 K higher than PHU while FVM predictions are greater by ca. 12 K compared to PSUC. Brown (2011) did not provide an explanation for the relatively large disagreement with the PHU predictions. After the initial temperature recovery, PHU and PSUC predict a steady drop in temperature whereas FVM prediction of the release temperature remains almost constant. This is then followed by second temperature recovery stage at ca. 35 s following depressurisation during which PSUC continues to over-predict the release temperature by ca. 2 k as compared to PHU.

In terms of computational run-time for puncture case, the corresponding CPU run-times for PHU, FVM and PSU are 439, 1,255 and 86 s respectively. Hence PSUC results in approximately 80% saving in CPU time as compared to PHU. The corresponding CPU run-times relating to FBR case for PHU, FVM and PSU are 377, 366 and 100 s respectively. This equates to ca. 73% saving in CPU run-time when compared to PHU.

Table 5.6: Shows the pipeline characteristics and prevailing conditions used for failure of a hypothetical pipeline.

Input		Full Bore Rupture	Puncture
Inlet Parameters	**Permanent Gas Inventory**		
	Feed composition (mole %)	methane- 95 %	methane- 95 %
		ethane-5 %	ethane-5 %
	Two-phase Inventory		
	Feed composition (mole %)	methane 50% n-butane 50%	methane 50% n-butane 50%
	Feed inlet temperature (K)	293.15	293.15
	Feed inlet pressure (bara)	60	60
	Ambient temperature (K)	293.15	293.15
	Ambient pressure (bara)	1.01	1.01
Pipe Characteristics	Length (m)	1000	1000
	External diameter (mm)	168.6	168.6
	Wall thickness (mm)	7.3	7.3
	Roughness (mm)	0.05	0.05
	Orientation to the horizontal plane (deg)	0	0
Rupture Conditions	Failure mode	FBR	Puncture along the length
	Failure location relative to high pressure end (m)	1000	500
	Puncture (orifice) diameter (mm)	154	50
	Discharge coefficient	1	1
Other Parameters	Feed flow rate prior to rupture (m^3/s)	0	0
	Pumping cessation time following pipeline failure (s)	0	0
	Pump shut-off head (bara)	NA	NA
	Grid system used	Simple	Simple
	Number of grid points specified	250	250
	Equation of State	Peng Robinson	Peng Robinson
	Friction factor correlation	Chen	Chen
	Heat transfer coefficient (W/m^2K)	Automatically Determined	Automatically Determined
	Total depressurisation time (s)	60	60

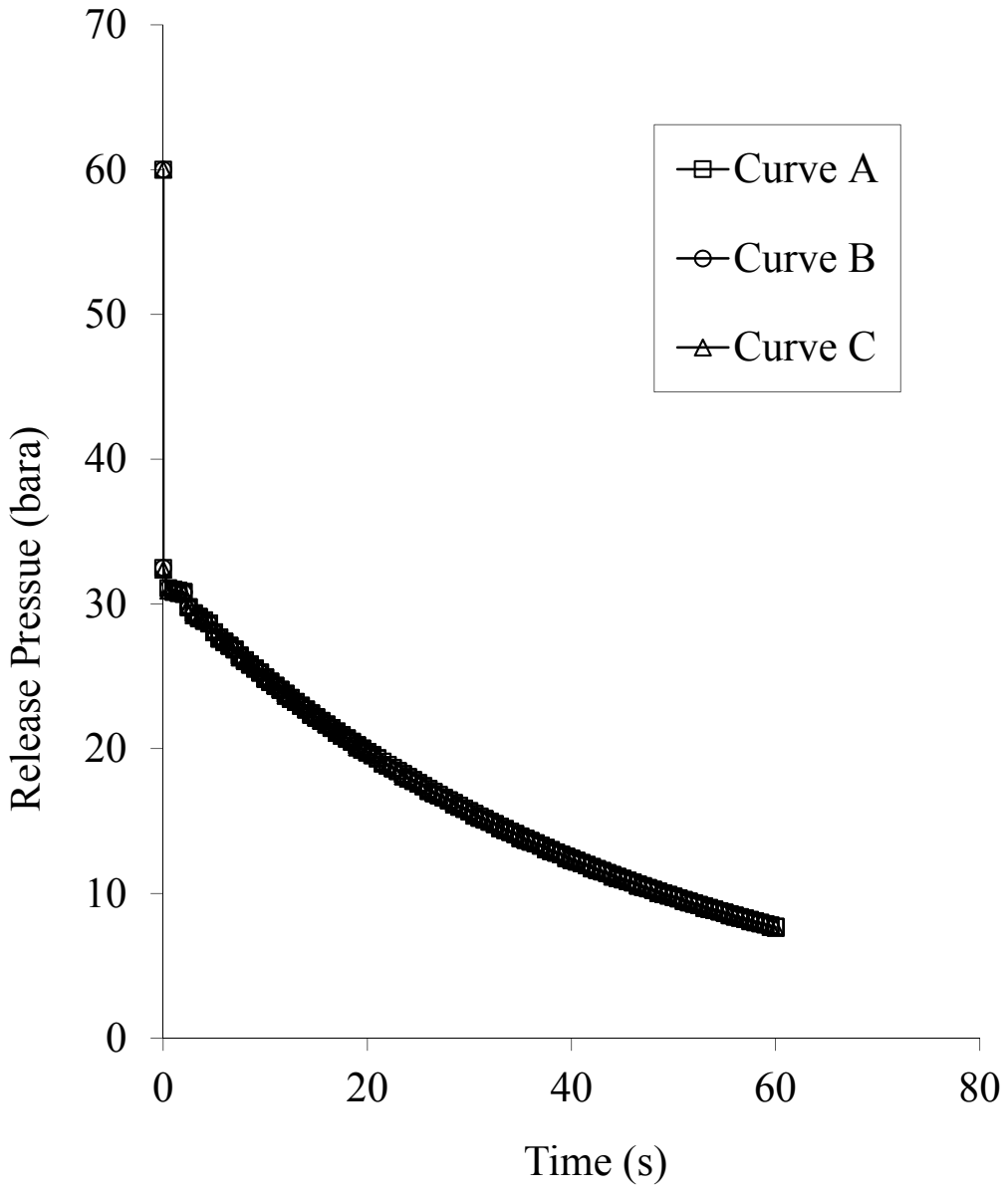

Figure 5.14: Variation of release pressure against depressurisation time of the pipeline with permanent gas inventory following puncture along the length.

Curve A: PHU, CPU run-time = 439 s

Curve B: FVM, CPU run-time = 1,255 s

Curve C: PSUC, CPU run-time =86 s

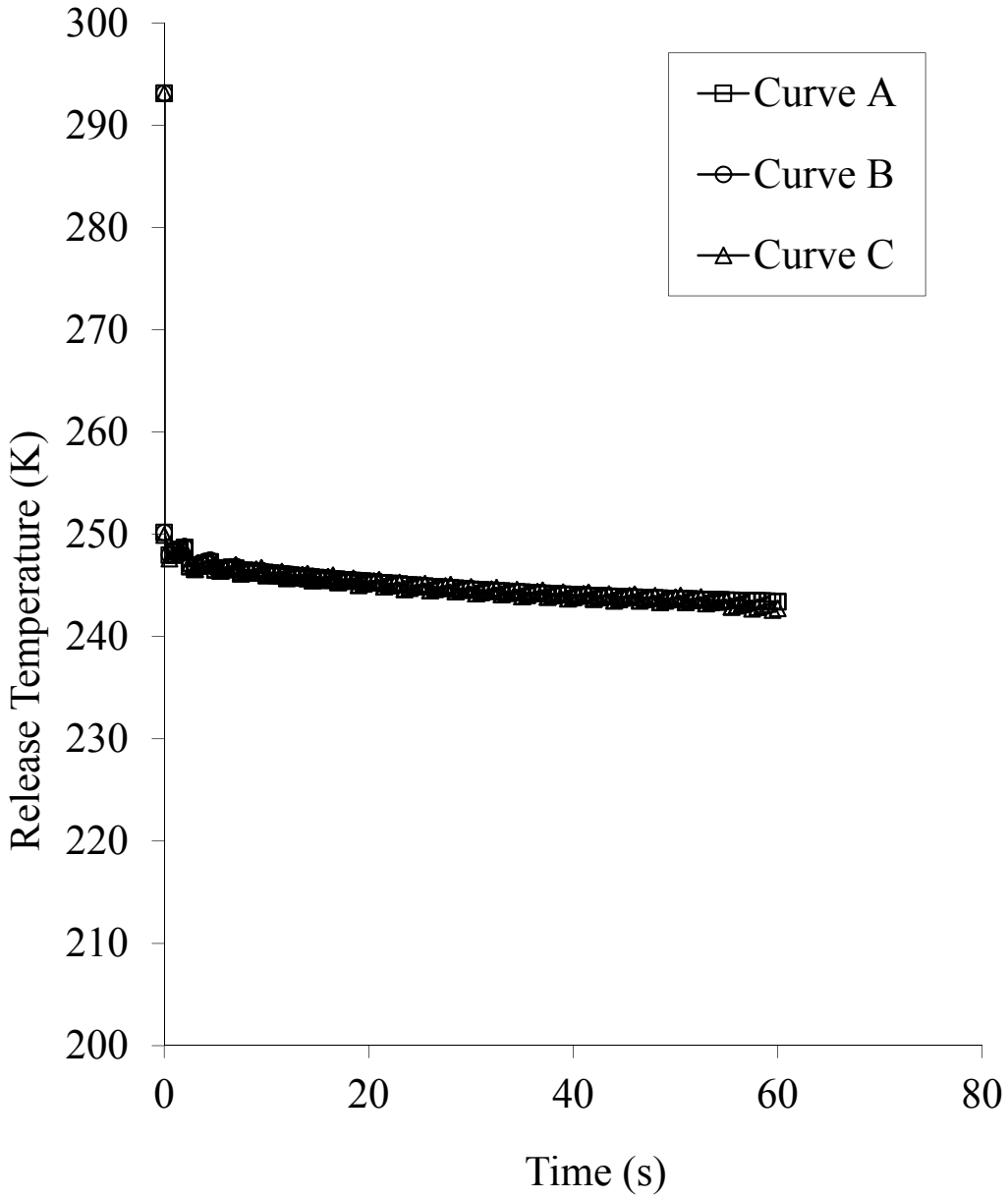

Figure 5.15: Variation of release temperature against depressurisation time of the pipeline with permanent gas inventory following puncture along the length.

Curve A: PHU, CPU run-time = 439 s

Curve B: FVM, CPU run-time = 1,255 s

Curve C: PSUC, CPU run-time = 86 s

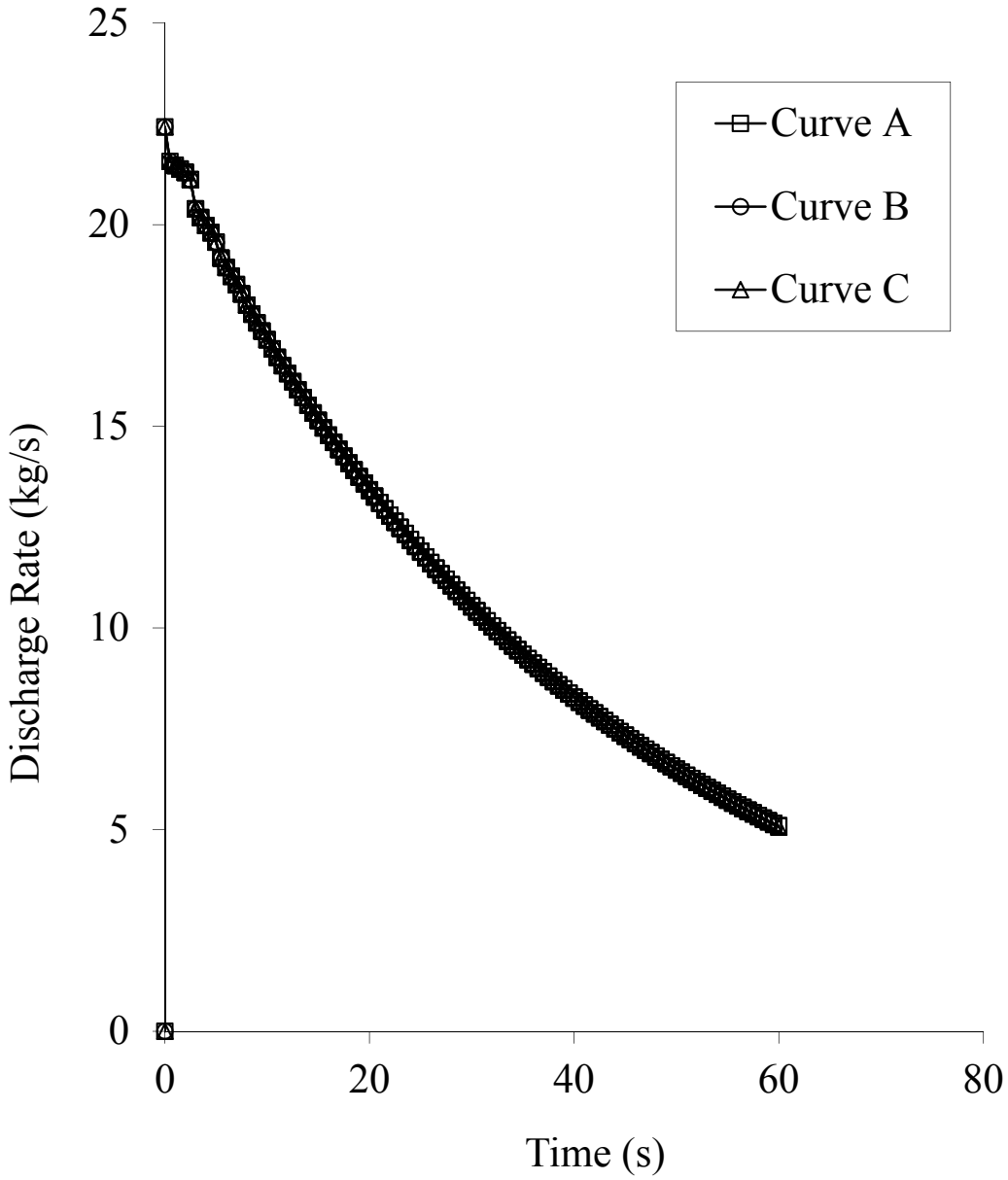

Figure 5.16: Variation of discharge rate against depressurisation time of the pipeline with permanent gas inventory following puncture along the length.

Curve A: PHU, CPU run-time = 439 s

Curve B: FVM, CPU run-time = 1,255 s

Curve C: PSUC, CPU run-time =86 s

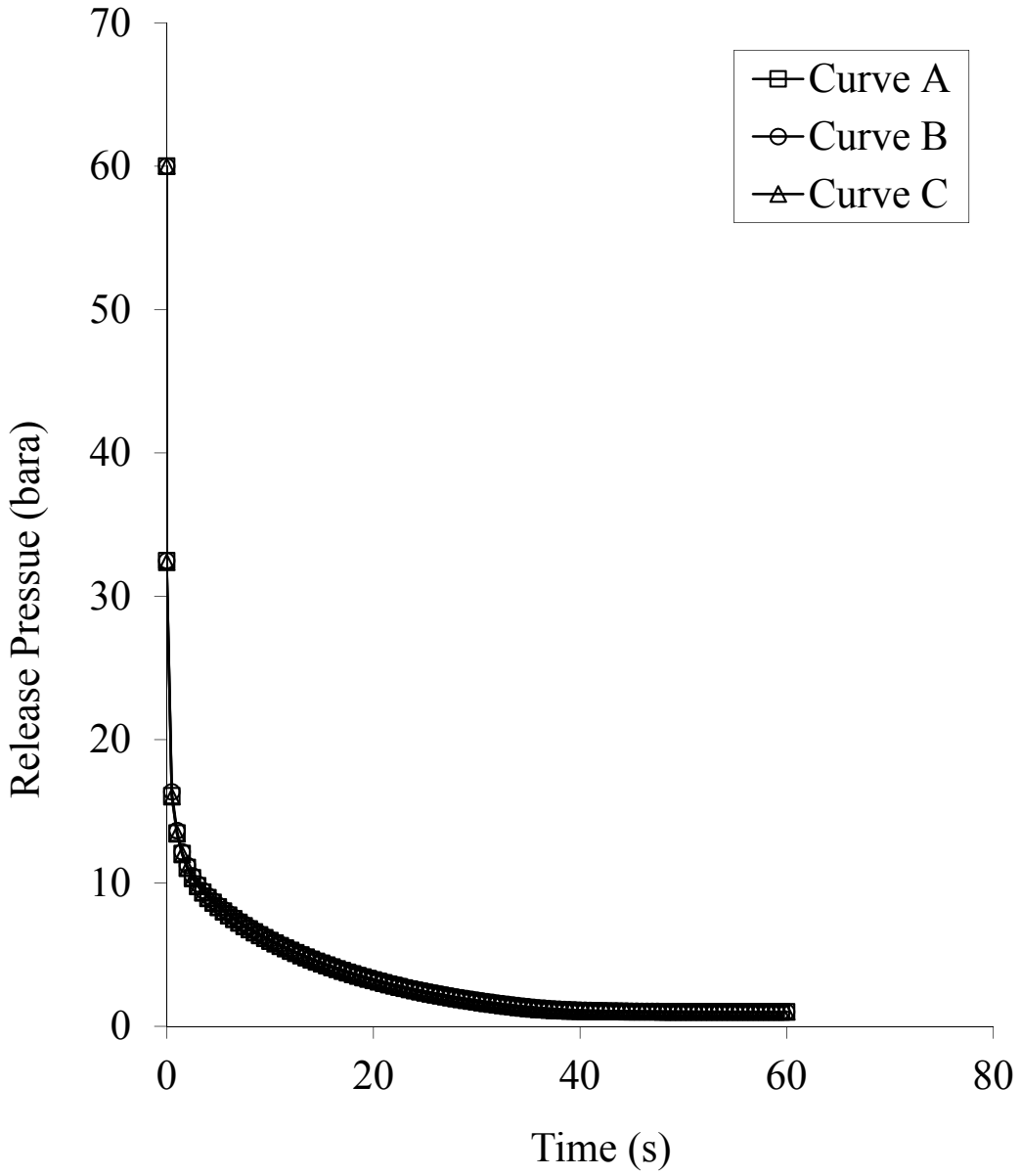

Figure 5.17: Variation of release pressure against depressurisation time of the pipeline with permanent gas inventory following FBR.

Curve A: PHU, CPU run-time = 377 s

Curve B: FVM, CPU run-time = 366 s

Curve C: PSUC, CPU run-time =100 s

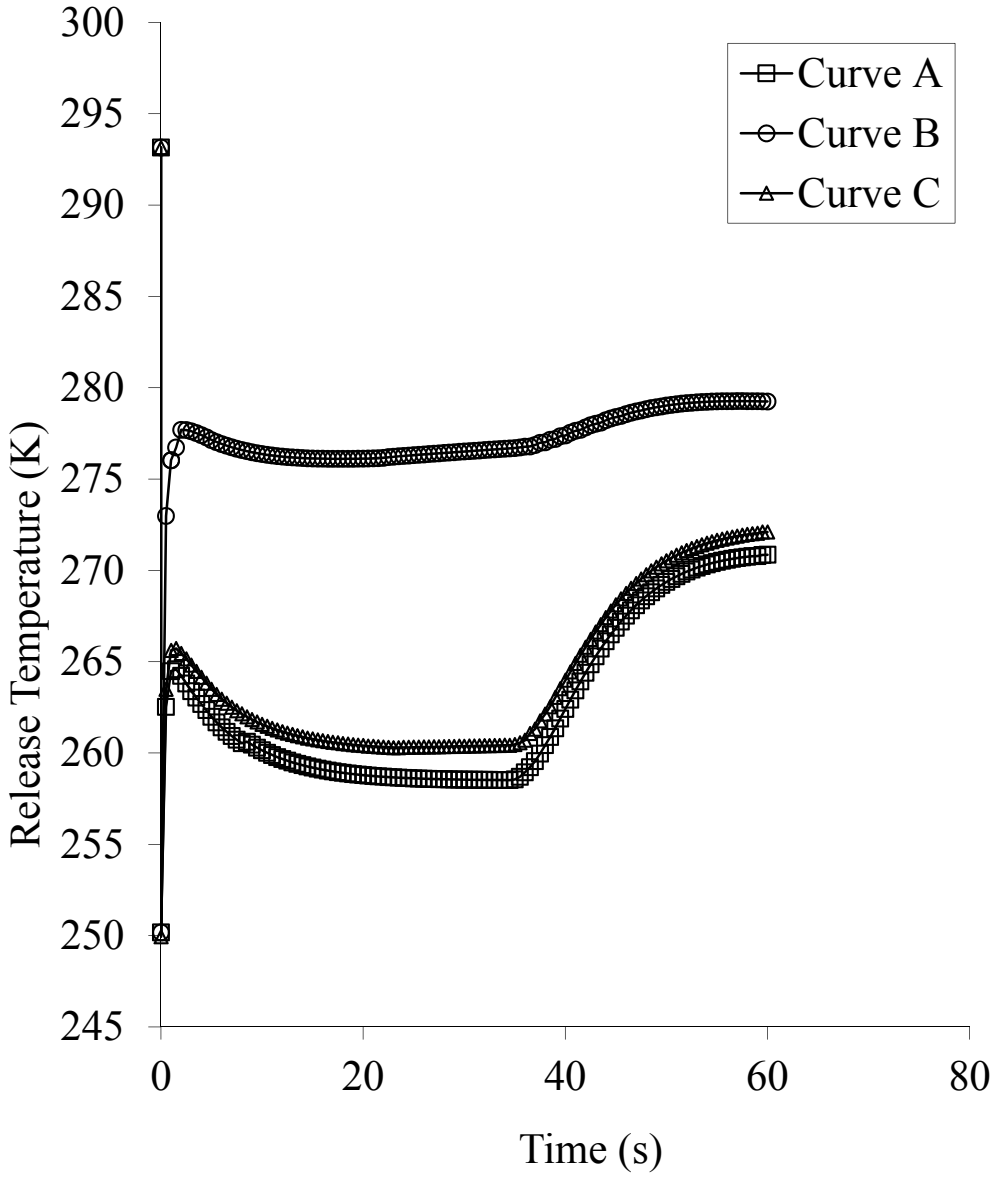

Figure 5.18: Variation of release temperature against depressurisation time of the pipeline with permanent gas inventory following FBR.

Curve A: PHU, CPU run-time = 377 s

Curve B: FVM, CPU run-time = 366 s

Curve C: PSUC, CPU run-time =100 s

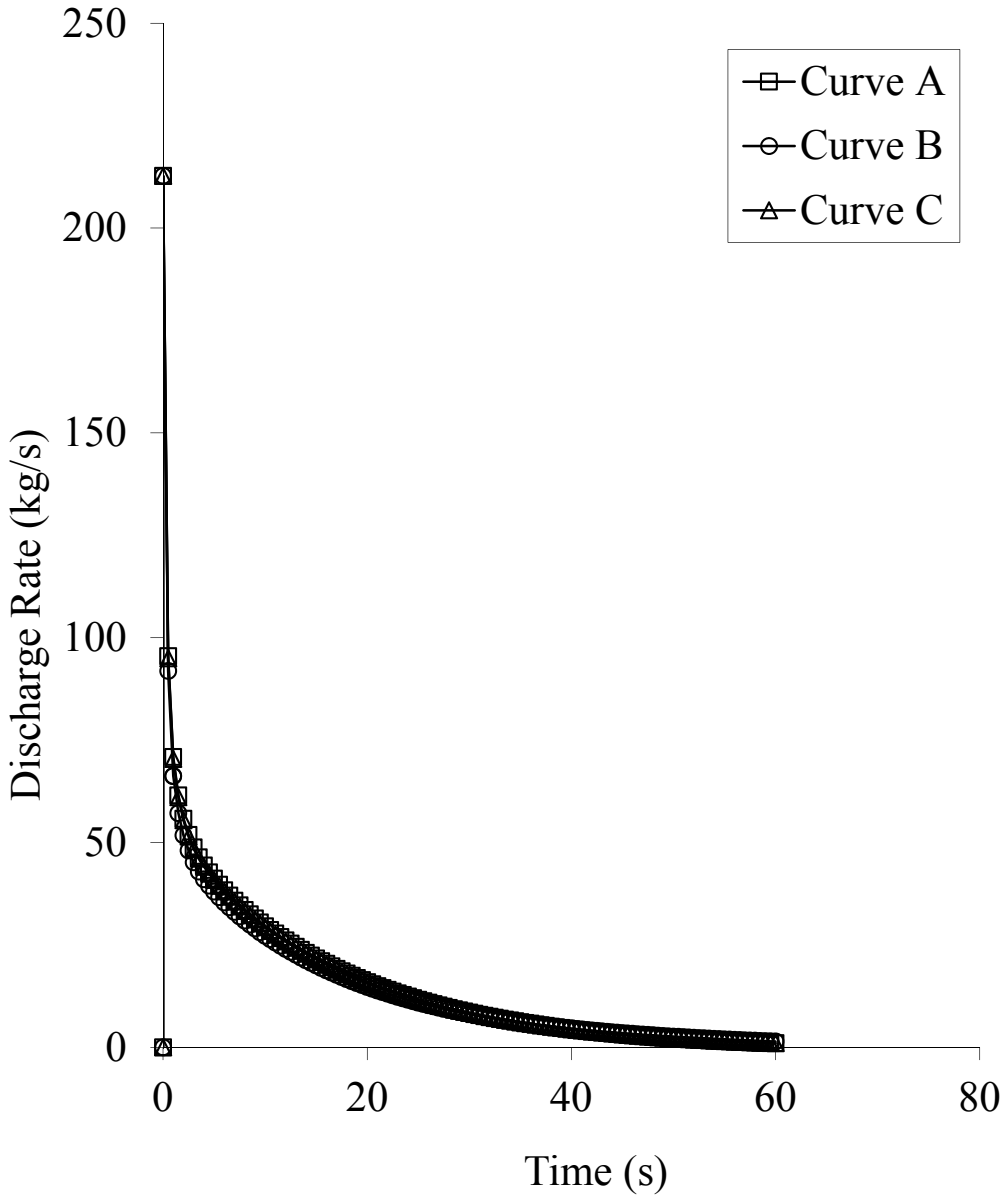

Figure 5.19: Variation of discharge rate against depressurisation time of the pipeline with permanent gas inventory following FBR.

Curve A: PHU, CPU run-time = 377 s

Curve B: FVM, CPU run-time = 366 s

Curve C: PSUC, CPU run-time =100 s

5.6.4 Two-phase Mixture

Variation of predicted release pressure, temperature and discharge rate against depressurisation time for the puncture failure are respectively presented in figures 5.20-22. The pipeline is assumed to contain a mixture of 50% methane and 50% n-butane at 60 barg. Under the conditions given in table 5.6, for case of two-phase inventory, the mixture remains in the two-phase state for the entire duration of the depressurisation. Curves A and B represent PHU and FVM predictions respectively while curve C represents PSUC predictions. Likewise, the variation of predicted release pressure, temperature and discharge rate against depressurisation time for FBR type failure are presented in figures 5.23-25 respectively.

As can be seen from figures 5.20-25, with the exception of the release temperature in figure 5.24, all three sets of predictions are also in excellent agreement showing no discernible differences. The predicted release temperature PSUC exhibits the same trend as predicted by PHU while FVM almost consistently over predicts the release temperature. The stepwise changes in release temperature in figure 5.21 is normally observed in puncture simulation and is due to the expansion and reflection waves formed after the failure. This behaviour is affected by several factors including the length of the pipe, inventory and the fact that for puncture simulations, the expansion and reflection waves die out considerably slower than the case of full bore rupture.

In terms of computational run-time, the corresponding CPU run-time of the puncture case for PHU, FVM and PSUC are 375, 874 and 64 s respectively. Hence the use of PSUC results in ca. 83% saving on CPU run-time when compared to PHU. The corresponding CPU times relating to FBR case for PHU, FVM and PSUC are 348, 274 and 81 s respectively resulting in ca. 77% reduction in CPU run-time as compared to PHU.

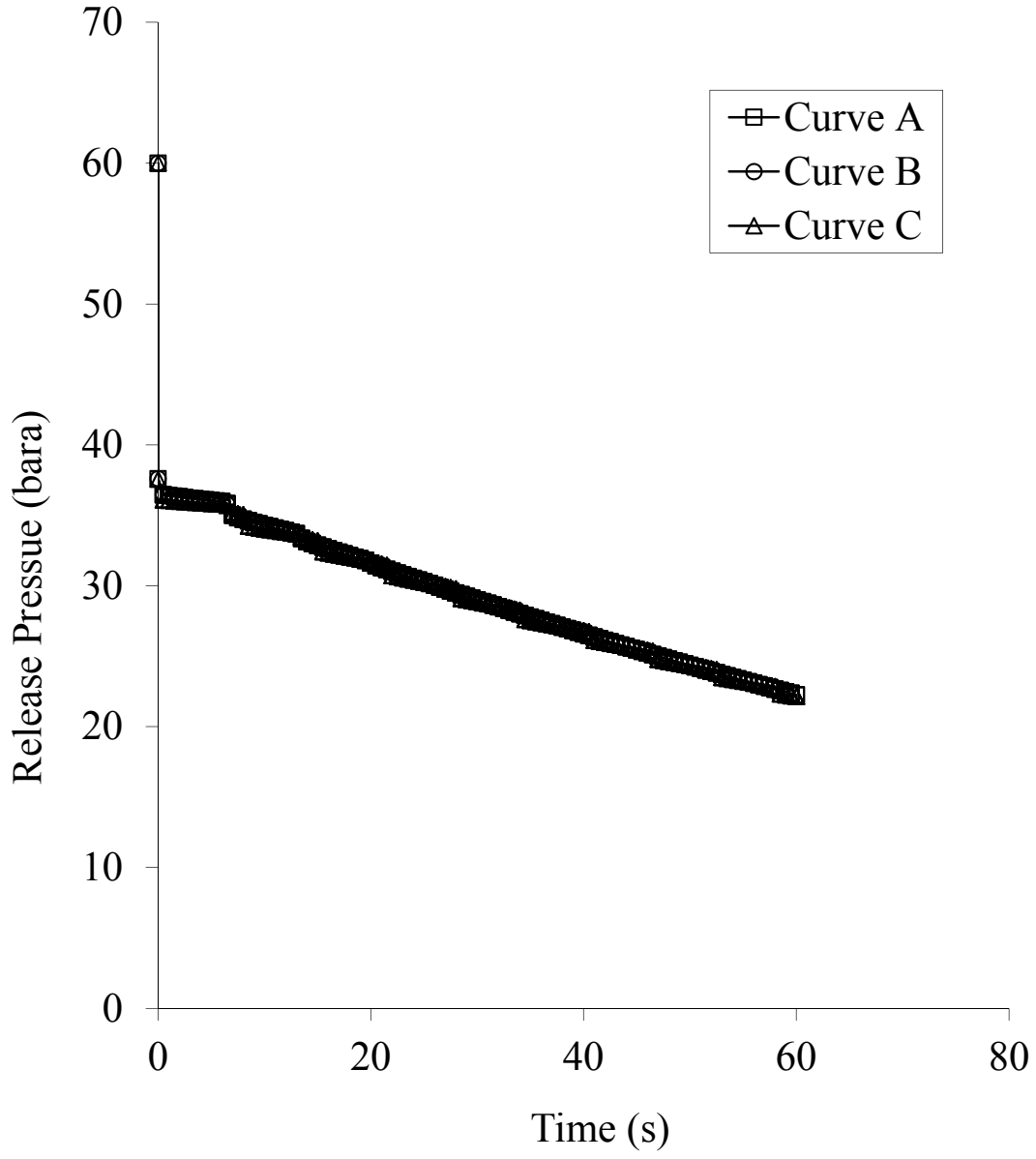

Figure 5.20: Variation of release pressure against depressurisation time of the pipeline with two-phase inventory following puncture along the length.

Curve A: PHU, CPU run-time = 375 s

Curve B: FVM, CPU run-time = 874 s

Curve C: PSUC, CPU run-time = 64 s

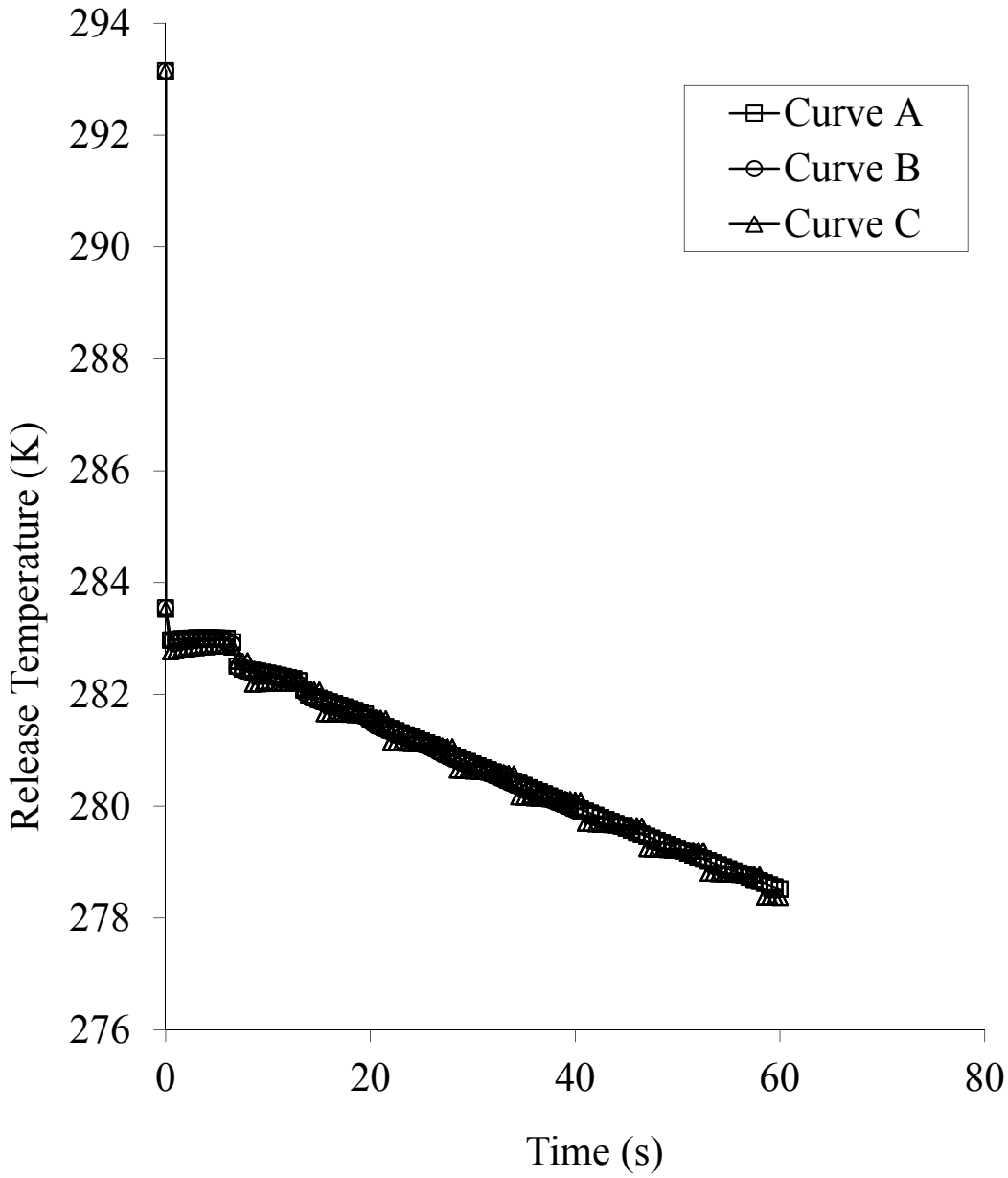

Figure 5.21: Variation of release temperature against depressurisation time of the pipeline with two-phase inventory following puncture.

Curve A: PHU, CPU run-time = 375 s

Curve B: FVM, CPU run-time = 874 s

Curve C: PSUC, CPU run-time = 64 s

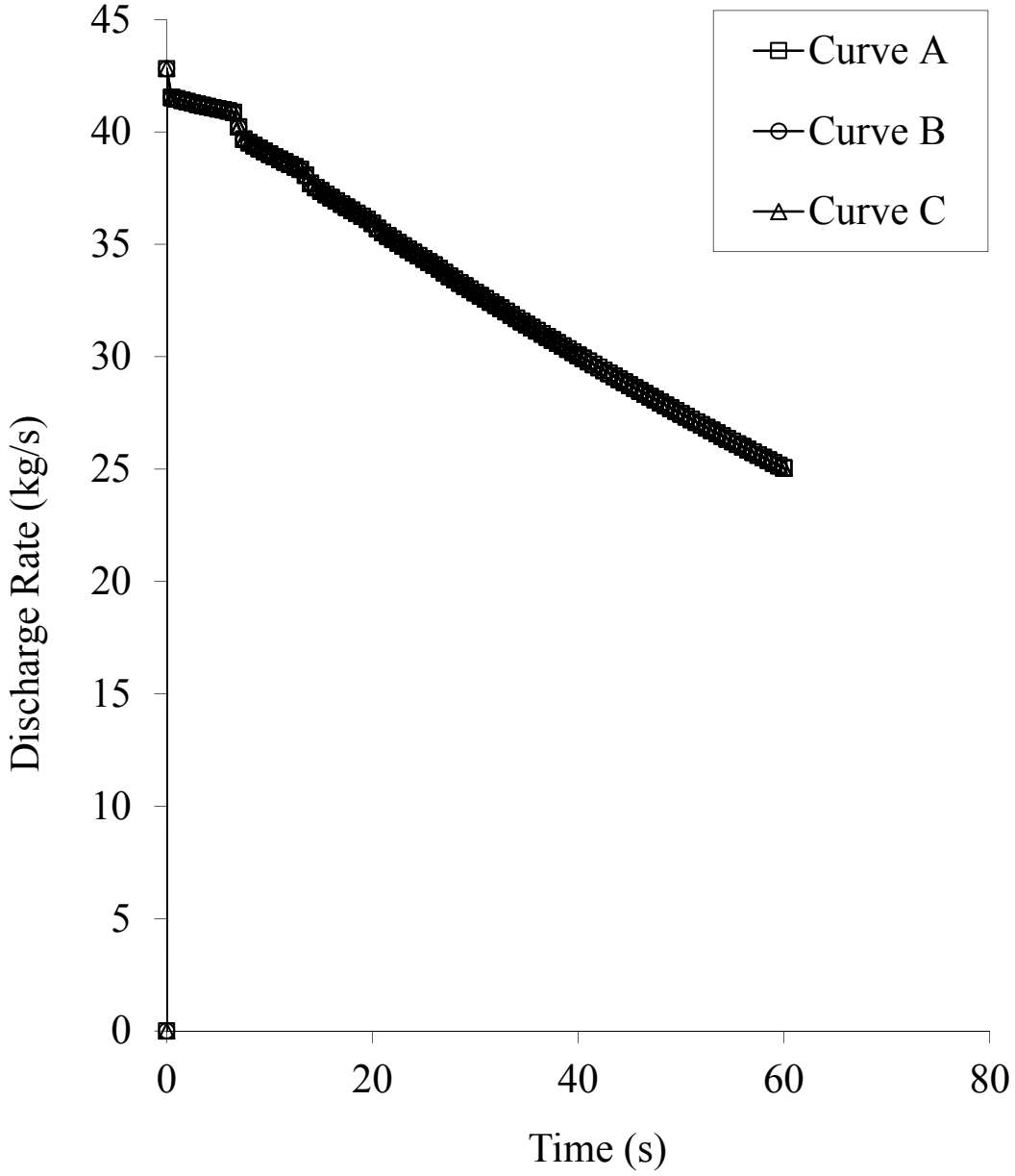

Figure 5.22: Variation of discharge rate against depressurisation time of the pipeline with two-phase inventory following puncture.

Curve A: PHU, CPU run-time = 375 s

Curve B: FVM, CPU run-time = 874 s

Curve C: PSUC, CPU run-time = 64 s

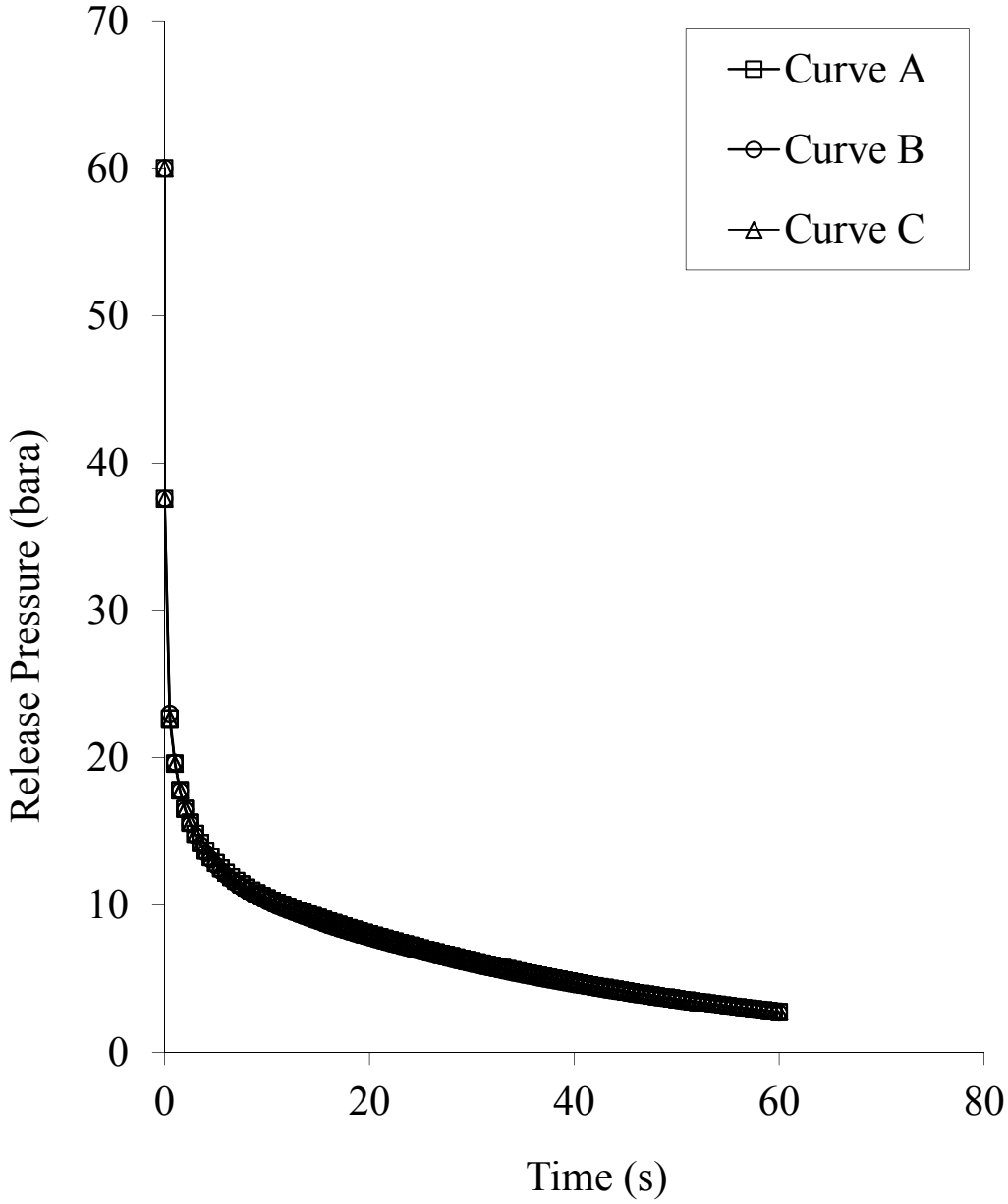

Figure 5.23: Variation of release pressure against depressurisation time of the pipeline with two-phase inventory following FBR.

Curve A: PHU, CPU run-time = 348 s

Curve B: FVM, CPU run-time = 274 s

Curve C: PSUC, CPU run-time = 81 s

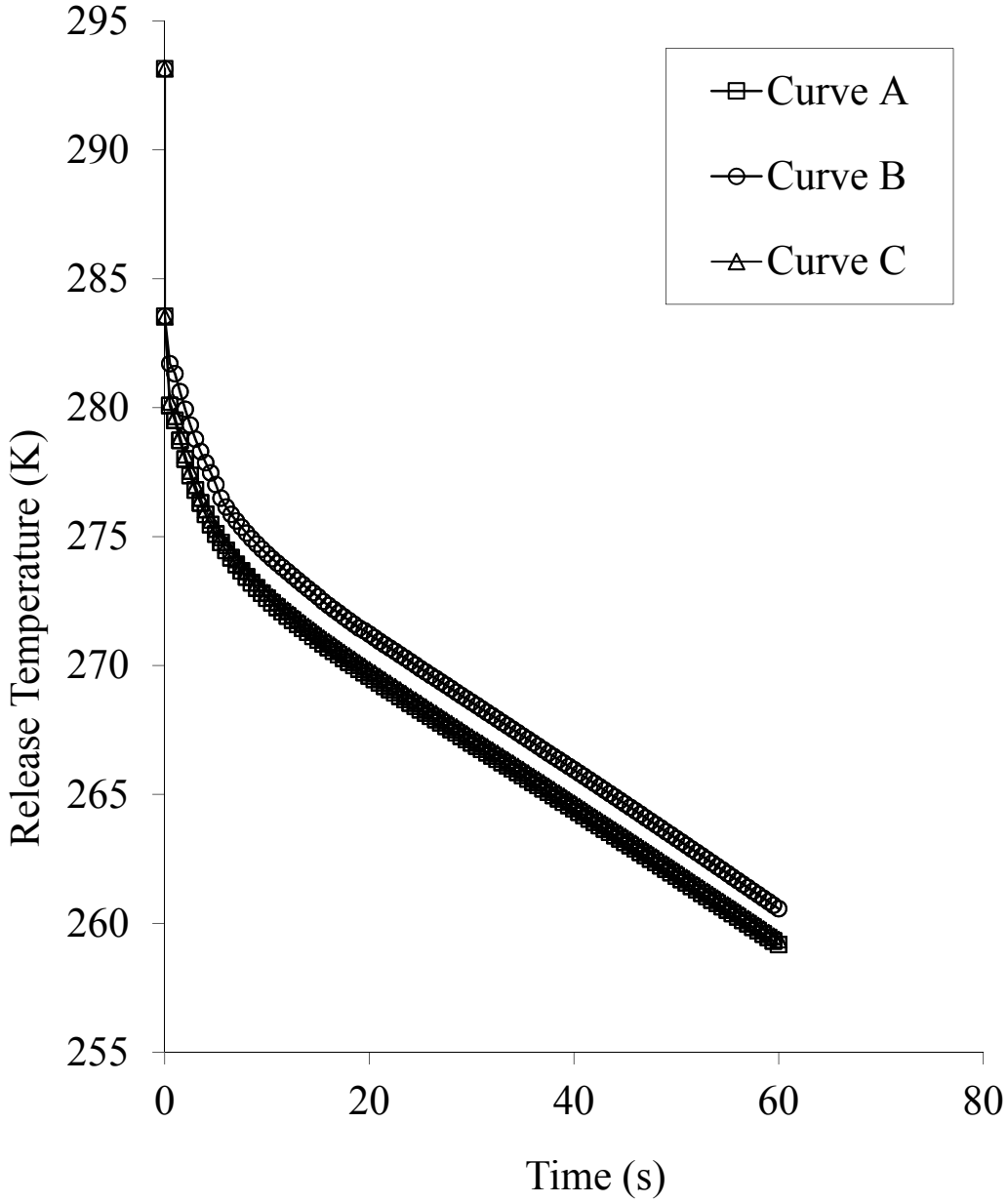

Figure 5.24: Variation of release temperature against depressurisation time of the pipeline with two-phase inventory following FBR.

Curve A: PHU, CPU run-time = 348 s

Curve B: FVM, CPU run-time = 274 s

Curve C: PSUC, CPU run-time = 81 s

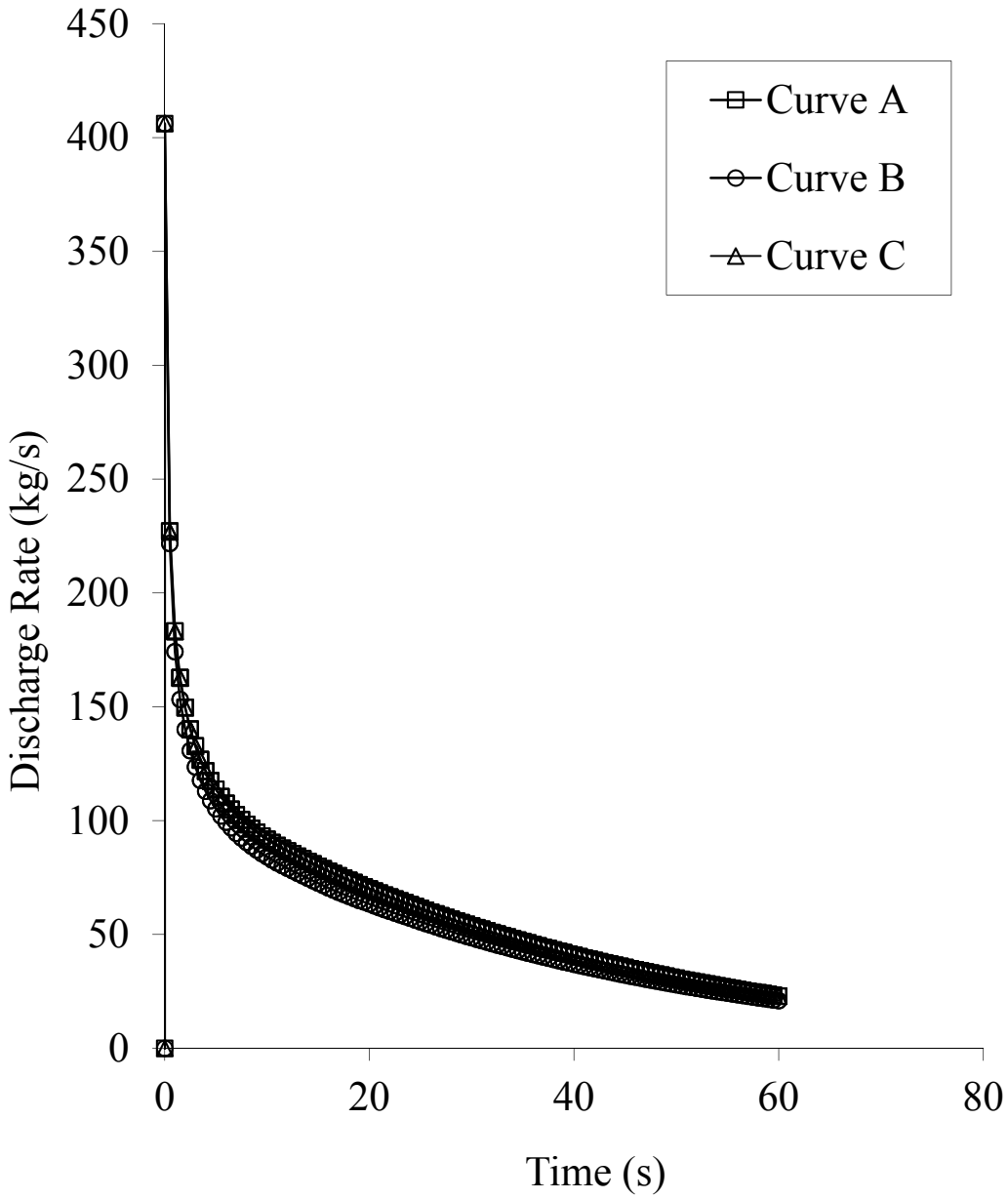

Figure 5.25: Variation of discharge rate against depressurisation time of the pipeline with two-phase inventory following FBR.

Curve A: PHU, CPU run-time = 348 s

Curve B: FVM, CPU run-time = 274 s

Curve C: PSUC, CPU run-time = 81 s

5.8 Concluding Remarks

This chapter presented the development of an alternative numerical model based on MOC. The model utilises the PSU conservation equations combined with Pressure Entropy (P-S) interpolation scheme. The above drastically reduces the number of P-S flash calculations required for calculating the critical discharge pressure at the release plane. Whilst maintaining almost the same level of accuracy as compared to PHU, the model primarily aims to reduce the long computational run-time associated with the numerically based models.

The performance of the PSUC was tested against available experimental data as well as the hypothetical case scenarios representing a realistic failure of a pipeline containing gas, two-phase and highly volatile liquid inventories. The predictions of the PSUC were compared against those from PHU and where available, FVM.

In general, PSUC predictions provided reasonable agreement with experimental data and the observed discrepancies were attributed to non-equilibrium effect, measurements uncertainties or errors. Also, the PSUC predictions were found to be in good accord with data obtained using PHU.

Different hypothetical case studies demonstrating the fluid transients in pipeline following a puncture along the length and FBR were presented. Similarly, the results obtained from PSUC, PHU and FVM were compared against each other in terms of their predictions and computational run-time.

For all the cases presented, PSUC consistently produced significant saving in CPU run-time with average reduction of ca. 84% as compared to PHU. All the CPU run-

times associated with the cases examined in this chapter are tabulated in table 5.7 for ready reference.

Table 5.7: Comparison of CPU run-times relating to PHU, FVM and PSUC for all simulations presented.

	CPU run-times (s)			CPU Saving % Compared to PHU	CPU Saving % Compared to FVM
	PHU	**FVM**	**PSUC**		
Validation against experimental data					
TransCanada	210	414	43	79.5	89.6
Piper Alpha	92,506	-	2,736	97	-
IOG P40	585	-	100	82.9	-
IOG P42	578	-	69	88.1	-
IOG P45	695	694	80	88.5	87.2
IOG P47	1,305	1,625	133	89.8	94.5
Verification Case Studies					
Full Bore Rupture					
Permanent Gas	377	366	100	73.5	72.7
Two-Phase	348	274	81	76.7	70.4
Puncture					
Permanent Gas	439	1,255	86	80.4	93.1
Two-Phase	375	874	64	82.9	92.7

Such models serve as a tool for safety engineers to carry out the consequence analysis. Considering that very long computational run-times are not uncommon

when simulating failures of long pipelines using numerical based outflow models, the presented work addresses the long computational run-time without compromising the accuracy. Accordingly, for the case of a very long pipeline, the PSUC performed particularly well in simulation of Piper Alpha in terms of accuracy and CPU run-time (see section 5.6.1).

Chapter 6: Development of the Semi-Analytical Vessel Blowdown Model for Pipeline Puncture Failures

6.1 Introduction

In the preceding chapter, the development and validation of a computationally efficient mathematical PSUC model for simulating outflow following pipeline failure was presented. It was shown that the model reduced the total computational run-time by ca. 84% as compared to PHU whilst maintaining the same level of accuracy. This chapter presents the development and testing of a semi-analytical model for predicting outflow from a pipeline following puncture type failure which requires negligible CPU resources. The conditions under which the transient outflow from a punctured pipeline may be approximated as that emanating from a vessel are determined so that an analytical solution based on a Vessel Blowdown Model (VBM) may be applied.

The chapter begins with presenting the main assumptions upon which the VBM is based. Next, an overview of the modelling of critical (or choked) flow through an orifice is presented. This is followed by formulation of the outflow for both two-phase and gas inventories for determining the exit pressure and discharge rate based on the VBM.

Finally, the results and discussion section presents a comparison of the predictions of the VBM against those obtained using the previously validated rigorous but computationally demanding numerical outflow model as presented in chapter 4. The model is based on PHU conservation equations together with P-H interpolation scheme developed by Atti (2006) herein referred to as PHU.

6.2 Development of the Vessel Blowdown Model

Error! Reference source not found. shows the pipe geometry used in development of VBM whereby the puncture of pressurised pipe between the block valves is approximated as a vessel with the same volume depressurising through an orifice with diameter corresponding to the punctured area. The pertinent physical and thermodynamic properties required for the formulation of the VBM are presented in Figure 6.2.

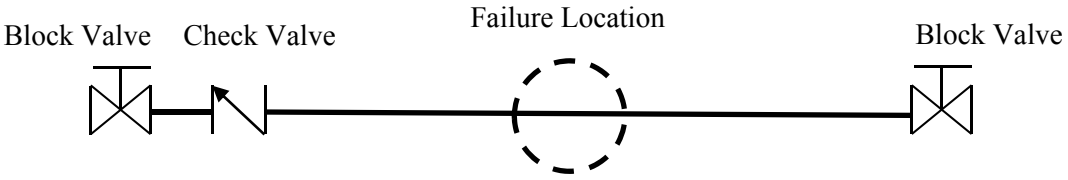

Figure 6.1: Pipeline geometry and illustration of valves with respect to failure location (DNV, 2010).

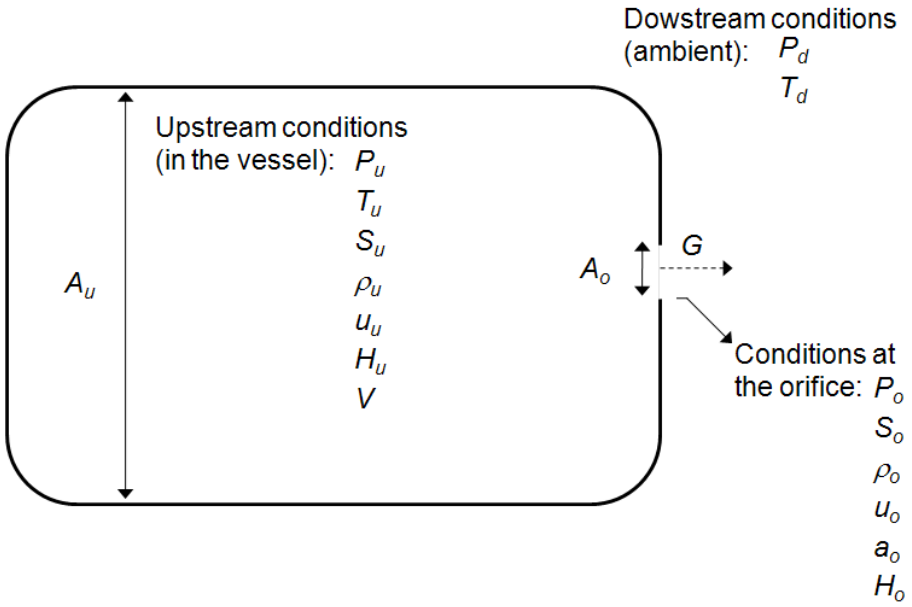

Figure 6.2: Schematic representation of a discharging vessel indicating the pertinent physical and thermodynamic properties required for the formulation of the VBM.

P: pressure; *T*: temperature; *S:* entropy; ρ: density; *H:* enthalpy; *u:* velocity; *V:* volume; *A:* cross sectional area; *G:* mass discharge rate; *a:* and speed of sound. Subscripts *u*, *o* and *d* refer to the upstream, orifice and downstream conditions respectively.

The conservation of energy for the fluid flowing through a restriction is given by the following equation (Coulson and Richardson, 1990):

$$udu + gdz + dH - \delta q + \delta W_s = 0 \qquad (6.1)$$

Where,

g = gravitational constant

z = distance in the "y" axis

q = net heat flow into the system

W_s = external work per unit mass

The following simplifications are applied to equation (6.1):

- The pipe is horizontal; $dz = 0$
- The discharge process is assumed to be isentropic
- No external work is done to the fluid; $\delta W_s = 0$

Based on the above assumptions, equation (6.1) is reduced to:

$$udu + dH = 0 \tag{6.2}$$

Integrating the above equation from the upstream (u) to the orifice (o) conditions gives:

$$H_u + \frac{1}{2}u_u^{\,2} = H_o + \frac{1}{2}u_o^{\,2} \tag{6.3}$$

Furthermore, assuming that the cross-sectional area (A_u) of the vessel is considerably larger than that for the orifice (A_o), the upstream fluid velocity relative to the downstream fluid velocity may be neglected (Vennard, 1996). Thus, equation (6.3) may be further simplified, giving:

$$H_u = H_o + \frac{1}{2}u_o^{\,2} \tag{6.4}$$

The methodology for solving equation (6.4) for obtaining the critical, or the choked pressure at orifice was presented in chapter 4, section 4.5.

6.2.1 Critical Flow Through an Orifice

When a compressible fluid with an upstream pressure, P_u is flowing through a restriction to a lower pressure P_d, to conserve mass, the downstream fluid velocity must increase. Assuming that the upstream pressure is fixed, the further P_d is reduced the higher is the velocity and consequently the mass flow rate increases. The flow is said to be choked when the mass flow rate does not increase further (i.e reaches its

maximum) with any further reduction in the downstream pressure. For homogeneous fluids, the physical point at which the choking occurs for an isentropic expansion (i.e. a frictionless and adiabatic flow) is when the exit plane velocity has reached the local speed of sound (Richarson and Saville, 1991). The corresponding mass flow rate is called the critical mass flow rate.

Under this condition, the velocity term in equation (6.4) can be replaced with the speed of sound as defined in equation (3.4) (Ghiaasiaan, 2008):

$$a_o^{\,2} = \left(\left. \frac{\partial P}{\partial \rho} \right|_S \right) \tag{3.4}$$

Where a is speed of sound.

Experimental observation reveals that the discharge area is always less than the orifice diameter (Coulson and Richardson, 1990). Figure 6.3 provides a schematic representation of the minimum flow area. This point of minimum flow area must be treated as the corresponding orifice area. As can be seen from Figure 6.3, the maximum contraction occurs slightly downstream of the orifice and is known as vena contracta.

This effect is taken into consideration by introducing a discharge coefficient in calculation of the mass flow rate.

The discharge coefficient is defined as:

$$C_D = \frac{\text{Area of vena contracta}}{\text{Area of orifice}} \tag{6.5}$$

And the critical mass flow rate can be calculated using the following equation (Coulson and Richardson, 1990):

$$G = C_D \rho_o u_o A_o \tag{6.6}$$

Where,

G = critical mass discharge rate

When the flow is choked, the discharged velocity u_o is replaced by the local speed of sound, a_o. Otherwise, using the fluid enthalpy at the orifice, equation (6.4) is solved for determining u_o.

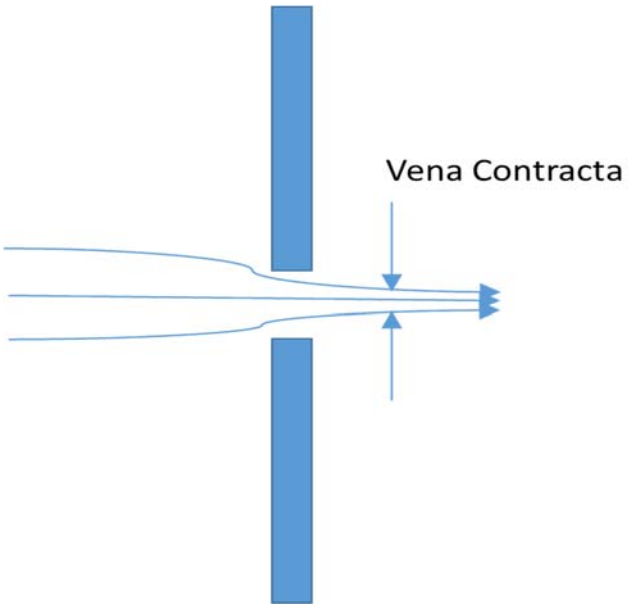

Figure 6.3: Schematic representation of the Vena Contracta during flow through an orifice.

6.3 Calculation of Choked Pressure for Single Phase Fluid

In order to calculate the discharge rate at the release plane, the choked pressure, P_o should first be determined. This allows for other properties such as speed of sound to be calculated at the exit plane.

The calculation flow algorithm for calculating the choked pressure for single phase flow through an orifice is given in Figure 6.4. It involves the following steps:

1. Perform pressure-temperature (P-T) flash in order to calculate the upstream entropy, S_u and enthalpy H_u

2. Guess an orifice pressure, P_o^i starting with a value between the upstream and ambient pressures. Superscript i denotes the corresponding depressurisation step

3. Since the fluid flowing through the restriction is assumed to follow an isentropic thermodynamic path, using the calculated upstream entropy and guessed orifice pressure, perform a pressure-entropy (P_o-S_u) flash to calculate the speed of sound, a_o and enthalpy, H_o at the orifice condition

4. Check if the a_o, H_o and H_u calculated in steps 1 to 3 satisfy equation (6.4). If no, repeat steps 1-3
5. If the pressure, P_o satisfying equation (6.4) is above the ambient pressure, it is then used as the choke pressure. Else the ambient pressure is set as the choke pressure

The Brent iteration method (Press et al., 1992) is employed to find the choked pressure.

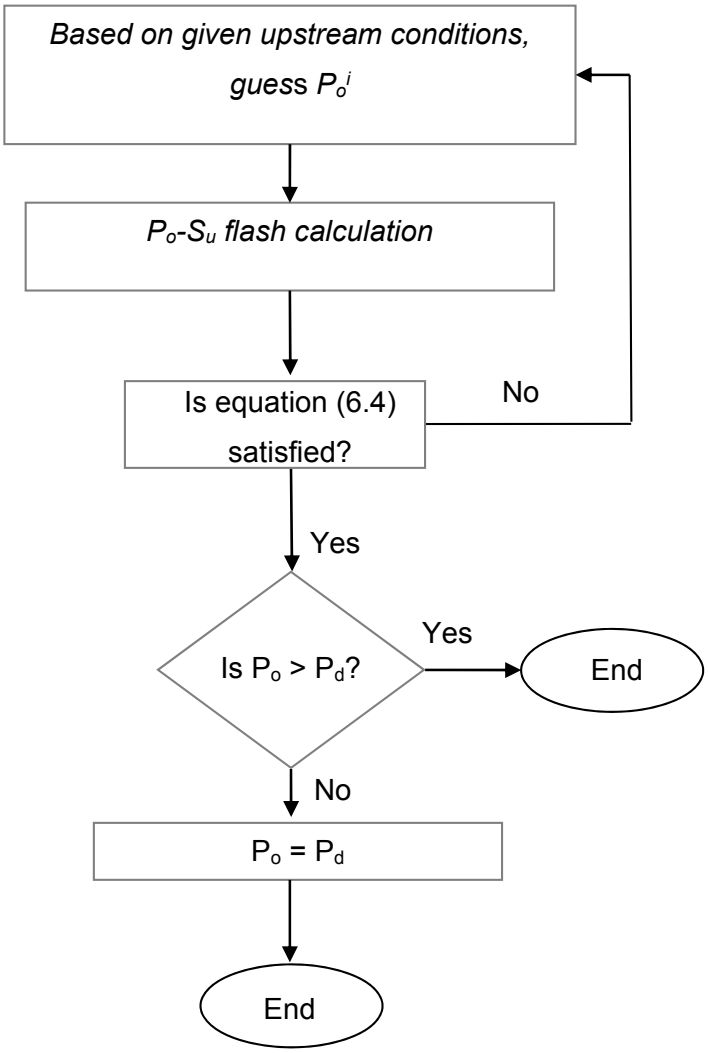

Figure 6.4: The calculation flow algorithm for determining the choked pressure for single phase fluid discharge though an orifice.

6.4 Calculation of Choked Pressure for Two-phase Flow

The ω-method (Leung, 1986) recommended by DIERS (The Design Institute for Emergency Relief Systems) is employed for calculating the choked pressure for two-phase flows. This method is also used for sizing emergency relief valves (Boicourt, 1995).

The critical mass flux is determined solely from the change in specific volume with respect to change in pressure at the choking location (i.e $(\frac{dv}{dP})_s$) derived from the momentum balance (Leung, 1990):

$$G^2 = \frac{-1}{(\frac{dv}{dP})_s} \tag{6.7}$$

Where,

v = mixture specific volume

The subscript, s denotes thermodynamic trajectory of constant entropy. For a homogeneous two-phase flow mixture $(\frac{dv}{dP})_s$ can be expanded giving:

$$\frac{dv}{dP} = \frac{d}{dP}[xv_v + (1-x)v_l] \tag{6.8}$$

Differentiation gives:

$$\frac{dv}{dP} = x\frac{dv_v}{dP} + v_{vl}\frac{dx}{dP} \tag{6.9}$$

Where,

v_v = vapour specific volume

v_l = liquid specific volume

v_{vl} = difference between specific volume in vapour and liquid phases

x = quality or gas mass fraction

The first term on RHS of the equation (6.9) represents the expansion of the vapour phase due to change in pressure. The second term corresponds to the rate of evaporation as a result of change in pressure.

Based on the conservation of energy under thermodynamic equilibrium:

$$\frac{dx}{dT} = -\frac{C_{pl,u}}{h_{vl,u}} \tag{6.10}$$

Where,

$C_{pl,u}$ = specific heat at constant pressure for liquid phase at upstream condition

$h_{vl,u}$ = latent heat of vaporisation at upstream condition

Clausius-Clapeyron equation for a system at thermodynamic equilibrium gives:

$$\frac{dT}{dP} = \frac{v_{vl,u}}{h_{vl,u}} \tag{6.11}$$

Eliminating, dT in equation (6.10) using (6.11) and substituting into equation (6.9) gives:

$$\frac{dv}{dP} = x\frac{dv_v}{dP} - C_{pl,u}T_u\left(\frac{v_{vl,u}}{h_{vl,u}}\right)^2 \tag{6.12}$$

In order to be able to integrate the above equation with respect to pressure, the following assumptions are made:

- Isothermal gas expansion. This is a valid approximation for two-phase flow since the condensed phase possesses far more sensible heat than the vapour phase (Leung, 1990)
- Ideal gas behaviour for the vapour phase
- The enthalpy of vaporisation, $h_{vl,u}$ is described by a constant average value

Integration and rearrangement of equation (6.12) yields:

$$\omega = \frac{\frac{v}{v_u} - 1}{\frac{P_u}{P} - 1} = \frac{x_u v_{v,u}}{v_u} + \frac{C_{pl,u}T_u P_u}{v_u}\left(\frac{v_{vl,u}}{h_{vl,u}}\right)^2 \tag{6.13}$$

Where ω is a dimensionless parameter.

As can be seen, the RHS of equation (6.13) involves only properties pertaining to the upstream conditions.

Recasting equation (6.4) yields:

$$G = [2(H_u - H_o)]^{1/2} / v \tag{6.14}$$

From the second law of thermodynamic for an isentropic process, equation (6.14) can be rewritten:

$$G = \frac{[2\int_{P_u}^{P_o} -v dP]^{1/2}}{v} \tag{6.15}$$

Grolmes and Leung (1984) correlated the P-v relation in the above equation and demonstrated that using ω, as defined in equation (6.13), satisfies the critical pressure ratio ($\eta = \frac{P_o}{P_u}$) in the non-linear equation as given below:

$$\eta^2 + (\omega^2 - 2\omega)(1-\eta)^2 + 2\omega^2 \ln \eta + 2\omega^2(1-\eta) = 0 \tag{6.16}$$

Finally, calculating the choked pressure for a two-phase mixture flowing through an orifice comprises the following three steps:

1. Perform a P-T flash based on the upstream conditions to determine the parameters required in the right hand side of equation (6.4)
2. Calculate ω from equation (6.13)
3. Solve equation (6.16) to obtain the choke pressure

6.5 Mathematical Modelling of the VBM

The following assumptions are made in the development of the VBM:

- The flow through the orifice is one-dimensional
- The discharge process through the orifice follows an isentropic path. The frictional loss is accounted for in the discharge coefficient (C_D)
- The ratio of orifice to vessel diameter is small in order to satisfy the assumption of negligible upstream orifice fluid velocity as compared to the velocity at the orifice
- The upstream fluid temperature remains constant during the depressurisation
- The pipe is assumed to be isolated upon puncture failure with no initial feed flow
- The state of the inventories remain unchanged throughout the depressurisation

6.5.1 Calculation Algorithm for VBM

The calculation algorithm for simulating the depressurisation of a punctured pipeline using VBM requires convergence of the energy balance equation (i.e. equation (6.4)) at the orifice. The variation of mass release rate with time is determined by approximating the depressurisation process using a series of small pressure steps from the initial feed pressure until completion of the depressurisation. Figure 6.5 shows the VBM calculation flow algorithm for determining the mass discharged and its variation with time as described below:

1. Given the initial upstream pressure P_u^i and temperature, T_u, a pressure-temperature flash calculation is performed to determine the upstream enthalpy (H_u), upstream entropy (S_u) and feed density (ρ_u)
2. Determine the orifice pressure, P_o using the procedures given in section 6.3 and 6.4 as applicable

3. The fluid enthalpy, speed of sound and density at orifice are determined using a pressure-entropy flash calculation at P_o and S_u

4. If P_o is greater than ambient pressure P_d, then the fluid speed of sound at the orifice is used for determination of the discharge velocity. Otherwise, using the fluid enthalpy at the orifice (as calculated in step 3), equation (6.4) is solved for determining u_o

5. The discharge rate is obtained using equation (6.6)

6. Calculate total mass of the inventory inside the vessel

7. Reduce the initial vessel pressure by ΔP and repeat steps 1-6

8. Calculate the mass released corresponding to ΔP using:

$$m_{lost}{}^{i} = m^{i-1} - m^{i} \tag{6.17}$$

Where,

m^i = mass inside the vessel in step i

m^{i-1} = mass inside the vessel in step i-1

9. Calculate the time required for the calculated mass released, $m_{lost}{}^{i}$ to be discharged from the vessel using:

$$\Delta t = \frac{m_{lost}{}^{i}}{G_{avg}} \tag{6.18}$$

Where G_{avg} is the average discharge rate between step i and i+1.

10. Apply ΔP and return to step 1

The calculations are terminated once the vessel pressure is equal to the ambient pressure.

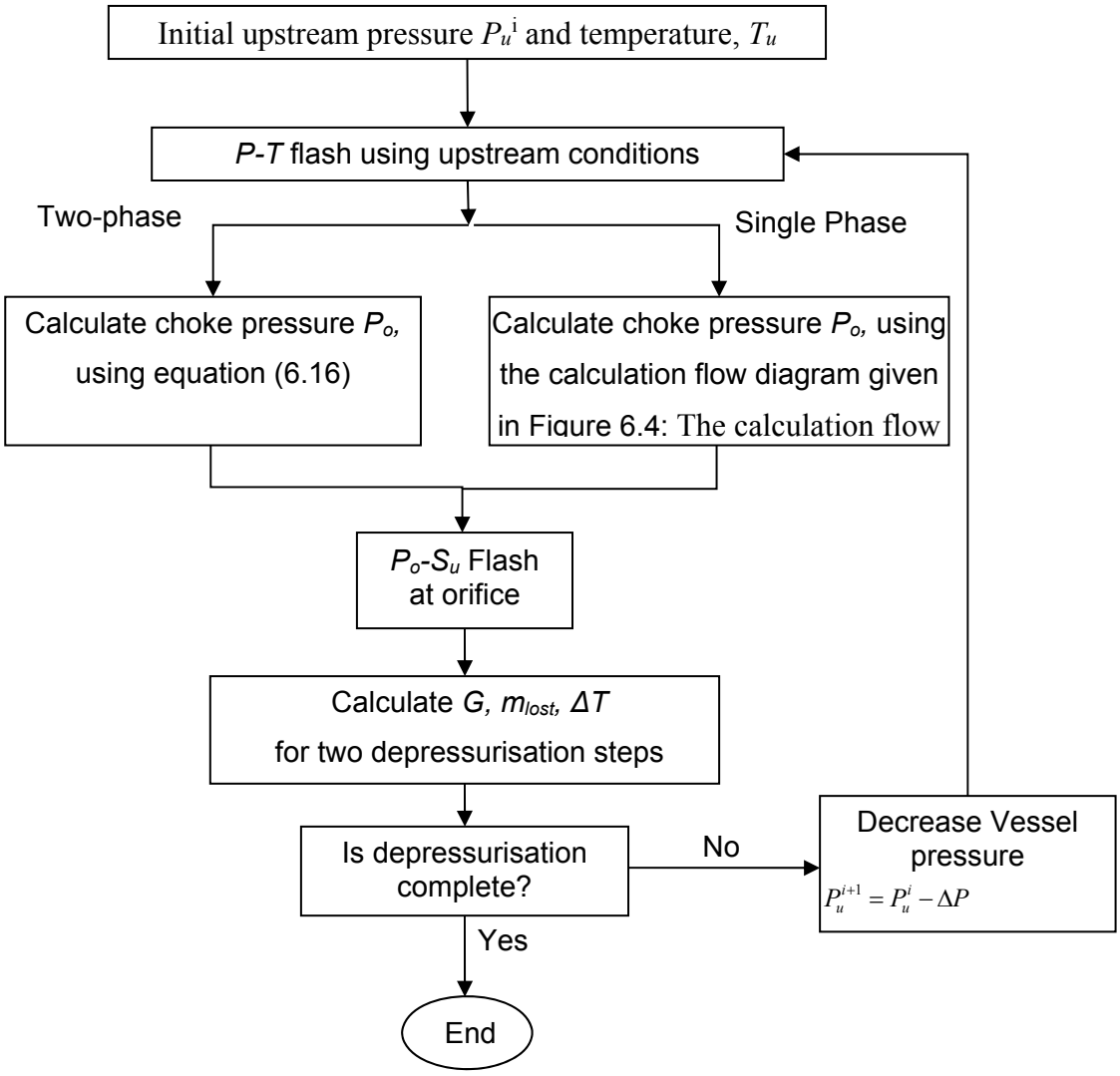

Figure 6.5: Vessel Blowdown Model calculation flow diagram.

6.6 Results and discussion based on the application of the VBM

The following describe the results for a series of investigations establishing the range of applicability of the VBM for simulating pipeline punctures. These investigations are based on comparison of the VBM predictions against those obtained using PHU.

The work commences with a sensitivity analysis for determining minimum depressurisation step, ΔP required for the solution of VBM based on its impact the on cumulative mass released data.

Throughout this work, only pipelines containing permanent gases and two-phase inventories are considered. Pressurised liquid pipelines are not considered here due to the almost instantaneous depressurisation to ambient conditions upon failure thus requiring little computational effort when simulating their behaviour. In the case of two-phase flow, an inventory which remains two-phase throughout the depressurisation is considered.

Changes to the following important parameters are made in order to test the range of applicability of the VBM for both permanent gas and two-phase inventories:

- Puncture to pipe diameter ratio, d_o/D
- Pipeline length
- Initial line pressure

Next, the average difference in prediction of cumulative mass released between VBM and PHU are determined. The sources of error are then discussed and the computational run-times associated with both models are presented.

6.7 Impact of Depressurisation Steps on VBM Performance

Clearly an increase in the number of depressurisation steps will improve the accuracy of the simulation. The following investigates the impact of the number of the

depressurisation steps, ΔP of 0.2 bar (50/100), 0.17 bar (50/300) and 0.1 bar (50/500) on the cumulative mass discharge convergence.

Table 6.1 represents the pipe characteristics and prevailing conditions used for this analysis. The corresponding cumulative mass released ΔP is shown in figure 6.6.

Table 6.1: The pipe characteristics used in the VBM for sensitivity analysis of the number of depressurisation steps.

Parameter	Value
Length (m)	1000
Inner Diameter (mm)	300
Initial Pressure (bara)	50
Initial Temperature (K)	300
Ambient Pressure (bara)	1.01
Ambient Temperature (K)	280
Puncture Diameter (mm)	120
Inventory	100 % methane
Failure Mode	Puncture in the middle
Discharge Coefficient	1

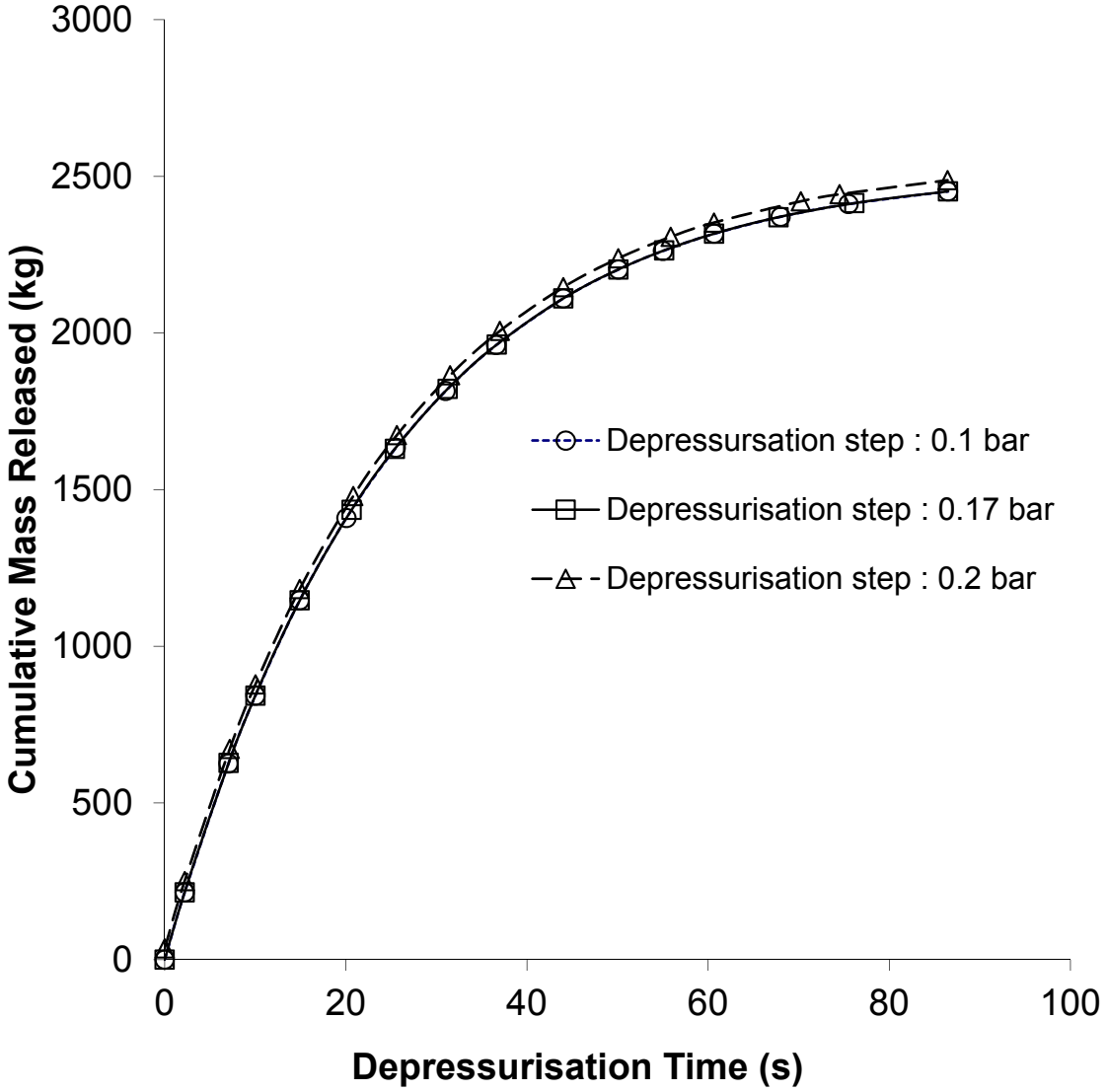

Figure 6.6: Variation of the cumulative mass released with time obtained from VBM for different number of depressurisation steps.

As it may be observed in figures 6.6, the decrease in ΔP from 0.17 to 0.1 bar has negligible impact on the cumulative data. Given the above, $\Delta P = 0.1$ bar is used in the proceeding investigations.

6.8 Definition of Error Analysis

The differences between VBM and PHU predictions of the cumulative mass released are examined for all the verification case studies presented. On average, 20 points are uniformly selected from each case study covering the entire depressurisation. The average and maximum percentage error for the cumulative mass released based on comparison with PHU are tabulated.

6.9 Verification of the VBM against PHU

6.9.1 Impact of the puncture to pipe diameter ratio, d_o/D

Table 6.2 presents the prevailing conditions, pipeline characteristics and the range of parameters employed in the proceeding investigations. The pipeline is assumed to be made of mild steel. Puncture to pipeline diameter ratios, d_o/D are in the range 0.1 – 0.4 covering realistic puncture failure scenarios. For the numerically based simulations (i.e PHU), an automatic nested grid system is used (see Mahgerefteh et al., 2008) in which smaller time and distance discretisation steps are employed near the puncture plane in order to reduce the computational run-times and improve accuracy of PHU.

Table 6.2: Pipeline characteristics, prevailing conditions and the range of parameters employed for VBM – PHU investigations.

Parameter	Value			
Pipe length, L (m)	100	1000	5000	
Pipe inner diameter, D (m)	0.3			
Pipe wall thickness (m)	0.01			
Line pressure (bara)	21	50	100	
Initial temperature (K)	300			
Ambient pressure (bara)	1.01			
Ambient temperature (K)	290			
Puncture location	Mid length			
Discharge coefficient	1			
Puncture diameter, d_o (m)	0.03	0.06	0.09	0.12
Puncture to inner pipe diameter ratio (d_o/D)	0.1	0.2	0.3	0.4
Pipe wall material	Carbon steel			
Pipe wall density (kg/m^3)	7854			
Wind velocity (m/s)	0			
Pipe wall thermal conductivity (W/m^2C)	53.65			
Pipe roughness (m)	0.0005			

For simplicity, a discharge coefficient of unity is assumed. All simulations are performed using a 2.66 GHz, 3.0 GB RAM PC. The failure is assumed to be in the form of a puncture mid-way along the uninsulated pipeline exposed to still air.

Throughout this chapter, the solid lines represent the VBM predictions whilst the data points represent PHU predictions.

Figures 6.7 and 6.8 represent the predicted cumulative mass released against time following pipeline puncture at 21 bara for pure gaseous methane and an equi-molar two-phase mixture of methane and n-pentane respectively. The VBM and PHU predictions are obtained at different puncture to pipe diameter ratios in the range of 0.1 – 0.4 for a 100 m pipeline. At the prevailing conditions tested (see table 6.2), methane remains in the gaseous state throughout the depressurisation to 1 bara.

To allow direct comparison, the vessel is assumed to have the same volume and at the same initial conditions as the pipeline. Given that the bulk fluid expansion within the vessel is assumed to be isothermal, other remaining vessel characteristics such as wall thickness, overall dimensions, shape and heat transfer coefficients are irrelevant.

As it may be observed in figures 6.7 and 6.8, in both cases the VBM predictions are generally in good agreement with PHU throughout. However, the degree of agreement between the models for prediction of the cumulative mass released reduces towards the end of depressurisation whereby VBM slightly over-predicts.

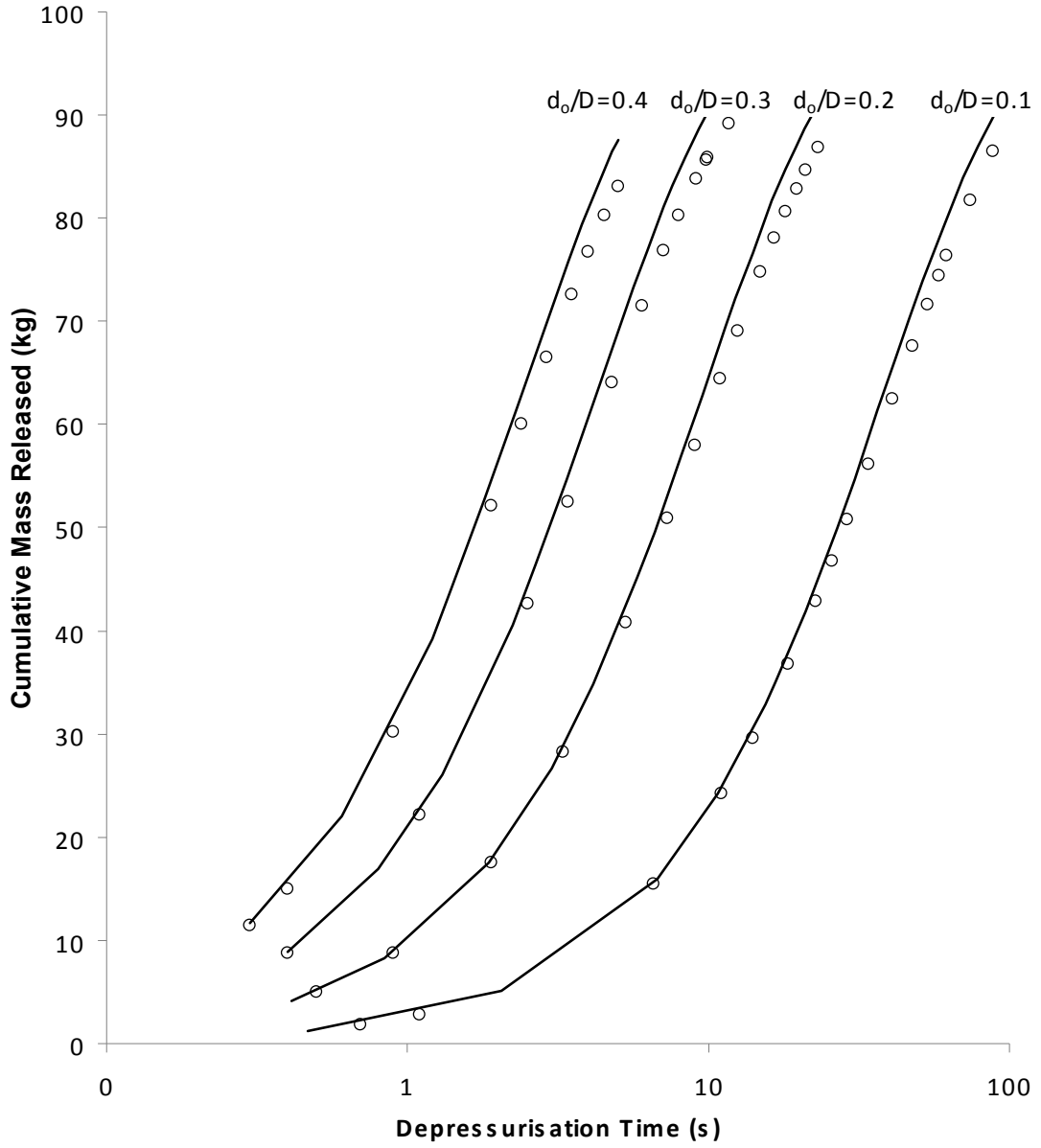

Figure 6.7: Comparison of cumulative mass released against depressurisation time to 1 bara for VBM (solid line) and PHU (data points) for different puncture to pipe diameter ratios, d_o/D. Inventory:
100% methane
Initial pressure: 21 bara
Pipeline length: 100 m

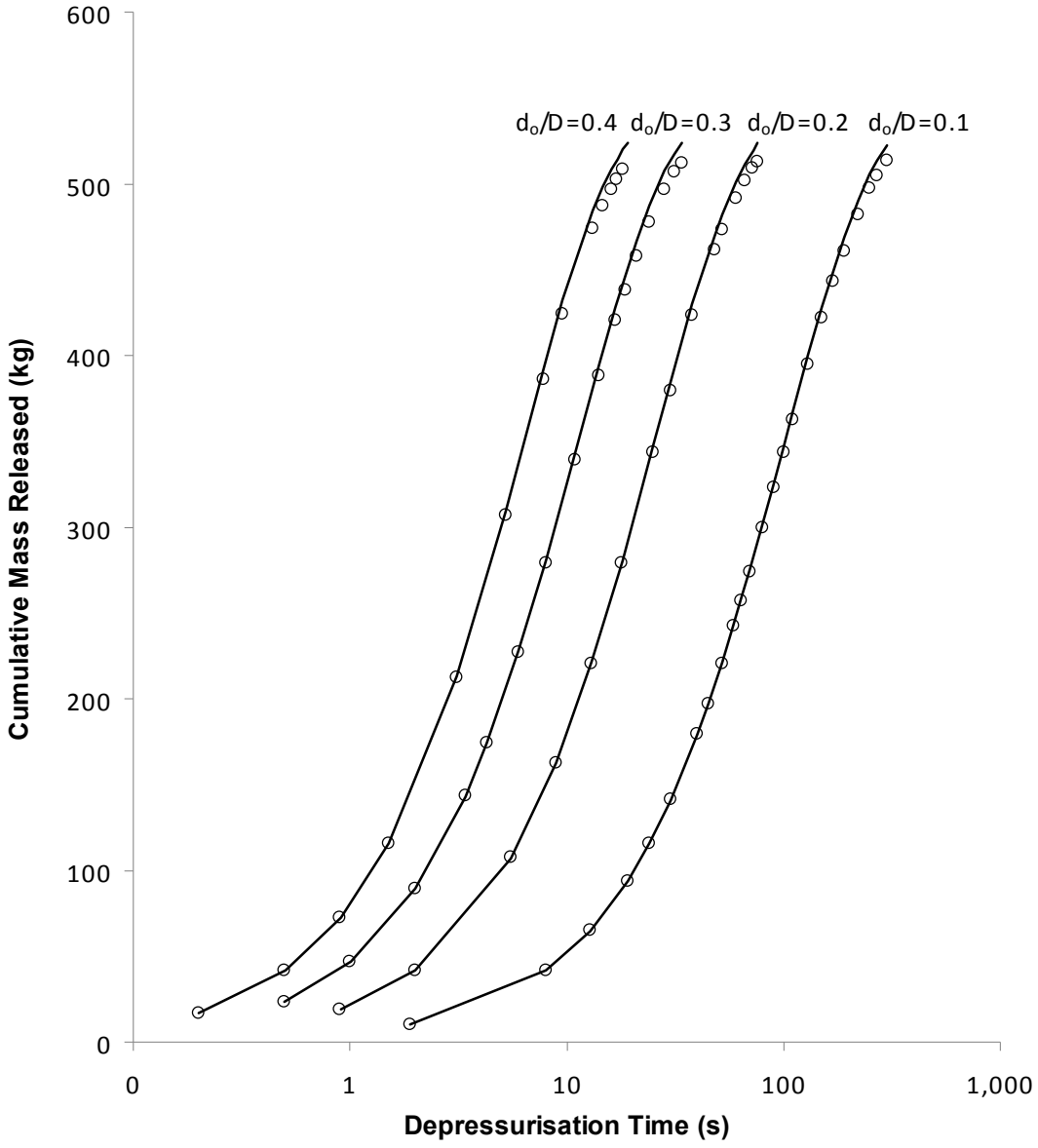

Figure 6.8: Comparison of cumulative mass released against time during depressurisation to 1 bara based on VBM (solid line) and PHU (data points) for different puncture to pipe diameter ratios, do/D.

Inventory: 50% methane and 50% n-pentane

Initial pressure: 21 bara

Pipeline length: 100 m

Table 6.3 presents the corresponding average and maximum percentage errors based on comparison with PHU for cumulative mass released data at different puncture to pipe diameter ratios. As can be seen, the percentage error in the VBM predictions increases with increase in the puncture-pipe diameter ratio. This is postulated to be as a result of increasing inapplicability of negligible bulk fluid motion assumption in the vessel with the increase in the puncture diameter.

Also, surprisingly, the VBM produces significantly smaller average errors in the case of the two-phase mixture as compared to the gaseous inventory.

Table 6.3: Average and maximum percentage errors of the cumulative mass released using VBM predictions relative to the PHU at different puncture to pipe diameter ratios for gaseous methane and an equi-molar two-phase mixture of methane and n-pentane.

Puncture/pipe diameter ratio, d_o/D	Permanent Gas (methane)		Two-phase mixture (methane and n-pentane)	
	Average % error	Maximum % error	Average % error	Maximum % error
0.1	3.52	4.95	0.96	1.73
0.2	3.86	5.02	1.25	2.04
0.3	4.08	5.21	1.32	2.27
0.4	4.29	5.19	1.46	2.46

Initial pressure: 21 bara; Pipeline length: 100 m.

In order to explain the observed trend in the data presented in table 6.3, the fluid velocity profiles using the PHU at 20 s following puncture failure mid-way along the 1000 m pipe for different puncture-pipe diameter ratios are presented in figures 6.9 and 6.10 for gaseous methane and equi-molar two-phase mixture of methane and n-

pentane respectively. All other pipeline characteristics and the prevailing conditions are the same as those given in table 6.2.

As it may be observed, at any given diameter ratio, the upstream velocity at mid-point along the pipe (the puncture location) for the gaseous methane is considerably greater than for the two-phase methane/n-pentane mixture.

Furthermore, as d_o/D is increased, the fluid velocity increases hence neglecting the kinetic energy upstream of the puncture location is postulated to be one of the main sources of error introduced in the VBM predictions.

In line with the findings presented in table 6.3, the above is also consistent with the better performance of the VBM prediction in the case of the two-phase mixture as compared to that for the permanent gas.

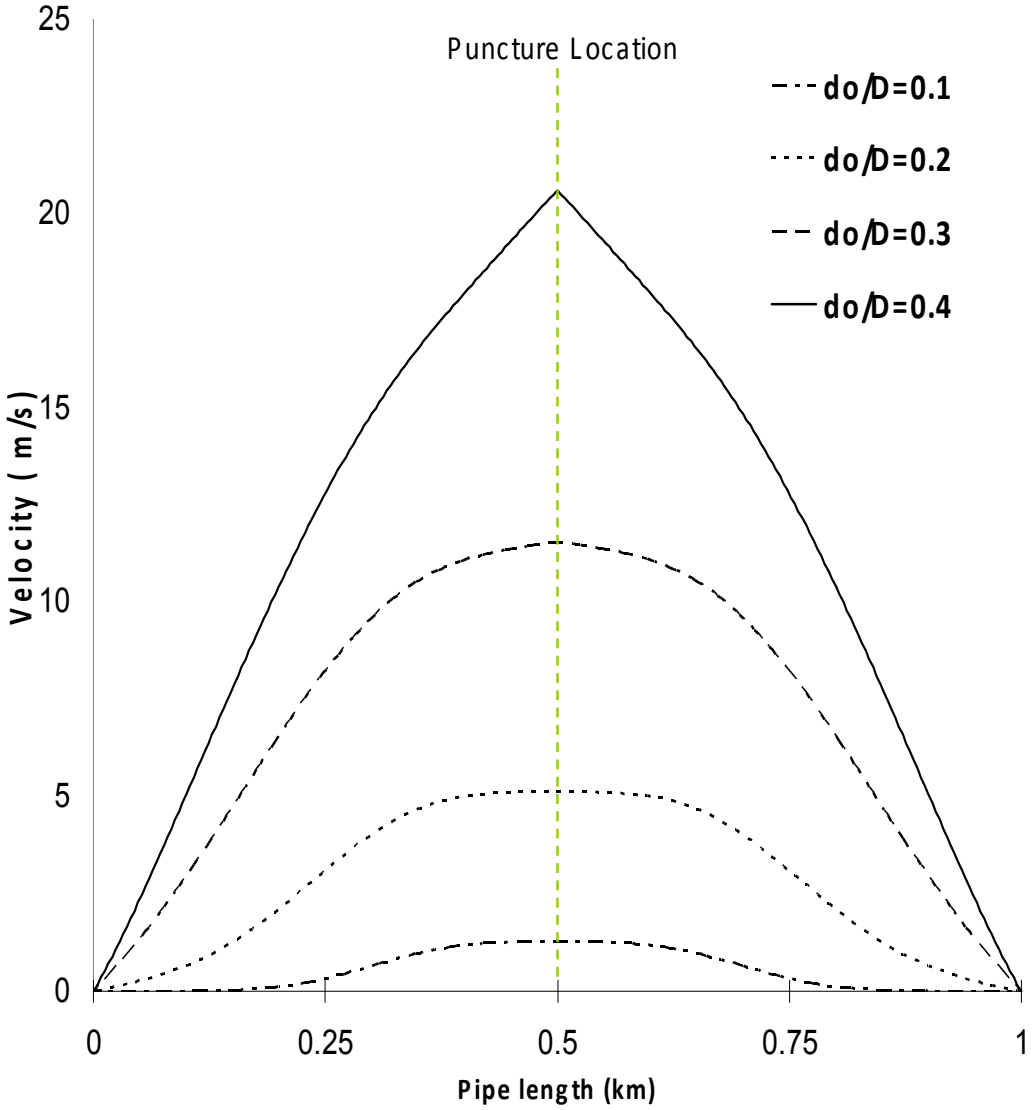

Figure 6.9: Velocity profile along the pipe for different puncture-pipe diameter ratios 20 s after the depressurisation using PHU.

Inventory: 100% methane

Initial pressure: 21 bara

Pipeline length: 100 m

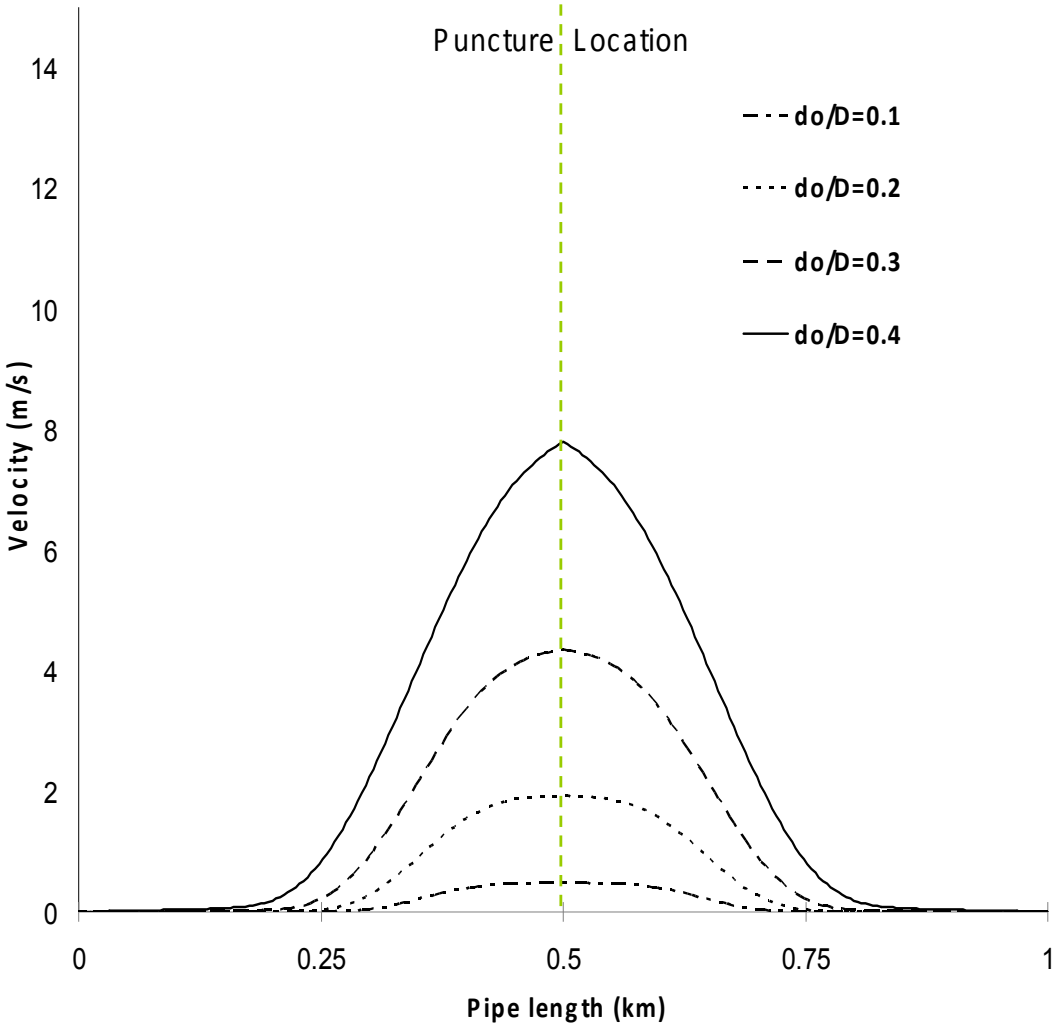

Figure 6.10: Velocity profile along the 1 km pipe for different puncture-pipe diameter ratios at 20 s following the depressurisation using PHU.

Inventory: 50% methane and 50% n-pentane

Initial pressure: 21 bara

Pipeline length: 100 m

6.9.2 Impact of Pipeline Length

Figure 6.111 and 6.12 show the cumulative mass released against depressurisation time based on predictions of VBM and PHU for different pipe lengths for gaseous and the two-phase inventories respectively. The data is presented for the largest puncture to pipe diameter ratio of 0.4 where the discrepancy between the two model predictions proved to be the largest.

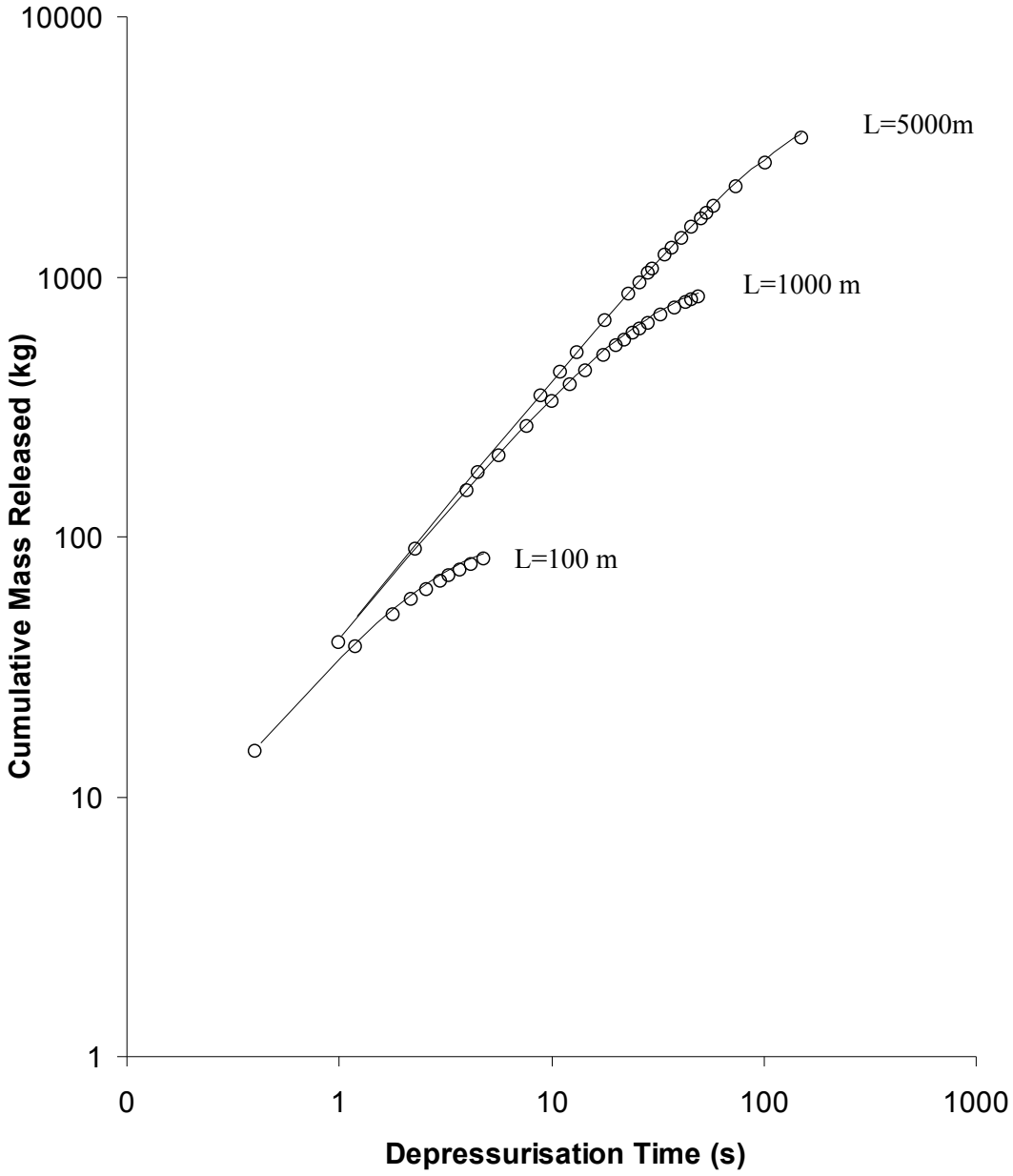

Figure 6.11: Comparison of the cumulative mass released against depressurisation time to 1 bara for VBM (solid line) and PHU (data points) at different pipe lengths, L.

Inventory: 100% methane

Puncture to pipe diameter ratio: 0.4

Initial pressure: 21 bara

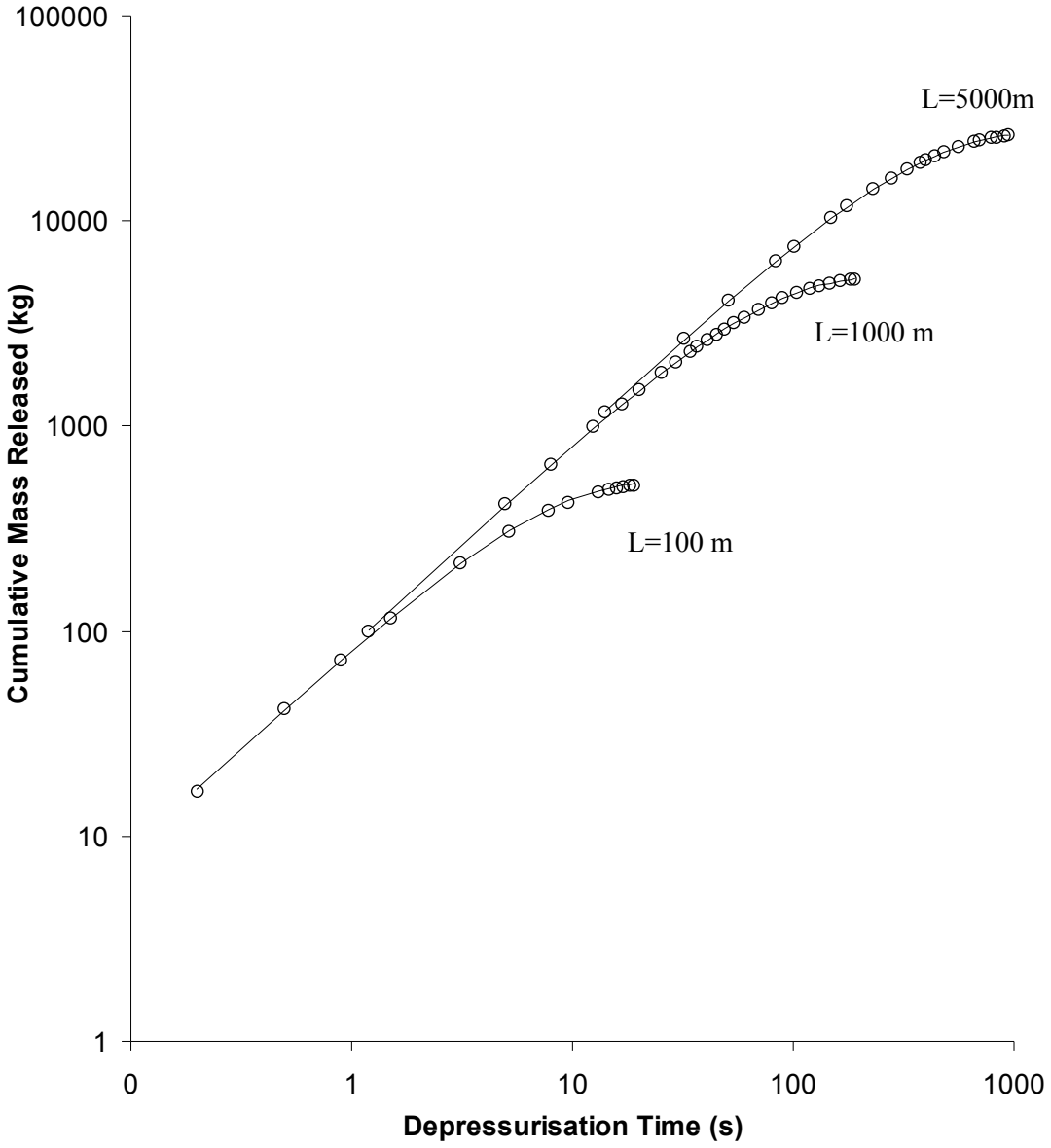

Figure 6.12: Comparison of the cumulative mass released against time during depressurisation to 1 bara for VBM (solid line) and PHU (data points) at different pipe lengths, L.

Inventory: 50% methane, 50% n-pentane

Puncture to pipe diameter ratio: 0.4

Initial pressure: 21 bara

Table 6.4 represents the corresponding average and maximum percentage errors in the VBM cumulative mass released predictions relative to the PHU predictions for both inventories at the different pipe lengths.

Table 6.4: Average and maximum percentage errors in the cumulative mass released using VBM predictions relative to the PHU predictions at different pipeline lengths for the gaseous methane and an equi-molar two-phase mixture of methane and n-pentane.

Pipe length, L (m)	Permanent Gas (methane)		Two-phase mixture (methane and n-pentane)	
	Average % error	Maximum % error	Average % error	Maximum % error
100	4.29	5.19	1.46	2.46
1000	2.55	6.45	0.42	1.64
5000	1.61	5.74	0.35	1.51

Puncture to pipe diameter ratio: 0.4; Initial pressure: 21 bara.

As it may be observed, good agreement between the two predictions are obtained for all the pipe lengths investigated. The largest average error of 4.29 % in the VBM prediction corresponds to the shortest pipeline length (100 m) for the gaseous phase.

Much the same as with the decreasing diameter ratio, the VBM performs better as the pipeline length is increased. This is consistent with the smaller impact of the bulk fluid motion within the pipeline on the discharge rate as the pipe length increases. Also, as it may be seen, the VBM performs better for the two-phase inventory as compared to the gaseous inventory. For the case of two-phase mixture a maximum error of ca. 2.46% is observed for the 100 m pipe whilst the corresponding maximum error for gaseous inventory is 6.47%.

To explain the observed trends in the data presented in figures 6.11-12 and table 6.4, it is important to consider the impact of the isothermal assumption on the VBM performance. The corresponding fluid temperature and pressure profiles using PHU for the 1000 m pipeline containing pure gaseous methane are presented in figures 6.13 and 6.14 respectively.

Based on the data in figure 6.13 (100% methane), as the depressurisation progresses, the temperature at the puncture location rapidly drops down to 292 K after 10 s and to 278 K after 20 s. Also, as expected the temperature further away from the puncture location changes at a much lower rate compared to the temperature at the release location.

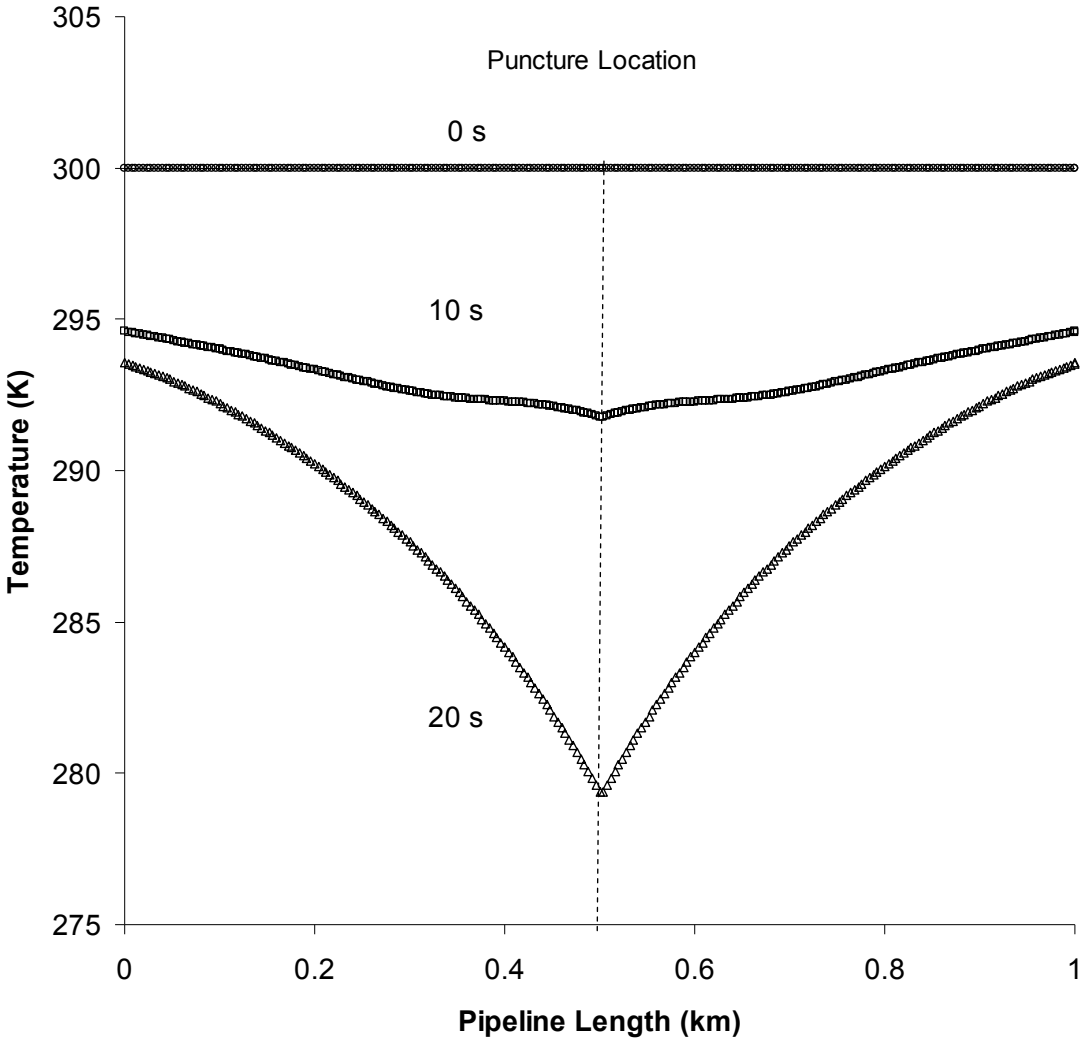

Figure 6.13: The variation of the fluid temperature profile along the length of the pipe at different time intervals following puncture.
Inventory: 100% methane
Puncture to pipe diameter ratio: 0.2
Pipeline length: 1000 m

This implies that the isothermal assumption in the VBM becomes more applicable with the increase in pipe length and hence its performance improves. The pressure profiles presented in figure 6.14 show that at any given time interval, the fluid pressure is

relatively uniform along the pipe. This is found to be consistent with the assumption of the constant pressure throughout the pipe at each depressurisation step.

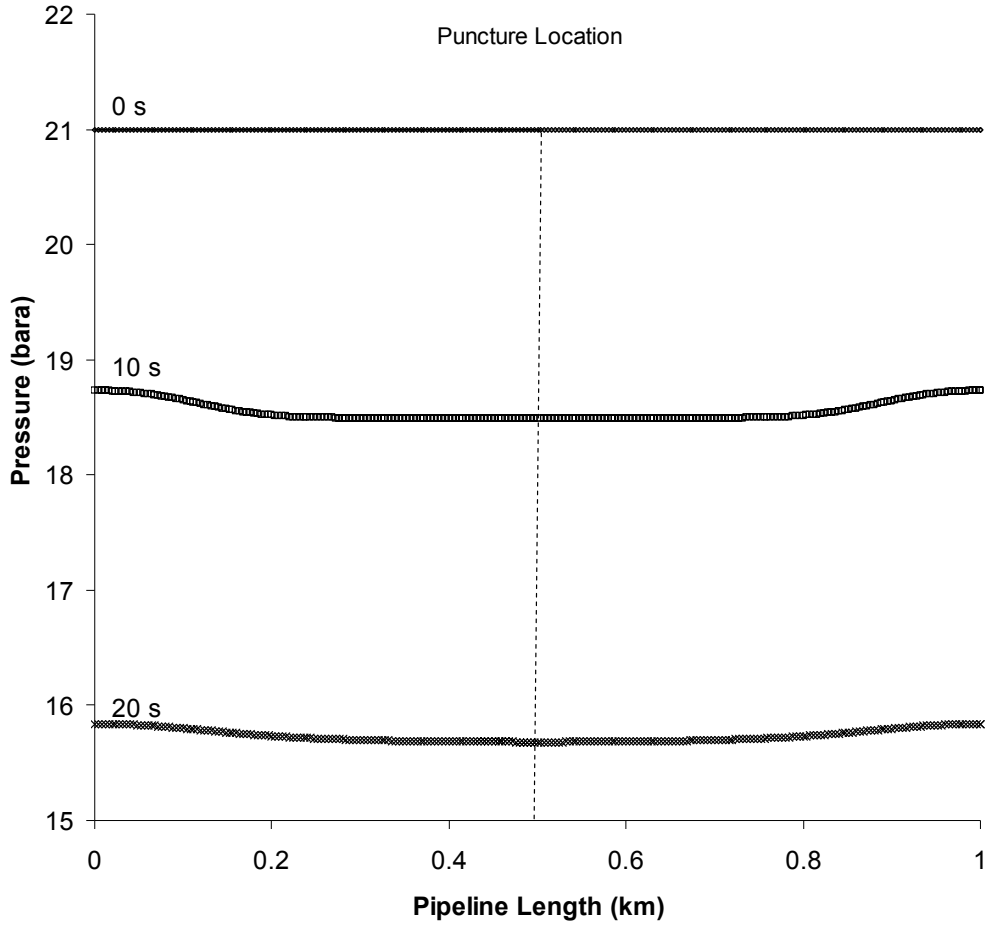

Figure 6.14: The variation of the fluid pressure profile in the vicinity of puncture at different time intervals following puncture.
Inventory: 100% methane
Puncture to pipe diameter ratio: 0.2
Pipeline length: 1000 m

Similarly, figures 6.15 and 6.16 respectively present the temperature and pressure profiles for a 1000 m metre pipe containing equi-molar two-phase mixture of methane and n-pentane.

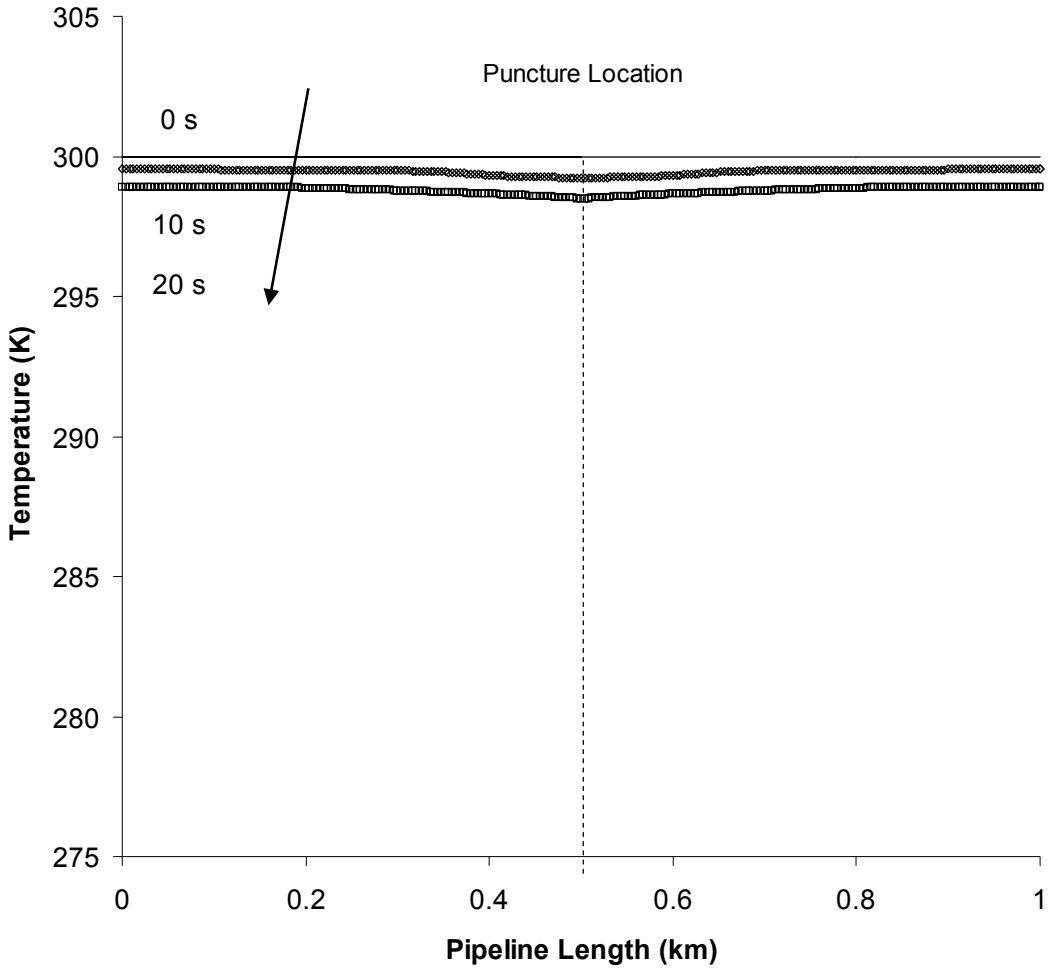

Figure 6.15: The variation of the fluid temperature profile in the vicinity of puncture at different time intervals following puncture.
Inventory: 50% methane, 50% n-pentane
Puncture to pipe diameter ratio: 0.2
Pipeline length: 1000 m

Referring to figure 6.15, it may be observed, the fluid within the pipeline is at 300 K prior to puncture. Following puncture, the fluid cools down at a much slower rate compared to the pure gas (cf. 20K with 2K at 20s). Based on the above, the validity of isothermal assumption increases for pipes containing two-phase inventories as opposed to permanent gas pipes. The pressure profiles presented in figure 6.16, show a stepwise behaviour for distribution of the pressure in the two-phase pipe. However, considering the data given in table 6.4, the assumption of the constant pressure throughout the pipe at each depressurisation step has not introduced significant errors. This may be due to, for example, the insignificant maximum pressure difference of ca. 0.8 % along the pipe after 20 s which continues to decrease as depressurisation proceeds.

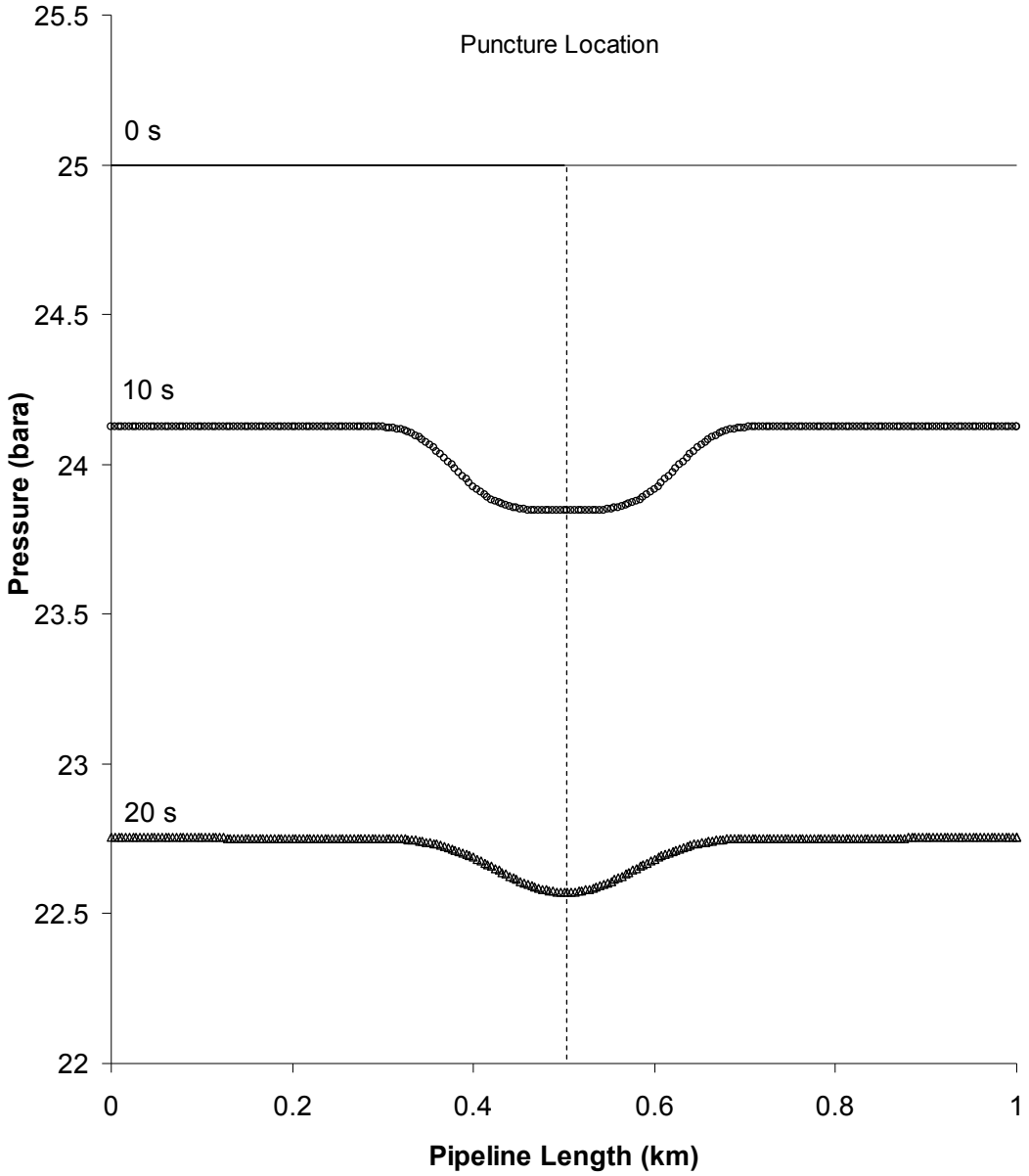

Figure 6.16: The variation of the fluid pressure profile in the vicinity of puncture at different time intervals following puncture.

Inventory: 50% methane, 50% n-pentane

Puncture to pipe diameter ratio: 0.2

Pipeline length: 1000 m

6.9.3 Impact of the Initial Pressure

Figures 6.17 and 6.18 show the comparisons of cumulative mass released against depressurisation time for different initial line pressures of 21, 50 and 100 bara based on VBM and PHU predictions. Figures 6.17-6.20 present the corresponding comparison of the discharge pressure and cumulative mass released against depressurisation time based on predictions of VBM and PHU for different line pressures. Figures 6.17 and 6.19 show the comparison of transient cumulative mass released and discharge pressure for gaseous methane respectively whereas figure 6.18 and 6.20 show the corresponding data for the two-phase methane/n-pentane mixture. The pipe length and puncture to pipe diameter ratio are 100 m and 0.4 respectively.

In line with the previous findings, for the case of gaseous methane, VBM predictions of cumulative mass released are higher than those obtained using PHU. Also, the degree of agreement between the predictions of the two models improves with decrease in the starting line pressure.

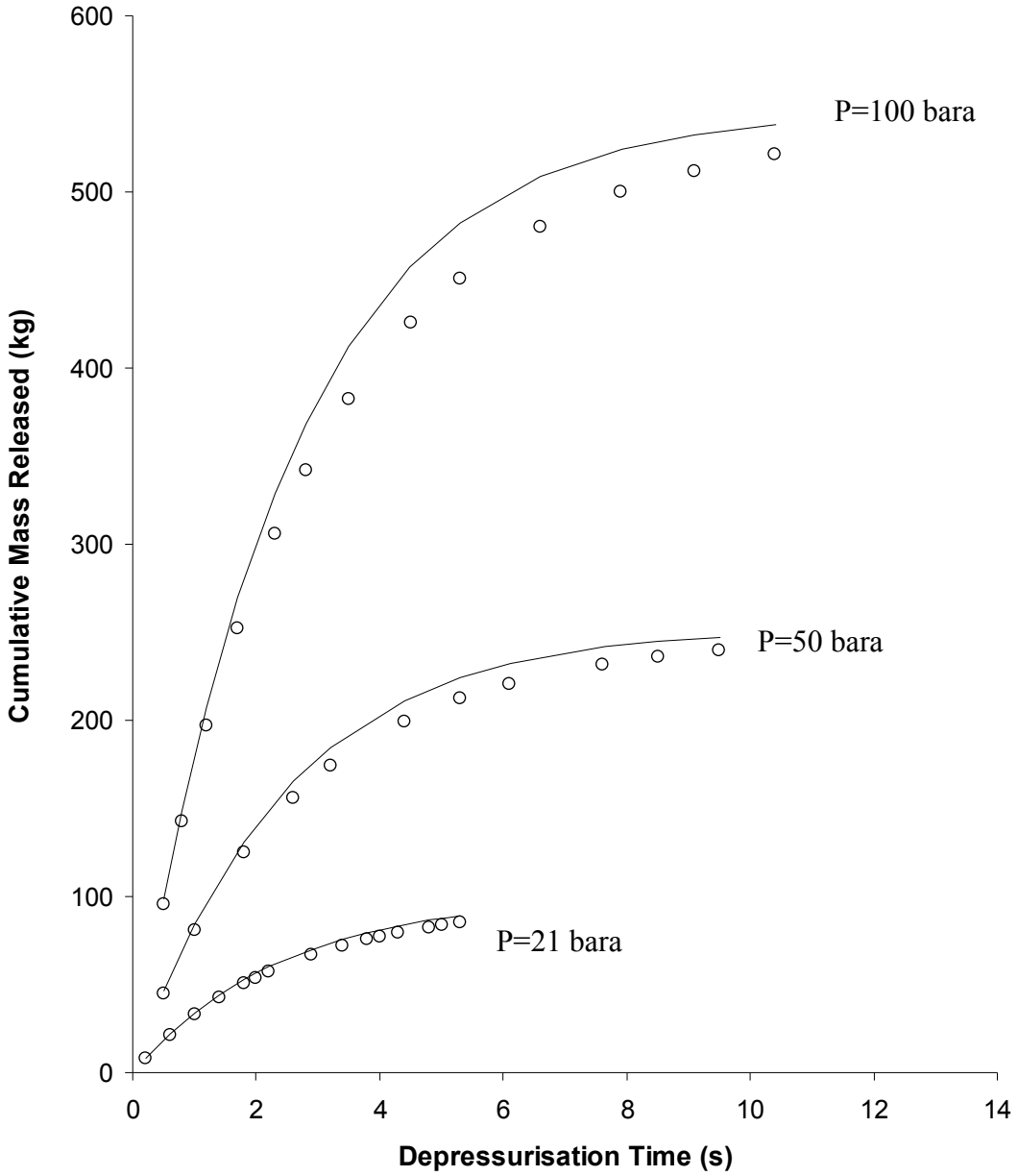

Figure 6.17: Comparison of the cumulative mass released against time during depressurisation to 1 bara based on VBM (solid line) and PHU (data points) predictions for different initial line pressures.

Inventory: 100% methane

Puncture to pipe diameter ratio: 0.4

Pipeline length: 100 m

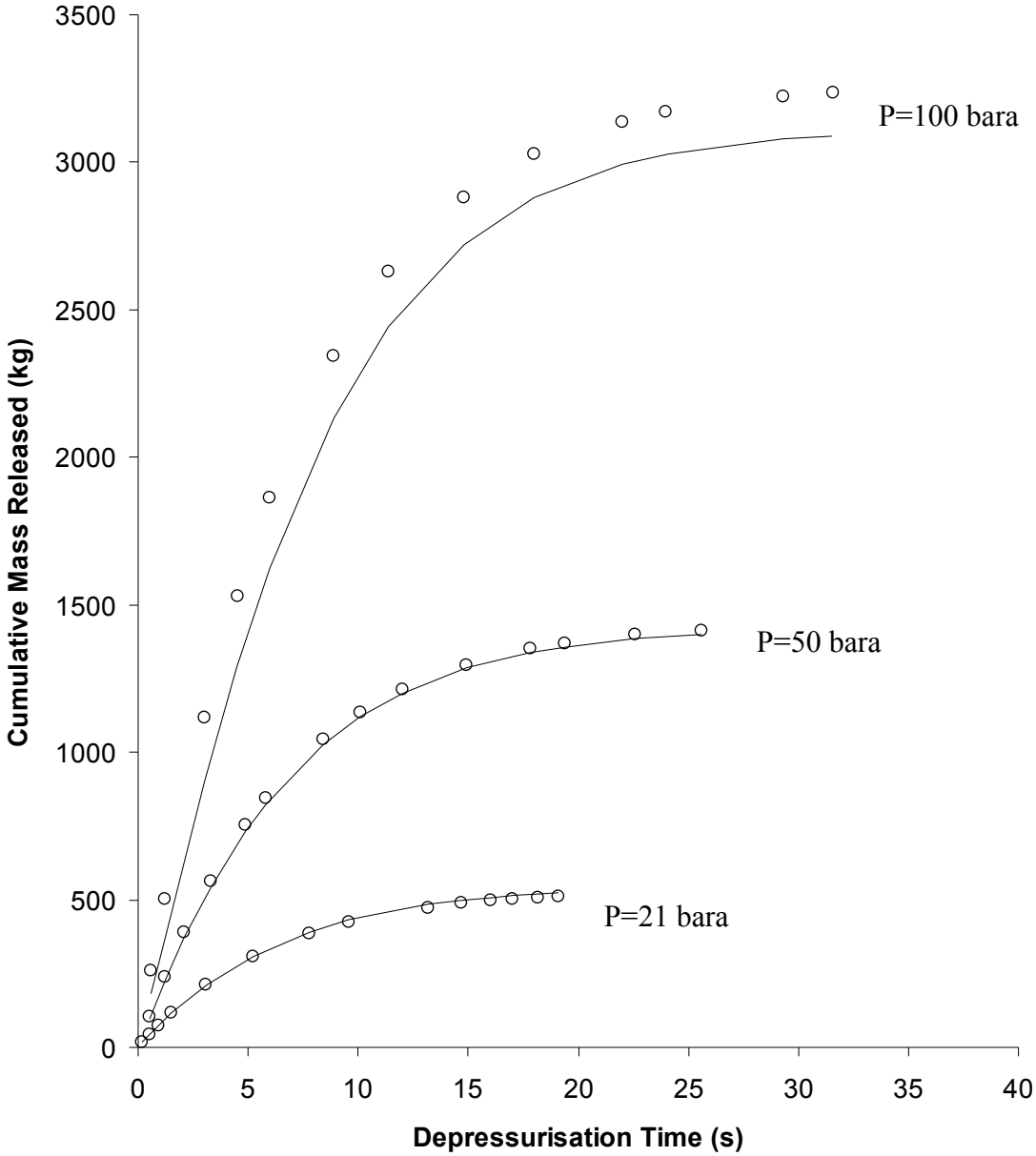

Figure 6.18: Comparison of the cumulative mass released against time during depressurisation to 1 bara based on VBM (solid line) and PHU (data points) predictions for different initial line pressures.

Inventory: 50% methane- 50% n-pentane

Puncture to pipe diameter ratio: 0.4

Pipe length: 100 m

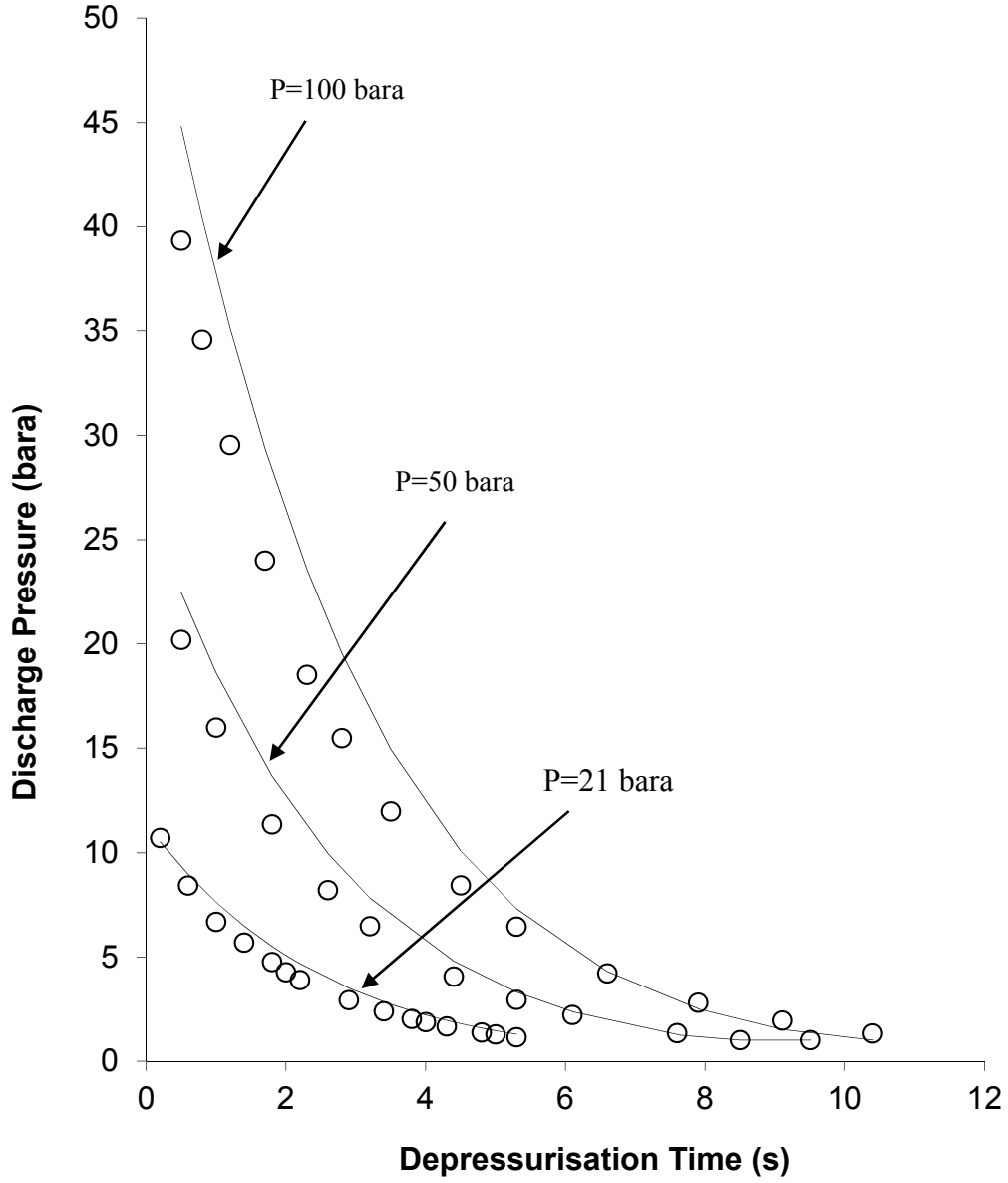

Figure 6.19: Comparison of the discharge pressure against depressurisation time to 1 bara based on VBM (solid line) and PHU (data points) predictions for different initial line pressures.

Inventory: 100% methane

Puncture to pipe diameter ratio: 0.4

Pipeline length: 100 m

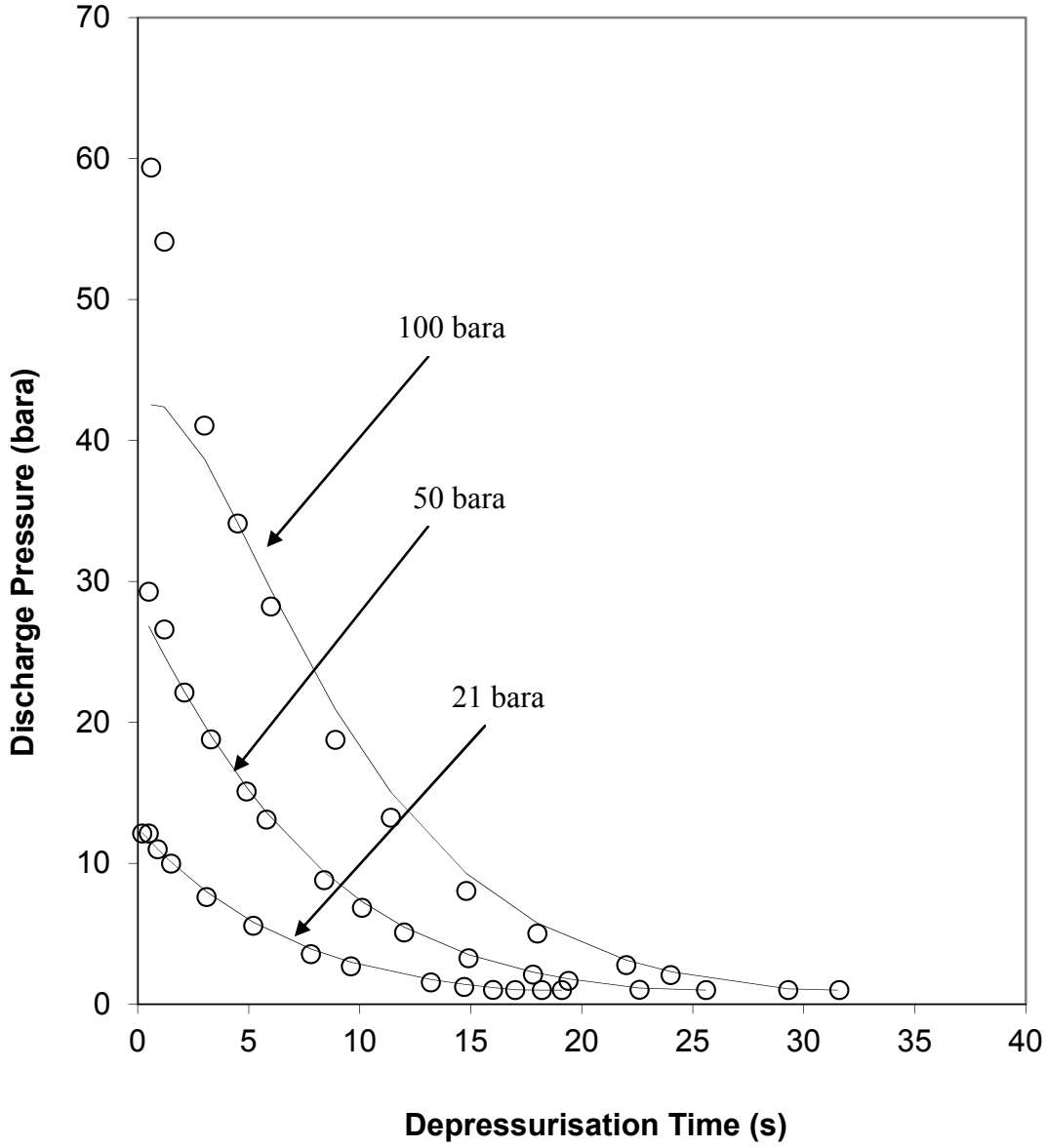

Figure 6.20: Comparison of the discharge pressure against time during depressurisation to 1 bara based on VBM (solid line) and PHU (data points) predictions for different initial line pressures.
Inventory: 50% methane- 50% n-pentane
Puncture to pipe diameter ratio: 0.4
Pipe length: 100 m

Table 6.5 presents the corresponding average and maximum error in VBM predictions of cumulative mass released at the different initial line pressures relative to PHU predictions.

As it may be observed in figures 6.17 and 6.18, VBM predictions are in good agreement against those obtained using PHU for all the conditions tested with the exception of 100 bara line pressure.

The discharge pressures calculated using VBM in figure 6.19 for gaseous inventory are relatively in good agreement with those of PHU for case of 21 bara. However the degree of agreement decrease with increase of line pressure. In figure 6.20, the discharge pressures calculated using VBM for the pipe with 100 bara initial pressure is considerably lower than PHU predictions. This marked difference is postulated to be due to failure of equation (6.27) in obtaining a correct choked pressure. Accordingly, the under-prediction of choked pressure results in under-prediction of the discharge rate which consequently results in a lower prediction of the cumulative mass released.

As can be seen in table 6.5, as the initial pressure in the pipe is increased from 21 bara to 100 bara the average error for the case of gaseous methane is increased from 4.30% to 6.77%. For two-phase mixture, very good agreement is observed with the exception of the 100 bara line pressure whereby VBM predictions of cumulative mass released is lower than PHU for the entire duration of depressurisation.

Table 6.5: Average and maximum percentage errors in the cumulative mass released using VBM predictions as compared to PHU predictions at different initial line pressures for the gaseous methane and an equi-molar two-phase mixture of methane and n-pentane.

Initial line pressure (bara)	Permanent Gas (100% methane)		Two-phase mixture (50% methane and 50% n-Pentane)	
	Average % error	Maximum % error	Average % error	Maximum % error
21	4.29	5.19	1.46	2.46
50	4.60	6.02	2.47	5.86
100	5.77	7.83	11.44	29.46

Puncture to pipe diameter ratio: 0.4; Pipe length: 100 m.

In order to explain this, the comparisons of the discharge rate against depressurisation time for both VBM and PHU are presented in figures 6.21 and 6.22 for gaseous and two-phase inventories respectively.

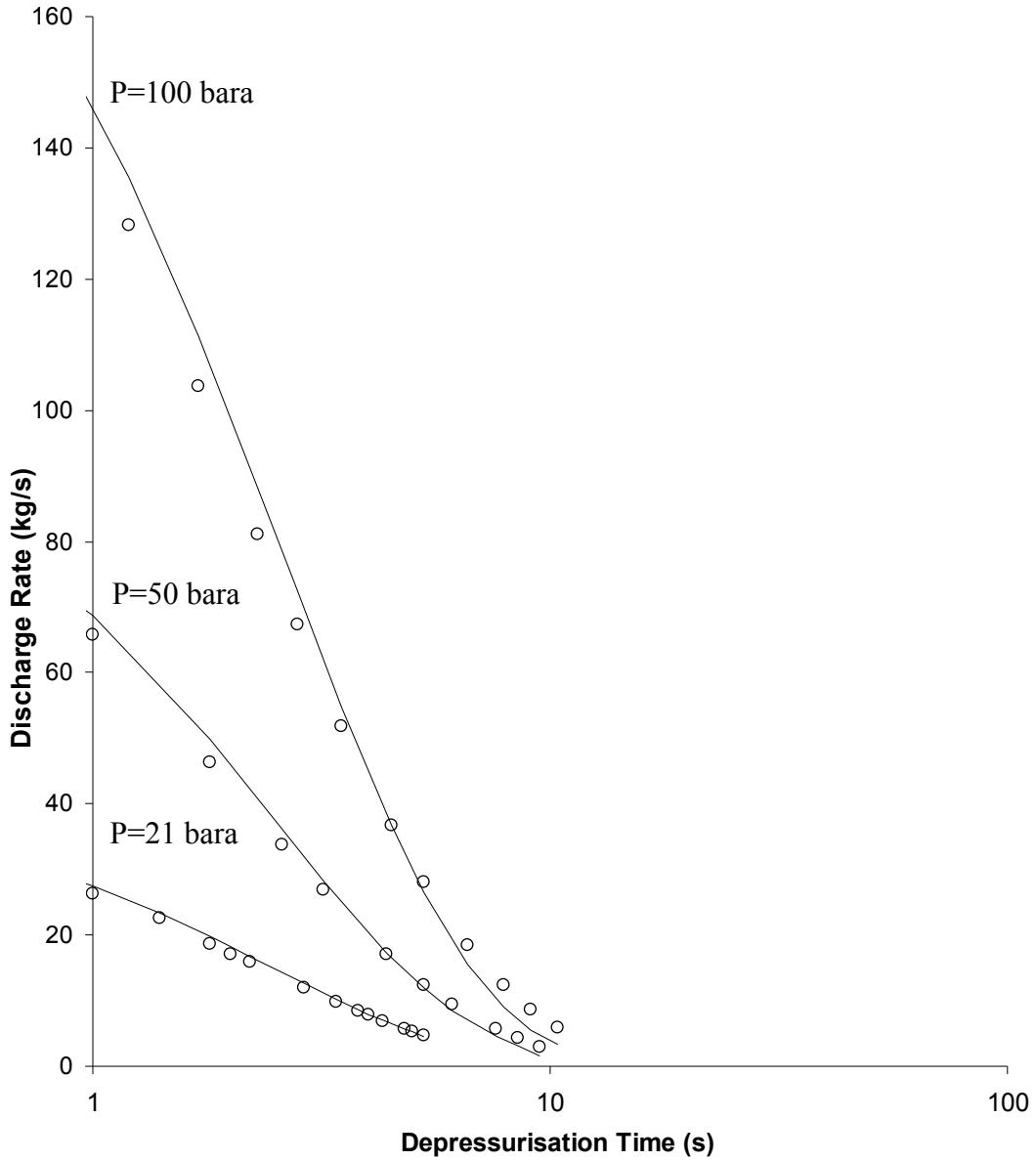

Figure 6.21: Comparison of the discharge rate against depressurisation time to 1 bara based on VBM (solid line) and PHU (data points) predictions for different initial line pressures.

Inventory: 100% methane

Puncture to pipe diameter ratio: 0.4

Pipeline length: 100 m

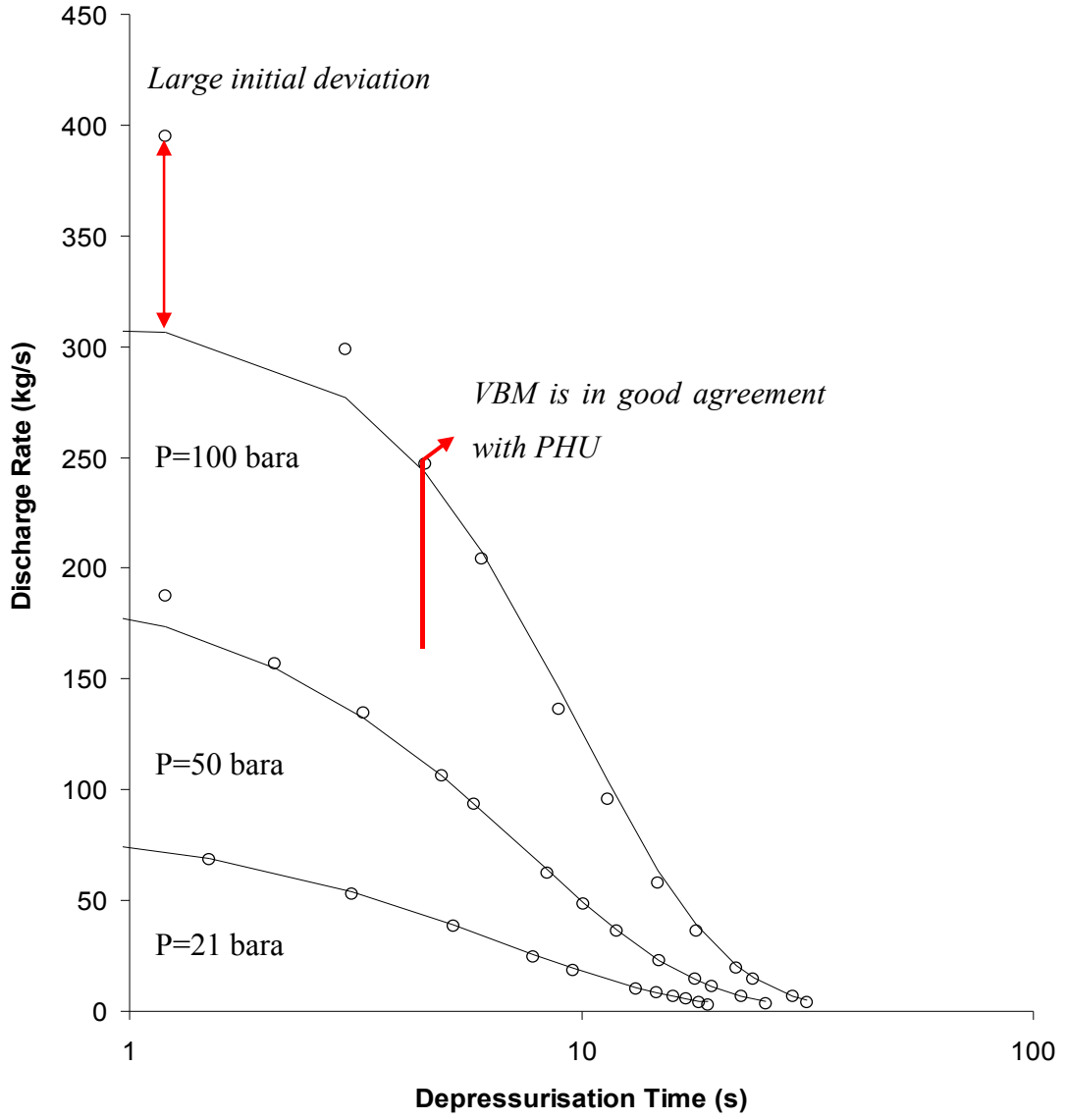

Figure 6.22: Comparison of the discharge rate against time during depressurisation to 1 bara based on VBM (solid line) and PHU (data points) predictions for different initial line pressures.

Inventory: 50% methane- 50% n-pentane

Puncture to pipe diameter ratio: 0.4

Pipe length: 100 m

In figure 6.22, the marked difference between the two models for the calculated mass discharge rates can be observed at the beginning of depressurisation (identified with arrow). As explained earlier, this deviation is due to the limitation of the Omega method and failure of equation 6.27 in predicting of the correct choked pressure. The 100 bara initial pressure of the pipe is very close to the two-phase mixture critical pressure of 103.1 bara which corresponds to reduced pressure of 0.94. This is considerably higher than the recommended reduced pressure range of <0.5 (Lenzing et al., 1998). Approximately 3 s following the depressurisation, the VBM prediction of the discharge rate provides a good agreement with the PHU and this trend continues till the end of depressurisation. This point corresponds to an upstream pressure of approximately 67 bara which is equivalent to the reduced pressure of 0.65.

6.10 Analysis of Computational Run-time

The main objective of this study was to address the long computational run-time associated with numerically based pipeline puncture simulations by developing a semi-analytical model which requires negligible computational resources.

Tables 6.6 and 6.7 respectively present the computational run-times for different pipeline lengths containing permanent gas (100% methane) and the two-phase (50% methane and 50% n-pentane) mixture. The line pressure is 21 bara and puncture to pipe diameter ratio of 0.2 are chosen as an example. Given that VBM is primarily a semi-analytical model, the corresponding computational run-time is comparatively insignificant.

As can be seen from table 6.6, the CPU run-time for PHU increases non-linearly with the increase of pipe length. This is because the number of nodes, when discretising time and space in PHU model, varies according to the length of the pipe. On the other

hand, the CPU run-time associated with VBM is unaffected by increase in pipe length and remains constant at ca. 0.320 s.The computational run-time of the PHU for two-phase pipelines, is almost three times higher than the permanent gas pipelines. This is due to the higher computationally demanding flash calculations involved which are required for determination of the physical properties of the two-phase inventory. Similarly, in table 6.7, the CPU run-time associated with PHU increases non-linearly with increase of pipe length in contrast to VBM which remains constant at ca. 1 s.

Table 6.6: Computational run-time reported for the simulations of VBM and PHU based on different pipe length.

Pipe Length (m)	CPU run-time for PHU	CPU run-time for VBM
100	4 min 2 s	0.321 s
1000	35 min 2 s	0.322 s
5000	4 h 12 min 33 s	0.320 s

Initial pressure, 21 bara; Inventory: 100% methane; Puncture to pipe diameter ratio, 0.2.

Table 6.7: Computational run-time reported for the simulations of VBM and PHU based on different pipe length.

Pipe Length (km)	CPU run-time for PHU	CPU run-time for VBM
100	2 hr 15 min 5 sec	1.022 sec
1000	5 hr 34 min 33 sec	1.022 sec
5000	12 hr 18 min 33 sec	1.019 sec

Initial pressure, 21 bara; Inventory: 50% methane and 50% n-Pentane; Puncture to pipe diameter ratio, 0.2.

As it may be observed, given that the VBM solution method is mainly analytically based, the corresponding computational run-times in all the cases presented are orders of magnitude smaller than those for PHU based simulations. Such reductions are especially marked for the two-phase mixture. For example, for the case of 5000 m pipe, the computational run-time is reduced from ca. 12 h down to ca. 1 s by employing the VBM whilst the corresponding maximum error is only 1.51% as compared to PHU.

6.11 Concluding Remarks

This chapter investigated the tantalizing important question of if and under what conditions the outflow from a punctured pipe can be modelled as that discharging from a vessel. Given that the latter may be solved analytically, this study addresses the fundamentally important drawback of the long computational run-times associated with the numerical techniques for simulating pipeline punctures.

The investigations involved development and testing of a simplified VBM and comparing its predictions against a rigorous but computationally demanding pipeline outflow model (i.e PHU) for a variety of test conditions.

These include variations in the pipe length, puncture/pipeline diameter ratio and line pressure for a permanent gas and a two-phase inventories. The results indicated that in the majority of cases, reasonably good agreement between the two methods exist. The degree of agreement was found to increase with decrease in the diameter ratio and line pressure. An increase in the pipe length also improved the degree of agreement.

In essence, the VBM performs well in predicting outflow from a punctured pipeline for as long as there is negligible relative bulk flow between the discharging fluid and the pipe wall.

Surprisingly, the VBM produces more accurate predictions for two-phase mixtures when compared with permanent gases. This is found to be a consequence of the better applicability of the isothermal bulk fluid decompression assumption within the pipeline in the case of two-phase mixtures.

Chapter 7: Development of Un-Isolated Vessel Blowdown Model (UVBM)

7.1 Introduction

This chapter deals with the extension of the VBM presented in chapter 6 for simulating the un-isolated puncture of pressurised pipelines. The application of the model hereby referred to as Un-isolated Vessel Blowdown Model (UVBM) is tested by comparison of its predictions against those obtained using the PHU.

The following three pipeline puncture scenarios are studied:

1. Isolated pipe with no initial feed flow
2. Isolated pipe with cessation of feed flow upon puncture
3. Cessation of feed flow 50 s post puncture

For the latter case, the computational run-time is compared with the corresponding computational run-time obtained using PHU

7.2 Development of the UVBM

Figure 7.1 schematically presents the pipe geometry used in the development of the UVBM whereby the puncture of a pressurised pipe between the block valves is approximated as a vessel with the same dimensions as the pipe depressurising through an orifice with an assumed diameter corresponding to the punctured area.

The pertinent physical and thermodynamic properties required for the formulation of the UVBM are presented in figure 7.2.

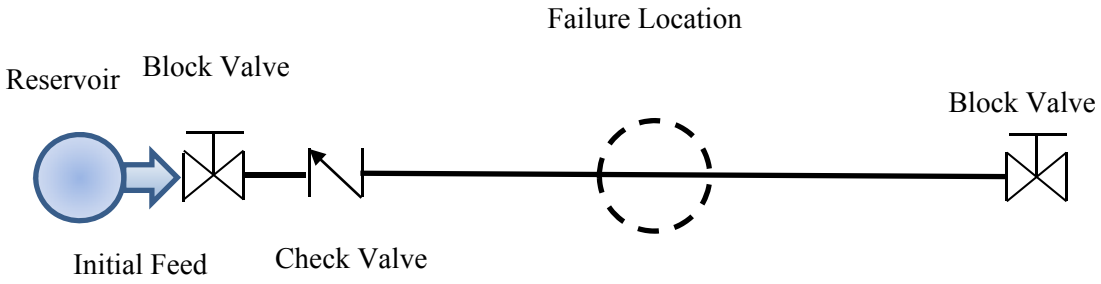

Figure 7.1: Pipeline geometry and illustration of reservoir, initial feed flow and valves with respect to failure location.

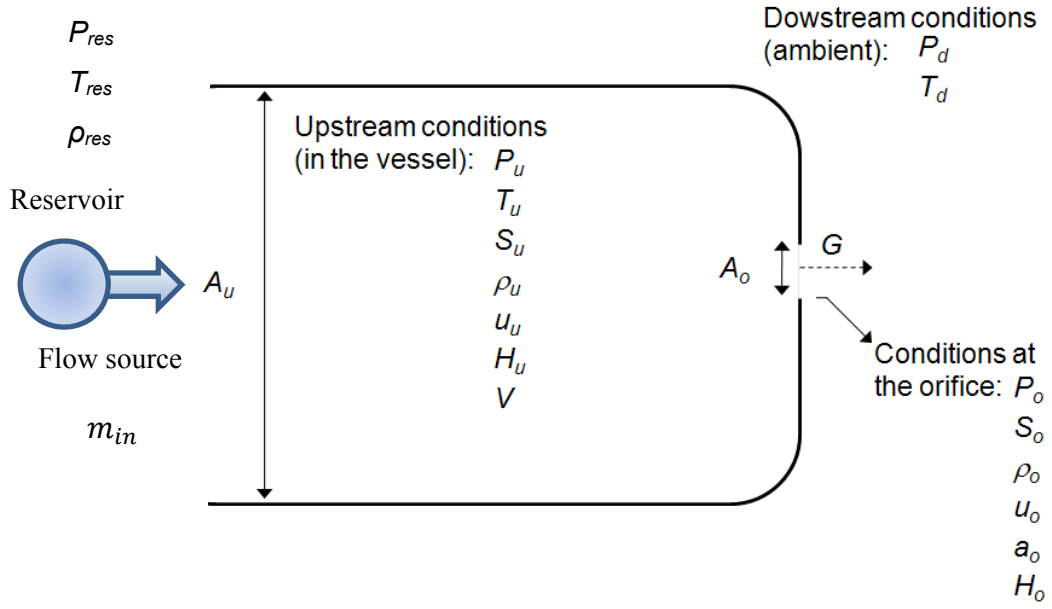

Figure 7.2: Schematic representation of a discharging vessel indicating the pertinent physical and thermodynamic properties required for the formulation of the UVBM.

P: pressure; T: temperature; S: entropy; ρ: density; H: enthalpy; u: velocity; V: volume; A: cross sectional area; G: mass discharge rate; a: speed of sound and m: mass flow rate. Subscripts u, o, d, in and res refer to the upstream, orifice, downstream, inlet and reservoir conditions respectively.

7.3 Mathematical Modelling of the UVBM

The following are the main assumptions employed in development of the UVBM in addition to those presented in chapter 6 for the VBM:

- The pipe is connected to an infinite reservoir (such as discharge from a wellhead)
- The pipeline inlet pressure is assumed to remain constant and equal to the reservoir pressure (P_{res})
- Vessel dimensions are the same as those of the pipe
- Prior to failure, the fluid flow in the pipe is in non-isothermal steady state condition
- No temperature stratification across the vessel wall
- Wall density ρ_w, specific heat capacity, C_{pw} and thermal conductivity, κ_w remain constant

Based on the above, the mass balance across the vessel is given by the following equation (Coulson and Richardson, 1999):

$$\frac{d(\rho V)}{dt} = m_{in} - G \qquad (7.1)$$

Where,

ρ = fluid density

t = time

V = vessel volume

G= mass discharge rate

m_{in}= inlet mass flow rate

Discharge rate is obtained using the following equation (see chapter 6: section 6.2.1)

$$G = C_D \rho_o u_o A_o \tag{6.1}$$

Given that the vessel volume is constant, the rate of change in density is given as:

$$\frac{d(\rho)}{dt} = (m_{in} - G)/V \tag{7.2}$$

Accordingly, the energy balance across the vessel is the sum of three components as given below:

$$\frac{VC_p d(\rho T)}{dt} = [(mC_p T)_{in} - \left(\mathrm{G}C_p T\right)_o] + \frac{d(PV)}{dt} + Q_h \tag{7.3}$$

Where,

C_p= fluid specific heat capacity

T_w= vessel wall temperature

T= fluid temperature

Q_h= heat transferred to the fluid given as (see chapter 3: section 3.7):

$$Q_h = \frac{4}{D_{in}} h_f^{i-1}(T_w - T) \quad (3.\ 1)$$

The first term on the RHS of equation 7.3 represents the energy flowing into and discharged from the vessel. The second term presents the work done by the fluid expansion during the depressurisation. The third component is the heat transferred from the vessel to the fluid.

The lumped body approach (Myers, 1971) is employed in UVBM whereby vessel wall temperature, T_w will get updated at each time step and used in Newton's cooling law (equation 3.27) to calculate the rate of heat transferred, Q_h to the fluid. T_w is obtained:

$$Ms_w C_{pw} \frac{dT_w}{dt} = h_{amb}^{i-1} A_{amb}(T_{amb} - T_w) - h_f^{i-1} A_{in}(T_w - T) \quad (7.\ 4)$$

Where,

Ms_w= mass of the steel

C_{pw}=heat capacity of pipe wall

A_{out} and A_{in} = the outside and inside surface areas along the walls of the vessel respectively

T_{amb}= the ambient temperature

h_{amb} and h_f =ambient and fluid heat transfer coefficients respectively

The fluid mixture density is calculated from:

$$\rho = \frac{PMw}{z\,RT} \tag{7. 5}$$

Where,

z = fluid compressibility factor

Mw=fluid molecular weight

R= Universal gas constant

For the case of two-phase flow, the mixture compressibility factor is determined from:

$$z = xz_g + (1 - x)z_l \tag{7. 6}$$

Where x is vapour fraction and subscripts g and l respectively denote gas and liquid phases.

In order to determine the second term on RHS of equation (7.3), equation (7.5) is rearranged and differentiated with respect to time giving:

$$\frac{d(PV)}{dt} = \frac{zVR}{Mw}\frac{d(\rho T)}{dt} \tag{7. 7}$$

Replacing equations (7.7) into (7.3) and rearranging gives:

$$\frac{d(\rho T)}{dt} = \frac{(mC_pT)_{in} - (\mathrm{G}C_pT)_o + Q_h}{V(C_p - \frac{zR}{Mw})} \tag{7. 8}$$

Using the rule of multiplication of derivatives for the left hand side of equation (7.8) yields:

$$\frac{d(\rho T)}{dt} = \rho \frac{dT}{dt} + T \frac{d\rho}{dt} \tag{7.9}$$

Rearranging gives:

$$\frac{dT}{dt} = \frac{(\frac{d(\rho T)}{dt} - T \frac{d\rho}{dt})}{\rho} \tag{7.10}$$

7.4 Determination of the Vessel Equivalent Pressure and Temperature

The pressure drop along the pipe during flow results in a corresponding drop in the fluid density. This means that at any given time, the amount of inventory within the pipe will be less than that for the no flow condition. Therefore, a steady state solution prior to puncture is required in order to determine the vessel equivalent pressure and temperature. Accordingly, the non-isothermal steady state model by Brown (2011) is utilised which involves numerical solution of the following equations:

$$u \frac{d\rho}{dx} + \rho \frac{du}{dx} = 0 \tag{3. 2}$$

$$\rho u \frac{\partial u}{\partial x} + \frac{\partial P}{\partial x} = \beta_x + \rho g \sin(\theta) \tag{3. 3}$$

$$\frac{\partial \mathrm{s}}{\partial \mathrm{x}} = \frac{Q_h + u\beta_x}{\rho u T} \tag{7.11}$$

The frictional force term (β_x) is given by:

$$\beta_x = \frac{2\rho u|u| f_w}{D} \quad (3.4)$$

Where,

f_w= fanning friction factor

D= pipeline diameter

The above equations are Ordinary Differential Equations (ODEs) and the Runge-Kutta method based on the Brankin (1989) algorithm is used for their numerical solution. The above is performed by employing the NAG sub-routine nag_ivp_ode_rk (Numerical Algorithms Group, 2000).

Once the pressure profile along the pipeline prior to failure is determined, the corresponding velocity profile and the total mass of the inventory inside the pipe may be determined. Using the volume of the pipe, the equivalent vessel pressure is determined using equation (7.5). The average temperature along the pipe is used as vessel equivalent temperature.

For calculation of the heat transfer coefficient, it is assumed that there is no drop in the fluid velocity along the vessel during the depressurisation.

7.5 Calculation Algorithm for UVBM

The calculation algorithm for simulating the depressurisation of a punctured pipeline using UVBM requires numerical solution of the following ODEs:

$$\frac{d(\rho)}{dt} = (m_{in} - G)/V \quad (7.2)$$

$$Ms_w C_{pw} \frac{dT_w}{dt} = h_{amb}^{i-1} A_{amb}(T_{amb} - T_w) - h_f^{i-1} A_{in}(T_w - T) \quad (7.7)$$

$$\frac{d(\rho T)}{dt} = \frac{(mC_pT)_{in} - (GC_pT)_o + Q_h}{V(C_p - \frac{zR}{Mw})} \quad (7.8)$$

$$\frac{dT}{dt} = \frac{(\frac{d(\rho T)}{dt} - T\frac{d\rho}{dt})}{\rho} \quad (7.10)$$

The calculation procedure for determining the discharge rate and release pressure and their variation with time is described below:

1. Given the pipe inlet conditions, the non-isothermal steady state model is utilised in order to calculate total mass of the inventory inside the vessel, vessel equivalent pressure, P^i_u and temperature, T^i_u

2. Using the pressure, P^i_u and temperature, T^i_u, a pressure-temperature flash calculation is performed to determine the upstream enthalpy (H_u), upstream entropy (S_u) and feed density (ρ_u)

3. Determine the orifice pressure, P_o using the procedures given in chapter 6 (see sections 6.3 and 6.4 as applicable)

4. Determine the fluid enthalpy, speed of sound and density at the release plane using a pressure-entropy flash calculation at P_o and S_u

5. Calculate the discharge rate using equation (6.6)

6. Calculate inlet mass flow rate. In the case of cessation of flow upon failure, m_{in} is equal to zero

7. Calculate $\frac{d(\rho)}{dt}$, $\frac{d(T_w)}{dt}$, $\frac{d(\rho T)}{dt}$ and $\frac{dT}{dt}$ using equations (7.2), (7.4), (7.8) and (7.10) respectively

8. Utilising the forward difference approximation of the above derivatives, calculate the ρ_u^{i+1}, T_u^{i+1} and T_w^{i+1} for the next time step

   A Δt of 0.2 s is used for all the simulations presented in this chapter.

9. Calculate P_u^{i+1} using equation (7.5). As the compressibility factor, z is a function of pressure and temperature, this needs to be solved iteratively. Using the z, obtained in previous time step, determine P_u^{i+1} and then calculate the new z. This is continued until convergence is achieved

10. Return to step 2. The calculations are terminated once the required depressurisation is reached or the vessel pressure is equal to ambient pressure.

7.6 Impact of Initial Feed Flow and Cessation of Flow

Table 7.1 presents the prevailing conditions, pipeline characteristics and the parameters employed in the proceeding investigations using the UVBM. The pipeline is assumed to be made of mild steel. A constant puncture to pipeline diameter ratio of 0.2 is used throughout. For simulations carried out using the PHU numerical simulation a nested grid system is used to reduce the CPU run-time.

For gaseous pipe, a mixture of 80 mol % methane and 20% mol % ethane and for the case of two-phase, an equi-molar mixture of methane and n-pentane are selected.

For simplicity, a discharge coefficient of unity is assumed. All simulations are performed using a 2.66 GHz, 3.0 GB RAM PC. Throughout this chapter, the solid lines represent the UVBM predictions whilst the data points represent PHU predictions. The UVBM predictions are obtained for different flow scenarios whilst the PHU predictions are only presented for the most prominent case which is cessation of flow 50 s after the depressurisation in order to improve the clarity of the figures presenting the comparison between UVBM and PHU. Although in each case, the differences between PHU and UVBM predictions were negligible.

7.6.1 Permanent Gas

Figures 7.3 and 7.4 respectively represent the predicted cumulative mass released and discharge pressure against time for different feed flow scenarios following the puncture (0.06 m dia) of a 10 km, 0.3 m i.d gas pipe. Curves A and B present UVBM predictions for an isolated pipe without and with initial feed flow respectively. Curve C and data points on the other hand present UVBM and PHU predictions for the case when feed flow is ceased 50 s after puncture. For the sake of an example, a typical feed velocity of 10 m/s is used (see table 7.1) As it may be observed in figure 7.3, curve B shows less mass being released as compared to curve A which is due to the impact of initial feed flow prior to failure. Similarly, given the flow is ceased 50 s after the failure, curve C shows more mass being released as compared to curve B and is in very good agreement with PHU prediction (data points). The average difference between UVBM (curve C) and PHU (data points) predictions is ca. 1.21%.

Table 7.1: Pipeline characteristics, prevailing conditions and the parameters employed in the proceeding investigations.

Parameter	Value	
Pipe length, L (m)	10,000	
Pipe inner diameter, D (m)	0.3	
Pipe wall thickness (m)	0.01	
Line pressure (bara)	21.6	
Initial temperature (K)	300	
Ambient pressure (bara)	1.01	
Ambient temperature (K)	290	
Puncture location	Mid length	
Discharge coefficient	1	
Puncture diameter, d_o (m)	0.06	
Puncture to inner pipe diameter ratio (d_o/D)	0.2	
Pipe wall material	Carbon steel	
Pipe wall density (kg/m^3)	7854	
Pipe wall thermal conductivity (W/m^{2}C)	53.65	
Pipe roughness (m)	0.0005	
Wind velocity (m/s)	0	
Initial Feed Velocity (m/s)	Two-phase pipe	2.5
	Gaseous pipe	10
Cessation of feed flow after failure (s)	50	

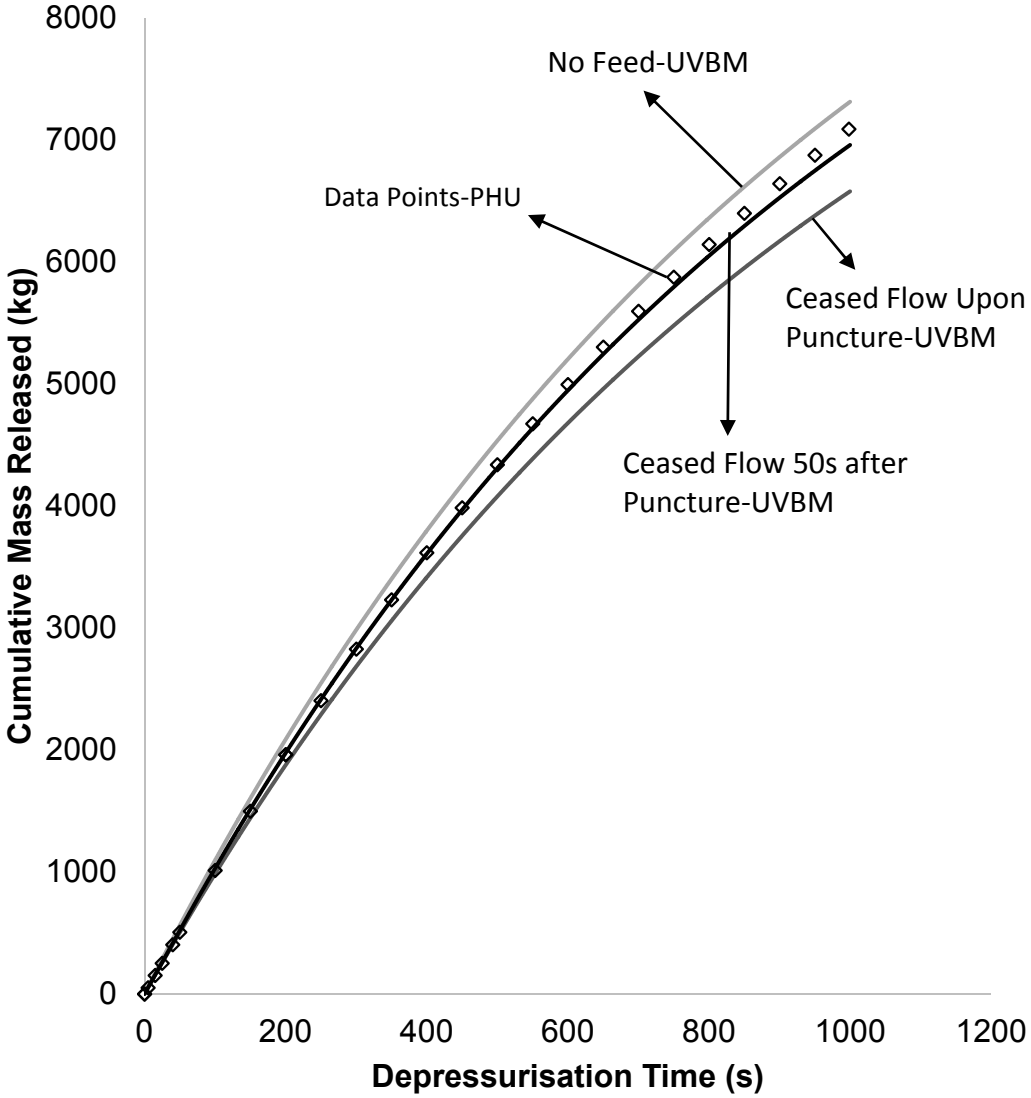

Figure 7.3: Comparison of cumulative mass released against depressurisation time for UVBM (solid lines) and PHU (data points) for different inlet feed scenarios:
Curve A: UVBM, isolated pipe with no initial feed flow, CPU run-time: 9.73 s
Curve B: UVBM, isolated pipe with initial feed flow, CPU run-time: 11.95 s
Curve C: UVBM, cessation of feed flow at 50 s, CPU run-time: 12.65 s
Data points: PHU, cessation of feed flow at 50 s, CPU run-time: 4,763 s

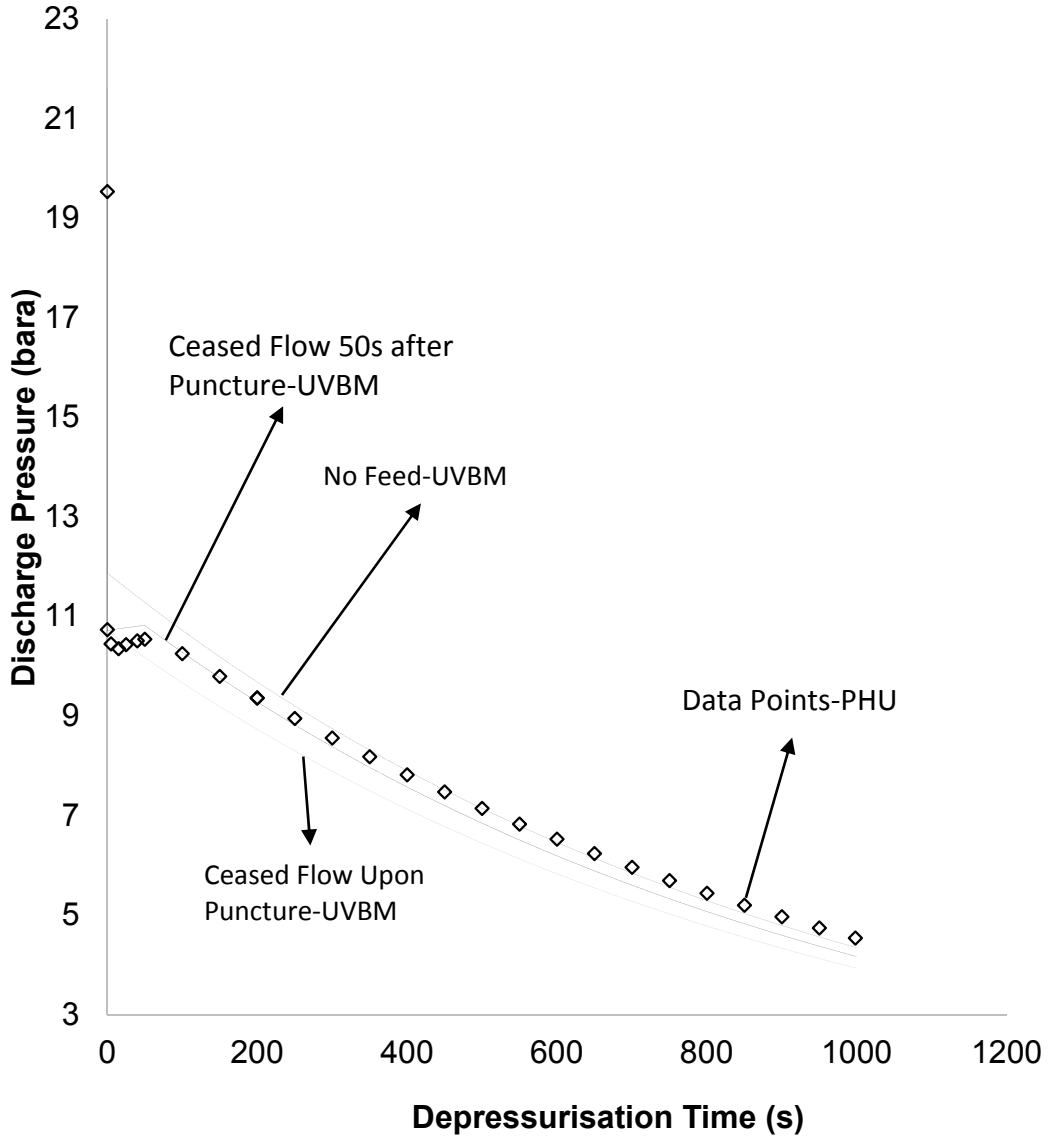

Figure 7.4: Comparison of discharge pressure against depressurisation time of the permanent gas pipe using UVBM (solid lines) and PHU (data points) for different scenarios:
Curve A: UVBM, isolated pipe with no initial feed flow, CPU run-time: 9.73 s
Curve B: UVBM, isolated pipe with initial feed flow, CPU run-time: 11.95 s
Curve C: UVBM, cessation of feed flow at 50 s, CPU run-time: 12.65 s
Data points: PHU, cessation of feed flow at 50 s, CPU run-time: 4,763 s

As it can be seen from figure 7.4, as expected, curve B depressurises faster than curve A due to the initial feed flow and curve C depressurises slower than curve B as a result of the incoming flow. The PHU prediction shows a slight drop in the discharge pressure until ca. 15 s post depressurisation followed by a gradual increase until the flow is ceased. This is postulated to be due the complex interactions between the incoming feed and the expansions waves travelling from the release plane towards the high pressure end. Thereafter, the PHU predicts a steady decrease in the discharge pressure. The UVBM, in line with PHU prediction, shows the initial increase in the release pressure which is caused by the feed flowing into the vessel followed by a steady drop. In general, the UVBM prediction of the release pressure (curve C) is in good agreement with PHU (data points) however the level of agreement is gradually reduced towards the end of the simulation.

7.6.2 Two-phase flow

Figures 7.5 and 7.6 respectively represent the predicted cumulative mass released and discharge pressure against time for different feed flow scenarios following the puncture of a 10 km pipe conveying two-phase inventory. Curve A and B present UVBM predictions for an isolated pipe with and without initial feed flow respectively. Curve C and data points present UVBM and PHU predictions for the case that flow is ceased 50 s after the depressurisation. A typical feed velocity of 2.5 m/s is used for initial feed (see table 7.1).

As it may be observed in figure 7.5, much the same as with the findings presented for the gas pipe, curve B shows less mass being released as compared to curve A which is due to the impact of initial feed flow prior to failure. Accordingly, curve C shows more mass being released as compared to curve B.

UVBM (curve C) and PHU (data points) predictions are in excellent agreement with the average difference of ca. 1.32%.

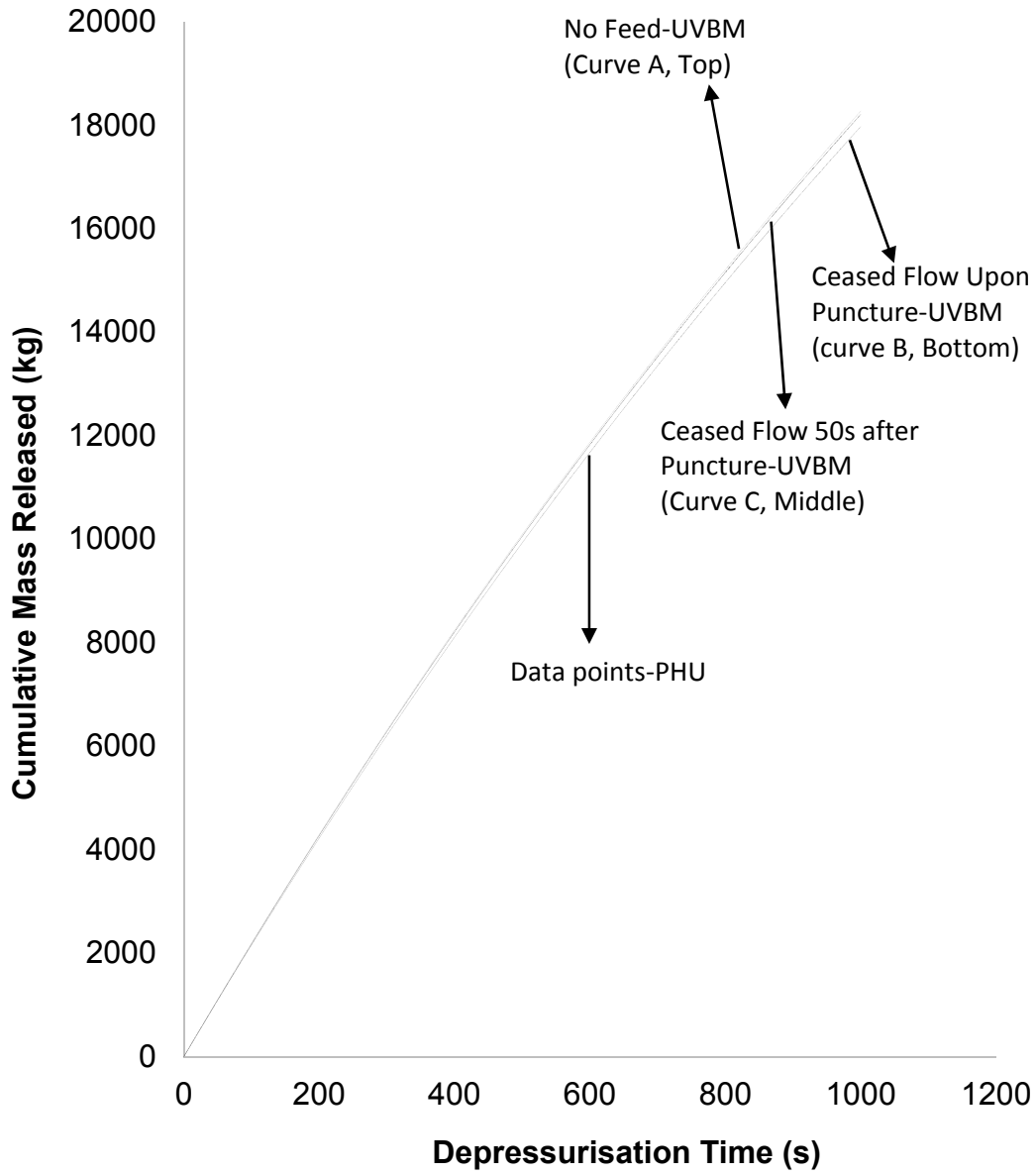

Figure 7.5: Comparison of cumulative mass released against depressurisation time of the two-phase pipe using UVBM (solid lines) and PHU (data points) for different scenarios:

Curve A: UVBM, isolated pipe with no initial feed flow, CPU run-time: 61.91 s

Curve B: UVBM, isolated pipe with initial feed flow, CPU run-time: 72.82 s

Curve C: UVBM, cessation of feed flow at 50 s, CPU run-time: 75 s

Data points: PHU, cessation of feed flow at 50 s, CPU run-time: 8,013 s

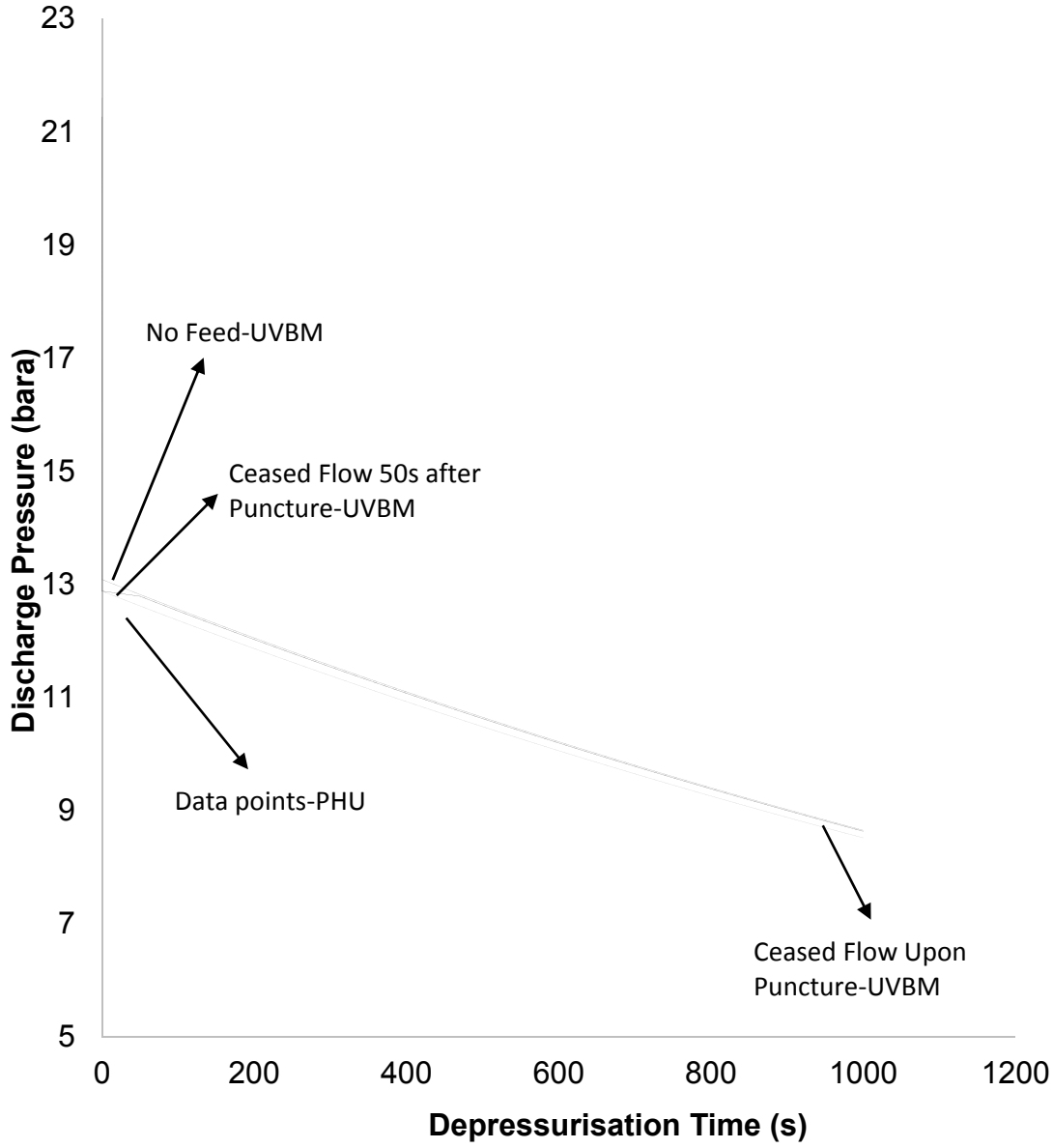

Figure 7.6: Comparison of discharge pressure against depressurisation time of the two-phase pipe using UVBM (solid lines) and PHU (data points) for different scenarios:

Curve A: UVBM, isolated pipe with no initial feed flow, CPU run-time: 61.91 s

Curve B: UVBM, isolated pipe with initial feed flow, CPU run-time: 72.82 s

Curve C: UVBM, cessation of feed flow at 50 s, CPU run-time: 75 s

Data points: PHU, cessation of feed flow at 50 s, CPU run-time: 8,013 s

7.7 Analysis of Computational Run-time

The main objective of this investigation was to address the long computational run-time associated with numerically based pipeline puncture simulations by developing the semi-analytical UVBM which requires negligible computational resources.

Tables 7.2 presents the computational run-times for different scenarios comprising permanent gas (80 mol % methane and 20mol % ethane) and the two-phase (50 mol % methane and 50 mol% n-pentane) mixture. Given that UVBM is primarily a semi-analytical model, the corresponding computational run-time is comparatively insignificant.

As it may be observed, the computational run-time for the PHU simulation for two-phase pipelines is almost two times higher than the permanent gas pipelines due to the higher computationally demanding flash calculations involved. The CPU run-time of the UVBM for two-phase pipelines is ca. 7 fold longer than the permanent gas pipe which is largely due the higher computation of flash calculations and the iterative solution of the pressure at the next time step (see step 9 of the calculation algorithm of UVBM).

Table 7.1: Computational run-time reported for the simulations of UVBM and PHU based on different feed flow scenarios.

Permanent Gas Pipe			
	CPU run-time		
Model	Case 1	Case 2	Case 3
UVBM	9.73 s	11.95 s	12.65 s
PHU	-	-	4,763
Two-phase Pipe			
	CPU run-time		
Model	Case 1	Case 2	Case 3
UVBM	61.91 s	72.82 s	75 s
PHU	-	-	8,013

Case 1: Isolated pipe with no initial feed flow

Case 2: Isolated pipe with initial feed flow

Case 3: Cessation of feed flow at 50 s post depressurisation

As it may be observed, given that the UVBM solution method is mainly analytically based, the corresponding computational run-times in case 3 are orders of magnitude smaller than those of PHU. Such reductions are especially marked for the case of the two-phase mixture.

7.8 Concluding Remarks

This chapter presented formulation and testing of the Un-isolated Vessel Blowdown Model (UVBM), as an extension of the VBM, which accounts for the impact of initial feed flow and fluid/wall heat transfer into the vessel during puncture. The

performance of the UVBM was tested using a hypothetical 10 km pipe following a puncture midway along the length of the pipe considering three failure scenarios. These include no initial feed flow, cessation of feed flow upon and 50 s after failure.

The UVBM and PHU predictions are found to be in very good accord. As compared to PHU, UVBM shows considerable promise given its negligible computational run-time and its ability to handle initial feed flow.

Although the model performed reasonably well for the cases presented using the typical feed velocities, higher feed velocities or pipeline lengths are expected to invalidate the assumption of uniform pressure along the length of the pipe inherent in VBM/UVBM due to resulting higher pressure drop.

Chapter 8: Conclusions and Suggestions for Future Work

8.1 Conclusions

The main contributions in this work are outlined below:

1- Review of the state of the art outflow models developed for simulating pipeline failures
2- Significant reduction in the computational run-time through development, validation and extensive testing of the efficient CFD model using the Pressure-Entropy (P-S) interpolation scheme and its coupling with Pressure (P), Entropy (S) and Velocity (U) based conservation equations
3- Development and extensive testing of a semi-analytical Vessel Blowdown Model (VBM) aimed at reducing the computational run-time to negligible levels
4- Investigating the conditions under which the transient outflow from a punctured pipeline may be approximated as a vessel discharging through an orifice using the VBM
5- Extending the VBM to account for the impact of initial feed flow and fluid/wall heat transfer

In what follows the main findings of the work are summarised:

In chapter 2, the models for simulating outflow following pressurised pipeline failure with various degree of sophistication were presented. A number of mathematical models were reviewed some of which were based on numerical solution of the

conservation equations and robust thermodynamic models whilst others relied on simplifying assumptions both in terms of fluid dynamic and thermodynamic aspects. The review highlighted how these assumptions undermine the accuracy of the predicted data.

The homogenous equilibrium models of Chen et al. (1995a, b) and Atti (2006) were found to be the most robust in terms of accuracy. The review indicated that in spite of earlier works of Atti (2006) and Brown (2011) focusing on the reduction in computational run-time associated with failure simulation of long pipelines, the CPU run-time still remains persistently long.

Based on the experimental work of Norris and Puls (1993), it was found that for 'small' size apertures, the blowdown behaviours of vessel and pipe become similar. This in turn posed the tantalising question of exactly under what conditions the above finding holds.

It was also found that considering the heat transfer between the fluid and pipe wall improved accuracy of the simulated data as the energy stored within the pipe wall itself is relatively readily available.

Chapter 3 presented and discussed the underlying assumptions upon which the system of conservation equations governing the fluid flow are formulated. The mass, momentum and energy conservation equations were expressed in terms of the primitive variables, pressure, enthalpy and velocity. The chapter highlighted that these equations are quasi-linear and hyperbolic in nature and their numerical solution must be selected appropriately.

The essential hydrodynamic and thermodynamic relations for predicting the pertinent fluid properties such as fluid speed of sound, isochoric thermodynamic function and phase dependent friction factor were presented. Following this, the mathematical expression for predicting the heat transferred to the fluid from the ambient/pipe wall based on the lumped body approach was presented.

In chapter 4, various numerical methods used for resolution of the partial differential equations were discussed. The Method of Characteristics (MOC) and its application for numerical solution of the conservation equations based on the Method of Specified Time were briefly reviewed.

The appropriate boundary conditions representing the fluid dynamics behaviour following the failure of pipeline were presented. These were:

- Intact end of pipeline (closed end)
- Full bore rupture or puncture at the pipe end
- Puncture along the pipe length
- Pump at pipe inlet

The numerical solution based on MOC involved converting the conservation equations into compatibility equations. These compatibility equations were then solved along the characteristic lines using the Euler predictor-corrector technique.

Chapter 5 presented the development of the PSUC. The model utilised the conservation equations based on Pressure (P), Entropy (S) and Velocity (U) as the primitive variables (PSU) coupled with Pressure-Entropy (P-S) interpolation scheme.

The performance of the PSUC was tested against available experimental data as well as hypothetical test cases involving the failure of realistic pipelines containing gas, two-phase and flashing hydrocarbons. In all the cases, the PSUC predictions were found to produce reasonable agreement with the published experimental data. In addition, the PSUC predictions remained in excellent accord with the previously developed but computationally demanding CFD model predictions employing Pressure (P), Enthalpy (H) and Velocity (U) (PHU) as the primitive variables.

More importantly, for all the cases presented, the PSUC consistently produced significant saving in CPU run-time with average reduction of ca. 84% as compared to the PHU.

In chapter 6, the development of a semi-analytical Vessel Blowdown Model (VBM) for predicting outflow from a pipeline following puncture type failure was presented. The conditions under which the transient outflow from a punctured pipeline may be approximated as that emanating from a vessel using the VMB were determined.

The applicability of the VBM was extensively tested by comparison of its predictions of the transient cumulative mass released against those obtained using the PHU. The parameters studied for testing the range of applicability of the VBM included the ratio of the puncture to pipe diameter (0.1 – 0.4), initial line pressure (21 bara, 50 bara and 100 bara) and pipeline length (100 m, 1 km and 5 km). The results revealed that the accuracy of the VBM improves with increasing pipeline length and decreasing line pressure and puncture to pipe diameter ratio. In general, it was shown that the VBM performed well in predicting outflow from a punctured pipeline for as long as there is negligible relative bulk flow between the discharging fluid and the pipe.

Surprisingly, the VBM produced better agreement with the PHU predictions for two-phase mixtures as compared to permanent gases. This was shown to be a consequence of the depressurisation induced cooling of the bulk fluid which is not accounted for in the VBM.

It was found that for high pressure two-phase pipelines (i.e. pressures higher than ca. 65 bara) VBM fails to accurately predict the release pressure. This was shown to be due the limitation of the omega method. Importantly though, the computational run-times were significantly reduced from several hours to ca.1 second using the VBM as compared to PHU.

Chapter 7 presented the development of the Un-isolated Vessel Blowdown Model (UVBM), as an extension of the VBM, which accounted for the impact of initial feed flow and fluid/wall heat transfer into the vessel during puncture. The following three pipeline puncture scenarios were studied:

1. Isolated pipe with no initial feed flow

2. Isolated pipe with cessation of feed flow upon puncture

3. Cessation of feed flow sometime after puncture

The applicability of the UVBM was tested by comparison of its predictions of transient cumulative mass released and discharge pressure against those obtained using the PHU. The UVBM predicted a faster depressurisation rate in the case of isolated pipe with cessation of feed flow upon puncture as compared to isolated pipe with no initial feed flow. This was found to be due to the pressure drop along the pipe caused by the feed flow. For the case of flow cessation sometime after the puncture, the UVBM predictions of transient cumulative mass released were found to

be in excellent accord with those obtained using the PHU for both permanent gases and two-phase pipelines. The average difference between the UVBM and PHU was ca. 1%

For the ranges tested, the VBM and UVBM were shown to present considerable promise given their significantly shorter computational run-time as compared to the PHU whilst maintaining a reasonable level of accuracy. However higher feed velocities or pipeline lengths are expected to invalidate the assumption of uniform pressure along the length of the pipe inherent in VBM/UVBM due to resulting higher pressure drop.

It is important to point out that the outflow models presented and developed in this work are based on the Homogenous Equilibrium Model (HEM) whereby the constituent fluid phases are assumed to remain at thermal and mechanical equilibrium during the depressurisation process. The validity of the above assumption has been supported by the reasonably good agreement of HEM predictions against real pipeline rupture test data. However, given the very limited number of such data available, it is difficult to establish the full range of the applicability of HEM based outflow models especially in the case of punctures where heterogeneous flow behaviour is expected to be more prevalent as compared to FBR.

It is hoped that the work presented in this study will help improve the safety of pressurised hydrocarbon transportation pipelines by enabling the more accurate prediction of the transient outflow following their accidental failure in a fast and reliable manner. Once such information is available, appropriate mitigation steps may be undertaken in an informed manner in order to reduce the consequences of their failure to a safe and manageable level thus helping to protect people, the environment and assets.

8.2 Suggestions for Future work

Hybrid Model

The depressurisation process of a pipeline containing gas or two-phase inventories is divided into two stages. The first stage involves the propagation of the decompression induced expansion waves from the ruptured or open end of the pipe towards the intact end. This stage is found to be highly transient lasting for a few seconds; the exact duration of which primarily depends on the pipe length, the fluid phase and its temperature and pressure. Once the expansion wave has reached the pipe intact end, the pressure at this location starts to fall. Thereafter, the flow inside the pipe is characterised as quasi-steady choked frictional flow and the main contribution to the pressure drop along the length of the pipe is caused by pipe wall friction.

Given the latter, it can be demonstrated that the inertia terms during this stage may be neglected in the transient equations. These terms are:

- Inertia associated with $\frac{\partial(\rho u^2)}{\partial x}$

- Inertia associated with $\frac{\partial(\rho u)}{\partial t}$

For brevity and demonstration purpose, the inertia associated with the first term (i.e. $\partial\ (\rho u^2)\ /\partial x$) is calculated at different times post depressurisation and presented in figure 8.1. The simulation is carried out based on a 5000 m pipe conveying pure methane following a puncture in the middle with puncture to pipe diameter ratio of

0.4. The feed flow is assumed to be ceased upon failure with the initial feed velocity of 10 m/s. All other prevailing conditions and pipeline characteristics are presented in table 6.2 (chapter 6).

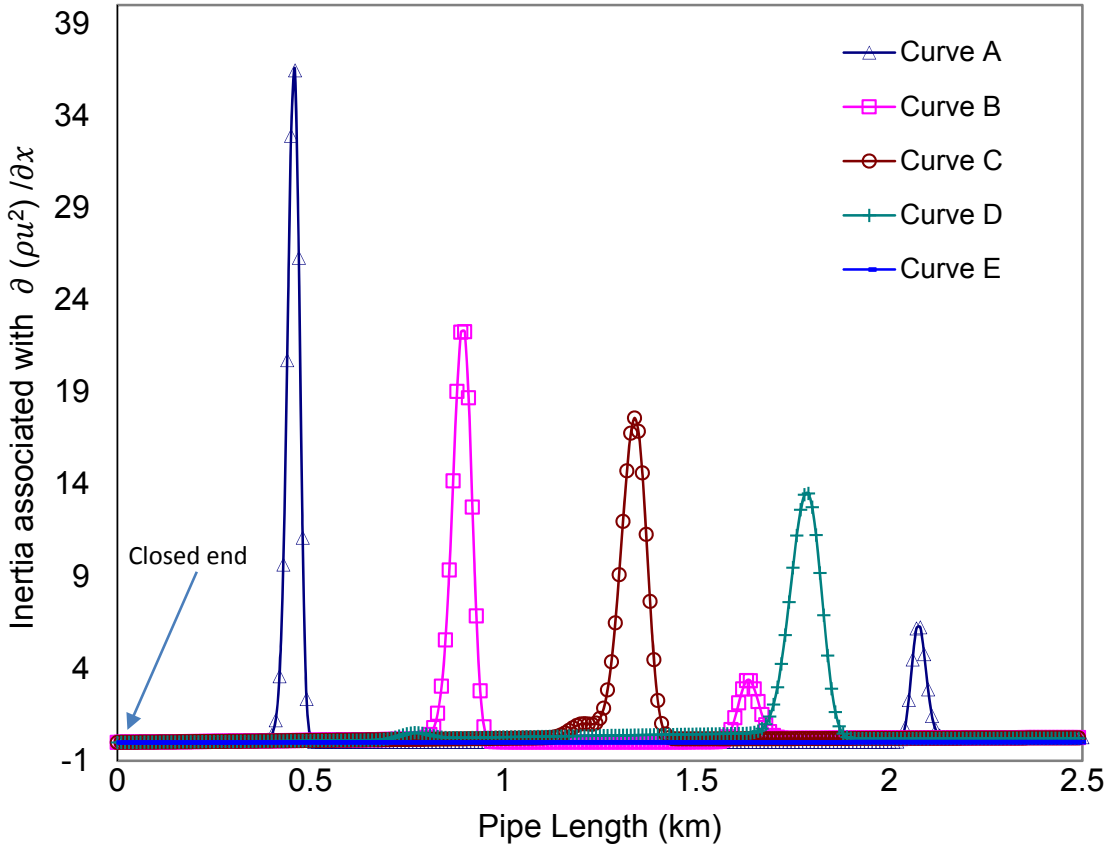

Figure 8.1: Inertia associated with $\partial\ (\rho u^2)/\partial x$ along the length of one section of the pipe at different times following puncture in the middle of the 5000m pipe.

Curve A: Inertia calculated at t=1s

Curve B: Inertia calculated at t=2s

Curve C: Inertia calculated at t=3s

Curve D: Inertia calculated at t=4s

Curve E: Inertia calculated at t=160s

Based on the figure 8.1, the inertia term arises because the gas accelerates as it expands from the closed end towards the open end. Once the highly transient regime has ended, the contribution of both inertia terms combined is less than ca. 1% of frictional term. Accordingly, the system of conservation equations can be reduced to a system of parabolic equations. The Method of Lines can then be utilised for the resolution of the parabolic equations whereby determination of time steps are no longer governed by the CFL stability criteria, thus allowing the use of larger time steps.

Based on the above, the computational run-time associated with the PSUC can further be reduced by way of developing a hybrid model. The hybrid model requires employing the PSUC for the highly transient stage of the depressurisation and the system of parabolic conservation equations (i.e. removing the inertia terms in the conservation equations) for the quasi-steady frictional flow.

Modelling Other Transient Boundary Conditions for UVBM

In the present model only a reservoir has been considered as the feed source in the UVBM. As part of future work, this can be further extended to account for pump or emergency shutdown valve at the high pressure end of the pipe.

Alternative Critical Discharge Rate Model

As an alternative to Omega method employed in VBM for predicting two-phase release pressure, the critical discharge solution methodology based on Elias and Lellouche (1994) known as the Critical Discharge Algorithm (CDA) can be implemented. Based on the CDA, the critical discharge pressure is obtained by maximising the discharge flow rate, G, in equation 6.6 (see chapter 6: section 6.2.1) with respect to pressure using the method of Brent (2002).

Heterogeneous Two-fluid Model

The validity of the HEM in the case of release from an inclined pipelines such as risers is in doubt due to the possibility of slug flow regime. The development of heterogeneous two-fluid model accounting for phase slip between the constituent phases is considered to be a useful tool. The modelling requires separate conservation equations for each constituent phase together with an appropriate liquid hold up correlation. The latter is empirically determined and will require the design of realistic experiments for the investigation of the various flow regimes and their transitions during pipeline failure.

References

APIGEC: Alberta Petroleum Industry Government Environmental Committee, "Hydrogen sulphide isopleth prediction-phase I: model sensitivity study," (1978).

Assael, M. J., J. P. M. Trussler and T. F. Tsolakis, *Thermophysical properties of fluids, an introduction to their prediction*, Imperial College Press (1996).

Atti, O., "Modelling outflow and low temperature induced crack propagation in pressurised pipelines", Ph.D. Thesis, University College London (2006).

Bendiksen, K. H., D. Malnes, I. Brandt, P. Fuchs, H. Linga, and R. Moe, "Two-phase flow research at SINTEF and IFE. Some experimental results and a demonstration of the dynamic two-phase flow simulator OLGA." *The Offshore Northern Seas Conference*, Stavanger (1986).

Bendiksen, K. H., D. Malnes, R. Moe, and S. Nuland, "The dynamic two fluid model OLGA: theory and application", *Society of Petroleum Engineers Production Engineering*, 6 (2), 171 (1991).

Boicourt, G. W., "Emergency Relief System (ERS) design: an integrated approach using DIERS methodology", *Process Safety Progress,* 14 (2), (1995).

Botros, K.K., J. Geerligs, J. Zhou, A. Glover, "Measurements of flow parameters and decompression wave speed following rupture of rich gas pipelines, and comparison with GASDECOM", *International Journal of Pressure Vessels and Piping*, 84, 358–367 (2007).

Brankin, R. W., "Algorithm 670: a Runge-Kutta-Nystrom code ACM", *transactions on mathematical software*, *15* (1), 31 (1989).

Brown, S., "CFD Modelling of Outflow and Ductile Fracture Propagation in Pressurised Pipelines", Ph.D. Thesis, University College London (2011).

Brown, S., and H. Mahgerefteh, "From Cradle to Burial: High Pressure Phase Equilibrium Behaviour of CO2 during CCS". *Proceedings of the 2009 AIChE Annual meeting. Nashville,* (2009).

Chen, J. R., S. M. Richardson, and G. Saville, "A simplified numerical method for transient two-phase pipe flow," *Trans IChemE*, 71A, 304 (1993).

Chen, J. R., S. M. Richardson and G. Saville, "Modelling of two-phase blowdown from pipelines: I. A hyperbolic model based on variational principles", *Chem. Eng. Sci*., 50,695 (1995a).

Chen, J. R., S. M. Richardson and G. Saville, "Modelling of two-phase blowdown from pipelines: II. A simplified numerical method for multicomponent mixtures", *Chem. Eng. Sci*., 50, 2173 (1995b).

Chen, N. H., "An explicit equation for friction factor in pipes," *Ind. Eng. Chem. Fundam.*, 18, No. 3, 296 (1979).

Cleaver, R. P., P. S. Cumber and A. Halford, "Modelling outflow from a ruptured pipeline transporting compressed volatile liquids", *J. of Loss Prevention in the Process Industries,* 16, 6, 533-543, (2003).

Coulson, J. M. and J. F. Richardson, *Chemical engineering vol.I.,* 6th. Edition, Butterworth, London (1999).

Courant, R., K. Friedrichs, and H. Lewy, "On the Partial Difference Equations of Mathematical Physics", *IBM Journal of Research and Development*, *11*(2), 215-234 (1967).

Cullen, W. D., "The public inquiry into the Piper Alpha disaster", (1990).

Cumber, P., "Outflow from fractured pipelines transporting supercritical ethylene", *J. of Loss Prevention in the Process Industries*, *20*(1), 26-37 (2007).

Daubert, T. E., and R. P. Danner, "Tables of physical and thermodynamic properties of pure compounds," DIPPR Project 801 Data Compilation (1990).

Denton, G., "*CFD* Simulation of Highly Transient Flows", Ph.D. Thesis, University College London (2009).

Elias, E. and G. Lellouche, "Two-phase critical flow". *International Journal of Multiphase Flow*, *20* (94), 91-168 (1994).

Ely, J. F., and H. J. M. Hanley, "Prediction of transport properties. 1. Viscosity of fluids and mixtures," *Ind. Eng. Chem. Fundam.,* 20, 323 (1981).

Ely, J. F., and H. J. M. Hanley, "Prediction of transport properties. 2. Thermal conductivity of pure fluids and mixtures," *Ind. Eng. Chem. Fundam.*, 22, 90 (1983).

Fairuzov, Y. V. "Blowdown of Pipelines Carrying Flashing Liquids", *AIChE Journal*, *44*(2), 245-254, (1998).

Fanneløp, T. K. and I. L. Ryhming "Massive release of gas from long pipelines" *AIAA Journal of Energy*, 6, 132-140 (1982).

Flatt, R., "Unsteady compressible flow in long pipelines following a rupture," *Int. J. Num. Meth. Fluids*, 6, 83 (1986).

Ghiaasiaan, M., *Two-phase flow: boiling and condensation in conventional and miniature systems*, Cambridge University Press, New York (2008).

Gottlieb, J., "Staggered and nonstaggered grids with variable node spacing and local time stepping for the random choice method". *Journal of Computational Physics*, 78(1), 160-177 (1988).

Grolmes, M. A., and J. C. Leung, "Scaling considerations for two-phase critical flow", *Multi-Phase Flow and Heat Transfer III, A: Fundamentals, 549,* (1984).

Haque, A., Chamberlain, G., Saville, G., Richardson, S. M., "Rapid depressurization of pressure vessels". *J. Loss Prev. Process Ind., 3*, 4-7 (1990).

Haque, M.A., S.M. Richardson, and Saville, G., Chamberlain, G., and Shirvill, L., "Blowdown of Pressure Vessels. II. Experimental Validation of Computer Model and Case Studies", Trans IChemE Part B: Process Safety Environmental Protection, 70, 10 - 17 (1992b).

Health and Safety Executive - Offshore, "http://www.hse.gov.uk/offshore/fireexp/riskasse.htm", (2009).

Hoffman, J. D., *Numerical methods for engineers and scientists*, McGraw-Hill, New York (1992).

Hyprotech, *PROFES-Transient user manual*, Aspentech, Houston (2001).

Kimambo, C. Z. and A. Thorley, "Computer modelling of transients ruptured high-pressure natural gas pipelines: a review of experimental and numerical studies", *IMechE*, C502/003, 55 (1995).

King, C.J., *Separation Processes*. McGraw-Hill Book Company, New York, (1980).

Lenzing, T., L. Friedel, J. Cremers, and M. Alhusein, "Prediction of the maximum full lift safety valve two-phase flow capacity", *Journal of Loss Prevention in the Process Industries*, 11, 307–321 (1998).

Leung, J. C., "A Generalized Correlation for one-component homogeneous equilibrium flashing choked flow", *AIChE Journal*., 32 (10), 1743 (1986).

Leung, J. C., "Similarity between flashing and non-flashing two-phase flows", *AIChE Journal*, 36 (5), 797-800 (1990).

Leveque, R. J., *Finite Volume Methods for Hyperbolic Problems*. Cambridge

University Press (2002).

Lydell, B. O. Y., "Pipe failure probability-the Thomas paper revisited", *Reliability Engineering and System Safety*, 68, 207 (2000).

Mahgerefteh,H., O. Atti, "Modeling low-temperature-induced failure of pressurized pipelines", A*IChE J.*, 52(3), 1248 (2006).

Mahgerefteh, H., G. Denton and Yuri Rykov, "A hybrid multiphase model", A*IChE J.*, 54 (9), 2261 (2008).

Mahgerefteh, H., A. Oke and O. Atti, "Modelling outflow following rupture in pipeline networks", Chem. Eng. Sci., 61(6), 1811 (2006a).

Mahgerefteh, H., A. Oke and Y. Rykov, "Efficient numerical simulation for highly transient flows", Chem. Eng. Sci., 61(15), 5049 (2006b).

Mahgerefteh, H., Y. Rykov, and G. Denton, "Courant, Riedrichs and Lewy (CFL) impact on numerical convergence of highly transient flows", *Chemical Engineering Science*, *64*(23), 4969-4975 (2009).

Mahgerefteh, H., P. Saha and I. G. Economou, "A study of the dynamic response of emergency shut-down valves following full bore rupture of gas pipelines", *Trans. Inst. Chem. Eng.*, Part B, 75, 201 (1997).

Mahgerefteh, H., P. Saha and I. G. Economou, "Fast numerical simulation for full bore rupture of pressurised pipelines", *AIChE J.*, 45, 1191 (1999).

Mahgerefteh, H., P. Saha and I. G. Economou, "Modelling fluid phase transition effects on dynamic behaviour of ESDV", *AICh E J.*, 46, 997 (2000).

Michelsen, M. L., "Multiphase isenthalpic and isentropic flash algorithms", *Fluid Phase Equil*., 33, 13 (1987).

Michelsen, M. L., "The isothermal flash problem: I. Stability", *Fluid Phase Equil.*, 9, 1 (1982a).

Michelsen, M. L., "The Isothermal flash problem: II. Phase-split calculation", *Fluid Phase Equil*., 9, 21 (1982b).

Montiel, H., J.A. Vílchez, J. Arnaldos and J. Casal, "Historical analysis of accidents in the transportation", *J. Hazard. Mater.* 51, 77–92 (1996).

Montiel, H., J. A. Vilchez, J. Casla and J. Arnaldos, "Mathematical modelling of accidental gas release", *J. Hazard. Mater.,* 59, 211 (1998).

Morrow, T. B., "Development of an improved pipeline break flow model", Final Report SwRI-6917/3, (1982).

Myers, G. E., *Analytical Methods in Conduction Heat Transfer,* McGraw-Hill Book Company, New York, (1971).

Norris, H. L., and R. C. Puls, "Single-Phase or Multiphase Blowdown of Vessels or Pipelines", *Society of Petroleum Engineers*, Paper SPE 26565, Huston, Texas, (1993).

Norris, H. L., "Hydrocarbon Blowdown from Vessels and Pipelines", *Society of Petroleum Engineers*, Paper SPE 28519, New Orleans, LA, (1994).

Oke, A., H. Mahgerefteh, I. Economou, and Y. Rykov, "A transient outflow model for pipeline puncture", Chem. Eng. Sci., 58(20), 4591 (2003).

Oke, A. "An efficient numerical simulation for modelling outflow following rupture or puncture of pressurised pipeline networks", PhD Thesis, University College London (2004).

Peng, D.Y. and D.B. Robinson, "A new two-constant equation of state", *Ind. Eng. Chem.*, 15, 58-64, (1976).

Picard, D. J., and P. R. Bishnoi, "Calculation of the thermodynamic sound velocity in two-phase multi-component fluids," *Int. J. Multiphase Flow*, 13(3), 295 (1987).

Prasad, P. and R. Ravindran, *Partial Differential Equations,* New Age International Publishers, (1985).

Press, W.H., S.A. Teukolsky, W.T. Vetterling and B.P. Flannery, *Numerical recipes in FORTRAN 77: The art of scientific computing*, 2nd. Edition, Cambridge University, Cambridge (1992).

Richardson, S. M., and G. Saville, "Blowdown of pipelines," *Society of Petroleum Engineers Europe 91*, Paper SPE 23070, Aberdeen, UK, (1991).

Richardson, S., and G. Saville, "Blowdown of LPG pipelines". P*rocess Safety and Environmental Protection*, 74(4), 235–244 (1996).

Rohsenow, W. M., J. P. Hartnett, and Y. I. Cho, eds., *Handbook of heat transfer*, 3rd ed., McGraw-Hill, New York (1998).

Saville, G., and R. Szczepanski, "Methane based equations of state for a corresponding states reference substance", *Chem. Eng. Sci*., 37, 719 (1982).

Shoup, G., J. J. Xiao and J. O. Romma, "Multiphase pipeline blowdown simulation and comparison to field data", *First North American conference on multiphase technology*, *BHR Group Conference Series No*. 31, (1998).

Tam, V. H. Y., and L. T. Cowley, "Consequences of pressurised LPG releases: the Isle of Grain full scale experiments", *Proceedings of GASTECH 88 (13th Int. LNG/LPG Conf.)*, Kuala Lumpur, 2 (1988).

Tam, V. H. Y., and R. B. Higgins, "Simple transient release rate models for releases of pressurised liquid petroleum gas from pipelines", *Journal of Hazardous Materials*, 25, 193–203 (1990).

Toro, E. F., and A. Siviglia, "PRICE: primitive centred schemes for hyperbolic systems", *International Journal for Numerical Methods in Fluids*, 42, 1263-1291 (2003).

Toro, E. F., *Riemann Solvers and Numerical Methods for Fluid Dynamics – A Practical Introduction* (3rd ed.), Springer, New York (2009).

Tubb, R., "Pipeline & Gas Journal's 2014 International Pipeline Construction Report", *Pipeline & Gas Journal*, *237*(2), (2014).

Twu, C. H., J. E. Coon and J. R. Cunnigham "New generalized alpha function for a cubic equation of state part 1. Peng-Robinson equation", *Fluid Phase Equilibria*, 105, 83-96 (1995).

U.S. Department of Transportation - Office of Pipeline Safety, "http://primis.phmsa.dot.gov/comm/reports/safety/PSI.html", (2014).

Walas, S. M. *Phase equilibria in chemical engineering*, Butterworth, London (1985).

Wylie, E. B., and V. L. Streeter, "*Fluid Transients in systems*", Englewood, NJ: Prentice-Hall, (1993).

Young, D. J. and A. Bum, "A simple model for the release rate of hazardous gas from a hole on high-pressure pipelines", *Journal of Hazardous Materials*, 97, 31-46, (2003).

Zucrow, M. J., and J. D. Hoffman, *Gas Dynamics*, Volume I and II, Wiley, New York, 297 (1975).